School of Applied Chemistry

The Characterisation of Polyacrylamide Flocculants

Richard Hecker

This thesis is presented as part of the requirement for the award of the

Degree of Doctor of Philosophy of the Curtin University of Technology

August 1998

"The habit of apprehending a technology in its completeness: this is the essence of technological humanism, and this is what we should expect education in higher technology to achieve. I believe it could be achieved by making specialist studies the core around which are grouped liberal studies. But they must be relevant; the path to culture should be through a man's specialism, not by-passing it...

"A student who can weave his technology into the fabric of society can claim to have a liberal education; a student who cannot weave his technology into the fabric of society cannot claim even to be a good technologist."

- Lord Ashby, *Technology and the Academics*

Abstract

Polyacrylamide is widely used as a flocculant but the influence of the molecular mass distribution upon flocculant activity is poorly understood. This thesis outlines the successful characterisation of ultrahigh molecular mass polyacrylamide solutions in terms of discrete solvated polymer coils and coil agglomerates. These features were correlated with the observed flocculation, demonstrating a number of solution state features required to improve flocculation activity.

Aqueous solutions of polyacrylamide exhibit time-dependant behaviour affecting viscosity and polymer agglomeration. Improving the solvation of the polymer suppressed the agglomerates, as did manipulation of hydrogen bonding through the presence of salts. Limiting agglomeration through improved solvation apparently lowers a barrier to polymer interaction, such that the coils disperse but become more susceptible to reagglomeration under mild shear. These solvent modifications did not fully suppress the agglomerates.

To fractionate polyacrylamide into a molecular mass distribution, flow field-flow fractionation (flow FFF) was chosen, coupled to a multi-angle laser light scattering (MALLS) photometer and a differential refractometer for molecular mass and concentration sensitive detection, respectively. For the first time, the analysis of high molecular mass polyacrylamides in water using the flow FFF-MALLS technique has been reported. However, a number of difficulties needed to be overcome, including shear artefacts, sample agglomeration and polymer-membrane interactions.

Both polyacrylamide standards and commercial flocculants were amenable to the technique. Commercial flocculants were found to vary not only with regard to viscosity and mean molecular mass, but also with sub- and supramicron size agglomerates. The flow FFF technique is size-sensitive, which for some low

molecular mass samples displayed an unusually wide elution profile, in apparent conflict with the molecular mass sensitive MALLS detector. It was concluded that polyacrylamide in solution exists simultaneously in three states: discrete polymer coils, entanglements of a several coils, and agglomerates with supramicron diameters.

This thesis concluded with a comparison between the characterised polyacrylamides and observed flocculation activity on a standard kaolin substrate. Results show polymer with supramicron agglomerates produce the largest and most shear-resistant kaolin aggregates with a definite optimum agitation intensity. Higher molecular mass flocculants with less agglomeration bind fine particles under more gentle conditions but are deficient under increasing stress. Flocculants exhibiting coil entanglements showed poor activity and formed only small aggregates. A modified flocculation mechanism was proposed, in which supramicron polymer agglomerates play a critical role.

Acknowledgments

Speak to th' mariners: fall to't - yarely - or we run ourselves aground. Bestir, bestir.

I am most grateful to the master and boatswain of the vessel, Dr. Phillip Fawell and Dr. John Farrow (A.J. Parker Cooperative Research Centre for Hydrometallurgy and CSIRO Minerals, Perth, Australia). Thanks to the navigators steering away from schoals: A/Prof. Alan Jefferson (Polymer Chemistry, Curtin University of Technology, Perth), and Jean Swift (Thickener Technology, CSIRO Minerals), and to Warren Jones (System Manager, CSIRO Minerals) for keeping the portholes clear. I offer a further thank you to the aesthetic eye of Phillip Fawell: if the figures within are especially clear, the credit is his.

Appreciation to the galley rowers below decks, the Particle Analysis Service and the Scientific Engineering Unit (CSIRO Minerals).

To the King of Naples and Duke of Milan for commissioning the voyage: the AJ Parker Cooperative Research Centre, in collaboration with the School of Applied Chemistry at Curtin University, and the Flocculation Chemistry Group at CSIRO Minerals.

To all the sprites, sylphs and faeries of the postgraduate island: the original inhabitants Franca J., David R. and Tony M; and to the later arrivals Melanie C., Gabriella S., Jo L., Melissa B., Justin M., Matt S. and Tian L. Especial thanks to Miranda, Mei L., for emergency coffee and film sessions.

Thanks finally to the many weathering the storm while Prospero tamed Caliban. In chronological order: Rob K., Roger H., Jason S., Scott B., Darryl H., Mei L., Susan K., Kitty vdH., Ange H., Rick H., Moo and Elmo.

Gentle breath of yours my sails / Must fill, or else my project fails

Contents

List of Figures

List of Tables

Glossary

This thesis links physicochemical parameters of polyacrylamides to an industrial process, and this glossary collates mineral processing terminology and polymer science acronyms and symbols employed in this work.

Terms

agglomerate	entangled polymer or microgel
aggregation	coalescence of discrete particles into a larger body
aggregate	the product of aggregation processes
cluster	an aggregate of aggregates
coagulation	aggregation brought about by addition of electrolyte
coagula	specific term for a coagulated aggregate
entanglement	smaller polymer agglomerate, less than 1 μm diameter
flocculation	aggregation brought about by addition of polymer

Acronyms

DLS	dynamic light scattering
DRI	differential refractive index
FBRM	focussed beam reflectance measurement
FFF	field-flow fractionation
GPC	gel-permeation chromatography
HDC	hydrodynamic chromatography
LALLS	low-angle laser light scattering
MALLS	multi-angle laser light scattering
M_n	number-averaged molecular mass
M_w	weight-averaged molecular mass
M_η	viscosity-averaged molecular mass
PAAm	polyacrylamide
PCS	photon correlation spectroscopy
SEC	size-exclusion chromatography

Symbols: Latin characters

A_2	second virial coefficient of polymer solution
a	polymer conformation exponent, $0.33 < a < 1.0$
b	(FFF) channel breadth
c	concentration
D	diffusion coefficient
d	particle or macromolecule hydrodynamic diameter
F	(FFF) force experienced by solute from applied field
f	(FFF) solute-carrier friction parameter
I_0	(MALLS) Intensity of incident polarised light
I_θ	(MALLS) Intensity of light at scattering angle θ
K	Mark-Houwink coefficient
K^*	(MALLS) optical constant
k	Boltzmann's constant; (MALLS) Debye plot constant
L	(FFF) channel length
l	(FFF) solute layer parameter
N_A	Avogadro's number
n	refractive index of a solution
n_0	refractive index of a solvent at for wavelength λ
$P(\theta)$	(MALLS) molecular architecture factor
R	(FFF) retention ratio
R_θ	(MALLS) Rayleigh ratio at scattering angle θ
r	(MALLS) distance between scattering medium and detector
$\langle r^2 \rangle^{\frac{1}{2}}$	root-mean-square polymer coil radius

S_d	(FFF) diameter-based solute selectivity
s	(FFF) solute field susceptibility parameter
T	temperature
t	time
t^0	(FFF) void time
t_r	(FFF) retention time
U	(FFF) solute drift velocity due to applied field
V	(MALLS) volume of the scattering medium
V^0	(FFF) channel void volume
V_r	(FFF) retention volume
$\dot{V}$	(FFF) volumetric channel (axial) flow rate
$\dot{V}_c$	(FFF) volumetric crossflow (field) flow rate
$\dot{V}_c^{\,i}$	(FFF) initial crossflow before programmed decay
$\langle v \rangle$	(FFF) mean linear velocity of carrier liquid
w	(FFF) channel thickness

Symbols: Greek characters

$\chi(\lambda)$	(FFF) mass transfer function
ϕ	(FFF) applied field
γ	shear rate
η	solution viscosity
η_0	solvent viscosity
λ	(FFF) solute layer parameter; (MALLS) wavelength of light
μ	(MALLS) molecular architecture function
θ	(MALLS) plane angle between incident and scattered light; Flory conditions
ρ	polydispersity index
σ^2	(FFF) contributor to band broadening
τ	(FFF) field decay time constant
τ_0	(FFF) time field held constant before decay

Publications

Material presented in this thesis has appeared in other forms.

Hecker R., Fawell P.D. and Jefferson A., "The Agglomeration of High Molecular Mass Polyacrylamide in Aqueous Solutions", *Journal of Applied Polymer Science*, in press.

Hecker, R., Fawell, P.D., Jefferson, A. and Farrow, J.B. "Flow Field-Flow Fractionation of High Molecular Mass Polyacrylamide", *manuscript submitted to Journal of Chromatography A.*

Hecker, R., Fawell, P.D., Jefferson, A. and Farrow, J.B. "Flow Field-Flow Fractionation of Polyacrylamide: Commercial Flocculants", *manuscript in CSIRO internal review for submission Journal of Applied Polymer Science.*

Hecker, R., Fawell, P.D. and Farrow, J.B. "The effect of flocculant properties and flocculation conditions on aggregate formation", *manuscript in preparation for submission to Colloids and Surfaces A: Physicochemical and Engineering Aspects.*

Johnson, R.R.M., Nguyen, T.V., Simic, K., Rudman, M., Blackburn, H.M., Swift, J.D., Fawell, P.D., Jones, W.G., Farrow, J.B., Fletcher, B.L., Collisson, M., Hecker, R. and Warren, L.J., "AMIRA Project P266A: Improving Thickener Technology" Stage 2, 4th Progress Report, CSIRO Division of Minerals, May 1995, pp. 105-110.

Johnson, R.R.M., Nguyen, T.V., Simic, K., Schwartz, M.P., Rudman, M., Blackburn, H.M., Swift, J.D., Fawell, P.D., Jones, W.G., Farrow, J.B., Fletcher, B.L., Collisson, M., Hecker, R. and Warren, L.J., "AMIRA Project P266A: Improving Thickener Technology" Stage 2, 5th Progress Report, CSIRO Division of Minerals, November 1995, pp. 125-130.

Chapter 1

Flocculants, Aggregation & Solid-Liquid Separation

1. *FLOCCULANTS, AGGREGATION AND SLURRY THICKENING*

Hydrometallurgical processing involves the use of substantial quantities of liquid, and at some point a solids concentrate must be separated from the process pulp. Dewatering the pulp aids both handling of the solids and retrieves process liquor. Clarified liquor is either recycled or sent for further processing (*i.e.* precipitation, electrowinning or solvent extraction), while the thickened solids may be pumped to tailings dams or disposed of by other means.

Solid-liquid separation is commonly achieved by sedimentation in a gravity thickener. The procedure depends upon sufficiently rapid settling of the solids, in turn dependant upon the size of the particles. By adding a flocculant to aggregate the solids the rate of settling is enhanced. Most effective flocculating agents are high molecular mass polymers able to adhere to the particulate surfaces.

Studies of flocculation have focussed upon the surface of the solids and mixing conditions, while consideration of the flocculant rarely extends beyond its charge density and mean molecular mass. While the molecular mass distribution of the flocculant is almost certainly a critical factor in flocculation performance, such information is not known due to difficulties in characterising the distribution of ultrahigh molecular mass polymers.

This thesis describes the development of methods to determine the molecular mass distribution and solution properties of polyacrylamide flocculants. Information gained from these methods, together with novel tools for the assessment of flocculation performance, were then used to establish a relationship between flocculation properties and the aggregation of a standard substrate.

This introductory Chapter provides a background in polymer adsorption and particulate aggregation, and concludes by demonstrating the industrial relevance of this work.

1.1 FLOCCULANTS

Polymeric flocculants are typically long, flexible chains of high molecular mass, usually in the range 1×10^6 to 25×10^6, and may possess a charge. They are derived from natural sources (such as starches), or synthetic (such as polyacrylamide, polyacrylate or polyethylene oxide). Some example monomer structures are shown in Figure 1-1.

Figure 1-1 Flocculant molecular structures: natural starch (amylose component) and synthetic (polyacrylamide monomers and acrylamide-sodium acrylate).

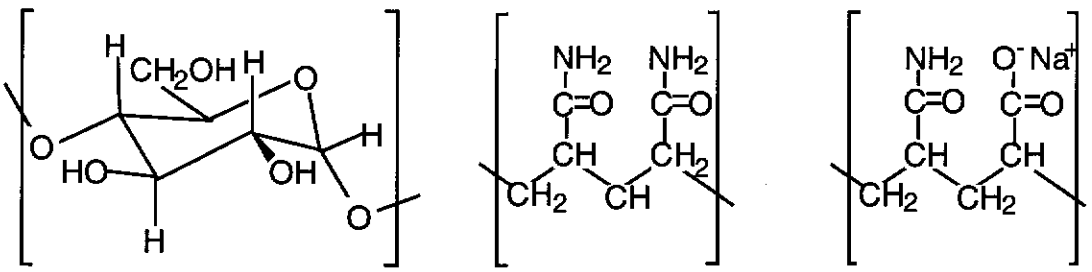

These macromolecules have a number of features as summarised by Table 1-1. Of the seven properties shown, the first three result from the type of monomer feedstock used in the production of the material, while the latter four are more subtle architectural features. The properties are intimately interrelated; for example functionality determines charge, which in turn influences solution coil dimensions. Molecular architectural features are functions of the polymerisation conditions. Higher reaction temperatures often favour branching and crosslinking, while poor mixing in a free-radical polymerisation produces a product with a wide molecular mass distribution. Table 1-1 highlights the advantage of synthetic flocculants, in which a greater variety of desired properties can be imparted onto the flocculant.

Table 1-1 Flocculant molecular features.

	Feature	Examples
Monomer properties	Monomer	moieties include amide, carboxylate or hydroxyl
	Composition	copolymers such as poly(acrylamide-*co*-acrylate) provide properties of both pendant moieties towards adsorption
	Charge	the charge and number of functional groups affects chain rigidity, coil radius and viscosity; also influences reactions to the ionic strength and acidity
Architecture	Tacticity	the arrangement of the units along the chain, whether random, alternating or in blocks, modify properties[A]
	Mean molecular mass	higher molecular mass corresponds to a longer linear molecules, greater ability to bridge across surfaces, and more "anchor" points for adsorption
	Molecular mass distribution	smaller molecules diffuse more rapidly to the surface, larger molecules bridge better; the effect of the mixture is unknown
	Branching	branching makes a polymer more compact at a given molecular mass as compared to a linear configuration

[A] Panzer and Halverson (1989).

Solutions of flocculant are viscous, due to their high molecular mass. Charged polymers have a greater solution viscosity from intramolecular repulsion "stiffening" the chain. For the same reason charged polymers are more sensitive to ionic strength than uncharged due to electrostatic shielding effects. Flocculant solutions are susceptible to degradation, where the macromolecule is cleaved, and to microbiological attack.

Flocculation requires polymer segment adsorption onto the surface from solution. Interaction between the flocculant and the surface is dependant principally upon the nature of the functional groups present, the first three items of Table 1-1. Mechanisms by which the adsorption is facilitated include the following:

- *hydrogen bonding*

  often hydroxyl, carbonyl or amine moieties of the macromolecule attach onto an oxide surface. The bonding may be bridged by a water molecule.

- *hydrophobic interaction*

  in which a polymer with significant hydrophobic character is "squeezed" out of the aqueous solvent to adsorb onto the surface. This mechanism requires that the surface is somewhat hydrophobic.

Charged polyelectrolytes interact with a surface by ionic mechanisms such as:

- *electrostatic interactions between oppositely charged polymer and surface*
- *polyvalent ion bridging between similarly charged polymer and surface*

For flocculants with mixed character, for example poly(acrylamide-*co*-acrylate), all of the adsorption mechanisms may be employed. Further, if a variety of surfaces are available in a slurry of mixed minerals, judicious selection of polymer to adsorb on only one type of surface may be employed to produce a selective flocculation. It is

the variation in properties available to synthetic flocculants that are their greatest advantage, allowing the material to be "tuned" to the application.

Of the synthetic flocculants in use, the polymers of acrylamide and its derivatives are the most common. The following discussion is therefore limited to polyacrylamide itself.

1.2 POLYACRYLAMIDE

Acrylamide (2-propenamide, $H_2C{=}CHCONH_2$) is a white crystalline solid soluble to 2.15 g mL^{-1} in water at 30°C, and prepared commercially from acrylonitrile, $CH_2{=}CHCN$. Ammoxidation of propylene vapour over a bismuth-molybdenum oxide heterogenous catalyst at 400-510°C and 50-200 kPa pressure gives a 98% conversion of propylene to acrylonitrile (Brazdil 1991). From a solution of acrylonitrile in water passage over a copper or Raney nickel catalyst at 85°C produces a near total conversion to acrylamide, a method in use by the major flocculant manufacturers including Allied Colloids and Nalco, although Nitto has recently developed an enzymatic and bacterial hydration process (Lipp and Kozakiewicz 1991). The final product is shipped as a 50 wt.-% solution in water (Habermann 1991) or dried as required.

Acrylamide is converted to polyacrylamide by a free-radical process, initiated physically by ultraviolet, x- or gamma-radiation, or chemically by azo, peroxide or redox reagents (Hunkeler and Hernández-Barajas 1996). The propagation to termination kinetic ratio of acrylamide, $k_p{:}k_t$, is 17.6±1.7, the highest of any commercial olefinic stock and features a pH independence (Hunkeler 1992) such that molecular masses in excess of $10{\times}10^6$ are easily achieved. Relatively high chain-transfer constants in the presence of sulphate and Cu^{2+} and Fe^{3+} salts are the greatest impediment to achieving high linearity and molecular mass in solution (Lipp and Kozakiewicz 1991). In a typical solution polymerisation a 20 wt.-% aqueous acrylamide solution is fed into a reactor with condenser and cooling jacket, and the reaction is initiated by sodium bisulphite/ammonium persulphate. Ultrahigh molecular masses may be produced by irradiation of monomer with cobalt-60 gamma radiation at a controlled rate to avoid crosslinking (Lipp and Kozakiewicz 1991). Emulsion, inverse emulsion and microemulsion polymerisation techniques for polyacrylamide are also available to avoid the extreme viscosities in excess of 10^6 cP

of the solution polymerisation (Hunkeler 1992, Hunkeler and Hernández-Barajas 1996) but necessitate removal of the emulsifying phase for many applications.

Polyacrylamide features an amide functionality on a hydrocarbon backbone. Referring to Table 1-1, these monomer properties provides the molecule with a remarkable flexibility and the amide allows binding to a variety of surfaces in an aqueous environment by hydrogen bonding. It is for these reasons polyacrylamide finds extensive use as a flocculant. These next Sections outline the properties of polyacrylamide. Following the convention used for describing proteins, the Sections are divided into *primary* structure of atomic arrangement, *secondary* structure of coils and folding, and the *tertiary* structure of supramolecular agglomerates.

1.2.1 Primary structure of polyacrylamide

Spectroscopic analysis of polymers is most widely used to ascertain copolymer ratios and degree of monomer block character, typically using infrared and nuclear magnetic resonance spectroscopies (Zurimendi *et al.* 1984). For the polyacrylamide homopolymer the primary structural features of interest are the head-to-tail versus head-to-head sequencing of the chain. Lancaster and O'Connor (1982) used ^{13}C NMR and failed to detect any head-to-head sequences, demonstrating that the amide groups are located only on every second carbon atom. The same study also quantified the tacticity of the pendant amide and determined a trend towards syndiotacticity. This result was matched with studies on higher molecular mass species (Inoue *et al.* 1983, Hikichi *et al.* 1988), showing polyacrylamide exhibits the usual syndiotactic sequences expected of vinylic polymers.

1.2.2 Secondary structure of polyacrylamide

The presence of the amide functionality in polyacrylamide allows for extensive hydrogen bonding in water. The hydrogen bonding activity was demonstrated with vibrational spectroscopy by monitoring the shift in the NH_2 modes when exchanging dynamically with D_2O solvent (Kulicke and Siesler 1982). Amide-amide interaction in polyacrylamide was found by Garces *et al.* (1994) to be pH independent on the basis of NMR relaxation studies, suggesting strongly that the amide group cannot be easily protonated.

Intramolecular associations are dependent upon the amide moieties being in near proximity. Factors affecting this will be molecular mass, concentration and conformation. Conformation in turn will be dependent upon the solvation of the polymer and somewhat upon the chain tacticity.

1.2.3 Tertiary structure of polyacrylamide

Tertiary structure in polyacrylamide solutions arises from intramolecular forces entwining polymer chains, or alternatively a loose collection of coils may agglomerate together. The presence of polymer dimers through multiple intermolecular hydrogen bonding is alluded to by a Raman study (Kulicke and Siesler 1982). They may be separated from solution by high-speed centrifugation (Muller *et al.* 1979) or filtration (Klein and Westerkamp 1981, Sugarman *et al.* 1987). The agglomerates were found by Boyadjian *et al.* (1976) to not be the result of permanent crosslinking but rather of weaker hydrogen bonding or physical entanglement. The proportion of the polyacrylamide entrapped in these microgels has not been quantified.

1.3 AGGREGATION OF PARTICLES

As defined in the Glossary, particle aggregation arising from addition of salts is termed *coagulation*, while *flocculation* is an aggregation arising from polymer addition.

Two-phase colloids are thermodynamically unstable with regard to surface area reduction and the use of the term "stability" refers therefore to a kinetic interpretation of aggregation (Myers 1991 pp. 194-198). An aggregation process may be halted in a metastable state in which activation energy barriers are greater than the energetic considerations. Further, if these conditions are satisfied by coarse colloids that only fuse together slowly but settle rapidly in the solution, then the particles are stable with respect to aggregation kinetics but unstable towards sedimentation, while the converse is true for a very fine dispersion. There are no universal terms in use for these conditions and clarification will be made as necessary.

1.3.1 Interactions between particles in suspension

For two particle in suspension in a medium the static component of the interaction influences the stability of the dispersion towards aggregation. For a simple monotonically decreasing potential energy, Figure 1-2a shows the interaction potential and force between two particles as a function of intervening distance. At the equilibrium separation the force vanishes, while the depth of the potential well determines the strength of the adhesion between the particles. For example, oil droplets in water possess a particularly deep well and consequently virtually irreversible coagulation, while micelles have a shallow potential well and remain dispersed.

Figure 1-2 Colloidal interactions depend on position and depth of energy potential wells. For a simple interaction there exists a single minimum well (a), but often a secondary minimum exists (b). The solid line indicates the electrostatic interaction and the dashed line the force.

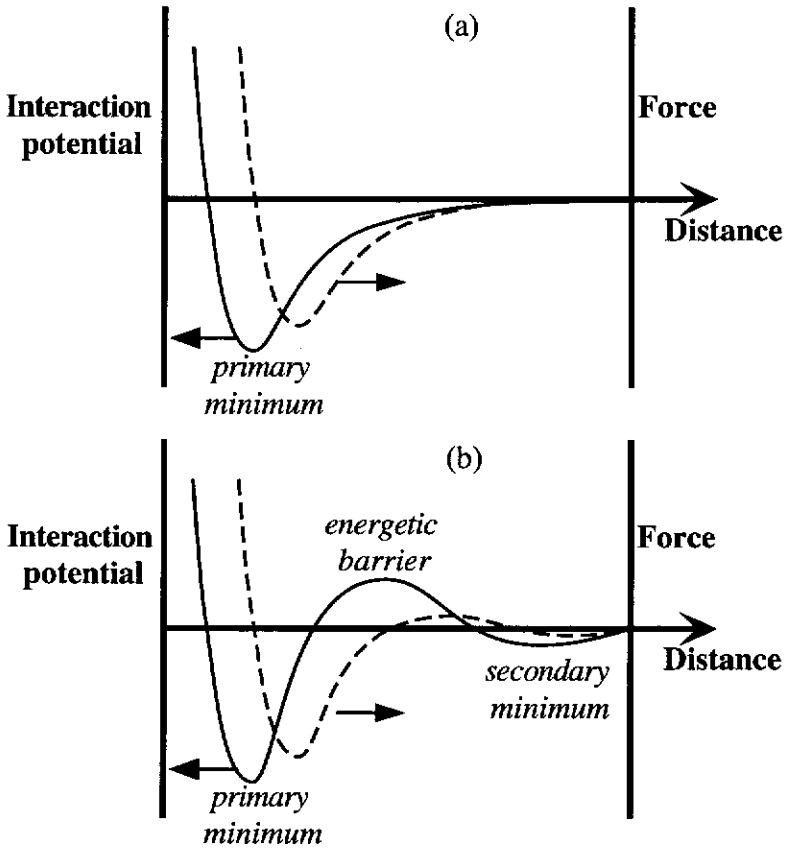

Most colloidal systems do not possess such a simple potential energy curve. For non-monotonically decreasing potentials the interaction shown by Figure 1-2b. The equilibrium separation seen for the simpler case remains but it is now separated from a secondary minimum by a potential barrier. The presence of the secondary minimum allows loose aggregate structures to form, and if the secondary minimum is sufficiently deep, these loose structures may become quite stable. The coagulation represented by the primary minimum may not be unreachable if the potential barrier is greater than thermal (few kT) energies, and while aggregation does not occur the system remains kinetically stable.

For real systems the model becomes more complex still with multiple interacting bodies and the medium attenuates the interactive forces. Clearly however, the

energy and the distance from the surface are the key components of colloid stability and are the topic of the next Section.

1.3.2 Electrostatic repulsion and coagulation

For an inorganic surface a charge arises by atomic substitution (analogous to doping aluminium or arsenic into silicon to produce semiconductors), preferential adsorption of ions, or surface specific reactions such as the hydrolysis or dissociation of surface moieties. Typically however the surface is negatively charged. Goüy (1910) and Chapman (1913) showed in a solvating electrolyte cations will approach the surface but owing to thermal motion tend to distribute themselves evenly. The result is a compromise in which the concentration of the cation is high near the surface and decreases gradually to the bulk electrolyte composition further away to form a diffuse double layer. A useful important concept is the "shear plane" parallel to the surface where a distinction between the atmosphere of counterions held tightly to the surface and the free, mobile counterions may be made. A further refinement to the model by Stern (1924) accounts for bound ions, which possess a finite volume, which form a steric barrier around the surface a few Ångströms in thickness (Gregory 1989).

A model for colloid stability based on the electrical double layer was developed over fifty years ago independently by Deryagin and Landau (1941), and by Verwey and Overbeek (1948). Their "DLVO" model quantifies the colloid interaction in terms of electrostatic repulsion versus attraction by London-van der Waals forces to predict the stability of a colloidal sol towards aggregation. According to DLVO theory the concentration of counterions decreases with distance from the surface. The electrical potential of the locus of points equidistant from the surface will be some value, Ψ, limiting to $\Psi=0$ in the bulk solution. The approximation by Debye and Hückel

(1923) presumes the rate of surface potential decay to be exponential which for some distance from the surface D

$$\Psi = \Psi_0 \, e^{-\kappa D} \tag{1-1}$$

where the constant κ is associated with the inverse of the "thickness" of the electrical double layer, known also as the Debye length. For low to moderate surface potential the Debye length (in inverse metres) may be calculated as follows

$$\kappa^{-1} = \left[\frac{(\varepsilon_0 \varepsilon)(kT)}{e^2 \left(\sum c_i z_i^2 \right)} \right]^{\frac{1}{2}} \cong 4.3 \times 10^{-10} \left(\sum c_i z_i^2 \right)^{-\frac{1}{2}} \tag{1-2}$$

where the approximate solution is for an aqueous solution at 25°C. This expression shows the Debye length is a function of electrolyte concentration and the ionic charge. Figure 1-3 shown schematically this effect in which increased electrolyte concentrations collapse the surface's electrical double layer for a surface of unit charge.

Figure 1-3 Surface potential schematic for high and low electrolyte concentration.

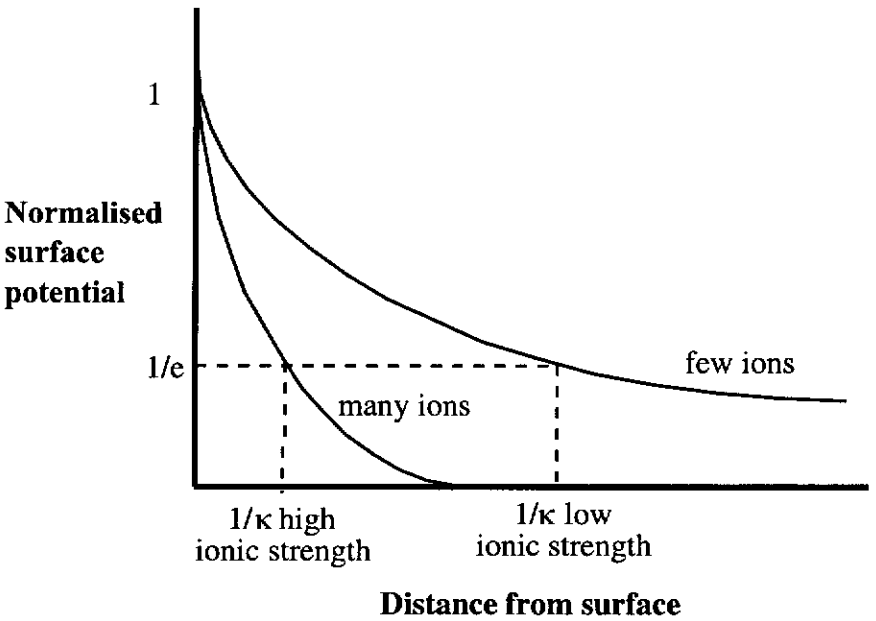

The Debye-Hückel model does not account for the ionic radius and hydration sphere, presumes point charges can approach infinitely closely, and the only

influence of the solvent is through its dielectric constant. These assumptions produce only minor deviations from observed behaviour.

Although the presence of electrolyte compress the electrical double layer and that the presence of salts with polyvalent ions such as Ca^{2+} or Fe^{3+} are even more effective at this compression, addition of ions with the opposite charge to the surface allow destabilisation by an "ion bridging" mechanism. The ion bridge arises from a polyvalent ion interacting via electrostatic means with two surfaces simultaneously. This effect may be promoted with pH changes modifying the charge of the surface. The multiple mechanisms, and often contrary effects, of additives is a common feature of colloid coagulation.

The coagula formed from the destabilisation of a sol by electrolytes exhibit a number of interesting properties. The increased diameters lead to increased settling as predicted by the Stokes' equation. Also, the coagula are sensitive to shear and will rupture easily but regenerate with time. Finally, the relatively close-packed nature of coagula leads to a decrease in available surface area. As will be shown, these properties mark coagula as different to polymer-aggregated particles.

1.3.3 Steric stabilisation: polymer overdosing

Even in an extremely dilute electrolyte a colloid may remain kinetically stable if the surfaces are kept separated at a distance greater than twice that of the position of the local maximum of the free energy curve, in essence making the potential well inaccessible. The most effective way to achieve this steric stabilisation is to cover the surface with a thick layer of polymer. Necessary characteristics of the polymer must include an affinity for the particulate surface to adsorb at a single or multiple points and a high molecular mass to make a sufficiently thick layer.

The proposed mechanism of steric stabilisation is based on two effects. Firstly, an entropic effect which favours the increase in volume per particle due to the added surface layer because of increased crowding (Mackor 1951, Mackor and van der Waals 1952). Secondly, there exists an osmotic effect in which the polymer layer, being relatively solvent-poor, allows liquid to enters the polymer coating and in resisting desolvation a energy barrier arises which resists colloid coagulation (Fischer 1958).

The thickness of the layer is strongly dependent upon the configuration of the polymer. With excessive affinity to the surface the polymer would lay flat and only a very thin layer is formed, while for very high molecular mass the polymer may be more firmly attached to the surface at multiple points and forms loops protruding into the solvent. Similar effects lead into the phenomenon of bridging flocculation and will be discussed thoroughly in Section 1.4.

1.4 Flocculation by Polymers

When a particle suspension is intimately mixed with the flocculating agent, and if the polymer adsorption onto the surface of the particle is energetically favourable, the polymer may "bridge" the particles and an aggregate is formed (Ruehrwein and Ward 1952). Figure 1-4 illustrates this effect. Polymers are efficient flocculants at low concentration as, by virtue of their length, they are able to span the two electric double layers, thereby alleviating the need for particles to approach closely to coagulate.

Figure 1-4 Flocculant molecules bridging particles (not to scale).

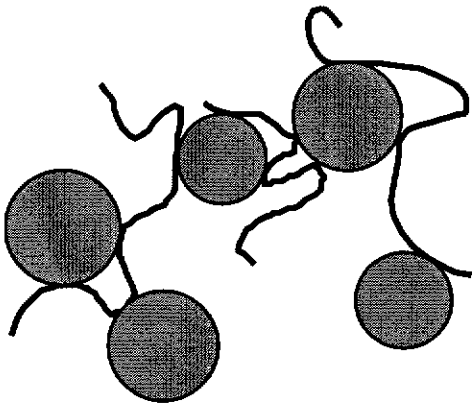

An alternative model is the electrostatic patch mechanism (Gregory 1989) similar to charge neutralisation by adsorbed counterions in the DLVO theory. A polyelectrolyte adsorbed onto a surface by electrostatic attraction creates a region on the surface differently charged from the remaining surface. This difference in charge is sufficient to allow other particles to bind into an agglomerate. Although this mechanism is possible for charged polymers it does not account for the action of nonionic flocculants and will not be considered further.

Compared to coagula, aggregates formed by flocculation are generally less-densely packed bodies, and unlike coagula the total available surface area is only reduced slightly from the free particles' total surface. Such aggregates generally exhibit a better resistance to shear disruption than coagula due to the physical binding of the

particle units (Smellie and La Mer 1958). However once the aggregate structure is broken the polymer will not re-bridge the particles and regeneration does not occur.

1.4.1 Thermodynamics of adsorption and surface coverage

For many of the polymer-surface interaction mechanisms described above, the extent of adsorption is dependant upon the partition between solvation and surface interaction. An individual polymer segment experiences this partition but the entire molecule is subject to the net effect of the segments. Limiting conditions for the polymer are therefore no affinity for the surface and total affinity for the surface depending upon segment-surface interaction. In between these limits the large polymer molecule has some segments adsorbed and some solvated. Figure 1-5 shows the polymer coil anchored onto the surface at multiple points while the ends ("tail") may be lying flat or protrude into the bulk solvent and the remaining polymer lying flat ("train") or protruding as "loops". Clearly if the partition favours solvation, the number of segments in the loops are more significant and the tails protrude, while a stronger surface affinity tends to compress the polymer onto the surface.

Figure 1-5 Polymer adsorbed on a surface.

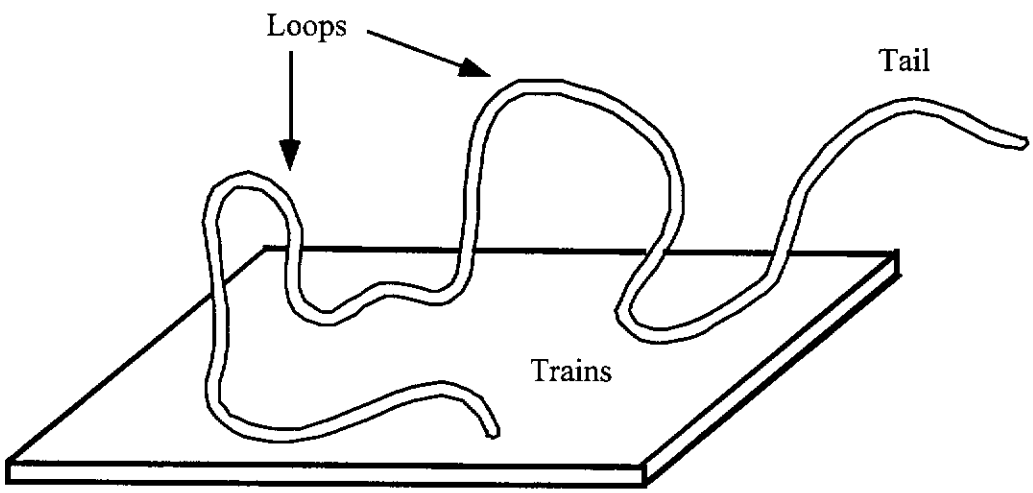

Polymer adsorption onto a surface is virtually irreversible. Although the adsorption of nonionic polymers onto silica facilitated by hydrogen bonding is approximately 16 to 20 kT per segment, multiple segment adsorption per molecule increase the net bonding proportionally. The multiple bonding with a small enthalpy gain exceeds the entropy loss of adsorption (Lyklema 1995) making adsorption spontaneous. Desorption of the polymer requires the release of *all* segments simultaneously (Lyklema 1989) and is, therefore, practically irreversible.

For bridging to be effective a competition arises between sufficient flocculant adsorbed onto a surface versus sufficient bare surface on another particle for the polymer to adsorb onto. La Mer and Healy (1963) modelled this competition with a surface coverage term $\theta(1-\theta)$ term where full particle surface coverage required θ polymer segments. The ideal coverage for flocculation occurs when this product maximised, at $\theta = 0.5$. Kitchener (1972) criticised the half-surface coverage model as simplistic since there is reference only to polymer segments attached to the surface and does not consider the loops which precludes, on steric grounds, new polymer from approaching the surface. This model has been refined since to account for polymer-polymer interactions, the possibility that two surface adsorbed loops may interact and form a bridge, and the possibilities for a single polymer chain to adsorb onto three or more particles simultaneously (Deason 1987, Hogg and Bunnaul 1992). Nevertheless, the models all predict an optimum flocculant dosage as some partial surface coverage, as total coverage invokes the steric stabilisation effect.

1.4.2 Polymer conformation on a surface

As alluded to earlier, the conformation of the polymer is dependant upon the quality of solvation, and surface affinity must be considered for predicting the size and protrusion of loops and tails. Empirical *in situ* methods for studying adsorbed

polymer conformation are few, based on neutron scattering or ellipsometry, while theoretical models abound.

Silberberg (1962a, 1962b) modified the random-walk model of solvated polymer to account for the presence of a surface and predicted that loops are very small, with no more than five polymer segments per loop. Further, if the adsorption energy per segment (the difference in free energy of adsorbed versus solvated segment) is greater than 1 kT the loops comprise less than two segments and the loose ends of the polymer eventually adsorb flat to the surface. However when structural restrictions were introduced simulating the precluded volume of the coil, loops of fifty segments long became common and the ratio of adsorbed to free segments was calculated to be 0.5. Fifty segments remains insufficiently large to cross two Debye thicknesses and flocculate. Since Silberberg's model is an equilibrium situation there must be sufficient polymer protruding off the surface to bridge only in the early stages of adsorption, as the final flattened configuration does not possess loops large enough to bridge.

More sophisticated statistical lattice models, compiled by Fleer (1995), refine Silberberg's model. At low coverage the polymer tends to flatten onto the surface similar to Silberberg's result, but at higher concentration the concentration profile off the surface decays much more slowly, due to steric crowding of the polymer and a layer up to 0.2 μm thick is present.

Recently Koopal (1992) and Fleer *et al.* (1993) have shown that the tails of adsorbed polymer are significant. While on the basis of segments, the number in the tails is small compared to the loops and trains, tails may protrude furthest from the surface. Presumably there is a time-dependency with the tails collapsing onto the surface, which is in turn dependant upon the polymer-solvent characteristics of the solvent. This solvent-tail effect was exploited by Marra and Hair (1989) using a triblock copolymer where the central block adsorbs onto the mica surface while the tail blocks remain protruding.

The above results clearly indicate that the conformation of the polymer, critical to successful flocculation, is dependant upon balancing the affinity of the polymer for the surface and solvent.

1.4.3 Effect of mean molecular mass

The effect of increasing molecular mass increases the coil dimensions dependant on conformation; for example doubling mean molecular mass will increase the radius of a spherical polymer by $2^{0.33}$-fold and $2^{0.5\text{-}0.7}$-fold for a helical coil. The increasing size influences flocculation through a greater bridging distance and more extensive flocculation for an equivalent dosage (number of molecules per unit surface area). Walles (1968) reported a doubling of polymer mean molecular mass increases the initial flocculation rate by ten to one hundred-fold.

Increasing chain length should allow an increase in the number and size of loops, but calculations by Silberberg (1962a) show the dependence is minimal for a degree of polymerisation over 10 000, equivalent to polyacrylamide of molecular mass 0.8×10^6. In terms of the polymer layer, Fleer and Scheutjens (1993) show the mean layer thickness increases with molecular mass at $(M_w)^a$ with exponent in the range 0.4 to 0.8, although whether the main contributions to this layer are from loops or tails was not clear.

The above studies presume a linear polymer. A branched polymer is more compact than a linear molecule for a given molecular mass, and linear polymers are more efficient flocculants than branched equivalents. For the same molecular mass, less unbranched flocculant is required for optimal performance (Anthony *et al.* 1975).

1.4.4 Effect of molecular mass distribution

The effects of molecular mass distribution upon flocculation are unclear. Smaller molecules diffuse to the surface more rapidly and by population are greater by number than the highest molecular mass species for a mass-based dosage. Conversely the larger molecules have more "anchor points" per molecule and the loss of entropy of mixing of the solution decreases less for the adsorption of longer chains, to favour keeping smaller molecules in solution. Published theory and empirical evidence indicates that the larger molecules adsorb preferentially (vander Linden 1978, Cohen Stuart *et al.* 1980, Fleer 1995, Lyklema 1995, de Laat and van den Heuvel 1995). The preference in adsorption effects is predicted only when surface saturation occurs and is unknown when the ratio of polymer per unit area is low. For the half-surface coverage the question of preferential adsorption on the basis of molecular mass is not addressed.

1.4.5 Flocculation kinetics

A flocculation "reaction" may be considered to take place in stages involving introduction of flocculant to slurry, dispersion of flocculant throughout the slurry, adsorption of flocculant onto slurry, initial formation of aggregates, growth of aggregates and eventually aggregate breakage (Farrow and Warren 1989). This complex process and macroscale observations are illustrated schematically by Figure 1-6. Initially the slurry is composed of a suspension of free particles (a) which settle only slowly. The flocculant, once introduced and dispersed evenly throughout the slurry loosely binds a number of the particles into highly porous aggregates (b) which have a large effective radius and settle rapidly, although the number of particles still free leave the liquid phase quite turbid. Further mixing and time (c) allow most of the particles to become entrapped to improve the liquid clarity and simultaneously the aggregates compact and dewater but with a smaller radius settle

more slowly. Continued agitation (d) forces rupture to many smaller, poorly settling aggregates. Although these processes of aggregation, compaction and rupture represent a progression for an individual aggregate, for the bulk material they are often observed simultaneously. Nevertheless, depending upon the type of aggregate required, there is an optimal extent of mixing.

Figure 1-6 Progress of a flocculation "reaction" versus time.

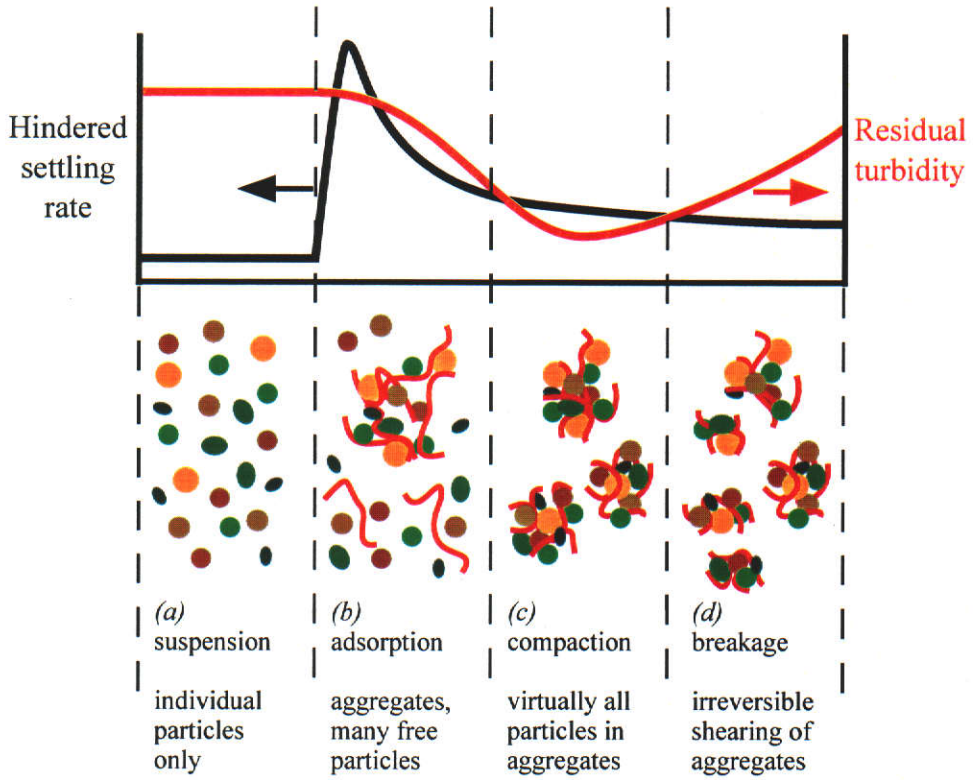

A substantial body of work exists on coagulation kinetics. Relating the rate of particle diffusion with the energetics of collision and probabilities of a successful collision gives rise to coagulation kinetics and begins with the von Smoluchowski (1916, 1917) model. The model presumes irreversible aggregation of primary spherical particles to higher order bodies. The rate of loss of the primary particles is dependant upon the transport processes: for two particles of radii r_i and r_j should motion and collision arise from fluid shear (mixing) is known as *orthokinetic* flocculation while collision from Brownian (thermal) effects is termed *perikinetic* flocculation. The rate constants k_{ij} of these processes are (Gregory 1989)

$$k_{ij} = \frac{4}{3}\gamma\left(r_i + r_j\right)^3 \qquad (1\text{-}3)$$

for orthokinetic flocculation for shear rate γ, while for perikinetic flocculation in a medium of viscosity η

$$k_{ij} = \frac{2kT}{3\eta}\frac{\left(r_i + r_j\right)^2}{r_i r_j} \qquad (1\text{-}4)$$

Clearly there is a critical collision radius ($r_i + r_j$) and the shear-derived orthokinetic flocculation is highly sensitive to particle size. The theory has been extended to the rate of appearance and aggregation of particulate dimers, trimers and so forth, as have the introduction of energy barriers to aggregation and particle adhesion probabilities. A coagulation process may use this reliable, rugged model.

From the model of the flocculation process (Figure 1-6) the model of coagulation kinetics cannot be transferred directly. For considerations of the flocculant itself the first two steps - mixing and adsorption - are critical, but poorly understood. Rates of polymer adsorption onto the primary particles (Healy and La Mer 1962, La Mer and Healy 1963) was shown to be initially very rapid but as less surface is available for further adsorption the rate of adsorption slows dramatically. More attention has been given to aggregate growth, where Hsu *et al.* (1995) successfully modelled growth by orthokinetic flocculation assuming polymer adsorption onto the surface was much faster than aggregate growth processes. Orthokinetic flocculation is very size-sensitive and the permanent rupture leads to a maximum aggregate size, with the limits to growth shown by Bremer *et al.* (1995) to be dependant upon shear and a projected area function related to the square of the mean aggregate radius.

1.5 THICKENER OPERATION

1.5.1 Solid-liquid separation

Hydrometallurgy refines crude ore to product by a series of solid-solution reactions. It represents an advance over pyrometallurgical processes in terms of energy requirements and gaseous pollutants but at the cost of process complexity.

Preliminary to processing, the mined ore must be ground to size. A primary crushing where the ore, with units as large as 1.5 m across, is reduced to bodies 10 to 20 cm in diameter; a secondary crushing to 0.5 to 2 cm; and a final grind to 10 to 300 μm (Wills 1985). Depending on the dispersal of mineral through the ore, each process has an optimal grinding size.

Ground ore is digested in an aqueous medium, often at elevated temperatures and pressures, and extreme pH conditions, such that the valuable material dissolves while gangue materials remain as a solid. Primary solid-liquid separation is accomplished in a thickener (Figure 1-7). Liquor enriched with dissolved minerals enters the thickening step as a slurry with the insoluble material. A stream of dilute flocculant is introduced to the slurry in the feedwell. In the feedwell, turbulent mixing disperses the flocculant through the slurry to aggregate the particles. As the flocculated suspension enters the body of the thickener, the solids settle rapidly and consolidate as a bed allowing removal as a dense underflow. These operations are illustrated in Figure 1-7. A typical thickener upgrade in a hydrometallurgical process would increase the slurry density from 3-10 wt.-% to an underflow at 25-60 wt.-%.

The remainder of the hydrometallurgical operation tends to focus on the enriched liquor. A second thickening stage is often used to clarify the liquid further by removing residual solids from the first thickener series. Depending upon the process, the liquor may be fed to an electrowinning or precipitation stage to complete the extraction.

Figure 1-7 Schematic of thickener operations.

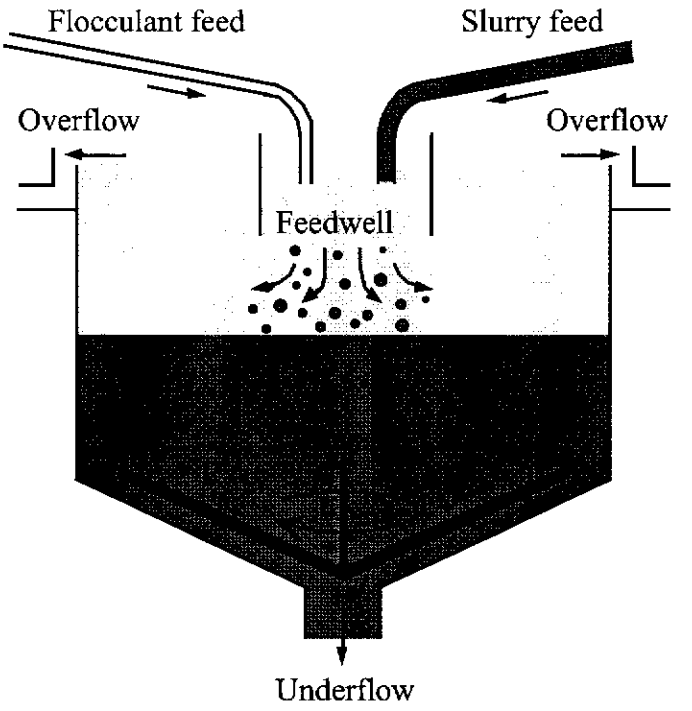

From this crude outline it is clear that the thickener occupies a pivotal position in mineral processing, needing to accommodate the fluctuation in throughput from the leaching to providing sufficient solids and liquids to their later treatment.

1.5.2 Aggregates

In the feedwell it is imperative that the flocculant be distributed evenly within the slurry to avoid regions of flocculant overdosing and steric stabilisation of the particles (Section 1.3.3). With flocculant mixed through the slurry the mechanisms of aggregate growth occur. A balance is needed between sufficient time to mix the slurry and flocculant streams and time to allow the solids to aggregate versus the increasing aggregate rupture with time (Section 1.4.5).

Mixing in the feedwell also establishes the type of aggregates. Aggregates may be classed as open or dense (Farrow and Warren 1989), depending upon the packing as shown by Figure 1-8. The rate of settling, as modelled by the Stokes' equation,

predicts a strong dependence upon aggregate size. Within the aggregate a quantity of liquor remains associated with the settling body, so for a given mass of particulates a large, open aggregate is preferred for rapid settling. Greater shear imparts a dewatering effect and the aggregate compacts to a smaller body with a higher proportion of solids per volume. Depending upon thickener performance required, high throughput or high underflow density, the type of aggregate varies.

Figure 1-8 Aggregate density and approximate aggregate radius. For a mass of particles the compact aggregate moves with less entrained liquor but the smaller hydrodynamic radius leads to slower settling.

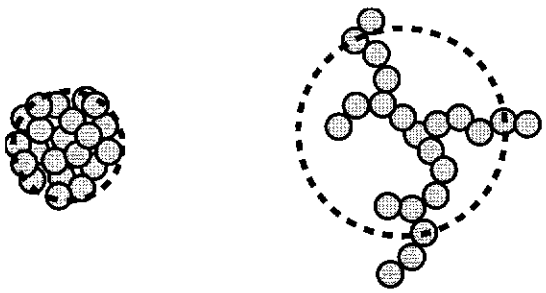

Departing the feedwell, aggregates settle under relatively quiescent conditions to avoid aggregate disruption. The time to settle must be as fast as possible to increase throughput, while being slow enough to establish a bed of solids at the base of the thickener. The presence of the bed compresses settled aggregates to force out entrained liquor, recalling it is the liquor bearing the dissolved valuable materials. The bed is continually raked to aid compaction and dewatering. It must be noted that some thickeners, used for specific high-throughput applications where underflow density is not critical, do not generate a bed.

Ideal thickener operation therefore exhibits

- good mixing in the feedwell for minimum flocculant consumption;
- fast settling for high throughput;
- minimum solids in the overflow for good clarity;
- minimum liquid in the underflow to limit loss of liquor.

Clearly the nature of aggregates produced in the feedwell affects performance.

1.6 Summary

This Section has outlined what features a commercial flocculant requires, with reference to mineral processing industries. The performance of synthetic polyacrylamide arises from high degree of polymerisation, good water solubility and a wide range of surface affinities. This Section has also shown that the dosage and mixing processes are of critical importance, determining whether the aggregates are compacted or loose, settling rapidly or providing good clarity, shear resistant or easily compressed.

What remains unknown are the effects of the polymer on aggregation. Lower molecular mass polymers diffuse more readily but are poorer at bridging. Higher molecular masses are more viscous, more easily precipitated and more shear sensitive. The performance of a commercial flocculant, with a range of molecular masses, needs to be related to the molecular mass distribution of the species present.

For ultrahigh molecular mass flocculant there are no readily available techniques to fully characterise the solution properties. Bulk characterisation techniques (*i.e.* viscosity) poorly predict flocculation activity.

Chapter 2 discusses available techniques for measuring the molecular mass and molecular mass distribution. Chapter 3 measures properties of PAAm solutions and the polymer agglomerates. Chapter 4 produces molecular mass distributions polyacrylamide standards by the novel flow FFF-MALLS technique proposed in Chapter 2. The latter half of Chapter 4 extends the work to commercial flocculants. Chapter 5 addresses the issues of molecular mass distribution on aggregates, using well-characterised polyacrylamides. Final conclusions from this study are presented in Chapter 6.

1.7 REFERENCES

Anthony, AJ, King, P.H. and Randall, C.W., 1975, 'The effects of branching and other physical properties of anionic polyacrylamides on the flocculation of domestic sewerage', *Journal of Applied Polymer Science*, vol. 19, pp. 37-48.

Boyadjian, R., Seytre, G., Berticat, P. and Vallet, G., 1976, 'Caracterisation physico-chimique de polyacrylamides utilises comme agents floculants. I. Etude en solution', *European Polymer Journal*, vol. 12, pp. 401-407.

Brazdil, J.F., 1991, 'Acrylonitrile', in *Encyclopaedia of Chemical Technology,* ed. Kroschwitz, J.I., vol. 1, John Wiley and Sons, New York,

Bremer, L.G.B., Walstra, P. and van Vliet, T., 1995, 'Estimations of the aggregation time of various colloidal systems', *Colloids and Surfaces*, vol. 99, pp. 121-127.

Chapman, D.D., 1913, *Philosophical Magazine*, vol. 25, no. 6, p. 457.

Cohen Stuart, M.A., Scheutjens, J.M.H.C. and Fleer, G.J., 1980, 'Polydispersity effects and the interpretation of polymer adsorption isotherms', *Journal of Polymer Science, Polymer Physics Edition*, vol. 18, no. 3, pp. 559-573.

de Laat, A.W.M. and van den Heuvel, G.L.T., 1995, 'Molecular weight fractionation in the adsorption of polyacrylic acid salts onto BaTiO3', *Colloids and Surfaces A: Physicochemical and Engineering Aspects*, vol. 98, pp. 53-59.

Deason, D.M., 1987, 'Statistical model for bridging efficiency in polymeric flocculation', in *Process Technology Proceedings 4: Flocculation in Biotechnology and Separation Systems,* ed. Attia, Y.A., Elsevier, Amsterdam, pp. 21-31.

Debye, P. and Hückel, E., 1923, 'Theory of electrolytes. II. The limiting law of electrical conductivity', *Physik Zeitschrift* , vol. 24, pp. 305-325.

Deryagin, B.V. and Landau, L.D., 1941, 'Theory of the stability of strongly charged lyophobic sols and the adhesion of strongly charged particles in solutions of electrolytes', *Acta Physicochimica URSS*, vol. 14, pp. 633-662.

Farrow, J.B. and Warren, L.J., 1989, 'The measurement of floc density-floc size distributions', in *Flocculation and Dewatering,* eds. Moudgil, B.M. and Scheiner, B.J., Engineering Foundation, New York, pp. 153-165.

Fischer, E.W., 1958, 'Elektronenmikroskopische Untersuchungen zur Stabilität von Suspensionen in Makromolekularen Lösungen', *Kolloid-Zeitschrift*, vol. 160, pp. 120-141.

Fleer, G.J., 1995, 'Multicomponent polymer adsorption: a useful approximation based upon ground-state solutions', *Colloids and Surfaces A: Physicochemical and Engineering Aspects*, vol. 104, pp. 271-284.

Fleer, G. J., Cohen Stuart, M. A., Scheutjens, J. M. H. M., Cosgrove, T., and Vincent, B., 1993, *Polymers at Interfaces,* Chapman and Hall, London.

Fleer, G.J. and Scheutjens, J.M.H.M., 1993, 'Modelling polymer adsorption, steric stabilization, and flocculation', in *Coagulation and Flocculation,* ed. Dobias, B., Marcel Dekker, New York NY, pp. 209-263.

Garces, F.O., Sivadasan, K., Somasundaran, P. and Turro, N.J., 1994, 'Interpolymer complexation of poly(acrylic acid) and poly(acrylamide): structural and dynamic studies by solution - and solid-state NMR', *Macromolecules*, vol. 27, pp. 272-278.

Goüy, G., 1910, *Journal of Physics*, vol. 9, no. 4, p. 457.

Gregory, J., 1989, 'Fundamentals of flocculation', *CRC Critical Reviews in Environmental Control*, vol. 19, no. 3, pp. 185-230.

Habermann, C.E., 1991, 'Acrylamide', in *Encyclopaedia of Chemical Technology,* ed. Kroschwitz, J.I., John Wiley and Sons, New York.

Healy, T.W. and La Mer, V.K., 1962, 'The adsorption-flocculation reactions of a polymer with an aqueous colloidal dispersion', *Journal of Physical Chemistry*, vol. 66, pp. 1835-1838.

Hikichi, K., Ikura, M. and Yasuda, M., 1988, 'Two-dimensional ^{1}H and ^{13}C nuclear magnetic resonance studies of poly(acrylamide)', *Polymer Journal*, vol. 20, pp. 851-859.

Hogg, R. and Bunnaul, P., 1992, 'Sediment compressibility in thickening of flocculated suspensions', *Minerals and Metallurgical Processing*, vol. 9, no. 4, pp. 184-188.

Hsu, J.-P., Lin, D.-P. and Tseng, S., 1995, 'The sticking probability of colloidal particles in polymer-induced flocculation', *Colloid and Polymer Science*, vol. 273, pp. 271-278.

Hunkeler, D., 1992, 'Synthesis and characterisation of high molecular weight water-soluble polymers', *Polymer International*, vol. 27, pp. 23-33.

Hunkeler, D. and Hernández-Barajas, J., 1996, 'A concise review of the influence of synthesis and technological factors on the structure and properties of polyacrylamides', in *Industrial Water Soluble Polymers,* ed. Finch, C.A., Royal Society of Chemistry, Cambridge, pp. 10-27.

Inoue, Y., Fukutomi, T. and Chûjô, R., 1983, 'Carbon-13 NMR analysis of the tacticity of polyacrylamide', *Polymer Journal*, vol. 15, pp. 103-105.

Kitchener, J.A., 1972, 'Principles of action of polymeric flocculants', *British Polymer Journal*, vol. 4, pp. 217-229.

Klein, J. and Westerkamp, A., 1981, 'Peculiarities of polyacrylamide analysis by aqueous GPC', *Journal of Polymer Science, Part A: Polymer Chemistry*, vol. 19, pp. 707-718.

Koopal, L.K., 1992, 'Adsorption', in *Colloid Chemistry in Mineral Processing,* eds. Laskowski, J.S. and Ralston, J., Elsevier, Amsterdam, pp. 37-90.

Kulicke, W.-M. and Siesler, H.W., 1982, 'IR studies of the deuteration of polyacrylamide', *Journal of Polymer Science: Polymer Physics Edition*, vol. 20, pp. 553-556.

La Mer, V.K. and Healy, T.W., 1963, 'Adsorption-flocculation reactions of macromolecules at the solid-liquid interface', *Reviews in Pure and Applied Chemistry*, vol. 13, pp. 112-133.

Lancaster, J.E. and O'Connor, M.N., 1982, 'High field 13C-NMR of the stereoregularity of polyacrylamide', *Journal of Polymer Science: Polymer Letters Edition*, vol. 20, pp. 547-550.

Lipp, D. and Kozakiewicz, J., 1991, 'Acrylamide Polymers', in *Encyclopaedia of Chemical Technology,* ed. Kroschwitz, J.I., John Wiley and Sons, New York.

Lyklema, J., 1989, in *Flocculation and Dewatering*, Engineering Foundation, New York, pp. 1-20.

Lyklema, J., 1995, *Fundamentals of Interface and Colloid Science. Volume II: Solid-Liquid Interfaces,* Academic Press, London.

Mackor, E.L., 1951, 'A theoretical approach to the colloid-chemical stability of dispersions in hydrocarbon', *Journal of Colloid Science*, vol. 6, pp. 492-495.

Mackor, E.L. and van der Waals, J.H., 1952, 'The statistics of the adsorption of rod-shaped molecules in connection with the stability of certain colloidal dispersions', *Journal of Colloid Science*, vol. 7, pp. 535-550.

Marra, J. and Hair, M.L., 1989, 'Interactions between two adsorbed layers of poly(ethylene oxide)/polystyrene diblock copolymers', *Colloids and Surfaces*, vol. 34, pp. 215-226.

Muller, G., Laine, J.P. and Fenyo, J.C., 1979, 'High-molecular-weight hydrolysed polyacrylamides. I. Characterisation. Effect of salts on the conformational properties', *Journal of Polymer Science, Part A: Polymer Chemistry*, vol. 17, pp. 659-672.

Myers, D., 1991, *Surfaces, Interfaces and Colloids,* VCH Publishers, Weinheim, Germany.

Panzer, H.P. and Halverson, F., 1989, 'Blockiness in hydrolyzed polyacrylamide', in *Flocculation and Dewatering*, eds. Moudgil, B.M. and Scheiner, B.J., Engineering Foundation, New York, pp. 239-249.

Ruehrwein, R.A. and Ward, D.W., 1952, 'Mechanism of clay aggregation by polyelectrolytes', *Soil Science*, vol. 73, pp. 485-492.

Silberberg, A., 1962a, 'The adsorption of flexible macromolecules. Part I. The isolated macromolecule at a plane interface', *Journal of Physical Chemistry*, vol. 66, pp. 1872-1883.

Silberberg, A., 1962b, 'The adsorption of flexible macromolecules. Part II. The shape of the adsorbed molecule. The adsorption isotherm, surface tension and pressure.', *Journal of Physical Chemistry*, vol. 66, pp. 1884-1907.

Smellie, R.H. and La Mer, V.K., 1958, 'Flocculation, subsidence and filtration of phosphate slimes. VI. A quantitatitive theory of filtration of flocculated suspensions', *Journal of Colloid Science*, vol. 23, pp. 589-599.

Stern, O., 1924, 'The theory of the electrolytic double layer', *Zeitscrift für Elektrochemie*, vol. 30, pp. 508-516.

Sugarman, J.H., Prud'homme, R.K., Langhorst, M.A. and Stanley, F.W., 1987, 'Detection of microgels in polyacrylamide solutions using microcapillary flow analysis', *Journal of Applied Polymer Science*, vol. 33, pp. 693-702.

vander Linden, C., 1978, 'Adsorbtion studies of polystyrene on silica. II. Polydisperse adsorbate', *Journal of Colloid and Interface Science*, vol. 67, no. 1, pp. 63-69.

Verwey, E. J. W., and Overbeek, J. T. G., 1948, *Theory of the Stability of Lyophobic Colloids,* Elsevier, Amsterdam.

von Smoluchowski, M., 1916, 'Drei Vorträge über Diffusion brownsche Bewegung und Koagulation von Kolloidteilchen', *Physik Zeitschrift*, vol. 17, p. 557

von Smoluchowski, M., 1917, 'Versuch einer Mathematischen Theories der Koagulations-Kinetic Kolloider Lösungen', *Zeitschrift Für Physikalische Chemie*, vol. 92, p. 129

Walles, W.E., 1968, 'Role of flocculant molecular weight in the coagulation of suspensions', *Journal of Colloid and Interface Science*, vol. 27, no. 4, pp. 797-803.

Wills, B. A., 1985, *Mineral Processing Technology*, Pergamon Press, Oxford.

Zurimendi, J.A., Guerrero, S.J. and Leon, V., 1984, 'The determination of the degree of hydrolysis in poly(acrylamides): simple methods using C13 n.m.r., and elementary analysis', *Polymer*, vol. 25, pp. 1314-1316.

Chapter 2

Review of Methods for Polymer Analysis

2. *REVIEW OF METHODS FOR POLYMER ANALYSIS*

Unlike simple organic species or ions, the analysis of the molecular mass of polymers is complicated by the physical properties of the long chain molecules such as viscosity and adsorption. These problems preclude many of the methods commonly used for simpler analytes. This Section covers the methods and complications of the analysis of polymers. The Section has been divided into four subsections, being methods for determining the mean molecular mass, methods for determining the molecular mass distribution, calibration procedures, and detectors for the separation. An ideal polymer characterisation tool would allow the separation of the polymer into near monodisperse fractions and the integrated mean molecular mass of the fractions produces a meaningful molecular mass distribution of the original sample.

A list of symbols used in this and following Chapters is collated into the Glossary, appearing at the beginning of this thesis.

2.1 METHODS FOR EMPIRICAL DETERMINATION OF MOLECULAR MASS

The measured mean molecular mass will vary depending upon the technique used. For a sample of N polymer molecules, with number n_i of molecular mass M_i or with mass w_i of molecular mass M_i, the number-averaged and weight-averaged mean molecular masses, M_n and M_w, are defined as

$$M_n = \frac{n_1 M_1 + n_2 M_2 + \ldots}{n_1 + n_2 + \ldots} = \frac{\sum_i n_i M_i}{\sum_i n_i} = \frac{\sum_i n_i M_i}{N} \qquad (2\text{-}1)$$

$$M_w = \frac{n_1 M_1^2 + n_2 M_2^2 + \ldots}{n_1 M_1 + n_2 M_2 + \ldots} = \frac{\sum_i n_i M_i^2}{\sum_i n_i M_i} = \frac{\sum_i w_i M_i}{\sum_i w_i} \qquad (2\text{-}2)$$

End-group analysis and colligative properties produce M_n, while light scattering gives M_w. Viscometry provides the viscosity average M_η, but unlike the other methods is not absolute and calibration of some form is necessary.

For a single component monodisperse system the degenerate case $M_n = M_w$ exists. A measure of the sample's deviation from this state, the polydispersity ρ, is defined as the ratio M_w to M_n. An anionically polymerised standard typically has ρ 1.05 to 1.1, a polyacrylamide standard $\rho \cong 2.5$ while for a commercial flocculant ρ is often greater than 10. Although this is does not measure the molecular mass distribution it is a useful and often quoted parameter nonetheless.

2.1.1 End-group analysis

The chain ends are chemically different as a result of polymerisation; for example a polyamide possesses a terminal amine or carboxylic acid moiety. Classic titration or spectrophotometric methods can be used to determine the quantity of end groups in

a given mass of polymer. The method is ineffective beyond low molecular masses of about M_n 25×10^3, as the proportion of end-groups becomes too low.

2.1.2 Colligative properties

Colligative methods determining M_n require techniques sensitive only to the number of molecules in solution. Typically the number of molecules in solution is so low only osmotic pressure is sufficiently sensitive with a maximum of approximately M_n 500×10^3. Osmometry features a polymer solution and pure solvent, separated by a membrane. The membrane is sufficiently fine to fully retain the polymer. As the solvent permeates the membrane in order to match the activities of solvent and polymer solution, the equilibrium point, measured by the osmotic pressure, is a function of the M_n of the polymer. Although the method is effective the equilibration often takes multiple hours.

2.1.3 Light scattering methods

The theory of light scattering from polymer solutions dates back fifty years (Debye 1944, Debye 1948, Zimm 1948). A Full derivation of the principles is presented in Wyatt (1993) but the important aspects are outlined below.

The angle-dependant light scattering, R_θ, for a coherent, monochromatic, vertically polarised source of wavelength λ_0 is defined as

$$R_\theta = \frac{I_\theta\, r^2}{I_0\, V} \qquad (2\text{-}3)$$

where I_0 the intensity of the incident beam, and I_θ is the scattered intensity measured at an angle θ from the vector of the incident beam from a scattering volume V to a detector at a distance r from the scattering medium. The Rayleigh ratio R_θ for a polymer solution is conveniently expressed as an excess scattering of the polymer solution as compared to the solute by replacing the I_θ term with $(I_{\theta,solution} - I_{\theta,solvent})$. Determination of the excess Rayleigh ratio at a number of angles leads directly to the weight-averaged molecular mass and a size factor from the following expression given to second order for polymer concentration c and second virial coefficient A_2

$$\frac{R_\theta}{K^*} = M_w c\, P(\theta)\left[1 - 2A_2 M_w P(\theta)\, c\right] \tag{2-4}$$

or more usefully for the purposes of data processing

$$\frac{R_\theta}{K^* c} = M_w P(\theta) - 2A_2 M_w^2 P^2(\theta)\, c \tag{2-5}$$

This expression may be expanded further to third order in c by introducing the third virial coefficient A_3 and another scattering term $Q(\theta)$ analogous to $P(\theta)$ as defined below. This term, and higher order virial coefficients, are vanishingly small and not considered further. The term K^* is an optical constant defined as follows

$$K^* = \frac{4\pi^2 n_0^2}{\lambda_0^4 N_A}\left(\frac{dn}{dc}\right)^2 \tag{2-6}$$

where $\left(\frac{dn}{dc}\right)$ is the differential refractive index increment with respect to a change in solute concentration. The strong dependence of K^* on the source wavelength λ_0 enforces the monochromatic requirement for analytical light scattering and the need to avoid fluorescent samples.

The term $P(\theta)$ is a molecular architecture factor related to the distance between the scattering centres of the molecule. For N scattering centres with centres N_i and N_j separated by a distance h_{ij} the form factor is

$$P(\theta) = \frac{1}{N^2}\sum_{i=1}^{i=N}\sum_{j=1}^{j=N}\left[1 - \frac{\mu^2 h_{ij}^2}{3!} + \frac{\mu^4 h_{ij}^4}{5!} - \ldots\right] \tag{2-7}$$

where $\mu = \left(\frac{4\pi}{\lambda_0}\right)\sin\left(\frac{\theta}{2}\right)$. The mean square radius of a molecule with respect to a centre of mass can be defined as follows

$$\langle r^2 \rangle = \frac{1}{2N^2}\sum_{i=1}^{i=N}\sum_{j=1}^{j=N} h_{ij}^2 \tag{2-8}$$

which on substitution of the architecture factor gives

$$P(\theta) = 1 - \frac{2\mu^2\langle r^2\rangle}{3!} + \ldots \tag{2-9}$$

provided $\mu^2\langle r^2\rangle << 1$ holds. This condition, in a physical sense, requires only partial destructive interference occurring and two waves encountering the same body must not be overly out of phase.

So far the relationship between the angular dependence upon scattering intensity has been shown to provide useful results such as the weight-averaged molecular mass and a sizing term. These data are extracted graphically using one of three methods known as the Debye, Zimm or Berry plot. The methods are similar so only the Debye method is outlined below.

The Debye form requires plotting the quantities $\frac{R_\theta}{K^* c}$ versus $\sin^2\left(\frac{\theta}{2}\right)$ and fitting a polynomial in $\sin^2\left(\frac{\theta}{2}\right)$ to the angular variation, and a polynomial in c to the concentration variation, then extrapolating to $\theta \to 0$ and $c \to 0$. The order of

polynomial is crudely dependent upon solution concentration and approximate radius of gyration but is chosen judiciously to minimise the residual fit error. The extrapolation to zero angle produces the following result

$$\lim_{\theta\to 0}\frac{R_\theta}{K^* c} = M_w - 2A_2 c M_w^2 \tag{2-10}$$

in which the slope at low concentrations with respect to concentration is

$$\frac{d}{dc}\left(\lim_{\theta\to 0}\frac{R_\theta}{K^* c}\right) = -2A_2 M_w^2 \tag{2-11}$$

and projection to zero angle and zero concentration gives

$$\lim_{c\to 0}\left(\lim_{\theta\to 0}\frac{R_\theta}{K^* c}\right) = M_w \tag{2-12}$$

An identical result is obtained should the choice be made to extrapolate first to zero concentration and then to zero angle

$$\lim_{\theta\to 0}\left(\lim_{\theta\to 0}\frac{R_\theta}{K^* c}\right) = \lim_{\theta\to 0}\left(M_w P(\theta)\right) = \lim_{\theta\to 0}\left(M_w\left[1 - \frac{16\pi^2\langle r^2\rangle}{3\lambda_0^2}\sin^2\left(\frac{\theta}{2}\right)\right]\right) = M_w \tag{2-13}$$

Once the doubly-extrapolated intercept M_w is determined, then substitution into the earlier equations produces the second virial coefficient A_2 and $\langle r^2\rangle$. The square root of the sizing expression $\langle r^2\rangle^{\frac{1}{2}}$ is often known as root-mean-square radius of gyration although unconnected with rotation or moments of inertia. The term "rms radius" will be used here instead. For a polydisperse system the returned rms radius is *z*-averaged.

One of the more useful outcomes of light scattering is the conformation plot. For the same polymer-solvent system an increase in molecular mass will increase the rms

radius as $\langle r^2 \rangle^{\frac{1}{2}} \propto (M_w)^a$, where the exponent $a = 1$ for rodlike molecules, 0.5 to 0.7 for coils and 0.33 for spheres.

2.1.4 Ultracentrifugation

A band of polymer placed on a less dense liquid will, under the influence of gravity, settle. The rate of settling is enhanced under centrifugal acceleration. For a modern ultracentrifuge, reaching 10^5 *g*, sedimentation times of a few hours are accessible. By monitoring sedimentation rate a sedimentation coefficient and thereby the hydrodynamic diameter is measured. which is a function of molecular mass. The calculation assumes that the polymers sediment independently (Suzuki 1992), and requires very dilute solutions.

Ultracentrifugation of moderate M_w (200×10^3) polyacrylamide was done nearly thirty years ago and the results agreed well with well-established viscometry determinations, although for higher molecular mass the method was reliable only at polymer concentrations less than 0.1% (Shyluk and Stow 1969). The relationship between sedimentation coefficient and mean molecular mass for polyacrylamide in water has been established (Klein and Conrad 1980), although Young *et al.* (1985) suggested that hydrodynamic sizes measured by ultracentrifugation are larger than the dimensions allowed by passage through well-characterised filters.

Ultracentrifugation is also applicable to the measurement of the molecular mass distribution and this issue is covered in Section 2.2.7.

2.1.5 Viscometry

Capillary viscometry of dilute polymer solutions produces the viscosity-averaged molecular mass M_η. The technique, unlike the others above, requires calibration but is the cheapest and arguably the most appropriate for routine analysis.

For a polymer solution of viscosity η and solvent viscosity η_0 measured at the same temperature the relative viscosity is the ratio of the two. For a dilute solution passing through a capillary the ratio of the time for identical volumes of solution and solvent to pass is equivalent to the viscosity ratio as expressed below.

$$\eta_{rel} = \frac{\eta}{\eta_0} = \frac{t}{t_0} \tag{2-14}$$

From the relative viscosity evaluated at a range of solution concentrations c the intrinsic viscosity $[\eta]$ is calculated as follows by either of the two derivations below, although both are usually employed simultaneously for the same solution

$$[\eta] = \lim_{c\to 0} \frac{\eta_{rel} - 1}{c} = \lim_{c\to 0} \frac{\ln(\eta_{rel})}{c} \tag{2-15}$$

The viscosity-averaged molecular mass is then derived from the intrinsic viscosity by the empirical Mark-Houwink equation

$$[\eta] = K(M_\eta)^a \tag{2-16}$$

where K and a are constants for a particular polymer-solvent system at a given temperature. Determination of the constants K and a is difficult for high molecular masses, as at that range the samples are far from ideal narrow molecular mass, and the derived values vary widely between laboratories. Nevertheless, the method is used extensively.

2.2 *Methods for Empirical Determination of Molecular Mass Distribution*

Numerous difficulties are encountered in the determination of the molecular mass distribution for high molecular mass polymers. These include low diffusion coefficients, shear sensitivity, conformation change, surface adsorption and viscosity. Liquid chromatographic methods to determine mass distributions must therefore

- be sensitive to low concentrations to limit the viscosity effects, which become predominant at high concentration;

- use low flow rates to avoid the effects of shear, which range from coil deformation to degradation. The low diffusion also demands relatively long experimental times;

- involve limited available surface, as any liquid-solid partitioning risks adsorption by polymer onto surface with resulting band distortions or loss of sample;

- account for electrolyte effects, as polymer sensitivity to other species often changes coil conformation and potentially increases the shear sensitivity and degradation.

The next Section compares some common methods for the separation of polymer chains for a molecular mass distribution determination. All methods necessarily imply the presence of an appropriate detector in the flow stream to identify the fractionated polymer.

2.2.1 Solvent fractionation

The Gibbs free energy of mixing quantifies solubility. As the entropic term $T\Delta S_M$ is necessarily positive the sign of ΔG_M is dependent upon the enthalpy of mixing ΔH_M. This enthalpy is in turn a function of the molecular mass such that higher molecular masses are less soluble. By careful addition of a non-solvent to a dilute polymer solution the energy of solvation changes and phase separation occurs when below the θ-temperature. Higher molecular mass species will precipitate, and with further addition of non-solvent lower molecular mass chains will follow in turn, allowing the fractions to be collected if required.

Although the method works adequately, the polymers precipitate only very slowly and are difficult to isolate from the bulk solution. The fractionated samples are still very polydisperse (Hashimoto *et al.* 1978, Caskey and Primus 1986), hence the technique is rarely used.

2.2.2 Continuous polymer fractionation (CPF)

The batch solvent fractionation (Section 2.2.1) has been extended to continuous fractionation applicable to preparative-scale separation. CPF requires a solvent in which the polymer is partially soluble such that higher mass fractions are insoluble and remain in a polymer-rich gel phase, while soluble lower mass fraction polymers dissolve into polymer-poor sol phase. A column, typically 2 m long by 25 mm diameter and oriented vertically, is arranged such that solvent is fed in the base, a moderately concentrated polymer solution for fractionation introduced higher up the column, and the sol phase removed from the top of the column. The gel phase tends to settle and is removed continuously from the base of the column adjacent to the solvent entry. The limit for fractionation is a function of the polymer-solvent interaction but may be tuned by the relative withdrawal of the sol and gel phases.

Advantages of CPF include the continuously generated fractions of moderate polydispersity (samples of ρ 1.3 have been produced from 2 kg of polymer) and minimal shear from the open column design. Disadvantages are in lengthy method development to select an effective solvent and long fractionation times due to the poor mass transfer characteristics of the gel phase.

The method has been successfully applied to polyisobutylene (Geerissen *et al.* 1987a, 1987b), polycarbonate (Weinmann *et al.* 1992) and polyacrylic acid (Haberer and Wolf 1995), but polyacrylamide fractionation has not yet been reported.

2.2.3 Size-exclusion chromatography (SEC)

SEC, synonymously known as gel-permeation chromatography (GPC), is the most widely used method for determining mass distributions on an analytical scale. In a column filled with a bed of porous material ("stationary phase") a polymer sample is carried by a flowing solvent ("mobile phase"). Passage through the column results in the size-exclusion effect in which smaller chains may enter a pore of the stationary phase while the larger chains cannot. The small chains therefore have their passage through the column retarded relative to the larger chains and as such separation occurs with the elution of the largest then smaller molecules. The fractionation by SEC is based upon hydrodynamic size and therefore calibration standards or molecular mass sensitive detectors are required.

Column band broadening due to poor mass transfer characteristics distorts the size distribution slightly but SEC has other more serious problems. The stationary phase has a large surface area, approximately 1000 m^2 per column (Benincasa and Giddings 1997), and although the separation is presumed to be derived solely from the exclusion effect, interaction between the analyte and stationary phase cannot be discounted (Dubin and Principi 1989). For this reason many modern columns use a

hydroxylated poly(methyl methacrylate) gel, rather than silica as packed in older columns, to reduce unwanted polymer-stationary phase adsorption (Meehan 1995). Within the SEC column the convoluted flow means high molecular mass polymers are susceptible to shearing and chain rupture, especially so at high flowrates. Kulicke and Böse (1984) showed that polyacrylamides in a silica packed column exhibited a clear flow rate dependant sample degradation with 5×10^5 molecular mass polymer degrading at flow rates over 1 mL min^{-1} while at molecular mass 9×10^6 it could not tolerate flow rates over 0.1 mL min^{-1}. This effect was explained in terms of the inability of the polymer to relax under elongation stress (Kulicke *et al.* 1988) where the chain is extended parallel to the flow velocity. In contrast, He *et al.* (1990) observed for 3×10^6 molecular mass polyacrylamide that increasing flow rates from 0.2 to 1.0 mL min^{-1} in a poly(methyl methacrylate) packing did not lead to a significant decrease in the molecular masses measured. Presumably the difference is due to packing materials with the polyacrylamide partially adsorbing onto the silica and being sheared by the carrier flow.

Polymer-substrate interactions may be reduced by additives to alter solvent properties. A formamide cosolvent in aqueous SEC has been used successfully for polyacrylamide (Onda *et al.* 1979, Onda *et al.* 1980, Biran and Dawkins 1984) as have nonionic surfactants (Campos *et al.* 1994). Partially hydrolysed (anionic) polyacrylamides in water are poorly fractionated by SEC even when polymer-substrate ionic interactions have been suppressed by addition of salt (Beazley 1985, Gharfeh and Moradi-Araghi 1986). For polyelectrolytes ionic strength influences the hydrodynamic volume and a changed exclusion effect will produce a different distribution profile (Leung *et al.* 1987). This underlies an important consideration of SEC in that polymer conformation must be known and invariant during the separation. Reports of the application of SEC to the analysis of polyacrylamides in the presence of common salts is presented in Klein and Westerkamp (1981), Kato *et al.* (1985), and Soponkanaporn and Gehr (1987), while Hunt *et al.* (1988) successfully linked the SEC separation with a light scattering detector.

In summary SEC is a widely used tool for the analysis of polyacrylamide but requires careful considerations of shear, conformation change and necessitates lengthy experimental times.

2.2.4 Hydrodynamic chromatography (HDC)

An HDC column is not dissimilar to that used in SEC but packed instead with solid, incompressible beads rather than a porous gel. The beads form a network of capillaries ensuring, as any liquid in a capillary occupies a range of velocities, the mobile phase in an HDC column moves slowly near the surface of the beads and faster away from the surface. A smaller polymer may more closely approach the bead's surface than a larger coil and as such elution from the column is in the order largest to smaller molecules.

HDC shares with SEC the flow rate limit problems of a packed column and polymer-stationary phase interaction. Shear degradation effects increase in severity with flow rate depending upon the molecular mass which places an upper limit on flow rate; for a 13×10^6 polyacrylamide analysis times of tens of hours were required (Langhorst *et al.* 1986). Polyacrylamide molecular mass distributions by HDC are concentration dependant over 50 ppm (Hoagland and Prud'homme 1988), and studies of the effects of shear on polyacrylamide concluded, since HDC is subject to such a range of influences, that any results are unacceptably ambiguous (Hoagland and Prud'homme 1989).

2.2.5 Field-flow fractionation (FFF)

Field-flow fractionation is a family of techniques based upon solutes in an open ribbonlike channel carried at differential rates when interacting with an applied field (Giddings 1985, Giddings 1988, Giddings 1993, Giddings 1995). A channel, typically 0.3 m long and less than 0.5 mm thick, forces carrier liquid to a parabolic velocity profile. The applied field forces the solute to migrate onto one of the ribbon walls ("accumulation wall") but this is moderated by the entropy-driven back diffusion. A solute will occupy a region above the wall with a mean position dependant upon the balance between the applied field and the solute diffusion. The FFF subtechniques are named according to the nature of the applied field, including gravitational or centrifugal sedimentation, hydraulic crossflow (flow-FFF), thermal gradient (thermal-FFF), or by a magnetic or electrical field. For macromolecular analysis both flow and thermal FFF have been found effective (Giddings *et al.* 1978, Giddings 1979) especially as the strength of the field can change over the duration of the separation to vastly increase the range of separation available in one channel. Field-flow fractionation began as a theoretical technique and, unlike SEC, there exists a rigorous basis for predicting elution times which does not demand calibration. A more thorough discussion of the theory and methods of FFF is provided in Chapter 4.

Thermal FFF is experimentally very simple with retention based upon the sample's thermal diffusion, which may be converted to a molecular mass. The technique has characterised ultra-high molecular mass linear polystyrenes (Gao *et al.* 1985) and has been shown to be highly sensitive to copolymer composition (Schimpf 1996). The technique performs poorly in aqueous systems, attributed to the thermal diffusion of polymers in water being too small for sufficient retention (Kirkland and Yau 1986).

Elution in flow FFF is based solely upon diffusion coefficient and since all solutes are influenced by the crossflow it is a universal technique. Experimentally the need

for a membrane by flow FFF introduces complexities of polymer-membrane interaction, empirically accounted for by observations of membrane texture, compressibility and surface chemistry. The separation of synthetic water-soluble macromolecule standards has been reported by Giddings *et al.* (1992) for poly(2-vinylpyridine) of molecular masses up to 0.24×10^6 in less than one hour and of polystyrene sulphonate up to 0.69×10^6 in 100 minutes. The overloading phenomenon, where the elution profile has a concentration dependence, was considered to be due to polymer-polymer interactions rather than a function of the membrane. Kirkland *et al.* (1992) noted the fractionation of 0.78×10^6 polystyrene sulphonate produced only a broad, diffuse profile. Recently reported is the fractionation of 1.40×10^6 polyacrylamide (Benincasa and Giddings 1997) but again the molecular mass profile is very broad, emerging over a 150 minute period.

Coupling of a multi-angle laser light scattering detector for a comprehensive polymer analysis was reported by Roessner and Kulicke (1994) and Thielking and Kulicke (1996) using a 13.4×10^6 molecular mass polystyrene latex, but discrete water-soluble polymers of an equivalent molecular mass have not been reported.

2.2.6 Photon Correlation Spectroscopy (PCS)

A polydisperse collection of particles may be routinely characterised by commercial PCS instruments, known also as dynamic light scattering (DLS). DiNapoli *et al.* (1982) applied the technique to M_w 0.2×10^6 polyacrylamide in a very clean solution, and using light scattering theory (Section 2.1.3) derived a reasonable rms radius and second virial coefficient. The paper also demonstrates three methods to derive the molecular mass distribution from line width analysis and the data was shown to match a parallel SEC study, although the conversion from PCS sizing to mass distribution required assumptions of polymer conformation similar to the SEC

calibration procedure. PCS analysis demands mathematically convoluted processing, however computer processing has improved and the technique is now widely employed by commercial instruments (Burchard 1983, Patterson 1983, Schmitz 1990, Ying *et al.* 1996).

2.2.7 Ultracentrifugation for molecular mass distribution

Polymer sedimentation rate is a function of sedimentation coefficient, which is in turn dependent upon molecular size (Section 2.1.4). Band sedimentation combined with light scattering has been proposed as an alternative to SEC (Holzwarth *et al.* 1986, Holzwarth *et al.* 1988), with the advantages of a packing-free technique including a low shear environment and no sample loss by adsorption. Molecular masses determined were generally higher than the SEC determinations and attributed to the poor performance of the exclusion effect for very large molecules, implying SEC does not reliably account for the highest mass fractions. Ultracentrifugation has very poor resolution and the sedimentation of low mass molecules leads to difficulties for very polydisperse samples.

In equilibrium ultracentrifugation, the gravitational field is maintained long enough for a dynamic equilibrium to be established at the bottom of the measuring cell (Schröder *et al.* 1988). A particle distribution will occur from which the mass and possible the distribution curve can be calculated. In practice, the method is limited to molecular masses from 10^3 to 10^6, as measurement times become excessive for larger polymers.

2.3 *Calibration and Standards for Polymer Analysis*

From a series of near-monodisperse polymer standards a calibration of the fractionation and band broadening arising from the separation may be established. While monodisperse materials (for example, anionically polymerised polystyrene with polydispersity less than 1.05) are available for organic-soluble polymers, water-soluble polyacrylamide standards have at best polydispersities 2.2 to 2.5. Published studies of the fractionation of polyacrylamide have used other water-soluble polymers for the calibration: polystyrene sulphonate (Muller and Yonnet 1984, Kulicke and Böse 1984, Bolte and Troquet 1990, Papazian 1990), polyethylene oxide (Lesec and Volet 1990, de Laat and van den Heuvel 1993, Cutié and Martin 1995), polyethylene glycol (Kato *et al.* 1985), poly(α-D-glucopyranosyl) "dextran" (Basedow *et al.* 1979) and polysaccharide "pullulan" (Lesec and Volet 1990), or by a polystyrene latex for calibration by size (Hoagland and Prud'homme 1988). In some cases a universal calibration procedure to relate hydrodynamic volume and molecular mass by intrinsic viscosity is used (Grubisic *et al.* 1967) with the aim to use well-defined samples for calibration, assuming that the behaviour of the calibration material and sample of interest are similar. Biran and Dawkins (1984) claim polystyrene is a good universal calibrant for polyacrylamide, while Reed (1995) showed a universal calibration is not appropriate for SEC columns analysing water-soluble polymers due to electrostatic and adsorption effects differing between calibrant and sample.

These problems are all avoided if a technique is chosen where calibration is not required, such as light scattering or flow FFF. The elution profile of a calibrant is still a useful test of instrument performance. However Caldwell (1991) has proposed instrumental band broadening in FFF is trivial for polydisperse samples in comparison to polydispersity effects and the elution profile is almost an accurate representation of the molecular mass distribution.

2.4 *Detection of Polyacrylamide*

Traditional liquid chromatography requires only a detector for the determination of analyte concentration, most typically a UV-Vis spectrophotometer. For polyacrylamide the spectrum exhibits a peak in the UV at 192.5 nm (Soponkanaporn and Gehr 1987). Detection is applied in the range 200-215 nm (Holzwarth *et al.* 1988, He *et al.* 1990, de Laat and van den Heuvel 1993) which has been claimed to be linear to 50 ppm in water (Langhorst *et al.* 1986) while others claim linearity to 2000 ppm (de Laat and van den Heuvel 1993). Quantification of dilute samples, as low as 5 ppm, has been achieved with the use of a fluorescence detector (Hoagland and Prud'homme 1988) although the sample required labelling of the polyacrylamide with a derivative of fluorescein. It is the lack of suitable chromophores which limits the sensitivity of spectrophotometric detection of polyacrylamide.

Differential refractometry (DRI), using a wavefront rotation technique similar to interference microscopy, offers higher concentration sensitivity for polyacrylamides (Hashimoto *et al.* 1978, Klein and Westerkamp 1981, Biran and Dawkins 1984, Kato *et al.* 1985, Campos *et al.* 1994, Cutié and Martin 1995). DRI detectors are susceptible to solution composition and temperature variations and an unstable baseline may produce a signal comparable in size and shape to that of the polymer (Hester and Puckett 1988).

For a given injected mass, a high mean molecular mass polymer has a concentration less than for a lower M_w polymer, and a greater detector response from concentration-sensitive detectors is demanded. For the study of ultra-high molecular masses a molecular-mass sensitive detector is advantageous. The capillary pressure (CP) detector measures the pressure drop as a viscous sample enters a capillary and as viscosity increases with increasing molecular mass the detector response increases (Hester and Puckett 1988); however under even moderate flow the narrow capillary may induce shear degradation of the polymer (Reed 1995). The CP detector is

essentially an on-line viscometer and similarly requires calibration to convert pressure signals to molecular mass information.

Light scattering as a method for determining mean molecular mass was described in Section 2.1.3 and the molecular mass dependence of excess scattering shown. Early instruments used low-angle laser light scattering (LALLS). This was used to observe a single scattering angle, typically 10°, and considered close enough to 0° that extrapolation was not required to determine the sizing term $P(\theta)$. Molecular mass calculations require concentration detection simultaneous with the scattering measurement, and this is usually provided by an in-line UV or DRI detector. Scattering theory needs also the second virial coefficient, A_2, to calculate the molecular mass. Measuring A_2 requires the angular dependence of scattering, which single-angle LALLS cannot evaluate, although for low polymer concentrations it may be assumed to be vanishingly small with little error (Muller and Yonnet 1984). Alternatively using LALLS and a concentration detector the excess Rayleigh ratio may be calculated at each interval and when plotted against the concentration of the sample slice extrapolation to infinite dilution gives M_w (Hunt *et al.* 1988).

An early SEC study of polyacrylamide using a LALLS detector was reported by Kim *et al.* (1982) but as the signal was so noisy the light scattering was used only to calibrate the system and a DRI detector was preferred for the mass distribution measurement. The signal improved when the column was flushed with mobile phase for periods up to a week. Subsequent studies have made full use of the LALLS detector (Kulicke and Böse 1984, Muller and Yonnet 1984, Lin and Getman 1987, Papazian 1990), and new methodologies for optimising polymer concentration for the LALLS detector have been developed (Hunkeler 1991, Hunkeler 1992). Lesec and Volet (1990) demonstrated a good agreement between SEC with a LALLS detector and SEC with universal calibration (Section 2.3) for the molecular mass of a 0.1×10^6 polyacrylamide, while Papazian (1990) could see little difference between molecular mass calculated from retention and from LALLS data. The SEC-LALLS

system is not appropriate for polyacrylamides over 1×10^6 as the molecular concentrations are difficult to measure (Lin and Getman 1987).

Measurement of the angular dependence of excess scattering at multiple angles simultaneously allows the sizing function $P(\theta)$ and second virial coefficient A_2 to be calculated in the one experiment (Wyatt 1993). Multi-angle laser light scattering, MALLS, is also less sensitive to particulate interferences, which have a greater effect at low angles. There are few examples of MALLS detection used with the fractionation of polyacrylamide, but Wyatt (1991) has presented data suggesting the presence of a polydisperse high molecular mass component. Comparison of MALLS, LALLS and CP detectors with a SEC separation showed the light scattering methods gave similar results but MALLS had greater scope for error reduction and rms size data, while the CP detector is more suited for sizing polymers with less than 0.01 μm radius (Reed 1995).

The greatest disadvantage of light scattering is the need for cleanliness, as the presence of dust and polymer microgels can overwhelm sample scattering. Clarification by filtration is often inappropriate for polymer samples because of their large size and shear sensitivity. These conditions are relaxed when the light scattering is employed as a chromatographic detector as the separation device also affects the contaminants and the mobile phase may be filtered separately from the polymer. Dust spikes still appear from the column packing shedding particles and the sample itself, but are infrequent enough to be ignored. For SEC-LALLS, ultracentrifugation of a polymer sample has been shown to be a reliable method to remove dust (Holzwarth *et al.* 1988).

2.5 *Conclusions for the Analysis of Polyacrylamide*

An ideal polymer characterisation tool would allow the separation of the polymer into near monodisperse fractions with the integrated mean molecular mass of the fractions producing a meaningful molecular mass distribution of the original sample. SEC or FFF are the techniques of choice for the separation of a general polymer sample into near-monodisperse fractions. For both detection and mean molecular mass measurement, light scattering combines both sensitivity and absolute (calibration-free) determination and is the best selection, although the molecular mass sensitivity of CP detection is an attractive alternative. For the analysis of high molecular mass polyacrylamides the SEC and CP methods are less attractive due to the shear environment. The selection of flow field-flow fractionation with a light scattering detection, ideally MALLS and DRI, is the preferred tool for the analysis of water-soluble, ultra-high molecular mass polyacrylamide. The use of PCS is also appropriate for polyacrylamide analysis, although since dust is not isolated from the sample a lower size limit exists for the technique.

2.6 *REFERENCES*

Basedow, A.M., Ebert, K.H. and Hunger, H., 1979, 'Effects of mechanical stress on the reactivity of polymers: shear degradation of polyacrylamide and dextran', *Makromoleculare Chemie*, vol. 180, pp. 411-427.

Beazley, P.M., 1985, 'Quantitative determination of partially hydrolysed polyacrylamide polymers in oil field production water', *Analytical Chemistry*, vol. 57, pp. 2098-2101.

Benincasa, M.A. and Giddings, J.C., 1997, 'Separation and characterization of cationic, anionic, and nonionic water-soluble polymers by flow FFF: sample recovery, overloading, and ionic strength effects', *Journal of Microcolumn Separations*, vol. 9, pp. 479-495.

Biran, R. and Dawkins, J.V., 1984, 'Separation system for fractionation of polyacrylamide by gel permeation chromatography', *European Polymer Journal* , vol. 20, pp. 129-133.

Bolte, M. and Troquet, M., 1990, 'Optimisation de la caracterisation de polymeres hydrosolubles par chromatographie a permeation de gel: utilisation de plans d'experiences, une methode rapide et efficace', *European Polymer Journal*, vol. 26, pp. 177-179.

Burchard, W., 1983, 'Static and dynamic light scattering from branched polymers and biopolymers', *Advances in Polymer Science*, vol. 48, pp. 1-124.

Caldwell, K.D., 1991, 'Polymer analysis by field-flow fractionation', in *Modern Methods of Polymer Characterisation,* eds. Barth, H.G. and Mays, J.W., John Wiley and Sons, New York, pp. 113-150.

Campos, A., Garcia, R., Porcar, I. and Soria, V., 1994, 'Solution properties of polyelectrolytes. XI. Adsorption effects in aqueous size-exclusion chromatography of polyanions', *Journal of Liquid Chromatography*, vol. 17, pp. 3261-3283.

Caskey, J.A. and Primus, R.J., 1986, 'The effect of anionic polyacrylamide molecular conformation and configuration on flocculation effectiveness', *Environmental Progress*, vol. 5, pp. 98-102.

Cutié, S.S. and Martin, S.J., 1995, 'Size-exclusion chromatography of cross-linked superadsorbent polymers', *Journal of Applied Polymer Science*, vol. 55, pp. 605-609.

de Laat, A.W.M. and van den Heuvel, G.L.T., 1993, 'Competitive and displacement adsorption of polyvinyl alcohol and the ammonium salt of a polyacrylic acid on $BaTiO_3$', *Colloids and Surfaces A: Physicochemical and Engineering Aspects*, vol. 70, pp. 179-187.

Debye, P., 1944, 'Light scattering in solutions', *Journal of Applied Physics*, vol. 15, pp. 338-342.

Debye, P., 1948, 'Molecular-weight determination by light scattering', *Journal of Physical and Colloid Chemistry*, vol. 16, pp. 18-32.

DiNapoli, A., Chu, B. and Cha, C., 1982, 'Molecular weight distributions of polyacrylamide by photon correlation spectroscopy', *Macromolecules*, vol. 15, pp. 1174-1180.

Dubin, P.L. and Principi, J.M., 1989, 'Failure of universal calibration for size exclusion chromatography of rodlike molecules versus random coils and globular proteins', *Macromolecules*, vol. 22, pp. 1891-1896.

Gao, Y.S., Caldwell, K.D., Myers, M.N. and Giddings, J.C., 1985, 'Extension of thermal field-flow fractionation to ultrahigh (20×10^6) molecular weight polystyrenes', *Macromolecules*, vol. 18, pp. 1272-1277.

Geerissen, H., Roos, J., Schützeichel, P. and Wolf, B.A., 1987a, 'Continuous fractionation and solution properties of PIB. I. Search for the best mixed solvent and first results of the continuous polymer fractionation', *Journal of Applied Polymer Science*, vol. 34, pp. 271-285.

Geerissen, H., Schützeichel, P. and Wolf, B.A., 1987b, 'Continuous fractionation and solution properties of PIB. II. CPF optimisation', *Journal of Applied Polymer Science*, vol. 34, pp. 287-305.

Gharfeh, S.G. and Moradi-Araghi, A., 1986, 'Determination of anionic high-molecular weight water-soluble polymers by size-exclusion chromatography', *Journal of Chromatography*, vol. 266, pp. 343-350.

Giddings, J.C., 1979, 'Field-flow fractionation of polymers: one-phase chromatography', *Pure and Applied Chemistry*, vol. 51, pp. 1459-1471.

Giddings, J.C., 1985, 'Optimised field-flow fractionation system based on dual stream splitters', *Analytical Chemistry*, vol. 57, pp. 945-947.

Giddings, J.C., 1988, 'Field-flow fractionation', *Chemical and Engineering News*, vol. 66, no. 41, pp. 34-45.

Giddings, J.C., 1993, 'Field-flow fractionation: analysis of macromolecular, colloidal, and particulate materials', *Science*, vol. 260, pp. 1456-1465.

Giddings, J.C., 1995, 'Measuring colloidal and macromolecular properties by FFF', *Analytical Chemistry*, vol. 67, pp. 592A-598A.

Giddings, J.C., Benincasa, M.A., Liu, M.-K. and Li, P., 1992, 'Separation of water soluble synthetic and biological macromolecules by flow field-flow fractionation', *Journal of Liquid Chromatography*, vol. 15, pp. 1729-1747.

Giddings, J.C., Lin, G.C. and Myers, M.N., 1978, 'Fractionation and size distribution of water soluble polymers by flow field-flow fractionation', *Journal of Liquid Chromatography*, vol. 1, pp. 1-20.

Grubisic, Z., Rempp, P. and Benoit, H., 1967, 'A universal calibration for gel permeation chromatography', *Journal of Polymer Science: Polymer Letters Edition*, vol. 5, pp. 753-759.

Haberer, M. and Wolf, B.A., 1995, 'Continuous fractionation of poly(acrylic acid)', *Die Angewandte Makromoleculare Chemie*, vol. 228, pp. 179-184.

Hashimoto, T., Sasaki, H., Aiura, M. and Kato, Y., 1978, 'High-speed aqueous gel-permeation chromatography', *Journal of Polymer Science: Polymer Physics Edition*, vol. 16, pp. 1789-1800.

He, Q., Young, T.-S., Willhite, G.P. and Green, D.W., 1990, 'Measurement of molecular weight distribution of polyacrylamides in core effluents', *Society of Petroleum Engineers Reservior Engineering*, vol. 5, pp. 333-338.

Hester, R.D. and Puckett, A.D., 1988, 'Size characterization of EOR polymers in solution', in *Water-Soluble Polymers for Petroleum Recovery,* eds. Stahl, G.A. and Schulz, D.N., Proceedings of the National Meeting of the American Chemical Society, Plenum, New York, pp. 201-213.

Hoagland, D.A. and Prud'homme, R.K., 1988, 'Analysis of water-soluble polymers using hydrodynamic chromatography', *Journal of Applied Polymer Science*, vol. 36, pp. 935-955.

Hoagland, D.A. and Prud'homme, R.K., 1989, 'Hydrodynamic chromatography as a probe of polymer dynamics during flow through porous media', *Macromolecules*, vol. 22, pp. 775-781.

Holzwarth, G., Soni, L. and Schulz, D.N., 1986, 'Molecular weight distribution of water-soluble polymers: a new absolute method', *Macromolecules*, vol. 19, pp. 422-426.

Holzwarth, G., Soni, L., Schulz, D.N. and Bock, J., 1988, 'Absolute MWD's of polyacrylamides by sedimentation and light scattering', in *Water-Soluble Polymers for Petroleum Recovery,* eds. Stahl, G.A. and Schulz, D.N., Proceedings of the National Meeting of the American Chemical Society, Plenum, New York, pp. 215-229.

Hunkeler, D., 1991, 'A high precision light scattering method for molecular weight determination', *Journal of Applied Polymer Science: Applied Polymer Symposium*, vol. 48, pp. 335-349.

Hunkeler, D., 1992, 'Synthesis and characterisation of high molecular weight water-soluble polymers', *Polymer International*, vol. 27, pp. 23-33.

Hunt, J.A., Young, T.S., Green, D.W. and Willhite, G.P., 1988, 'Size-exclusion chromatography in the measurement of concentration and molecular weight of some EOR polymers', *Society of Petroleum Engineers Reservior Engineering*, vol. 3, pp. 835-841.

Kato, Y., Matsuda, T. and Hashimoto, T., 1985, 'New gel permeation column for the separation of water-soluble polymers', *Journal of Chromatography*, vol. 332, pp. 39-46.

Kim, C.J., Hamielec, A.E. and Benedek, A., 1982, 'Characterization of nonionic polyacrylamides by aqueous size exclusion chromatography using a DRI/LALLS detector system', *Journal of Liquid Chromatography*, vol. 5, pp. 1277-1294.

Kirkland, J.J., Dilks, C.H. and Rementer, S.W., 1992, 'Molecular weight distributions of water-soluble polymers by flow field-flow fractionation', *Analytical Chemistry*, vol. 64, pp. 1295-1303.

Kirkland, J.J. and Yau, W.W., 1986, 'Thermal field-flow fractionation of water-soluble macromolecules', *Journal of Chromatography*, vol. 353, pp. 95-107.

Klein, J. and Conrad, K.-D., 1980, 'Characterisation of poly(acrylamide) in solution', *Makromoleculare Chemie*, vol. 181, pp. 227-240.

Klein, J. and Westerkamp, A., 1981, 'Peculiarities of polyacrylamide analysis by aqueous GPC', *Journal of Polymer Science: Polymer Chemistry Edition*, vol. 19, pp. 707-718.

Kulicke, W.-M. and Böse, N., 1984, 'Bestimmung der Molmassenverteilung sowie Stabilitätsgrenze von Polyacrylamiden unter Benutzung einer kombinierten Ausschlußchromatographie/Kleinwinkel-Laser-Streulichtphotometer Anlage', *Colloid and Polymer Science*, vol. 262, pp. 197-207.

Kulicke, W.-M., Böse, N. and Bouldin, M., 1988, 'The role of polymers in enhanced oil recovery', in *Water-Soluble Polymers for Petroleum Recovery,* eds. Stahl, G.A. and Schulz, D.N., Proceeding of the National Meeting of the American Chemical Society, Plenum, New York, pp. 201-213.

Langhorst, M.A., Stanley, F.W., Cutié, S.S., Sugarman, J.H., Wilson, L.R., Hoagland, D.A. and Prud'homme, R.K., 1986, 'Determination of nonionic and partially hydrolysed polyacrylamide molecular weight distributions using hydrodynamic chromatography', *Analytical Chemistry*, vol. 58, pp. 2242-2247.

Lesec, J. and Volet, G., 1990, 'Data treatment in aqueous GPC with online viscometer and light-scattering detectors', *Journal of Liquid Chromatography*, vol. 13, no. 5, pp. 831-849.

Leung, R.W.M., Pandey, R.N. and Das, B.S., 1987, 'Determination of polyacrylamides in coal washery effluents by ultrafiltration/size-exclusion chromatography-ultraviolet detection techniques', *Environmental Science and Technology*, vol. 21, pp. 476-481.

Lin, F.C. and Getman, G.D., 1987, 'Gel permeation chromatography analysis of water soluble polymers', at *International GPC Symposium*, Millipore Corporation, Midford Massachusetts, pp. 225-45.

Meehan, E., 1995, 'Semirigid polymer gels for size exclusion chromatography', in *Handbook of Size Exclusion Chromatography*, ed. Wu, C., Marcel Dekker, New York, pp. 25-46.

Muller, G. and Yonnet, C., 1984, 'Aqueous gel permeation chromatography of high molecular weight water soluble polymers', *Makromoleculare Chemie, Rapid Communications*, vol. 5, pp. 197-201.

Onda, N., Furusawa, K., Yamaguchi, N. and Komuro, S., 1979, 'Gel permeation chromatography using controlled-porosity glass. I. Polyacrylamide-formamide solution', *Journal of Applied Polymer Science*, vol. 23, pp. 3631-3638.

Onda, N., Furusawa, K., Yamaguchi, N., Tokiwa, M. and Hirai, Y., 1980, 'Gel permeation chromatography using controlled-porosity glass. II. Polyacrylamide aqueous solutions', *Journal of Applied Polymer Science*, vol. 25, pp. 2363-2372.

Papazian, L.A., 1990, 'A pH effect in the HPSEC separation of polyacrylamide-based copolymers', *Journal of Liquid Chromatography*, vol. 13, pp. 3389-3398.

Patterson, G.D., 1983, 'Photon correlation spectroscopy of bulk polymers', *Advances in Polymer Science*, vol. 48, pp. 125-159.

Reed, W.F., 1995, 'Data evaluation for unified multi-detector size exclusion chromatography - molar mass, viscosity and radius of gyration distributions', *Macromolecular Chemistry and Physics*, vol. 196, pp. 1539-1575.

Roessner, D. and Kulicke, W.-M., 1994, 'On-line coupling of flow field-flow fractionation and multi-angle laser light scattering', *Journal of Chromatography A*, vol. 687, pp. 249-258.

Schimpf, M.E., 1996, 'Advances in field-flow fractionation for polymer analysis', *Trends in Polymer Science*, vol. 4, no. 4, pp. 114-121.

Schmitz, K.S., 1990, *An Introduction to Dynamic Light Scattering by Macromolecules,* Academic Press, Boston.

Schröder, E., Müller, G. and Arndt, K.-F., 1988, *Polymer Characterization*, Hanser Publishers, Munich.

Shyluk, W.P. and Stow, F.S., 1969, 'Aging and loss of flocculation activity of aqueous polyacrylamide solutions', *Journal of Applied Polymer Science*, vol. 13, pp. 1023-1036.

Soponkanaporn, T. and Gehr, R., 1987, 'Quantitative determination and peak molecular weight analysis of acrylamide-based polyelectrolytes by size exclusion chromatography', *International Journal of Environmental Analytical Chemistry*, vol. 29, pp. 1-14.

Suzuki, H., 1992, 'Sedimentation analysis of synthetic polymers', in *Analytical Ultracentrifugation in Biochemistry and Polymer Science*, eds. Harding, S.E., Rowe, A.J. and Horton, J.C., Royal Society of Chemistry, Cambridge, pp. 568-592.

Thielking, H. and Kulicke, W.-M., 1996, 'On-line coupling of flow field-flow fractionation and multiangle laser light scattering for the characterisation of macromolecules in aqueous solution as illustrated by sulphonated polystyrene samples', *Analytical Chemistry*, vol. 68, pp. 1169-1173.

Weinmann, K., Wolf, B.A., Rätzsch, M.T. and Tschersich, L., 1992, 'Theory-based improvements for continuous polymer fractionation demonstrated for poly(carbonate)', *Journal of Applied Polymer Science*, vol. 45, pp. 1265-1279.

Wyatt, P.J., 1991, 'Combined differential light scattering with various liquid chromatography separation techniques', *Biochemical Society Transactions*, vol. 19, p. 485.

Wyatt, P.J., 1993, 'Light scattering and the absolute characterization of macromolecules', *Analytica Chimica Acta*, vol. 272, pp. 1-40.

Ying, Q., Wu, G., Chu, B., Farinato, R. and Jackson, L., 1996, 'Laser light scattering of poly(acrylamide) in 1 M NaCl aqueous solution', *Macromolecules*, vol. 29, pp. 4646-4654.

Young, T.S., Yan, X., Hogen-Esch, T.E. and Butler, G.B., 1985, 'Measurement of hydrodynamic sizes of ultralarge water-soluble polymers by Nucleopore filtration and multicell equilibrium dialysis', *Journal of Macromolecular Science-Chemistry*, vol. A22, pp. 437-453.

Zimm, B.H., 1948, 'The scattering of light and the radial distribution function of high-polymer solutions', *Journal of Chemical Physics*, vol. 16, pp. 1093-1099.

Chapter 3

Polyacrylamide in an Aqueous Solution

3. POLYACRYLAMIDE IN AN AQUEOUS SOLUTION

Studies of the molecular mass distribution of high molecular mass polyacrylamide (PAAm) are complicated by the instability of the polymer in aqueous solutions. As the solid polymer swells and disperses there are processes of polymer coil entanglement, conformation change and agglomeration occurring simultaneously, and under acid, alkaline or warm conditions chemical modification of the functional amide group occurs. An understanding of these processes is a necessary precondition to achieving meaningful molecular mass characterisation and is reviewed in Section 3.1. Section 3.3 of this Chapter shows how the ageing of PAAm is related to changes in the mass distribution and the presence of agglomerates in solution. The effect of solution composition to enhance or disperse the agglomerates is reported.

The existence of any agglomerated species in a polymer solution will have a detrimental effect on fractionation techniques based on hydrodynamic volume. Section 3.4 shows that heating produces poorly soluble agglomerates which resist dissolution. The final Section of this Chapter shows how agglomerates may be created by applying shear to a polymer solution. The magnitude of the shear is comparable to that present in a liquid chromatography environment. Results are shown which place limits on the flow rates and tube thinness such that any analytical technique does not inadvertently create agglomerates. These limits find direct application in the molecular mass fractionation of Chapter 4.

3.1 Self Agglomeration of Polyacrylamide

In water, solid PAAm swells to a gel as the liquid permeates into the polymer, and as more water enters a dispersed polymer solution forms. The solution viscosity may therefore be expected to increase with time from that of water to a maximum determined by the polymer concentration and molecular mass. However, early studies observed decreasing solution viscosities with time (Narkis and Rebhun 1966, Shyluk and Stow 1969). A closer examination showed that PAAm solutions experienced a rapid increase in viscosity to a maximum after 24 hours, before a slower viscosity decrease to a local minimum after 160 to 180 hours (Gardner *et al.* 1978).

Explanations for viscosity changes have included chain scission due to the action of residual catalyst (Shyluk and Stow 1969, Haas and MacDonald 1972, Henderson and Wheatley 1987), microorganisms (Chmelir *et al.* 1980), crosslinking (Haas and MacDonald 1972, Boyadjian *et al.* 1976b), hydrolysis (Stejskal and Horska 1982), chain disentanglement (Narkis and Rebhun 1966, Gardner *et al.* 1978) and conformation changes (Kulicke and Kniewske 1980). However, degradation by chain scission has largely been ruled out from static light scattering studies (Kulicke and Kniewske 1980, Kulicke *et al.* 1982). Biocides have been shown to have little effect (Kulicke *et al.* 1982), while hydrolysis and crosslinking have only been observed at elevated temperatures. Aggregated polymer will contribute less to the overall solution viscosity than the individual polymer chains, and therefore chain disentanglement is inconsistent with any observed decrease in viscosity over extended periods. The majority of evidence favours a model for solution instability based on polymer conformational changes derived from intramolecular hydrogen bonds between amide groups, as shown in Figure 3-1 (adapted from Kulicke and Kniewske 1980). The polymer initially takes a highly extended conformation, corresponding to the maximum in viscosity. The hydrogen bonds may be classified as chain stiffening between adjacent segments (X), forming helical structures (Y) and

random intramolecular links (Z). With time, the oriented bond types (X and Y) are destroyed as the hydrogen bonds are hydrolysed, resulting in a more stable, compact coil with predominantly random hydrogen bonding. This model does not specifically address the function of water in the bonding. Shown in Figure 3-2 is the proposed hydrogen bonding for the oriented regions, but whether the bonding features direct carbonyl to amine bonding between amide groups or is facilitated by water "bridging" the bond is unclear.

While the above model is quite satisfactory to explain the observed viscosity changes, another possibility is the agglomeration of multiple polymer chains to form an agglomerate. Such microgel agglomerates may be expected to have a lower viscosity contribution than the individual polymer chains (Muller *et al.* 1979). The presence of agglomerates in PAAm solution has been previously noted, although rarely studied. Klein and Westerkamp (1981) stated that low levels of agglomerates could result in the plugging of columns during GPC analysis of polyacrylamides. They have been removed from solution by high-speed centrifugation (Muller *et al.* 1979) or filtration through a large pore-size filter (Klein and Westerkamp 1981, Sugarman *et al.* 1987).

Boyadjian *et al.* (1976a) found that high salt levels were able to disperse agglomerates, and therefore concluded that agglomerates were not the result of permanent (covalent) crosslinking but of weaker hydrogen bonding or physical entanglement. However, polymer crosslinking as a result of thermally or chemically induced imide bridges may also lead to agglomeration (Sugarman *et al.* 1987).

Figure 3-1 Inter- and intramolecular hydrogen bonding in polyacrylamide. Stiff, oriented hydrogen bonds (X, Y) hydrolyse eventually leaving only random bonding (Z) and a more compact coil.

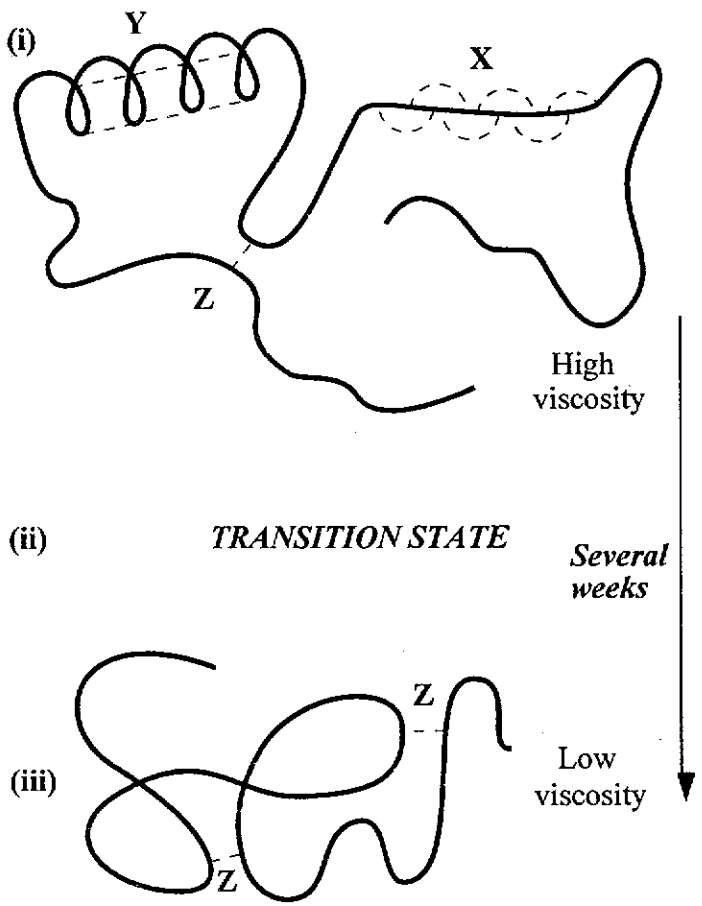

Figure 3-2 Local hydrogen bonding in between nearby amide moieties. The hydrogen bonds may be bridged by water.

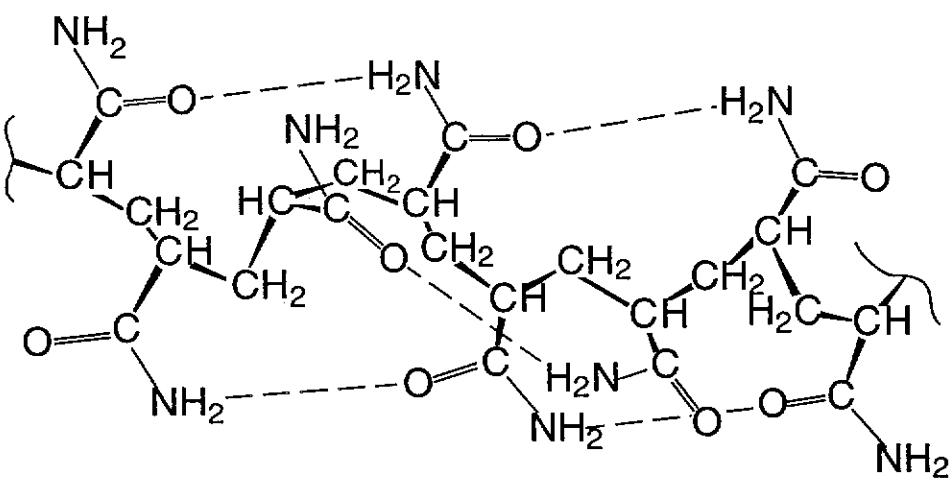

3.2 EXPERIMENTAL

3.2.1 High purity water

Aqueous solutions were made up in high purity deionised water (Milli-Q plus 185, Millipore, Bedford, Massachusetts) freshly filtered through a 0.2 μm prefilter (Opticap, Millipore) with further 0.1 μm filtration (Millipak 40, Millipore) immediately prior to use.

3.2.2 Reagents

A commercial, high molecular mass, nonionic PAAm, Magnafloc 333 ("M333", Allied Colloids, Bradford, Great Britain), common in mineral processing applications was used. The weight-average molecular mass M_w of this polymer as measured by MALLS was 20×10^6 (Section 3.2.8). For the shear study (Section 3.2.12) a lower molecular mass polyacrylamide FA920MPM (SNF Floerger, Saint-Etienne, France) was also used, with M_w 10×10^6. All other chemicals used were of analytical reagent grade. Solutions containing salts or additives were filtered through a 0.2 μm syringe filter (Acrodisc, Gelman, Ann Arbor Michigan).

Reagents used as received for the FIA procedure (Section 3.2.9) were: acetamide (Aldrich, 99%), acetic acid (Ajax, 99.7%), bromine (BDH, 99.5%), potassium dihydrogen phosphate (BDH, 99%), disodium hydrogen phosphate dodecahydrate (Univar, 99%), sodium dodecyl sulphate (Biorad, 99%), sodium formate (Ajax, 99.0%), soluble starch (Aldrich, 99.6%).

Flocculation tests were carried out with a standard kaolin substrate (Kaolin RF, Commercial Minerals, Perth, Australia), having a d_{50} of 3.9 μm as measured by laser diffraction (MasterSizer, Malvern, England).

3.2.3 Flocculant dissolution procedure

A wide-mouth glass jar with a screwtop lid was rinsed thoroughly with three 50 mL quantities of 0.1 μm filtered Milli-Q water. The container was filled with approximately 80% of the total solvent and the polymer was added portionwise with swirling between addition over approximately fifteen minutes. The addition of polymer was performed in a laminar flow cabinet (Gelman HWS). Once the entire polymer was added, the remaining solvent was added and the container sealed. The container now containing swelling polymer was kept moving manually until the polymer had sufficiently swelled and dispersed so that visible white inhomogenities had vanished and only polymer gel was visible. The container was then mechanically swirled on a shaking table (Chiltern Scientific SS70) at 150±5 rpm until the solution became a clear, homogenous and viscous fluid, typically two hours but occasionally overnight.

3.2.4 Nuclear magnetic resonance

The ^{13}C NMR procedures are described in Appendix 1. The polyacrylamides showed no hydrolysis or imidisation.

3.2.5 Ageing experiments

Polymer stock solutions were aged at ambient indoor temperature (20°C) for periods of up to three months. The solutions were diluted for size analysis by adding 5.0 mL of stock, dropwise with swirling, to 100±2 mL of filtered water containing salt or additive at the same level as that in the stock.

3.2.6 Polymer agglomerate size

The size distributions of agglomerates in PAAm solutions were measured with a Hiac Royco 9064 Sizing Counter (Pacific Scientific, Silver Spring, Maryland) fitted with a MicroCount-05 liquid sensor and controlled by Hiac Royco Particle Distribution Analysis Software (PDAS, Version 2.1). Flow past the detectors (60 ± 1 mL min^{-1}) was initiated by applying overpressure to the solution with compressed air from an AW3000 filter-regulator (SMC, Sydney, Australia) adjusted to 75 kPa over atmospheric pressure.

The Sizing Counter provides the number of counts measured over each of a range of size channels. Light from the 50 mW laser diode interacts with samples passing through the sensor to the collection optics. The sensor's optical system utilises light scattering signals to detect particles as small as 0.5 μm in size, and light obscuration to count particles from 1.6 μm to 350 μm diameter. Each particle passing through the sensor therefore generates an analogue electrical pulse of size-dependant magnitude, which is converted into a "count". For all experiments, the flow past the detectors was kept constant at 60 mL min^{-1} over the 20.0 mL sample volume.

Numerous repeat runs with 0.1 μm filtered water indicated that the signals for the two smallest channels (0.50 and 0.55 μm threshold size) fluctuated considerably. These fluctuations were established as resulting solely from electronic noise. Consequently, only those channels corresponding to sizes over 0.61 μm were used in size distributions. While the instrument is typically used for solid particle sizing, light scattering is commonly used to study PAAm solutions (Kulicke *et al.* 1982), and light obscuration has proved sensitive to the presence of PAAm agglomerates (Sommer *et al.* 1992).

Background correction over the lower size channels is trivial - for the 0.70 μm channel the background is typical fifty counts, compared with 5000 in the measured

solution. Greater care was required for sizes over 1.5 μm, where the low number of counts per channel may be influenced by stray dust from poorly filtered background solutions. The distributions were averaged from triplicate determinations of each dilution. Weighting of the counts may be applied to the size distributions to enhance the contribution of the small number of large species, but the effect of any dust contamination will also be enhanced.

3.2.7 Viscosity

An Ubbelohde capillary viscometer (no. 75, 0.01017 cSt s^{-1}) was used to measure dilute polymer solution viscosities at 30°C. The viscosity trends reported in Section 3.3.2 were measured by Julian Scott and his data is gratefully acknowledged.

3.2.8 Mean molecular mass

MALLS measurements were performed on selected flocculant stock solutions using a Dawn-DSP photometer (Wyatt Technology Corporation, Santa Barbara, California) fitted with a helium-neon laser (wavelength 632.8 nm) and a K5 flow cell. The instrument was calibrated with 0.02 μm filtered toluene and the detectors normalised with a 0.2 μm filtered solution of low molecular mass dextran (T10, Pharmacia, Uppsala, Sweden). A schematic of the arrangement of the flow cell and detectors is shown in Figure 3-3.

The molecular mass of PAAm by MALLS was determined by injecting at least four samples of polymer at various dilutions from a syringe pump at a constant low flow rate through a 5.0 μm pore membrane filter (Acrodisc, Gelman) and into the flow cell. A refractive index increment of 0.180 mL g^{-1} was used.

The sensitivity of the photodiodes was set at the maximum level. Measured scattered light intensities were treated by the DAWN 3.01 software from Wyatt Technology using Debye formalism, as discussed in Section 2.1.3. The data was fitted to a polynomial of the lowest order that gave a satisfactory residual error, usually fourth order.

For the shear studies (Section 3.2.12), the data was collected using the ASTRA 4.20 software from Wyatt Technology. Data processing was unchanged from above.

Figure 3-3 Plan view of the MALLS arrangement: (a) a single detector observes a fixed angle, as modified by solvent and cell refraction, and (b) a number of detectors over a range of angles. Low angle detectors 1-3 are unavailable due to light scattering by water.

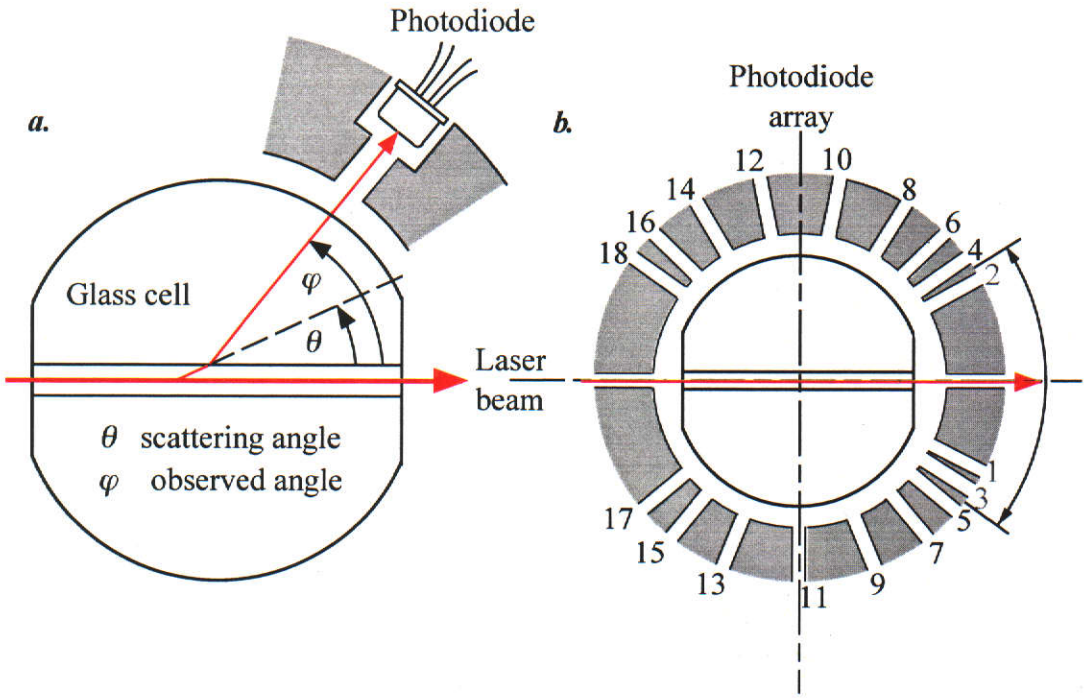

3.2.9 Polymer solution concentration

The method developed by Scoggins and Miller (1975) for the determination of polyacrylamide concentration was used. The amide functional group is oxidised by bromine to form a bromoamide product while excess bromine was destroyed by sodium formate to water, carbon dioxide and sodium bromide. The bromoamide undergoes a rapid redox reaction with iodide oxidising it to the triiodide anion, which is detected spectrophotometrically as a starch-triiodide complex. Gharfeh and Moradi-Araghi (1986) automated the solution mixing procedure and demonstrated the applicability of the technique in the presence of common interferents found in brine solutions. Taylor (1993) refined the technique by the addition of a surfactant into the starch complex to shift the peak to 500-525 nm and by adding the iodine as CdI_2 enabled adaptation of the technique to a flow-injection analysis (FIA) method. The FIA technique provides excellent reproducibility by eliminating the operator-dependant variations (Karlberg and Pacey 1989). This is important since the detectable starch-surfactant-triiodide species is unstable, with the signal at 525 nm decaying steadily with time.

Figure 3-4 FIA apparatus: schematic of experimental arrangement.

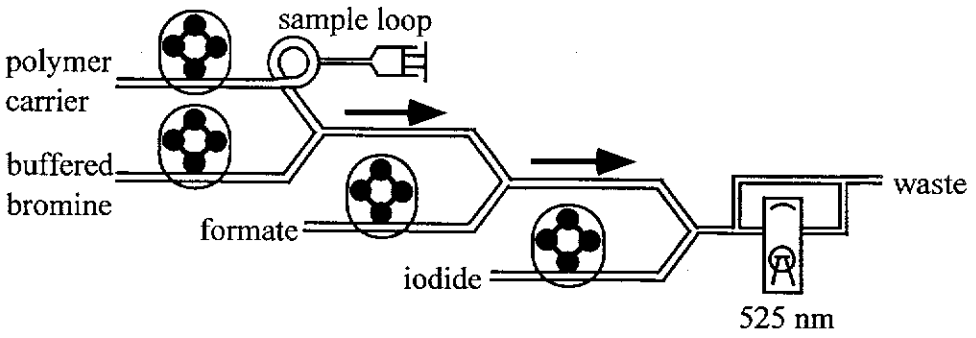

The water carrier, sodium formate and surfactant-starch-iodide solutions were delivered by three peristaltic pumps (Watson-Marlow 101U, Falmouth, England) fitted with 0.040" i.d. Silastic tubing (Dow Corning, Midland, Michigan). Bromine was incompatible with Silastic tubing, so was delivered using a Masterflex pump and

size 14 Tygon tubing (Cole-Parmer, Chicago, Illinois). Tubing connections and the six-port sample injector were low-pressure fittings made from polypropylene (Bio-Rad, Richmond, California). Reaction tubing employed the knitted coil configuration (Karlberg and Pacey 1989) made of Silastic tubing except for the bromine-water-polymer mixing, which employed Tygon tubing immersed in a water bath at 60°C (Julabo VC/3, Seelbach, Germany).

Detection of the active species required a spectrophotometer (Varian Cary 3E, Palo Alto, California) and 10 mm flow cell observing 525 nm at a 1 s response. The least-squares fit between detector signal and polymer concentration gave a correlation coefficient greater than 0.98 whether the signal was measured by height or area. The method was modified slightly from Taylor *et al.* (1995) by installing another peristaltic pump after the detector and the addition of a T-piece before the detector to bleed bubbles of CO_2 (from the formate-bromine reaction) and prevent their entry into the quartz flow cell. The T-piece also eliminated most of the pulsing disturbance derived from the peristaltic pumps. A final modification employed was to replace the water by a phosphate buffer at pH 7.0, which also helped in maintaining baseline stability.

3.2.10 Flocculant activity

Cylinder tests were conducted using stoppered 100 mL graduated cylinders. Approximately 8 L of a 5 wt.-% kaolin slurry was stirred at high speed for 90 minutes prior to use. A peristaltic pump was used to transfer 50 mL of the kaolin slurry from the bulk slurry to a graduated cylinder. Sufficient water was then added to the cylinder so the final volume of slurry, water and flocculant was 100 mL. After ten inversions at 30 rpm on a cylinder rotator the required volume of polymer solution was added by syringe. After a further ten inversion cycles, the cylinder was returned to the vertical position and the rate of fall of the mudline was followed.

The hindered settling rate was taken as the initial linear slope of a plot of the mudline height against time.

3.2.11 Heating polyacrylamide

Approximately 5 g of the commercial polyacrylamide M333 was dispersed over a watchglass and placed in a laboratory oven (Contherm Series Five, Lower Hutt, New Zealand). A 1 g sample of the polymer was retrieved after one, three and six hours heating. Three such experiments were performed simultaneously with ovens operating at 100, 150 and 200°C. After removal from the heat, the polymer was stored in a vial within a vacuum desiccator. One final sample was given two months continuous exposure at 100°C.

Solutions of heated PAAm were prepared as per Section 3.2.3 to 5 mg mL^{-1} concentration. The solutions were observed by the Hiac Royco Sizing Counter over a period of two weeks (Section 3.2.6).

The remaining solid polymer stored in the vacuum desiccator was investigated by Raman spectroscopy (RFS, Bruker, Rheinstetten, Germany) employing a 1064 nm Nd-YAG source laser, and emissions were detected by a germanium detector cooled in liquid nitrogen. Sample heating and associated interference was observed if the laser power was over 150 mW, so the power was kept at 100 mW. Of 256 scans collected for Fourier transformation, approximately ten were rejected automatically due to muon interference. Data was processed using the Bruker OPUS 2.0 software. Deconvolution of the region 1410 to 1460 cm^{-1} used the Levenberg-Marquardt algorithm with the two dominant peaks fitted to a curve of character equally Lorentzian and Gaussian ("Voight function"), and in all cases a third minor peak was indicated.

3.2.12 Shear studies

Commercial polyacrylamide M333 (Section 3.2.2) was used. Experiments were repeated with FA920MPM (SNF Floerger, Saint-Etienne, France), identical in all respects but with molecular mass 10×10^6. Aqueous solutions were made identical to the earlier description (Section 3.2.3). Polymer solutions *circa* 0.50 mg mL^{-1} are referred to as *dilute* while solutions at 5.00 mg mL^{-1} are termed *concentrated.* Actual solution concentrations were 0.58 and 5.19 mg mL^{-1} in water, and 0.49 and 5.09 mg mL^{-1} in 2%-v/v formamide for dilute and concentrated, respectively.

Shear was applied to polymer stock solutions by extrusion through poly(ether-ether-ketone) ("PEEK") tubing (Alltech, Sydney, Australia) of lengths 0.3, 1.0 or 2.4 m and internal diameters 0.25 mm (0.010") or 0.51 mm (0.020"). Flow was controlled using a syringe pump (pump: Razel A-99, Stamford, Massachusetts; syringes: Terumo, Elkton, Maryland). In some cases the backpressure generated by the narrow tube and viscous polymer limited the ability of the syringe pump to reach the higher flow rates. For experiments requiring inline filtration, a 5 μm Acrodisc syringe filter (Gelman, Ann Arbor, Michigan) was installed between the syringe and the shear tubing.

Effluent from the shear tube fed into the MALLS instrument for polymer coil radius measurements, identical to Section 3.2.8. From the MALLS detector, the solution passed through silicone tubing (Silastic, Dow Corning, Midland, Michigan) of internal diameter 1.0 mm (0.040") to collection for Hiac Royco sizing. A vial of 100±0.5 g of either water or 2%-v/v formamide was prepared. Sheared polymer solution (5.0±0.1 g) from the MALLS detector was collected in the same solvent filled vial. Agglomerate sizing measurements of these solutions were identical to those described in Section 3.2.6. Time between the final polymer effluent collection and sizing did not exceed five minutes.

3.3 AGEING AND AGGLOMERATION

3.3.1 Agglomerate size

MALLS measurements on aqueous solutions of the 2×10^7 molecular mass polyacrylamide indicated that the polymer molecules have rms diameters (Section 2.1.3) in the order of 0.35 μm in deionised water at ambient temperature. On this basis, the Sizing Counter would only be expected to show counts in the lowest size channels. Figure 3-5a shows the typical size distribution for a solution aged for six weeks in the dark, conditions under which the solution exhibited little remaining dynamic instability. A high level of counts were observed at sizes near 1.0 μm, with measurable counts up to sizes of 15 μm, well in excess of the expected dimensions for the polymer molecules. The possibility that dilution of the stock solution for the sizing affected the agglomerates was eliminated through a range of dilutions of stock solution. The number of agglomerates above the background varied linearly with dilution, and agglomeration is a function only of stock concentration, as reported below. There may exist a time component, in that allowing the diluted stock to stand aids dispersion of agglomerates, but the time from dilution to analysis was kept constant and was not considered an issue.

Using the MALLS estimate of individual PAAm coil size, polymer agglomerates measured in the 0.7 μm channel of the size distribution may possibly represent 4 to 6 associated molecules, while a 15 μm agglomerate may involve over 10^4 individual molecules. Figure 3-5a provides comparison with the same solution after 5.0 μm filtration, showing the effect removal of the agglomerates has on the size distribution. The spikes observed in the background 0.1 μm filtered water and filtered polymer solution correspond to discrete and irreproducible channel counts, and were attributed to residual dust contamination.

Figure 3-5 Overlaid size distributions measured for a 5.20 mg mL^{-1} aqueous solution of PAAm (M333) before and after 5.0 µm filtration; (a) raw counts distribution, (b) volume-based distribution.

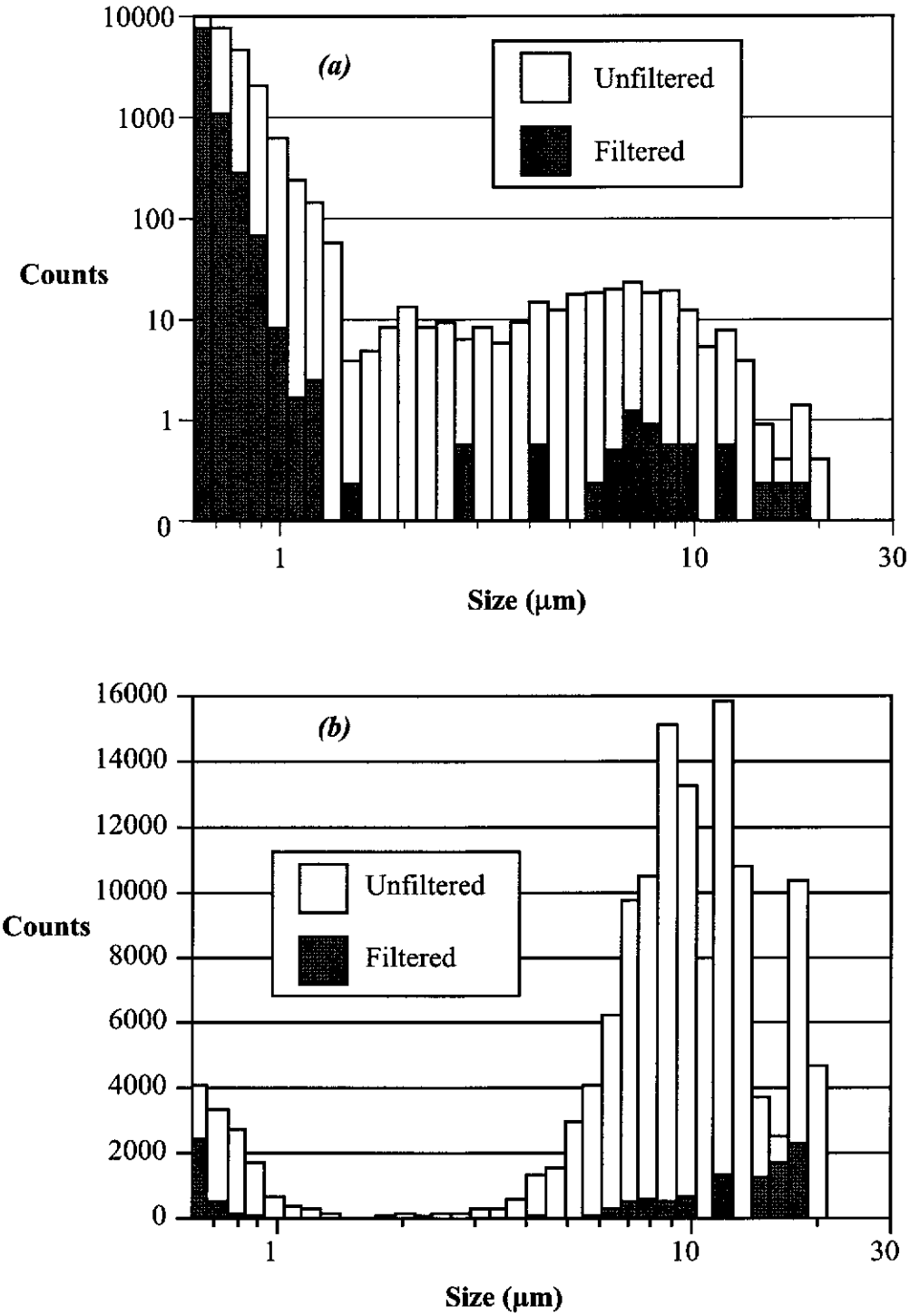

The same data is also presented as a volume-based distribution in Figure 3-5b, emphasising that the relatively low number of agglomerates have an enormous contribution to a volume-based sizing technique. However, difficulties arise in comparing volume distributions because the influence of dust spikes at the larger channel sizes has a disproportionate influence. The following discussion is therefore limited to only the raw counts per channel in excess of the background.

Static light scattering at low detector angles is strongly affected by the presence of large particles. For a polydisperse system, light scattering returns a *z*-averaged radius (Section 2.1.3) and as such any 10-15 μm polymer agglomerates present in solution should drastically interfere with MALLS size measurements. Considering a sample of monodisperse 0.4 μm diameter polymer coils, if there exists 0.1% by number agglomerated to 10 μm, a crude calculation shows that the light scattering should return a mean radius of over 4 μm. The diameter of the polymer coil calculated from MALLS is of the expected magnitude for a polymer of this size within light scattering error (±3%), and suggests that the number of agglomerates and agglomerated polymer was extremely low compared to the bulk polymer concentration. A similar conclusion was drawn by François *et al.* (1979), who found that known agglomerates were not detected by light scattering. Using the above model system, if the 10 μm agglomerates are of the order 0.001% by number, an overall light scattering radius of 0.43 μm is obtained, and represents an approximate upper limit to the agglomerate concentration. Disruption of large species by passage through the MALLS flow cell and associated capillary tubing may be discounted, as distributions measured with the Sizing Counter were identical before and after passage through the MALLS system.

While the Sizing Counter is well suited to the study of agglomerated polymer, its lower size limit precludes measurement of full population size distributions down to individual polymer dimensions. The polymer solution concentration was therefore determined before and after membrane filtration by FIA (Section 3.2.9). No

significant change could be detected after 5.0 μm filtration, while 0.8 μm filtration resulted in a 2.5% reduction in concentration (Table 3-1). Although these results imply that the population of agglomerates in solution is low, there is also the possibility that any large agglomerates are quite fragile and that passage through a membrane causes rupture to smaller sized agglomerates.

Table 3-1 Effect of membrane filtration on the concentration and flocculant activity of polyacrylamide solutions aged for 5 days.

Solution	Measured concentration ($mg\ mL^{-1}$)	Hindered settling rate ($m\ h^{-1}$)[A]
Unfiltered	5.52±0.03	22.0±1.0
0.8 μm filtered	5.38±0.03	13.3±0.5
5.0 μm filtered	5.52±0.03	10.8±0.3

A. Values interpolated for a dosage of 250 $mg\ kg^{-1}$.

Table 3-1 also shows the effect of filtration on the flocculation activity for solutions of PAAm. While 5.0 μm filtration had no effect on the measured polymer concentration, the activity was found to drop substantially. This was consistent with the observations of Shyluk and Stow (1969), who felt that agglomerates were less likely to take a flattened conformation when adsorbed on a particle, and may enhance polymer bridging. If this is the case, then the consequence of filtration is almost certainly the rupture of any large agglomerates. Interestingly, the reduction in flocculant activity was not quite as large after 0.8 μm filtration, despite a slight reduction in concentration. Apparently, small entanglements of only a few polymer chains do not contribute greatly to activity. The flocculation activity of supramicron agglomerates and low activity of the submicron species will be shown significant for the flocculant activity studies of Chapter 5.

3.3.2 Ageing of polyacrylamide solutions

Viscometry yields a single, solution-averaged measurement of polymer properties, and as such is not highly sensitive to minor changes resulting from solution instability. The reduced viscosity of the solution as a function of time was compared with the counts measured in both the sub- and supra-micron range of the size distribution (Figure 3-6). The reduced viscosity exhibited only a 13% increase over the 80 day ageing period, while counts in the selected size regions varied over a much wider range. The number of counts in the submicron range and solution reduced viscosity both increased rapidly after five to eight days ageing (Figure 3-6a). This is in good agreement with the viscosity results of Gardner *et al.* (1978), who believed the changing polymer-solvent interactions favoured a chain disentanglement mechanism.

Figure 3-6a also shows that the solution viscosity increased further between 30 and 40 days. However, this behaviour was not mirrored by the submicron counts, which displayed a steady downward trend after 20 days. Examination of the supramicron counts (Figure 3-6b) indicates that the agglomerate concentration reached a minimum during the first week of ageing but then increased steadily. This previously unreported ageing behaviour for polyacrylamide was observed repeatedly in aqueous solutions of PAAm containing no salts or additives. The increase in supramicron counts following the peak in the number of submicron counts was consistent with the conclusions of Raos and Allegra (1996), who predicted from free energy calculations that substantial coil agglomeration may predate the appearance of larger agglomerates for solvated polymers under the θ-temperature.

Figure 3-6 Comparison of viscometry and Sizing Counter for M333 ageing in water. (a) counts in the range 0.68 to 0.72 μm; (b) counts > 1 μm.

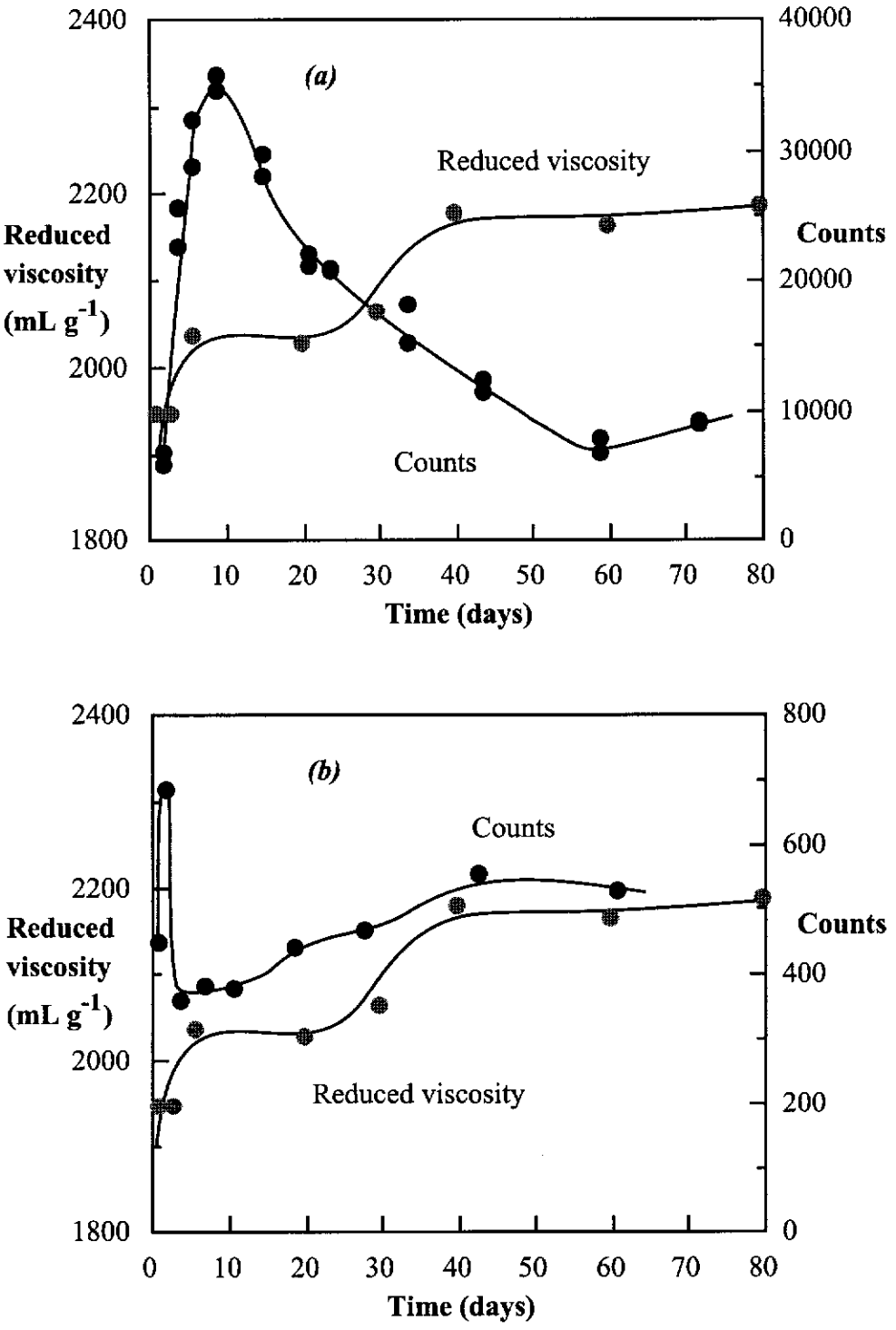

3.3.3 Effect of concentration

The ageing of PAAm solutions at lower polymer concentrations was monitored over several months. Figure 3-7 shows the effect of concentration on the submicron counts. Lowering the solution concentration delayed the onset of the peak in the submicron counts, from eight days at 5.20 mg mL^{-1} to nearly three weeks at 2.00 mg mL^{-1}. The magnitude of the measured counts was also substantially lower than expected, even after taking into consideration the reduction in concentration.

Figure 3-7 Submicron counts (0.68 to 0.72 μm) for the ageing of M333 solutions at different stock concentrations.

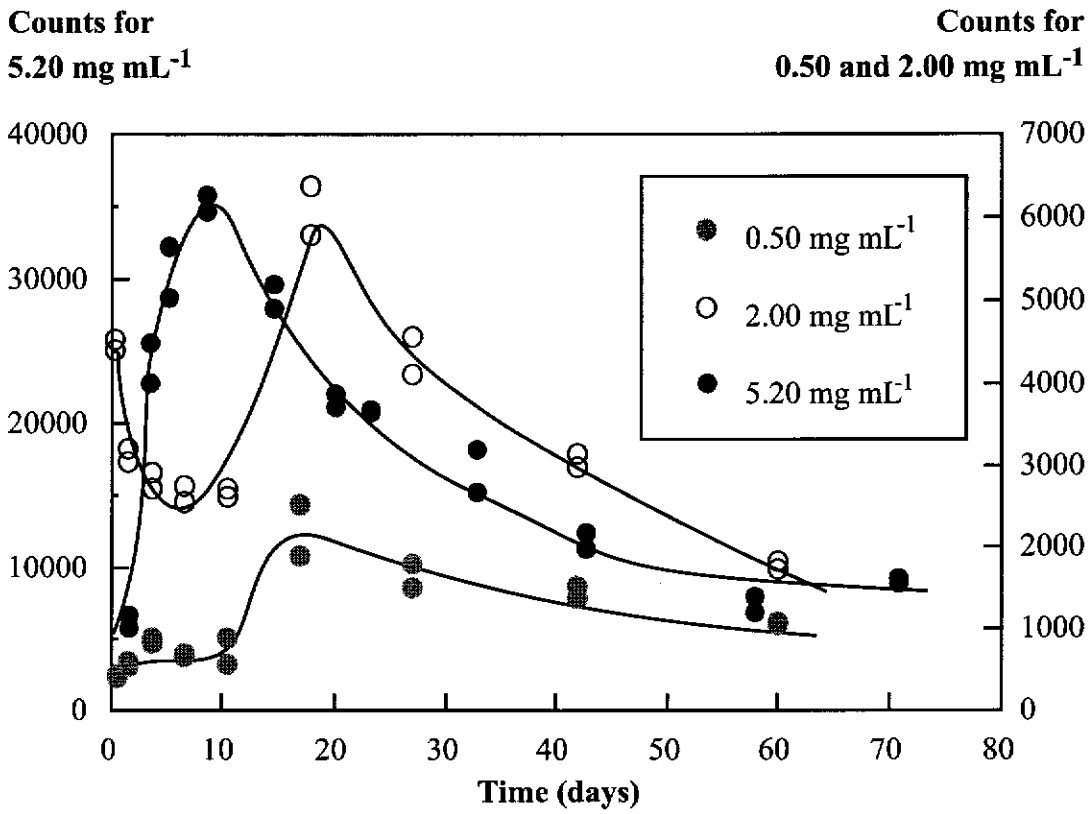

Solutions containing 0.1 mg mL^{-1} or less of PAAm had no supramicron counts and showed no signs of agglomeration whatsoever. A number of polymer-solvent systems are known to exhibit a threshold level for agglomeration, defined as a critical entanglement concentration, c^*, below which the solution remains well solvated and essentially homogenous (Aharoni 1983, de Jaeger *et al.* 1991). For PAAm, this

critical concentration has been related to the intrinsic viscosity, $[\eta]$, by the relationship $c^* = 2.5\ [\eta]^{-1}$ (Kulicke *et al.* 1982). In water this results in a c^* of approximately 1.25 mg mL^{-1}. The results obtained show that significant agglomeration may still be observed at concentrations below c^*.

3.3.4 Effect of chemical additives - organic cosolvents

The addition of an alcohol, typically 2-propanol, has been demonstrated to result in enhanced solution stability as measured by viscometry (Chmelir *et al.* 1980, Henderson and Wheatley 1987). Such additives are thought to prevent microbial or radical attack, although their effect has been questioned (Kulicke *et al.* 1982). The use of formamide as a solvent for PAAm has also been found to result in higher stability, as a consequence of improved solvation of the polymer (Kulicke *et al.* 1982, Biran and Dawkins 1984). The ageing of aqueous solutions of 5.00 mg mL^{-1} PAAm containing either 2%-v/v 2-propanol or 2%-v/v formamide was examined. The aggregation of the polymer over time was monitored by following the 0.68 to 0.72 μm channel of the size distribution (Figure 3-8).

Over an initial period of two weeks the presence of 2-propanol did indeed suppress the ageing effects, but after this time the alcohol enhanced agglomeration, with the submicron counts steadily increasing to high levels. In contrast, 2%-v/v formamide, known to be a good solvent for PAAm, efficiently suppressed agglomeration over the full ageing period.

Figure 3-8 Submicron counts (0.68 to 0.72 μm) for the ageing of 5.00 mg mL^{-1} M333 solutions in water, and in the presence of 2%-v/v 2-propanol or formamide.

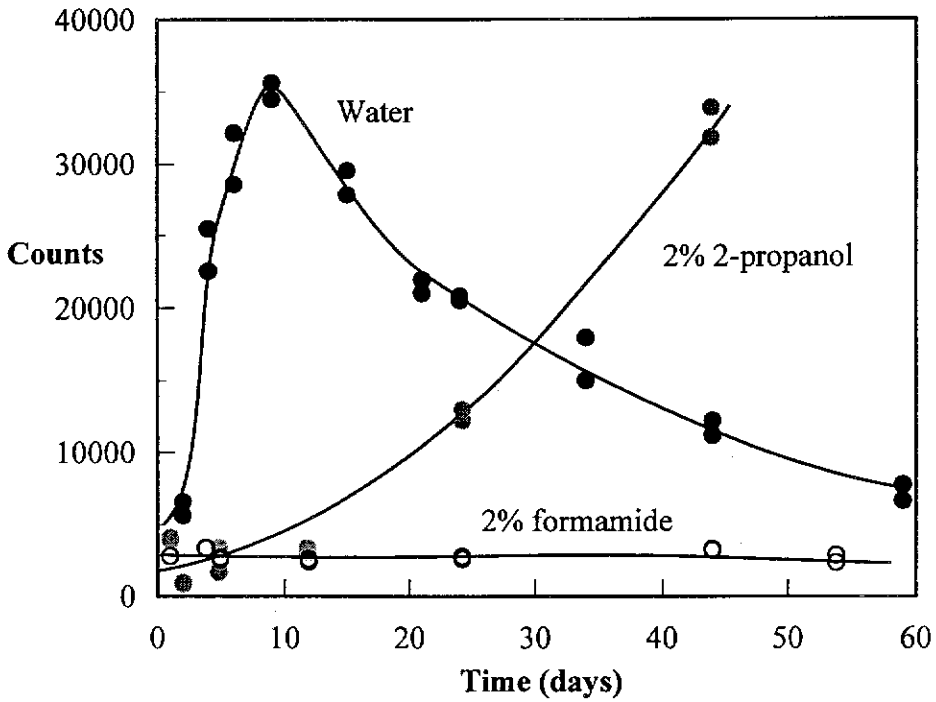

The effect of both additives on supramicron counts is shown by Figure 3-9. After one day of ageing a distinct agglomerate contribution can be seen in the range 4 to 11 μm for a solution containing 2-propanol (Figure 3-9a). By 12 days the concentration of agglomerates in this solution has dropped, possibly reflecting optimum dissolution of the polymer (Figure 3-9b). However, by 74 days a substantial increase in the supramicron counts was observed, as well as an increase in the agglomerate size range to include diameters of up to 20 μm. The contradiction with previous ageing studies may be a consequence of the relative insensitivity of viscosity measurements to agglomerate formation, or the fact that many of these studies were not carried out for long enough to show the instability. Again, counts measured in the presence of formamide remained at low levels throughout the same period.

Figure 3-9 Overlaid distributions for M333 solution containing 2%-v/v 2-propanol or formamide after ageing for (a) 1 day, (b) 12 days and (c) 74 days.

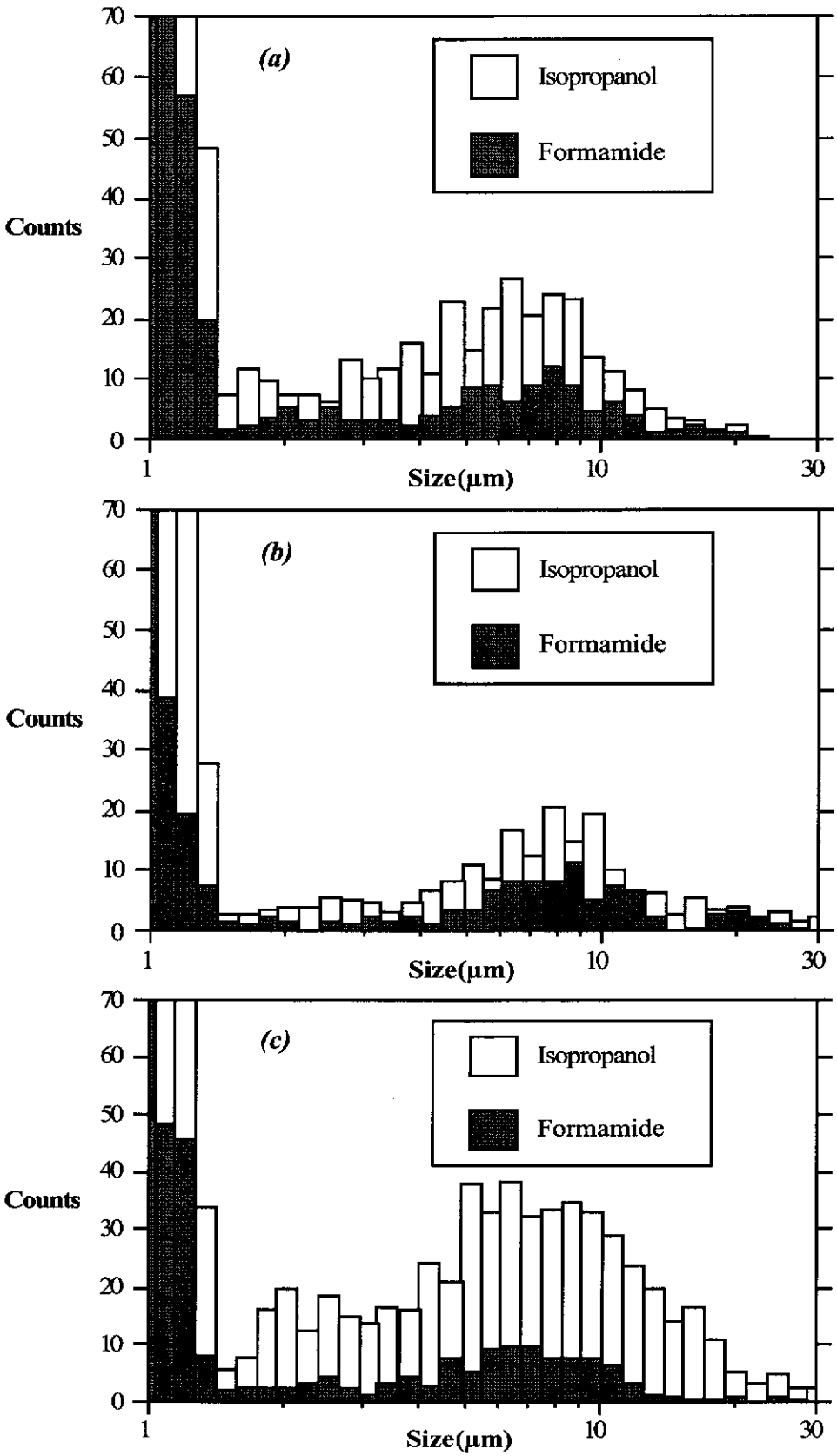

3.3.5 Effect of chemical additives - salts

Solutions of PAAm at 5.00 mg mL^{-1} were aged in the presence of varying concentrations of thiocyanate, chloride and acetate salts, chosen to modify hydrogen bonding (Millero 1972, Franks 1983). Ageing behaviour was found to be influenced by the salt concentration. At high salt concentrations (500 mmol L^{-1}), the formation of submicron agglomerates was suppressed, similar to the effect of 2%-v/v formamide.

In the presence of dilute salts (5 mmol L^{-1}), ageing did result in peaks in the submicron counts (Figure 3-10), although this effect was reduced and delayed compared to that in pure water. In water the peak in the 0.68 to 0.72 μm channel occurred after 6 to 8 days, whilst in dilute salt solutions the equivalent peaks were only observed in the range 12 to 25 days. The extent of agglomeration in the presence of thiocyanate was only slightly reduced compared to that in water, while with acetate the measured peak counts were more than halved. Chloride was the most effective of the dilute salts studied for suppressing agglomeration, with the counts almost reduced to the level seen in formamide solution.

Salts at 500 mmol L^{-1} appeared to limit the formation of submicron agglomerates, but the behaviour in the supramicron range was dependent upon the salt type. In the case of potassium thiocyanate solutions, agglomerate formation remained low over the first weeks of ageing (Figure 3-11a). However, after 42 days significant levels of agglomerates could be seen in solution, and subsequently exceeded the levels measured in salt-free solutions. Ageing in chloride solution also initially resulted in low supramicron counts (Figure 3-11b). Like the thiocyanate solutions, an increase in agglomerate counts did occur in the presence of chloride after 43 days, but this trend was not maintained, with counts returning to lower levels. Sodium acetate produced the strongest suppression of agglomeration during initial ageing, although a significant increase in counts was observed after one month (Figure 3-11c).

Figure 3-10 Submicron counts (0.68 to 0.72 μm) for the ageing of M333 solutions in the presence of 5 mmol L^{-1} salts.

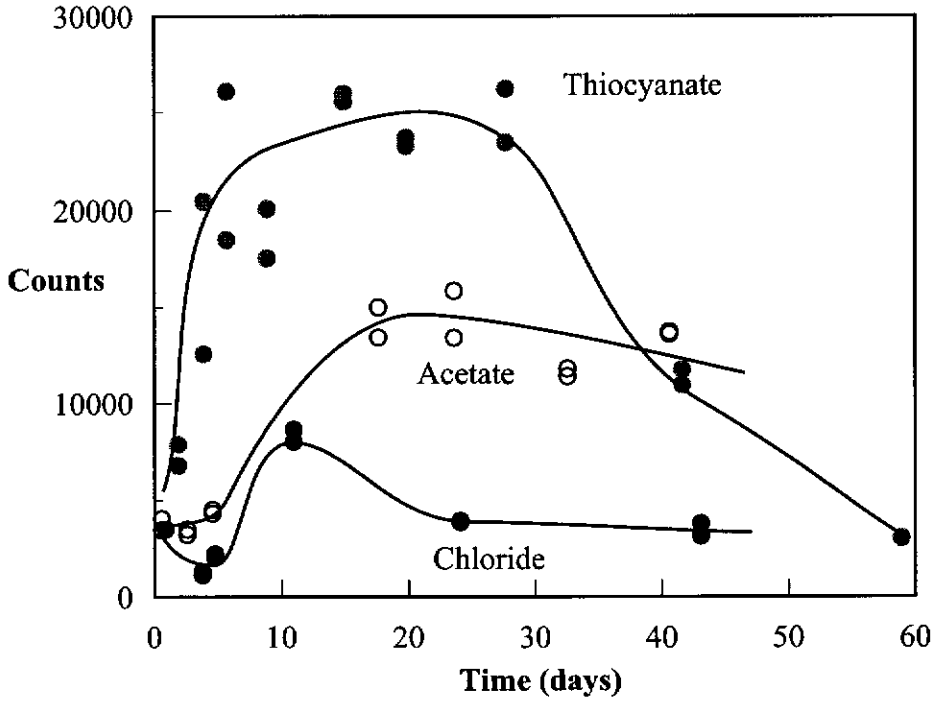

Supramicron counts displayed very similar behaviour in either 5 mmol L^{-1} or 500 mmol L^{-1} chloride solutions. Dilute levels of thiocyanate or acetate did not significantly change the extent of agglomerate formation from that seen in salt-free solutions.

Figure 3-11 Overlaid distributions for M333 solution containing 500 mmol L^{-1} (a) thiocyanate, (b) chloride or (c) acetate as a function of time.

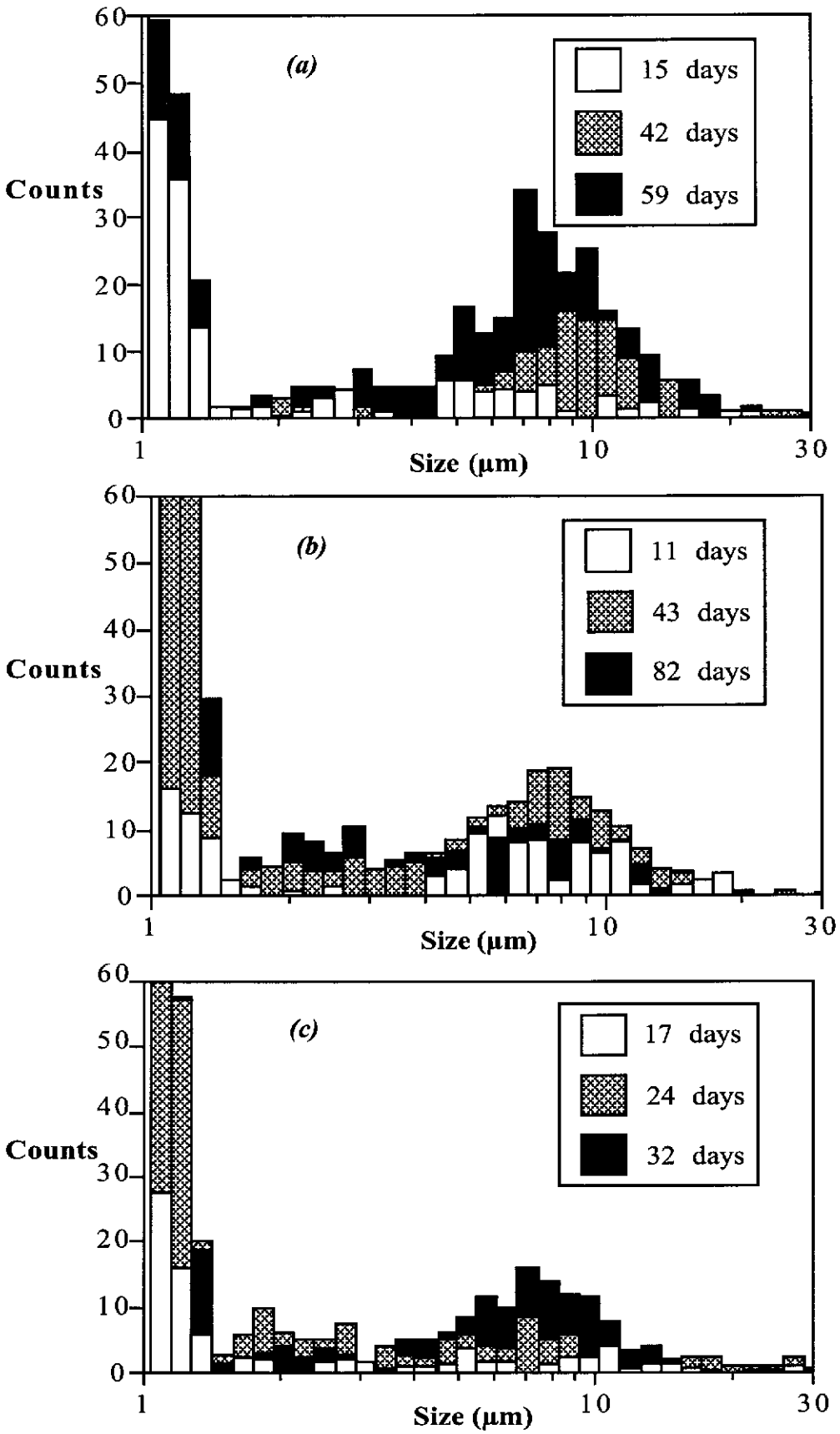

3.3.6 Solution state features of polyacrylamide

The dissolution of PAAm in water is favoured due to the high heat of solution of the amide functionality, which compensates for the hydrophobicity of the nonpolar backbone (Nicholson 1991). Dupuis *et al.* (1994) have stated that collisions between polymer molecules can result in association if the strength of the polymer-polymer and polymer-solvent interactions are similar. At dilute concentrations the formation of large agglomerates was thought unlikely due to the low probability of multiple collisions. At higher concentrations chain overlap may favour intermolecular interactions and larger agglomerates may be expected. These conclusions are consistent with the results shown in Figure 3-7 for the effect of concentration on submicron counts.

Dupuis *et al.* (1994) claimed that while large agglomerates may only be favoured at higher concentrations, doublets are observed over a wide range of concentrations. A recent study using dynamic light scattering has also detected non-covalent, soluble agglomerates in aqueous solutions of PAAm, which were thought to consist of about four linear chains (Ying *et al.* 1996). This compares favourably with the observations that counts in the size distribution near 0.7 μm (Figure 3-5) may result from the association of 4 to 6 molecules. The Sizing Counter used in this study, while unable to detect non-associated PAAm, has proved highly sensitive to the presence of agglomerated polymer.

The size parameter changes for PAAm (Figure 3-6) show an early peak in the submicron counts, followed by a steady decrease, the latter coinciding with an increase in the supramicron counts. Such behaviour is consistent with general predictions for agglomerating polymers (Raos and Allegra 1996), and reflects the balance between polymer-polymer and polymer-solvent interactions. As the conformation of the polymer changes, necessarily the proportion of polar or nonpolar character presented to the solvent varies, and the solvation energies of the

polymer changes. Modification of the solvation properties, which reduce polymer-polymer interactions may delay or prevent the formation of large agglomerates that are bound by hydrophobicity.

The observed reduction of submicron counts as the ionic strength was increased suggests that the presence of salt limits PAAm agglomeration. Karlström *et al.* (1990) linked the solubility behaviour of nonionic polymers as a partition between the polar and nonpolar coil segments, which for polyacrylamide are the amide moieties and hydrocarbon backbone respectively. Presumably, the salt effect occurs by improving the solvation of the amide. A study of lower molecular mass polyacrylamides found that high levels of salt (0.1 mol L^{-1} NaCl) were required to disperse agglomerates in solution (Boyadjian *et al.* 1976a). However, results obtained with this study show that ionic strength alone was not effective at preventing the formation of large agglomerates (*i.e.* over 2 μm diameter).

Hydrogen bonding is of critical importance in determining the conformation of PAAm (Kulicke and Kniewske 1980), and therefore the modification of hydrogen bonding by salts may explain their effect on the measured size distributions. Anions may be classified as hydrogen bond makers, which impose a local order by water dipole-ion interaction, and hydrogen bond breakers, which can disrupt existing order (Millero 1972, Franks 1983). This approach was used by Leca (1986) to explain how viscosity and coil dimensions of PAAm in 1.0 mol L^{-1} salt solutions increased with hydrogen bond breaking ability. Of the anions studied here, thiocyanate is a strong structure breaker, chloride a weak breaker and acetate a weak maker. High concentrations of the bond breaking thiocyanate interfere with the water-amide interactions, thereby favouring polymer-polymer interactions and allowing agglomeration processes to continue unabated. While submicron counts were slightly reduced in the presence of thiocyanate, this may be a consequence of the higher supramicron particles observed.

Chloride does not greatly change polymer interactions so the agglomerate levels are largely unchanged, although the increase in ionic strength does allow better dispersal of the submicron agglomerates compared to the salt free solutions. As a weak hydrogen bond maker, acetate appears to inhibit the formation of supramicron agglomerates (Figure 3-11c).

These same effects are more dramatically illustrated in the case of the organic modifiers. The addition of alcohols such as 2-propanol at dilute levels is known to reduce the solvation of polyacrylamide as compared with water (Basedow *et al.* 1979, Leca 1986). Polymer-polymer interactions are therefore favoured, and as Figure 3-8 and Figure 3-9 clearly show, agglomeration and the formation of agglomerates are greatly enhanced. In contrast, formamide is known to be a good solvent for polyacrylamide. Ying *et al.* (1996) found that submicron agglomerates readily dissociate in 100% formamide to the constituent linear chains. Even at 2%-v/v formamide, the improved solvency almost totally suppresses sub- and supramicron counts, with no evidence of ageing over an extended period.

3.4 HEATING AND IMIDISATION

In Section 3.3 it was shown that polyacrylamide in solution contains agglomerates. Although it was demonstrated that their extent could be manipulated by solvation properties, they were never removed completely, indicating agglomerates may be inherent to polyacrylamide. It is known that amide moieties may lose an equivalent of ammonia to condense to an imide upon heating (Figure 3-12). Imidisation would feature as intermolecular crosslinking, or as cyclisation should it occur on adjacent polymer segments. Either outcome would modify the solution properties of the material and produce agglomerates resistant to solvent modification. Commercial, powdered polyacrylamide is dried before distribution and since imidisation occurs upon heating, there exists a mechanism to form agglomerates. Commercial flocculant from SNF-Floerger commonly produce a haze in solution, while material of the same quoted mean molecular mass from Allied Colloids remained clear. If this haze does represent poorly dispersed polymer due to heating and imidisation, the polymer solution may be less effective as a flocculant according to the bridging mechanism.

Figure 3-12 Imidisation of PAAm and loss of ammonia. Shown is imidisation of adjacent amides and cyclisation, but intermolecular crosslinking may occur.

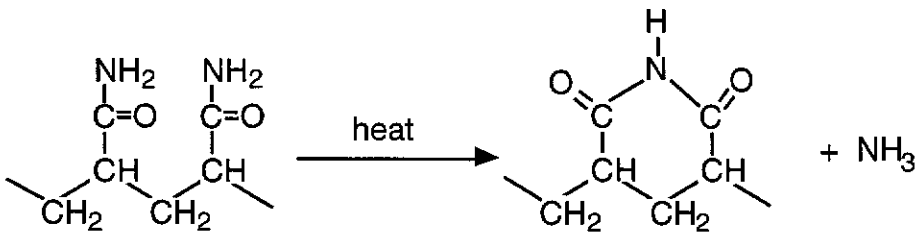

3.4.1 Effects of heat on polyacrylamide

Solid PAAm heated to 175 to 300°C will undergo thermal degradation to imides with concurrent release of ammonia, while over 300°C the polymer decomposes to hydrogen and carbon dioxide (Smith *et al.* 1996). Even at a constant temperature of 37°C the solid polymer will eventually become brittle. Anhydrous heating of PAAm in sulphuric acid or formamide reached a limiting situation once two-thirds of the initial amide was transformed to imide, while one-third remained as free amide after 15 hours at 150°C (Haas and MacDonald 1971). The authors proposed, on the basis of microanalytical data, that the imidisation occurs predominantly as cyclisation between two adjacent amide groups. The presence of imide was confirmed by infrared spectroscopy with the amide carbonyl bands at 1640-1650 cm^{-1} and N-H at 1620 cm^{-1} shifting to 1680 cm^{-1} and vanishing, respectively.

Aqueous pH-neutral PAAm solutions slowly hydrolyse the acrylamide to acrylate and a smaller amount of imide with heating (Moradi-Araghi *et al.* 1988), although the presence of water alone will not produce hydrolysis (Maurer *et al.* 1988). The extent of imidisation has been quantified by infrared spectroscopy observing the optical density ratio of imide to methylene bands at D_{2860}:D_{2930} and D_{1190}:D_{1450} with the latter being more sensitive (Boyadjian *et al.* 1976b). These authors also noted by differential scanning calorimetry that PAAm experiences transitions at 150°C and 200°C.

3.4.2 Observation of heated solid polyacrylamide

For convenience, heated PAAm is labelled as *ttt-d* where *ttt* is the temperature of heating (°C) and *d* is the duration of heating in hours. Exceptions are for unheated PAAm sample, labelled *unmodified*, and for 2 months heating at 100°C, labelled *100-2m*.

After heating, the samples at 100 and 150°C appeared identical to the original white, grain-like sample, while exposure to 200°C discoloured the sample to a pastel yellow after one hour and a dark mustard after three hours. The discoloured samples were increasingly fragile, as the grains crushed easily to powder.

Upon solution preparation, PAAm heated to 100°C swelled and dispersed as expected. The 150°C heated samples swelled and dispersed, but even after a week definite loose "blobs" could be seen up to 4 mm diameter. The number and size of these gels were visibly greater with longer heating. The viscosity of the 150°C solutions was also obviously less than the 100°C solutions but did increase with solution ageing. In order to quantify this viscosity observation the solutions were placed into an Ubbhelode capillary viscometer (Section 3.2.7) but the "blobs" blocked the capillary and prevented the measurement. PAAm samples heated to 200°C were quite hydrophobic, consequently there was no swelling or dissolution after a fortnight exposure, and after three months the *200-1* sample had only begun to disperse. The *100-2m* sample exhibited no colour change, although in solution the polymer did not swell well, remaining as discrete, adhesive pieces.

3.4.3 Solid-state Raman study

The poor solubility of the heat-affected polyacrylamide limits the techniques available for quantifying the presence of imide. Of techniques applicable to the solid state, Raman emission spectroscopy was chosen. Initial experiments using a visible (632.8 nm) source were not appropriate for the 200°C heated samples, in which a fluorescence band dominated the signals.

Following the method of Boyadjian *et al.* (1976b), the signals around 2960 cm^{-1} were compared with 2870 cm^{-1}, diagnostic for the presence of imide functionality. For these signals there was sufficient overlap to warrant deconvolution in the manner described above (Section 3.2.11) and in all cases a third low-intensity peak was required at 2930 cm^{-1} to fit the original spectra to a residual rms error of less than 0.05%. Comparing the area of the 2870 cm^{-1} peak with the total area of the region shows that this ratio is approximately 0.105, averaged over all samples, but increases sharply with increasing heating. This signal ratio is shown in Figure 3-13. The experiments where the ratio increases were matched by a small shift of the position of the deconvoluted peak from 2960 to 2965 cm^{-1}. The presence of the imide was shown to be linked to the 200°C exposed polyacrylamide and matches the observed insolubility. The sample *150-6* also exhibited a retarded rate of dissolution, examined further in Section 3.4.4, and the peak ratio increased. In contrast, the sample *100-2m* produced a very poorly swelling polyacrylamide but the peak ratio indicated imide at levels of the *unmodified* PAAm. Other transitions used by Boyadjian *et al.* (1976b) at 1450 cm^{-1} were investigated requiring deconvolution of the peak into dominant 1420 and 1455 and a lesser peak at 1440 cm^{-1}. A similar result to the above was produced showing enrichment of the 1440 cm^{-1} as compared to the neighbouring 1420 and 1455 cm^{-1} transitions.

An extensive analysis of the vibrational spectrum of polyacrylamide by Mohan and Murugan (1997) led to assignation of the 2960 cm^{-1} region to an asymmetric CH_2

stretch and 1440 cm^{-1} to the C-N stretch. It is feasible that if the heating induces imidisation then the C-N stretching frequency would change but it is unexpected that a mode characteristic of the polymer backbone at least three bonds remote should be affected as well. The other interesting result is that the spectra show a definite change with heating intensity rather than the duration, seen on comparing the *200-1* and *100-2m* samples.

Figure 3-13 Raman signal area ratio of 2870 cm^{-1} to the 2800-3000 cm^{-1} region for heat treated solid polyacrylamides.

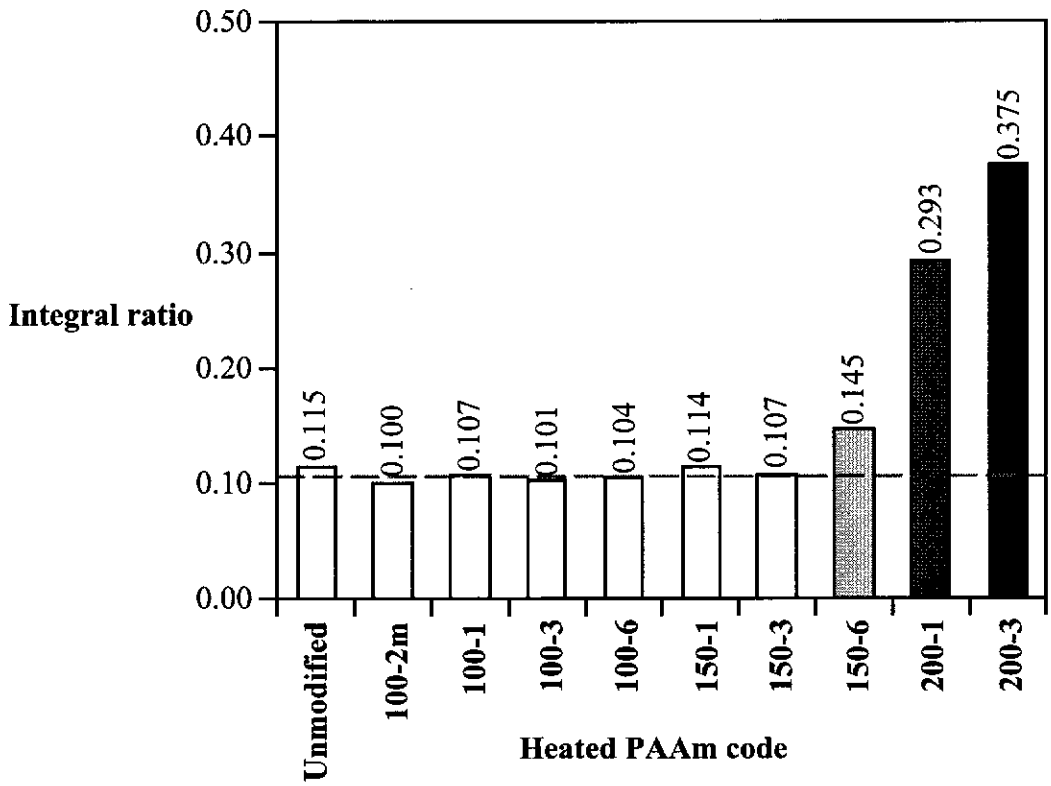

3.4.4 Solution state study

Agglomerate size distributions were measured for the solutions of the heat treated polyacrylamides. The following figures presents for each size fraction the normalised integrated counts, where the number of counts is square (area) weighted by the procedure described in Section 3.2.6. Each colour of the plot is assigned to a time after exposure to water.

Figure 3-14a shows, for *unmodified* PAAm after 1.8 days ageing, that the number of submicron counts is quite small, with a few agglomerates present. The analysis repeated after 2.9 days shows a loss of virtually all of the agglomerates, and between 2.9 and 3.8 days the dissolution is complete and counts have stabilised with regard to the sub- and supramicron counts. This is a definite indication that a polymer solution ideally should be aged approximately three days before use in order to disperse agglomerates. Sample *100-1* showed no visible differences from the *unmodified* sample, although the dissolution is retarded. After 3.8 days the agglomerate integral was equivalent to 2.9 days ageing for *unmodified* PAAm, and stabilised by 4.8 days. This suggests that relatively gentle heating affects the PAAm dissolution. Six hours heating at 100°C is shown by Figure 3-14b where the dissolution is retarded further still. The integral curve at 4.8 days for 6 hours heating matches the 3.8 days integral for 1 hour heating and the 2.9 days curve for no heating. Only after 8.5 days does the integral show dissolution of the aggregates. These curves show components around 4 to 7 μm in diameter which resist dissolution.

Figure 3-15a shows that after heating the PAAm to 150°C for only 1 hour, dissolution of agglomerates was not achieved even after 10.9 days. For *150-1* the largest agglomerates, over 20 μm diameter, disperse over the first 70 hours. Agglomerates of 4 to 7 μm diameter remain for more than five days, and only after this period do the submicron counts increase reflecting free polymer. For the *150-3*

and *150-6* samples (4.40 and 4.78 mg mL^{-1}, respectively) the same 4 to 7 μm band remains intact and the initial dissolution of the supra-20 μm gels is retarded. For the *150-6* sample, Figure 3-15b illustrates this effect very clearly, with significant submicron counts present only after 8.5 days. Presumably the submicron counts continue to increase with a resultant effect on the supra-20 μm counts. The distributions of both the three and six hour heated samples also show many more agglomerates over 50 μm.

Although not shown here, sample *100-2m* shows rapid dissolution of the polymer, but agglomerates in the 4 to 7 μm range were present for two weeks of observed solution ageing without dissolution. The submicron counts did show an increase after about four days, but this was matched in an increase in the over 15 μm agglomerates, suggesting that there were species greater than 50 μm dispersing into individual coils and smaller agglomerates.

Finally, a solution of FA920MPM, known to exhibit a haze, was sampled for agglomerate distribution. The haze is denser than the bulk solution and settles. Two samples were taken, one from an upper, clearer section of the solution and one taken from the lower haze-enriched region. Both samples showed a pronounced 4-7 μm size agglomeration but the hazy sample possessed an order of magnitude more agglomerates of this size.

Figure 3-14 Dissolution curves for (a) *unmodified* PAAm at 4.95 mg mL^{-1} and (b) *100-6* at 4.76 mg mL^{-1}. Values represent period of ageing in days.

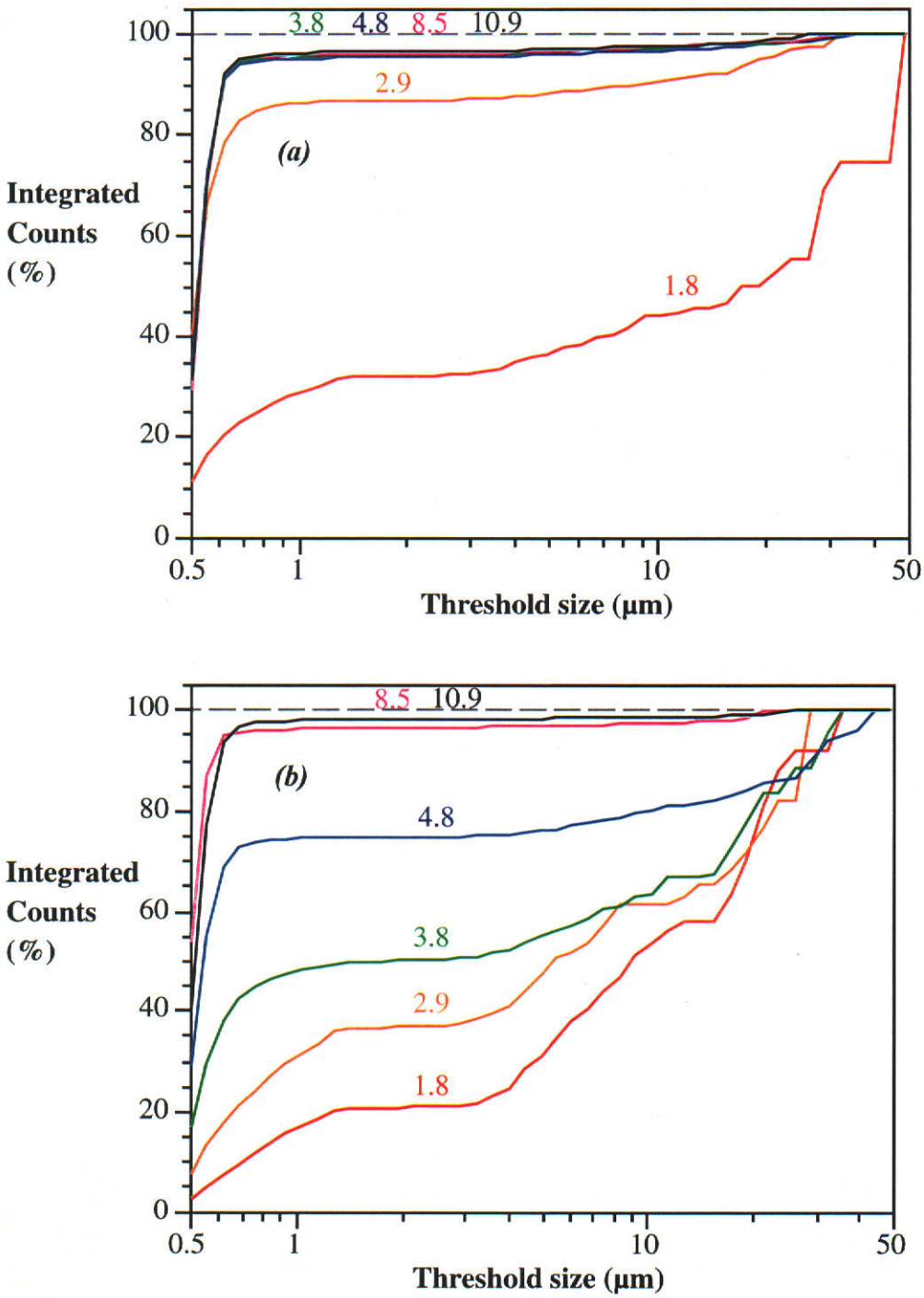

Figure 3-15 Dissolution curves for (a) PAAm *150-1* at 5.25 mg mL^{-1} and (b) *150-6* at 4.78 mg mL^{-1}. Values represent period of ageing in days.

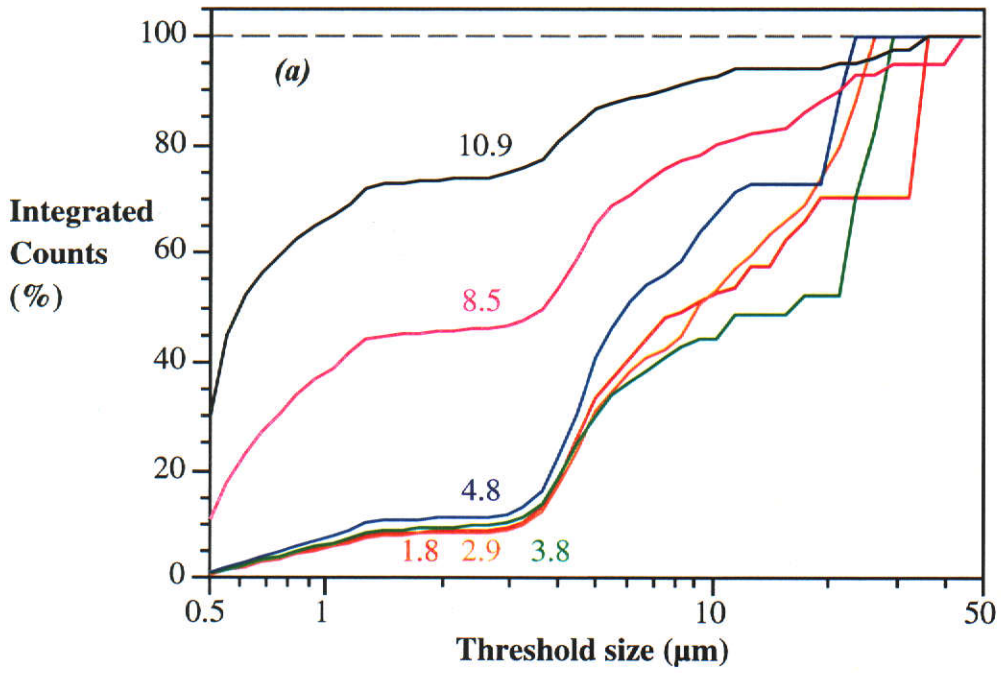

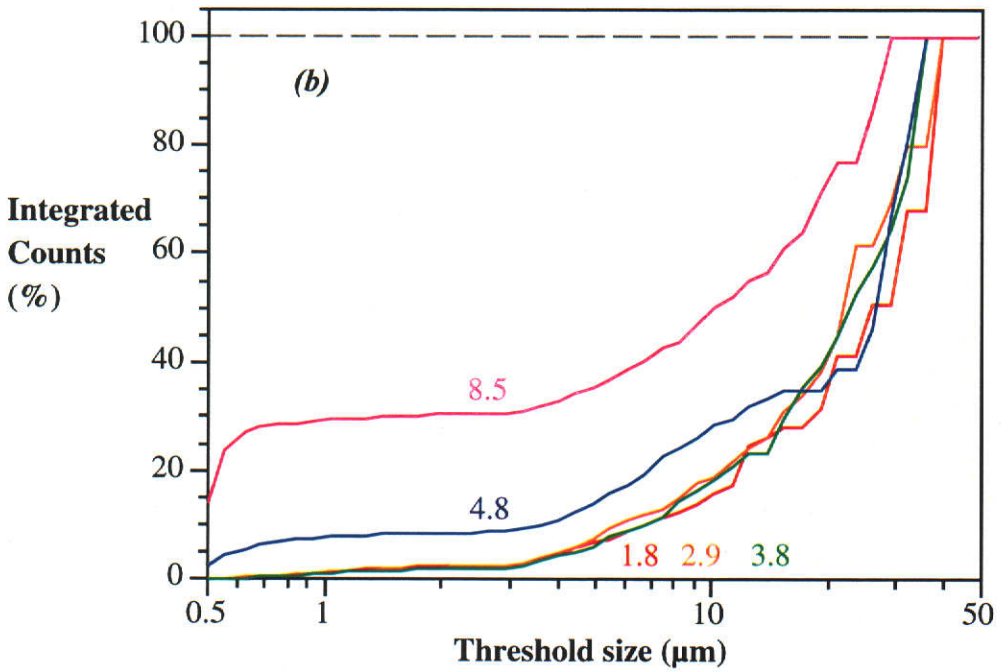

3.4.5 The effects of heating on polyacrylamide

The dissolution of polyacrylamide in an aqueous solution is a complicated process involving swelling, dispersion and conformation change. Comparison of the heated and *unmodified* PAAm samples shows exposure to heat affects the rate and extent of dissolution of the polymer. For heating of less than six hours, the intensity of heat is more significant than duration, with the effect of forming stable material 4 to 7 μm in diameter which resists dissolution. Published literature attributes this to the hydrophobic imide groups but a significant amount of imide was detected only for the discoloured, insoluble samples. The poorly soluble polyacrylamides exhibited no characteristic imide signal beyond background levels. However, all of the heat-modified polyacrylamides showed an increased intensity of a C-N stretching mode compared to the unheated sample. What this correlated to in terms of a partial thermal decomposition remains unknown.

This Section has shown agglomerates are inherent to commercial polyacrylamides, and any technique to characterise this material must account for these bodies. The effect of a chromatographic environment on polymer agglomerates is the topic of the next Section of this Chapter.

3.5 Shearing and Filtration

Studies of the molecular mass distribution of PAAm solutions are complicated by the polymer's sensitivity to shear. Liquid chromatographic methods to study PAAm will inevitably impose a shear stress. Quantifying these shear effects is a necessary precondition to determining a meaningful molecular mass distribution.

A solvated PAAm coil conformation may be reliably related to solution viscosity, η. Unperturbed coils under no shear have the limiting zero-shear viscosity, η_0, dependant upon molecular mass and distribution, branching ratio, concentration and temperature (Kulicke *et al.* 1982, Müller and Klein 1988). However, under pipe shear the polymer coil occupies a range of flow laminae, and as the shear increases the coil reduces stress by deforming from a sphere to a prolate ellipsoid (Chmelir *et al.* 1980, Dupuis *et al.* 1994). Consequently, the polymer coil packing changes, and solution viscosity increases from the zero-shear limit. In narrow tubing the shear stress is a function of the shear rate, in turn a function of the velocity gradient perpendicular to the direction of flow (Barth and Carlin 1984). Tubing inner diameter (and hence both tubing cross-sectional area and velocity gradient), is therefore predicted to be the single most important shear function for this coil deformation mechanism.

Increasing the shear, the polymer experiences a transition in which the coil unravels to a highly extended conformation (Muller *et al.* 1988). The extended coil has a greater viscosity and, depending upon molecular mass, concentration and flow field, a network structure may form (Peterlin 1966, Müller and Klein 1988). For PAAm, the network arises from intermolecular hydrogen bonds or by a simple physical entanglement of the coils. Hence, applied shear may result in polymer agglomeration. When the shear is increased, an upper viscosity limit η_∞ arises in which the polymer coil is fully extended. At and beyond this shear rate the

possibility of polymer degradation by chain scission increases and the molecular mass distribution will become irreversibly changed.

In an analytical environment such as liquid chromatography, improved resolution of solutes is gained by reducing void volumes, or minimising band broadening through shorter analysis times. Reducing the void volume is typically achieved by using thinner tubing while analysis time is lowered with more rapid solution flow. The determination of polymer molecular mass distribution is therefore likely to demand shear stresses that potentially distort the molecular mass distribution by mechanisms described above.

This Section compares the rms radius and polymer agglomeration measurements with shear from capillary flow in both water and 2%-v/v formamide, a solvent known to limit ageing and agglomeration behaviour (Section 3.3). The effect of filtration is also reported. All reported data for this Section refers to the higher molecular mass M333 except where explicitly noted.

3.5.1 Results of shearing of polyacrylamides

Shear in these experiments was generated from extrusion through tubing of varying lengths and diameters. In the following discussion the tubing used in the experiment is given a code for three different tube lengths and two internal diameters (Table 3-2).

Table 3-2 Shear tubing code for tubing internal diameter and length.

	0.26 mm i.d.	0.51 mm i.d.
0.3 m long	T03	W03
1.0 m long	T10	W10
2.4 m long	T24	W24

3.5.1.1 Polyacrylamide in water

The mean error in radii determinations of PAAm arising from light scattering was 3%, approximately 5 nm. For a given tube configuration, Figure 3-16a shows dilute PAAm (M333, exact concentrations were noted in Section 3.2.12) is not greatly affected by shear, as the coil radii is invariant over the flow rate range, remaining within error.

Figure 3-16b shows the shear pattern for high concentration, high molecular mass M333 solutions. The 0.51 mm tubing shows a radius increase with tubing length, but now exhibits a distinct flow rate effect, with the radius increasing with shear rate. A new feature is a plateau in the sizing trend for the 2.4 m tube (W24). The same set of shearing experiments with lower molecular mass PAAm (sample FA920MPM) showed the same sizing trends, although the extent of any observed changes were smaller than for the higher mass flocculant.

Agglomerate distributions from the Sizing Counter for W03 are compared in Figure 3-17a for concentrated M333. The MALLS mean radii differed by less than 1% over the flow rate range (Figure 3-16b). The extent of agglomeration is shown as normalised, surface-weighted counts integrated from 0.6 to 40.0 μm diameters, identical to the format displayed in Section 3.4.4. There is an amount of the polymer agglomerated to the 5 to 20 μm range, vastly greater than the typical 0.35 μm MALLS mean diameters observed. The agglomerate distribution matched the MALLS sizing trend, showing little change in agglomeration over the flow rates studied, although there is a slight shift to smaller agglomerate diameter at the higher flow rates.

Figure 3-16 Effects of rms radii of (a) dilute and (b) concentrated M333 observed by MALLS. Tubing dimensions are described in Table 3-2.

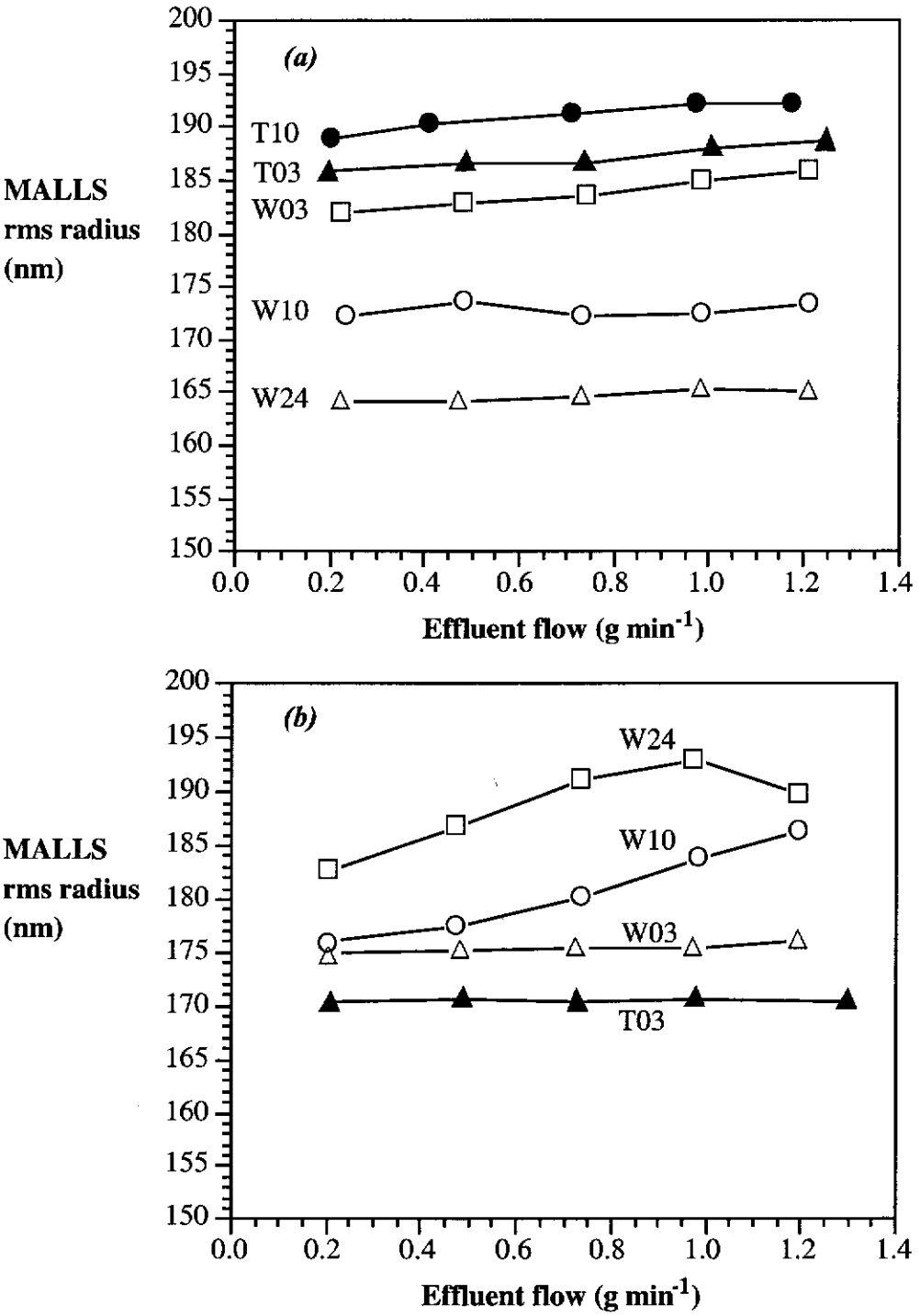

Figure 3-17 Shear agglomeration of 5.00 mg mL^{-1} M333 of molecular mass 20×10^6 in water after shear in (a) 0.3 m long by 0.51 mm i.d. (W03) and (b) 2.4 m by 0.51 mm i.d. (W24) tubes.

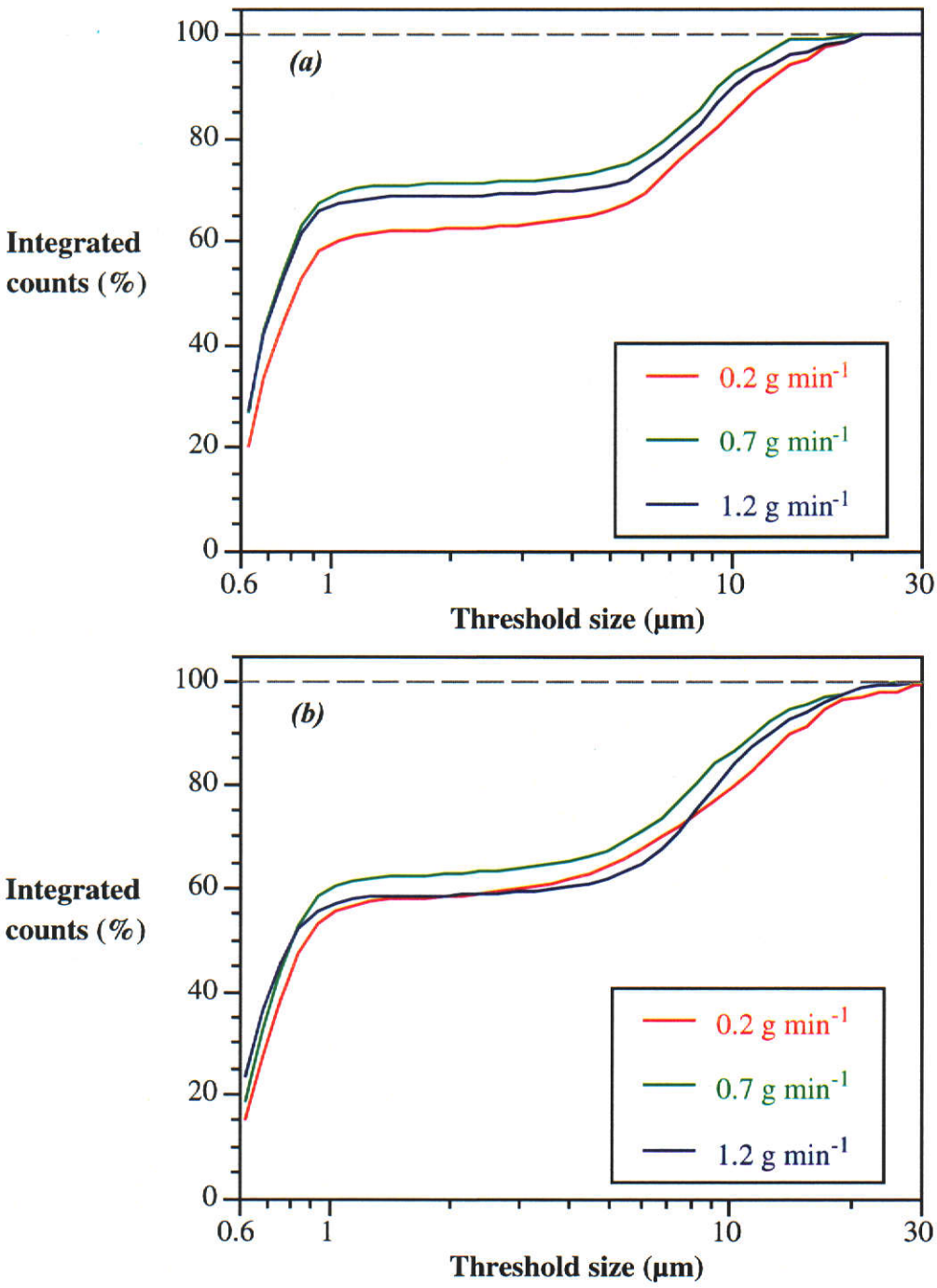

Figure 3-17b shows results for a similar experiment performed for the W24 tube. The MALLS radii (Figure 3-16b) showed a plateau at high flow rates. The integrated counts for this experiment shows, for agglomerates over 5 μm diameter, a shift to smaller diameters with increasing flow rate. The maximum agglomerate diameter from W24 is over 30 μm diameter, while for the shorter shear tube W03 the maximum diameter observed was only 21 μm.

3.5.1.2 Polyacrylamide in 2%-v/v formamide

The presence of 2%-v/v formamide inhibited the ageing/agglomeration effects of PAAm (Section 3.3). For the dilute polymer extruded through 0.51 mm diameter tubing, the MALLS rms radius remained around 168 nm, independent of tube length and flow rate. This result matches the behaviour of dilute PAAm in water (Figure 3-16a), although the radii are 10 nm smaller, commensurate with decreased agglomerate size and number.

Figure 3-18a shows the effect of shear on concentrated PAAm in 2%-v/v formamide. The mean radii are again 10 nm smaller compared to water solvation only, but the radii plateau feature, observed only for W24 in water, is present in the shorter W10 tube as well. The agglomerate size distribution for W24 is shown in Figure 3-18b, analogous to Figure 3-17b in water. The increasing number of submicron species, or equivalently loss of supramicron agglomerates, shows flow rate dependence. The maximum observed agglomerate also shifts from over 30 μm diameter at 0.2 mL min^{-1} to 18 μm at 1.2 mL min^{-1}.

Figure 3-18 Shear agglomeration of 5.00 mg mL^{-1} M333 of molecular mass 20×10^6 in 2%-v/v formamide for (a) MALLS mean radii and (b) Sizing Counter agglomerate distribution. Tubing dimensions are described in Table 3-2.

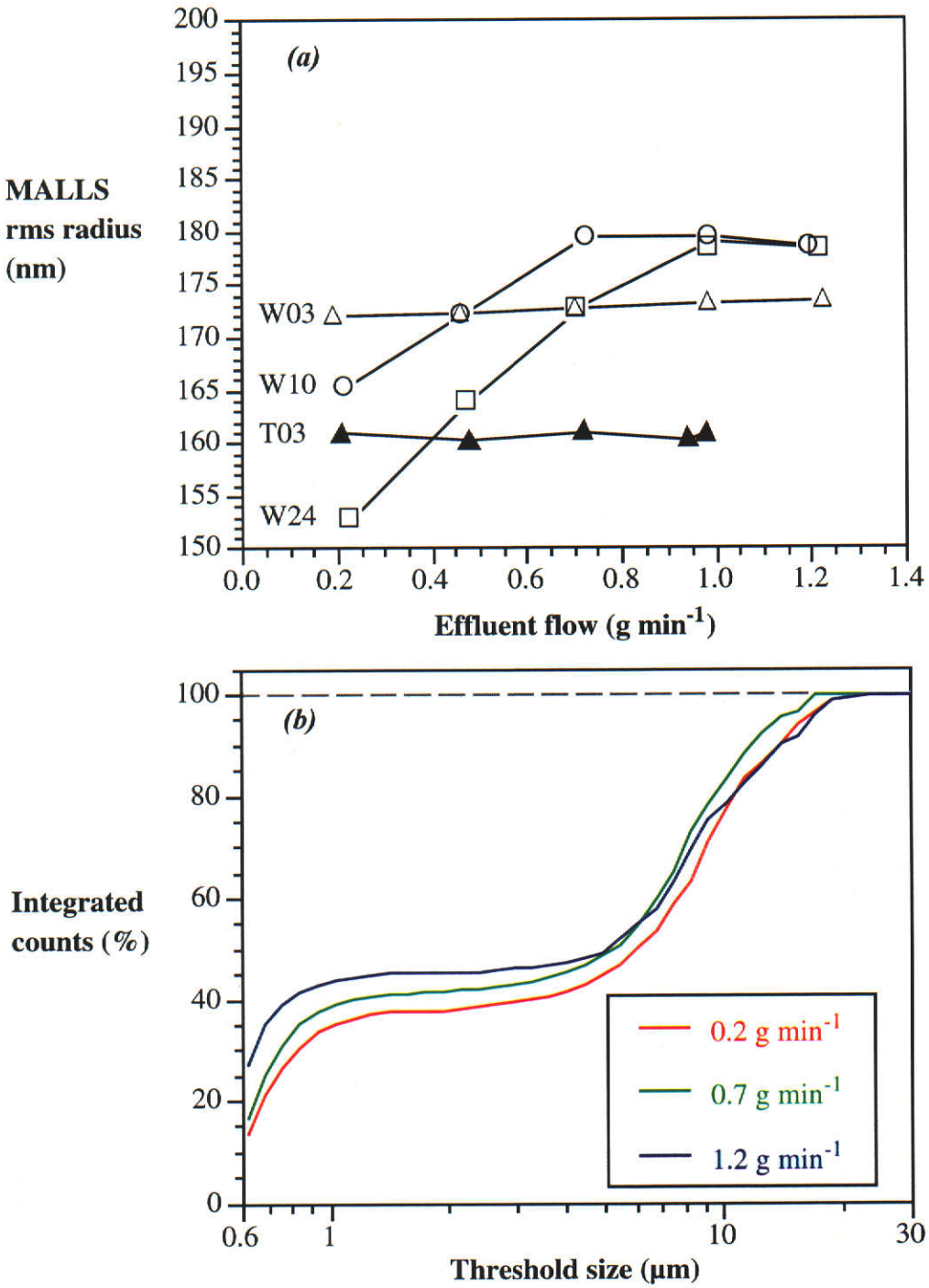

3.5.1.3 Polyacrylamide with 5.0 μm filtration

Figure 3-19a shows the rms radii after 5 μm inline filtration for the concentrated polymer solution in water. At a low flowrate, filtration had little effect on the mean radius, while increased flowrate increased the coil radius. The agglomerate distribution of solution subject to 5 μm filtration is shown by Figure 3-19b. Clearly, the agglomerate disruption improved dramatically at greater flow rates. The same experiment, for high concentration PAAm in 2%-v/v formamide, showed that while agglomerates are disrupted at low flow rates, the extent of agglomeration actually increased with flow rate. This is an inversion of the water-solvated trend.

3.5.2 Effects of shear and filtration on polyacrylamide

3.5.2.1 In water

The light scattering measurements have, given identical volume and number of polymer coils, less angular dependence from a sphere than from an ellipsoid, therefore the measured radius increases with ellipsoid eccentricity. It was observed for the dilute polymer solutions in water (Figure 3-16a) that the mean radius was greater in the narrower shear tube, which may be attributed to the coil deformation mechanism.

Based purely upon shear stress considerations for ideal fluids, the tube length is not relevant, yet it clearly influenced the rms radius results for concentrated polymer (Figure 3-16b). A reason for this arises from viscosity-shear relationships, where shear increases the solution viscosity commensurate with the polymer coil deformation, but recovery to the initial viscosity is achieved only after some period of no shear.

Figure 3-19 Shear agglomeration of 5.00 mg mL^{-1} PAAm of molecular mass 20×10^6, in water, with 5 µm inline filtration followed by passage through W03. (a) MALLS mean radii and (b) Sizing Counter agglomerate distribution. Tubing dimensions are described in Table 3-2.

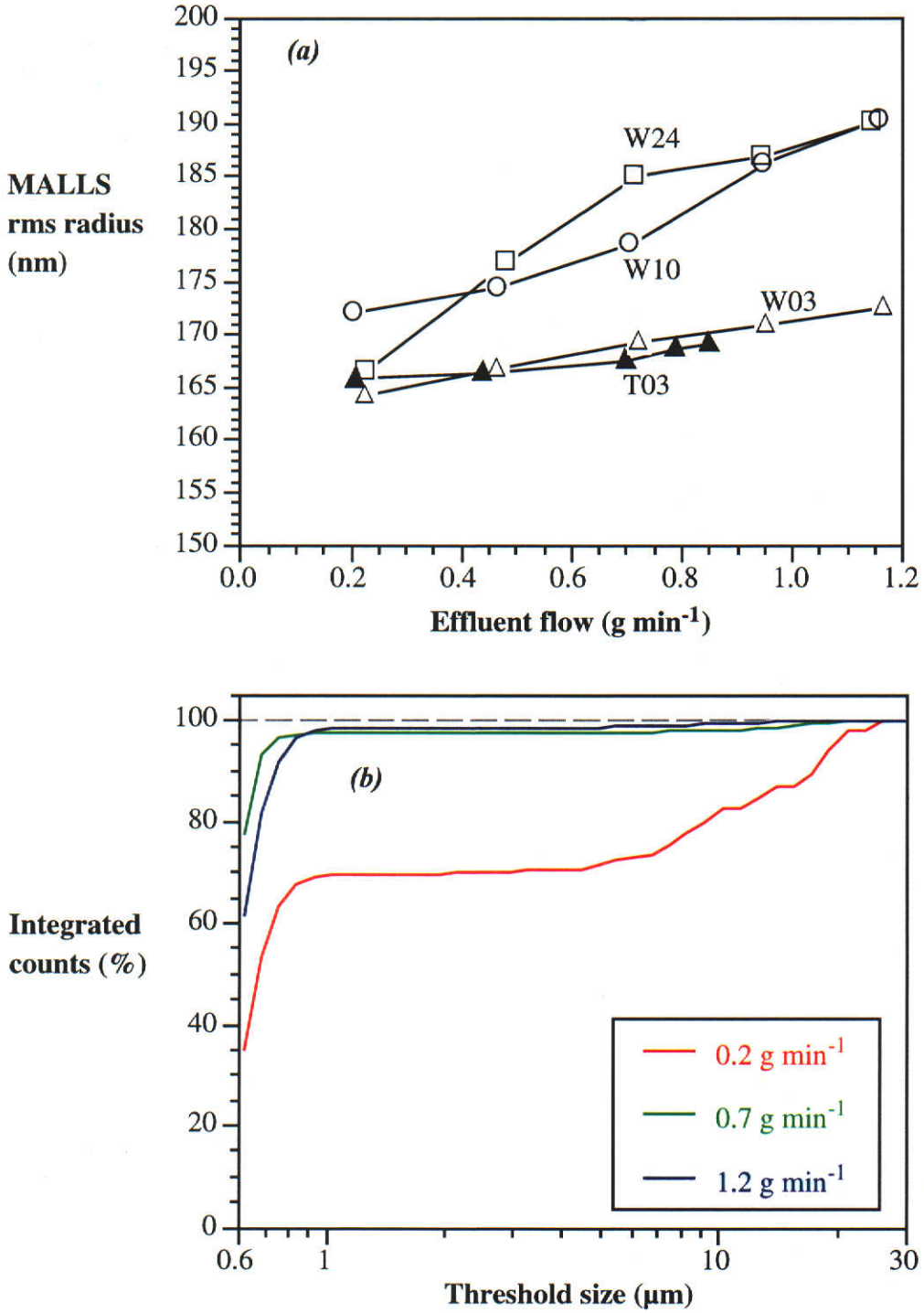

For PAAm, Chmelir *et al.* (1980) observed that relaxation times range from a few minutes to an hour. This interval is matched by Barham (1986), where an individual 3×10^6 molecular mass PAAm coil in water takes approximately an hour to recover from polymer-polymer entanglement induced by solution flow. Thus the product of shear stress and tube length allow the polymer coils time to entangle and these newly-formed agglomerates increase the mean MALLS sizing, as observed.

The agglomerate size integral of Figure 3-17a shows a slight trend to smaller agglomerates for PAAm in water with increasing flow rate for both W03 and W24. This apparent contradiction with the rms radii results was clarified in Section 3.3.1 where supramicron agglomerates were shown to be too few to affect the MALLS detector. The changes do not indicate whether this is a compression of the agglomerates upon passage through the tubing or a degradation process, ranging from coilwise abrasion to a catastrophic shattering of the agglomerates. Significantly, the maximum agglomerate size is affected by tube length, where longer shear duration leads to larger agglomerates.

3.5.2.2 In formamide

Comparison between the W03 shear tube experiments in water and dilute formamide (Figure 3-16b and Figure 3-18a, respectively) show the rms radius constant with flow rate. In water, little change in agglomerate distribution is noted, but the agglomerate distribution shifted in 2%-v/v formamide with increasing flowrate. This shows that shear in the 0.51 mm diameter tubing favoured agglomerate dispersion in dilute formamide, while the poorer solvation of PAAm in water limited the extent of dispersion by physical shear. The presence of formamide for both W10 and W24 shear tubes exhibit a similar sizing plateau (Figure 3-18a), where again improved solvation allowed agglomerate dispersion to occur more readily.

3.5.2.3 Effect of filtration

The effect of filtration was addressed for two reasons. Firstly, the agglomerates may be efficiently removed by filtration rather than solvent modification and filtration is easy to impart with an inline filter. Secondly, when the filtration is accomplished MALLS sizing trends are of the individual polymer coils, unmasked by agglomerate effects. It has been shown in Section 3.3 that 5 μm filtration has no detectable effect on polymer concentration.

The increasing rms radius with flow rate for filtered PAAm in water (Figure 3-19a) matches the shear deformation mechanism (Section 3.5.2.1), while 5 μm inline filtration removes agglomerates well, as shown in Figure 3-19b. Agglomerate disruption is more effective at higher flow rates, although it remains unclear whether the agglomerates may deform to pass the filter at slow flow rates, or are reduced to free coils so that at faster flow rates there is insufficient time to re-agglomerate in the tubing.

For concentrated PAAm in 2%-v/v formamide was filtered, an increase in the agglomeration with flow rate was shown. In water, where the coils are contracted, filtration removes most of the agglomerates, and further shear is unable to induce re-agglomeration. In dilute formamide, where the coils are expanded due to better solvation, greater coil collision and agglomerate reformation occurs. This mechanism qualitatively explains the filtration observations.

3.6 *Conclusions for Aqueous Solutions*

Before the molecular mass distribution of PAAm may be determined, the effects of ageing and shear upon the solution need to be understood. This Section has provided an outline of these properties.

While the individual polymer molecules had diameters in the order of 0.35 μm, a high number of agglomerates were seen which may contain 4 to 6 polymer chains. As the solution age increased, a detectable level of agglomerates (2 to 15 μm) were observed. The number of agglomerates can be controlled by the manipulation of hydrogen bonding, through added salts or solvents. For example, the addition of formamide was shown to improve the solvation of PAAm such that agglomeration was at a minimal level and ageing effects were eliminated.

Salts or solvents never suppressed the presence of agglomerated PAAm completely. Heating solid PAAm is known to produce imides, and was shown to increase solution agglomeration. While the presence of imides was detected for samples subject to excessive heating, many samples exhibited the retarded dissolution without detectable imides. This indicated that imides are influential at very low concentrations or that heating has multiple effects.

High molecular mass PAAm may undergo shear degradation, however, simulating conditions of analytical environments shows that only shear-induced entanglement occurs. Improving the solvent quality, such that the initial agglomeration is less, makes the polymer more susceptible to the shear-agglomeration. Filtration does remove the agglomerates, but deforms the polymer coils.

To avoid shear-agglomeration for concentrated PAAm, polymer-carrying tubing 0.51 mm i.d. and as short as possible is acceptable for flow rates less than 0.5 mL min^{-1}. This information was utilised in the fractionation method development for determining molecular mass distributions (Chapter 4).

3.7 REFERENCES

Aharoni, S.M., 1983, 'On entanglements of flexible and rodlike polymers', *Macromolecules*, vol. 16, pp. 1722-1728.

Barham, P.J., 1986, 'Adsorption-entanglement layers in flowing high molecular weight polymer solutions. IV. The rates of layer formation and decay', *Colloid and Polymer Science*, vol. 264, pp. 917-923.

Barth, H.G. and Carlin, F.J., 1984, 'A review of polymer shear degradation in size-exclusion chromatography', *Journal of Liquid Chromatography*, vol. 7, pp. 1717-1738.

Basedow, A.M., Ebert, K.H. and Hunger, H., 1979, 'Effects of mechanical stress on the reactivity of polymers: shear degradation of polyacrylamide and dextran', *Makromolekulare Chemie*, vol. 180, pp. 411-427.

Biran, R. and Dawkins, J.V., 1984, 'Separation system for fractionation of polyacrylamide by gel permeation chromatography', *European Polymer Journal*, vol. 20, pp. 129-133.

Boyadjian, R., Seytre, G., Berticat, P. and Vallet, G., 1976, 'Caracterisation physico-chimique de polyacrylamides utilises comme agents floculants. I. Etude en solution', *European Polymer Journal*, vol. 12, pp. 401-407.

Boyadjian, R., Seytre, G., Berticat, P. and Vallet, G., 1976, 'Caracterisation physico-chimique de polyacrylamides utilises comme agents floculants. II. Etude des fractions insolubles', *European Polymer Journal*, vol. 12, pp. 409-413.

Chmelir, M., Künschner, A. and Barthell, E., 1980, 'Water soluble acrylamide polymers, 2. Aging and viscous flow of aqueous solutions of polyacrylamide and hydrolysed polyacrylamide', *Angewandte Makromolekulare Chemie*, vol. 89, pp. 145-165.

de Jaeger, N.C., Gilleir, J. and Verdyck, W., 1991, 'Monitoring the amount of microgel structures in aqueous solutions of ionic and non-ionic polymers, using the electrical sensing zone technique', in *Advances in the Measurement and Control of Colloidal Processes*, eds. Williams, R.A. and de Jaeger, N.C., Butterworth-Heinemann, Oxford, pp. 150-160.

Dupuis, D., Lewandowski, F.Y., Steiert, P. and Wolff, C., 1994, 'Shear thickening and time-dependent phenomena: the case of polyacrylamide solutions', *Journal of Non-Newtonian Fluid Mechanics*, vol. 54, pp. 11-32.

François, J., Sarazin, D., Schwartz, T. and Weill, G., 1979, 'Polyacrylamide in water: molecular weight dependence of $<R^2>$ and $[\eta]$ and the problem of the excluded volume exponent', *Polymer* , vol. 20, pp. 969-975.

Franks, F., 1983, *Water,* Royal Society of Chemistry, Cambridge.

Gardner, K.L., Murphy, W.R. and Geehan, T.G., 1978, 'Polyacrylamide solution aging', *Journal of Applied Polymer Science*, vol. 22, pp. 881-882.

Gharfeh, S.G. and Moradi-Araghi, A., 1986, 'Determination of anionic high-molecular weight water-soluble polymers by size-exclusion chromatography', *Journal of Chromatography*, vol. 266, pp. 343-350.

Haas, H.C. and MacDonald, R.L., 1971, 'Imidisation reaction in polyvinylamides', *Journal of Polymer Science: Part A-1*, vol. 9, pp. 3583-3593.

Haas, H.C. and MacDonald, R.L., 1972, 'Dichotomies in the viscosity stability of polyacrylamide solutions. I.', *Journal of Polymer Science, Part B: Polymer Physics*, vol. 10, pp. 461-467.

Henderson, J.M. and Wheatley, A.D., 1987, 'Factors effecting a loss of flocculation activity of polyacrylamide solutions - shear degradation, cation complexation and solution aging', *Journal of Applied Polymer Science*, vol. 33, pp. 669-684.

Karlberg, B., and Pacey, G.E., 1989, *Flow Injection Analysis: a Practical Guide*, Elsevier, Amsterdam.

Karlström, G., Carlsson, A. and Lindman, B., 1990, 'Phase diagrams of nonionic polymer-water systems. Experimental and theoretical studies of the effects of surfactants and other cosolutes', *Journal of Physical Chemistry*, vol. 94, pp. 5005-5015.

Klein, J. and Westerkamp, A., 1981, 'Peculiarities of polyacrylamide analysis by aqueous GPC', *Journal of Polymer Science, Part A: Polymer Chemistry*, vol. 19, pp. 707-718.

Kulicke, W.-M. and Kniewske, R., 1980, 'Purification of aqueous and non-aqueous polymer solutions for light scattering measurements and comparison of molecular weights determined with a low-angle and a wide-angle photometer', *Makromolekulare Chemie, Rapid Communications*, vol. 1, pp. 719-727.

Kulicke, W.-M., Kniewske, R. and Klein, J., 1982, 'Preparation, characterization, solution properties and rheological behaviour of polyacrylamide', *Progress in Polymer Science*, vol. 8, pp. 373-468.

Leca, M., 1986, 'Influence of denaturing agents on macromolecular coil dimensions of polyacrylamides in diluted aqueous solutions', *Polymer Bulletin (Berlin)*, vol. 16, pp. 537-543.

Maurer, J.J., Harvey, G.D. and Klemann, L.P., 1988, 'Thermally promoted hydrolysis of polyacrylamide', in *Water-Soluble Polymers for Petroleum Recovery,* eds. Stahl, G.A. and Schulz, D.N., Proceedings of the National Meeting of the American Chemical Society, Plenum, New York, pp. 261-270.

Millero, F.J., 1972, 'The partial molar volumes of electrolytes in aqueous solutions', in *Water and Aqueous Solutions: Structure, Thermodynamics and Transport Processes,* ed. Horne, R.A., Wiley-Interscience, New York, pp. 519-564.

Mohan, S. and Murugan, R., 1997, 'Vibrational spectra, assignments, and normal coordinate analysis of polyacrylamide', *Arabian Journal of Science and Engineering*, vol. 22, no. 2A, pp. 155-164.

Moradi-Araghi, A., Hsieh, E.T. and Westerman, I.J., 1988, 'Role of imidization in thermal hydrolysis of polyacrylamides', in *Water-Soluble Polymers for Petroleum Recovery,* eds. Stahl, G.A. and Schulz, D.N., Proceedings of the National Meeting of the American Chemical Society, Plenum, New York, pp. 271-278.

Muller, A.J., Odell, J.A. and Keller, A., 1988, 'Elongational flow and rheology of monodispersive polymers in solution', *Journal of Non-Newtonian Fluid Mechanics*, vol. 30, pp. 99-118.

Muller, G., Laine, J.P. and Fenyo, J.C., 1979, 'High-molecular-weight hydrolysed polyacrylamides. I. Characterisation. Effect of salts on the conformational properties', *Journal of Polymer Science, Part A: Polymer Chemistry*, vol. 17, pp. 659-672.

Müller, R.-J. and Klein, J., 1988, 'Correlation of viscoelastic properties with the molar mass distribution for aqueous polyacrylamide solutions', *Makromolekulare Chemie* pp. 2341-2355.

Narkis, N. and Rebhun, M., 1966, 'Ageing effects in measurement of polyacrylamide solution viscosities', *Polymer (London)*, vol. 7, pp. 507-512.

Nicholson, J.W., 1991, *The Chemistry of Polymers,* Royal Society of Chemistry, Cambridge.

Peterlin, A., 1966, 'Hydrodynamics of macromolecules in a velocity field with longitudinal gradient', *Journal of Polymer Science, Part B: Polymer Physics*, vol. 4, pp. 287-291.

Raos, G. and Allegra, G., 1996, 'Chain interactions in poor-solvent polymer solutions: equilibrium and non-equilibrium aspects', *Macromolecules*, vol. 29, pp. 6663-6670.

Scoggins, M.W. and Miller, J.W., 1975, 'Spectrophotometric determination of water soluble organic amides', *Analytical Chemistry*, vol. 47, pp. 152-154.

Shyluk, W.P. and Stow, F.S., 1969, 'Aging and loss of flocculation activity of aqueous polyacrylamide solutions', *Journal of Applied Polymer Science*, vol. 13, pp. 1023-1036.

Smith, E.A., Prues, S.L. and Oehme, F.W., 1996, 'Environmental degradation of polyacrylamides. I. Effects of artificial environmental conditions: temperature, light, and pH', *Ecotoxicology and Environmental Safety*, vol. 35, pp. 121-135.

Sommer, H.T., Harrison, C.F. and Montague, C.E., 1992, 'Particle size distribution from light scattering', in *Particle Size Analysis,* eds. Stanley-Wood, N.G. and Lines, R.W., Royal Society of Chemistry, Cambridge, pp. 163-171.

Stejskal, J. and Horska, J., 1982, 'Refractive index increments of polyacrylamide and comments on the light scattering from its solutions', *Makromolekulare Chemie*, vol. 183, pp. 2527-2335.

Sugarman, J.H., Prud'homme, R.K., Langhorst, M.A. and Stanley, F.W., 1987, 'Detection of microgels in polyacrylamide solutions using microcapillary flow analysis', *Journal of Applied Polymer Science*, vol. 33, pp. 693-702.

Taylor, K.C., 1993, 'Spectrophotometric determination of acrylamide polymers by flow injection analysis', *Society of Petroleum Engineers Advanced Technology Series*, vol. 1, no. 2, pp. 130-133.

Taylor, K.C., Burke, R.A., Nasr-El-Din, H.A. and Schramm, L.L., 1995, 'Development of a flow injection analysis method for the determination of acrylamide copolymers in oilfield brines', at *SPE International Symposium on Oilfield Chemistry*, Society of Petroleum Engineers, San Antonio, Texas, pp. 691-700.

Ying, Q., Wu, G., Chu, B., Farinato, R. and Jackson, L., 1996, 'Laser light scattering of poly(acrylamide) in 1 M NaCl aqueous solution', *Macromolecules*, vol. 29, pp. 4646-4654.

Chapter 4

Polyacrylamide Characterisation by Flow FFF

4. *POLYACRYLAMIDE CHARACTERISATION BY FLOW FFF*

Chapter 3 provided the supramicron (agglomerate) distribution of PAAm in aqueous solutions. This Chapter supplies the submicron complement. Recalling Chapter 2, the fractionation of high molecular mass PAAm by size exclusion chromatography is complicated by concerns over adsorption and shear degradation. The coupling of flow FFF, a MALLS detector and a concentration-sensitive detector was proposed in Chapter 2 to give absolute measurement of molecular mass distributions in a low shear environment.

The first Sections of this Chapter comprise a thorough theoretical background to separation by FFF techniques. The theory provides a guide to optimisation of the system for polymeric samples. Aspects under consideration include hydrodynamic effects, carrier solution, membrane chemistry and agglomeration of the polymer. Section 4.4 describes the central part of this Chapter, the fractionation of commercial PAAm standards of mean molecular masses in the range 0.35 to 9.00×10^6. The breadths of the distributions complement the polymer agglomeration reported in Chapter 3, indicating the presence of entangled polymer. The final Section describes the fractionation of commercial PAAm flocculants, and demonstrates extensions of the technique to degradation studies and hydrolysed PAAms.

4.1 FFF APPLIED TO POLYMERS

The principles of the field flow fractionation method have been described in general for comparison against other analytical methods (Section 2.2.5), but the following Sections describes the theoretical basis for the technique. As will be shown, the methods are directly applicable to particulate analysis, but polymers have proved thus far to be somewhat intractable. The critical result for this work, relating measured retention time to the polymer dimensions, is provided by equation (4-21) in Section 4.1.1.4.

4.1.1 Theoretical basis of FFF

4.1.1.1 Mean position of the sample

The cross-section of a FFF cell of thickness w is shown by Figure 4-1. Other dimensions of the cell are length L, breadth b and void volume V^0. For an applied field of strength ϕ, a sample experiences a force F from the field whose magnitude is moderated by its susceptibility to the field, s (Janca 1988)

$$F = \phi s \tag{4-1}$$

The force provides an impetus and the sample accelerates rapidly to a steady-state drift velocity, U, which is a function of the force imposed and a friction coefficient f

$$U = \frac{F}{f} \tag{4-2}$$

The accumulation wall limits migration and the sample concentrates to form a layer adjacent to the wall. The sample concentration varies with proximity from the wall such that there is an exponential decay with a characteristic thickness, expressed as a

competition between the sample's diffusion coefficient D and the drift velocity U (Caldwell 1991)

$$c_x = c_{x=0} \exp\left(-\frac{xU}{D}\right) = c_{x=0} \exp\left(-\frac{x}{l}\right) \tag{4-3}$$

where c_x is the solute concentration at a distance x ($0 \leq x \leq w$) from the accumulation wall. At the wall, $x = 0$, and the solute concentration is given by $c_{x=0}$.

Figure 4-1 Mechanism of FFF for submicron solutes: "normal mode" operation. The improved back-diffusion of smaller solutes leads to their more rapid elution.

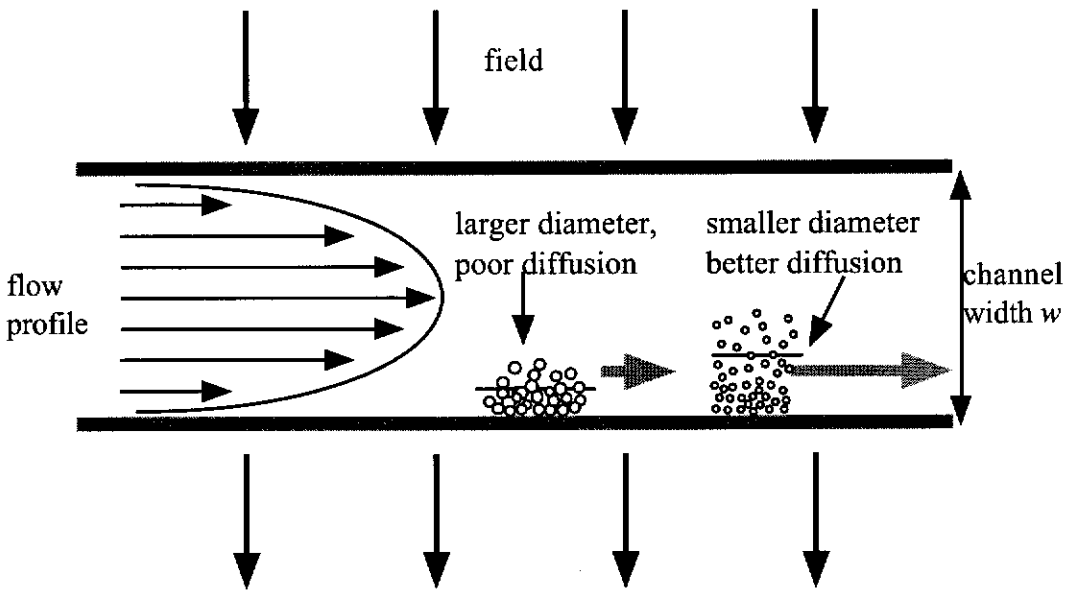

The parameter l is a measure of the thickness of the solute atmosphere (Caldwell 1991)

$$l = \frac{D}{U} \tag{4-4}$$

Clearly, an increase in field strength ϕ will result in a more compact layer with a smaller characteristic parameter l. The diffusion coefficient is dependent upon f by

$$D = \frac{kT}{f} \tag{4-5}$$

where k is Boltzmann's constant and T temperature. Upon substitution of (4-1) and (4-5) into (4-4) a general expression for the layer thickness results characteristic for each sample

$$l = \frac{kT}{\phi s} \tag{4-6}$$

The effect of the thickness of the atmosphere protruding into the FFF channel (not to scale) is illustrated by Figure 4-1. As will be shown this mean layer thickness directly determines the retention of the sample.

It is more convenient for the following retention discussion to express this characteristic solute layer thickness in a dimensionless form as the ratio to the channel thickness w

$$\lambda = \frac{l}{w} \tag{4-7}$$

4.1.1.2 Theory of retention

A sample injected into the thin FFF channel relaxes into the equilibrium exponential distributions as described above. The complication of sample injection will be discussed in detail in Section 4.1.1.8. When the axial ("channel") flow is reintroduced, the thin channel forces a parabolic carrier liquid flow profile. A sample susceptible to the field occupies a more compressed mean position (small λ), and will be carried at a slower rate than the less compact profiles which are carried by the more rapidly moving laminae (Caldwell 1991). By such a process separation occurs. To a good approximation, the velocity profile is parabolic and symmetric around the centre of the channel and for a mean channel flow rate of $\dot{V}$ gives rise to the mean linear velocity of the carrier liquid $\langle v \rangle$

$$\langle v \rangle = \frac{\dot{V}}{bw} \tag{4-8}$$

and the velocity of the lamina v_x at a distance x ($0 \leq x \leq w$) from the accumulation wall will, for a parabolic velocity profile, be given by

$$v_x = 6\langle v \rangle \left(\frac{x}{w} - \frac{x^2}{w^2} \right) \tag{4-9}$$

The sample retention ratio is defined as the ratio of the mean zone migration velocity $\langle V \rangle$, the average of the product of concentration and laminae velocities for all values of x the sample occupies, to the mean carrier linear velocity $\langle v \rangle$

$$R = \frac{\langle V \rangle}{\langle v \rangle} = \frac{\langle c_x . v_x \rangle}{\langle c_x \rangle \langle v \rangle} \tag{4-10}$$

Combining the relevant equations, the retention ratio can be expressed in the classic FFF form (Janca 1988, Caldwell 1991)

$$R = 6\frac{l}{w}\left[\coth\left(\frac{w}{2l} \right) - \left(\frac{2l}{w} \right) \right] = 6\lambda \left[\coth\left(\frac{1}{2}\lambda \right) - 2\lambda \right] \tag{4-11}$$

Retention, therefore, is strictly a function of the ratio of the mean sample thickness to the channel width, and by manipulating the mean layer thickness (governed by the field strength) and the flow velocities (with the channel flow rate) the retention of a sample may be controlled. For well retained samples, where $l \rightarrow 0$, the *coth* function rapidly approaches unity and the ratio simplifies to

$$R = 6\lambda \tag{4-12}$$

Experimentally, R is determined from retention volumes or retention times of a sample (V_r, t_r) as compared to a void volume or void time (V^0, t^0) which may be calculated from the channel dimensions or measured for an unretained component

$$R = \frac{V^0}{V_r} = \frac{t^0}{t_r} \tag{4-13}$$

Studies for the refinement of the above theory to account for deviations in the parabolic flow profile due to viscosity inhomogenities and drag effects on the channel walls show the corrections are minor for model solutes (Giddings and Schure 1987, Martin *et al.* 1997, Giddings 1997).

4.1.1.3 Flow FFF

Subtechniques of FFF differ in the manner in which the drift velocity U is imparted. For the case of flow FFF, all samples are equally susceptible to the crossflow and the same U is imparted upon all species, which makes it unique in the family of FFF. The accumulation wall is permeable to the crossflow, and a membrane covering the accumulation wall allows the sample to establish the solute concentration gradient, which generates a diffusive flux as described above. The balance between the impelling field and the entropy-driven diffusion results in an equilibrium position described by

$$\lambda = \frac{l}{w} = \frac{D}{Uw} \tag{4-14}$$

The area of the accumulation wall is given by the quotient of the void volume, V^0, to the channel thickness, w. Since the drift velocity, U, is identical to the ratio of the volumetric crossflow, $\dot{V}_c$, to the area of the accumulation wall, substitution for U gives (Giddings *et al.* 1976)

$$\lambda = \frac{D}{w^2}\frac{V^0}{\dot{V}_c} \tag{4-15}$$

This last result reveals that retention in flow FFF, shown to be a function of λ, is in turn dependant solely on the differences in diffusion coefficients of the solutes. Since diffusion is an effective measure of hydrodynamic diameter, retention therefore is a function of a solute's diameter.

4.1.1.4 Selectivity and programming

From the retention times of different samples, the diameter-based selectivity S_d arises from a comparison of the analyte retention with diameter d, and is defined as

$$S_d = \left| \frac{\partial \ln(t_r)}{\partial \ln(d)} \right|_{\dot{V},\dot{V}_c} \tag{4-16}$$

The retention for flow FFF is based solely upon diffusion and as such $S_d = 1$. By the same reasoning the selectivity is also unity for thermal FFF while for sedimentation FFF the experienced force is a function of the cube of the diameter and $S_d = 3$. For comparison, selectivity for a SEC separation falls in the range 0.03 to 0.22 (Giddings 1979).

By manipulating the volumetric channel and field flow, the sample characteristic λ may be modified. For example, increased channel flow rate decreases analysis time but at cost to resolution, while increased crossflow has the opposite effect. This balance, the "general elution problem", is the goal of optimising separation. For a polydisperse sample, the conditions chosen to resolve the small components retain the larger species excessively, while optimising for these larger solutes requires a loss of selectivity for the smaller species. Flow programming solves this problem. Programming requires that one or both of the flows change with time, most commonly the crossflow (field) decreases with time. In the early stages of the separation, the field is strong enough to resolve the smaller components, while later it is sufficiently low to allow the larger species to elute in a reasonable time. Retention time t_r in a field-programmed experiment is given by the integrated time dependence of the retention (Giddings and Caldwell 1984)

$$t^0 = \int_{t=0}^{t=t_r} R(t)dt \tag{4-17}$$

This expression may be complicated by a threshold field, $\dot{V}_c^{th}$, above which the sample is held immobile upon the membrane and during this time retention $R = 0$ (Wahlund *et al.* 1986). It is necessary to choose initial field strength, $\dot{V}_c^{i}$, sufficient to give the required selectivity while being low enough to avoid immobilisation. After a period τ_0, for the crossflow undergoing an exponential decay with time constant τ, the time-dependant crossflow function is

$$\dot{V}_c(t) = \dot{V}_c^{i} \exp\left(-\frac{t-\tau_0}{\tau}\right) \tag{4-18}$$

By integrating the time-dependant field expression (4-18) by (4-17), the retention time for a component in the decaying field is given by

$$t_r = \tau_0 + \tau \exp\left(\frac{t_r - \tau_0}{\tau} - 1\right) \tag{4-19}$$

Upon rearranging (4-15) to express diffusion coefficients in terms of crossflow and retention, then substituting (4-13) and $\dot{V} = \frac{V^0}{t^0}$, the following expression arises (Wahlund *et al.* 1986)

$$D = \frac{w^2}{6}\frac{\dot{V}_c R}{V^0} = \frac{w^2}{6}\frac{\dot{V}_c}{\dot{V}}\frac{1}{t_r} \tag{4-20}$$

which on substitution of (4-19) gives

$$D = \frac{w^2 \dot{V}_c}{6\dot{V}}\left[\tau_0 + \tau \exp\left(\frac{t_r - \tau_0}{\tau} - 1\right)\right]^{-1} \tag{4-21}$$

Diffusion coefficients of samples may be determined from first principles by flow FFF, providing that a judicious choice of time and decay constant is made. A diffusion coefficient is a revealing datum for a macromolecule, being dependent upon hydrodynamic size, and therefore molecular mass and coil configuration. The exponential decay program has an elution profile in which the retention time is a logarithmic function of the sample's diffusion coefficient and therefore a logarithmic

dependence upon size. Other decay programs exist, such as a linear, parabolic or power decay, providing different size-elution patterns.

Programmed FFF presumes the sample responds immediately to changes in field strength. Changing field strength produces a sample-field response ("secondary relaxation", as opposed to the stopflow "primary relaxation", see Section 4.1.1.8) which complicates elution, and judicious use of programming was emphasised by Giddings and Caldwell (1984) in response to the elaborate corrections deemed necessary by Yau and Kirkland (1984). A later study of the secondary relaxation by Hansen *et al.* (1988) showed that the differences are minimal and of account only for ultrafast separations. Programming theory also presumes the solutes are point masses. Corrections to the elution time-diffusion coefficient relationship accounting for the size of real samples require only a linear function of sample size (Williams and Giddings 1994) providing the field decay is not too rapid. Finally, the programming method has been shown to reduce band width of late eluting components, but the initial high crossflow rate may be incompatible with the sample as immobilisation and overloading occur (Section 4.1.1.7).

4.1.1.5 The steric inversion

The lower limit to fractionation is determined by the porosity of the retaining membrane, balanced against the higher crossflow required for retention of small solutes and commensurate trans-membrane pressure drop. For polymer fractionation the upper size limit is of greater concern and needs to be considered carefully. The theory presented so far refers to "normal" mode FFF, where the back-diffusion mechanism is significant. For larger particles, nominally over 0.7 to 0.8 μm diameter, the diffusion is negligible compared to their protrusion into the flow stream from the accumulation wall (Myers and Giddings 1982). The centre of

mass of a larger particle in the parabolic channel flow will be acted upon by more swiftly moving laminae as compared to a smaller one, as shown by Figure 4-2.

Figure 4-2 Mechanism of FFF for supramicron solutes: "steric" mode operation. Larger samples elute more rapidly, a reversal of "normal" mode.

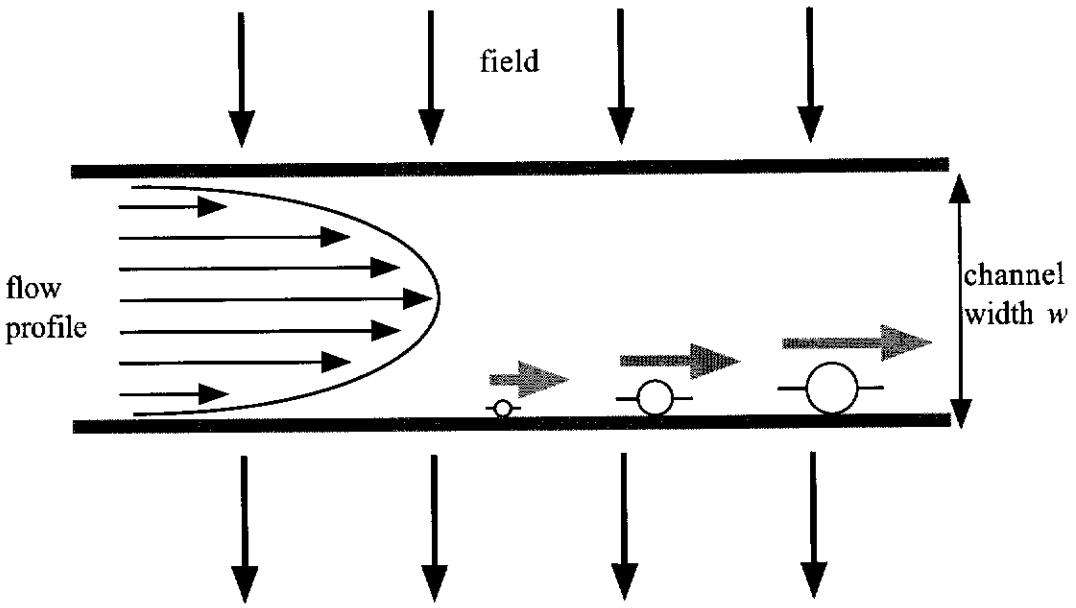

The retention ratio for the "steric" mode is given by

$$R = 3\gamma \frac{d}{w} \tag{4-22}$$

for a particle of diameter d. The factor γ is a dimensionless constant approximately equal to unity and physically is a measure of the lift forces derived from shear on the particle occupying a range of carrier fluid laminae. This factor is still poorly understood so, unlike normal mode FFF, prediction of retention ratio in the steric mode remains reliant upon empirical data. The most significant issue of steric mode operation is a reversal of elution, where for a highly polydisperse sample the finest material experiencing the normal mode mechanism may coelute with the largest diameter particles subject to the steric mode operation. This is a problem intrinsic to the FFF methodology, although the critical diameter d_i, where the steric inversion occurs, shifts according to the flow rates applied (Jensen *et al.* 1996).

For polymer analysis the lower bound of molecular mass is somewhat less than 1 000 and is of particular interest to the analysis of humic and fulvic acids (Giddings 1989). The upper bound for polymers prior to the onset of steric effects has not been studied extensively. Based upon equivalent particle diameters, the upper bound for normal mode (diffusion controlled) elution range from a molecular mass of 10^7 (Kirkland and Dilks 1992) to 10^{10} (Caldwell 1991) prior to the onset of steric effects.

4.1.1.6 Band broadening

During fractionation, an injected sample slug with a square concentration profile broadens parallel to the channel flow coordinate to emerge in a Gaussian concentration profile. The degree of the band broadening as measured by the variance in the peak profile, σ^2, has a number of contributing factors, as described below (Caldwell *et al.* 1988).

The contribution due to the size of the injected pulse σ_{inj}^2 is a function of the injected volume V_{inj} and total channel length L

$$\sigma_{inj}^2 = \frac{1}{12}\left(\frac{V_{inj}L}{V^o}\right) \tag{4-23}$$

The contribution due to mass transfer and non-equilibrium effects σ_{neq}^2 is dependant upon the time spent fractionating the solute, most significant for well-retained samples positioned very near the accumulation wall. Factors include the mean sample height λ (Section 4.1.1.1) as a mass transport function $\chi(\lambda)$ approximated by $\chi(\lambda) = 24\lambda^3$, the mean channel flow velocity $\langle v \rangle$, diffusion coefficient D and the distance travelled by the sample profile Z ($Z \leq L$) expressed as

$$\sigma_{neq}^2 = \chi(\lambda)\, w^2\, \langle v \rangle \frac{Z}{D} \tag{4-24}$$

Finally, the contribution due to the differential migration of sample components arising from polydispersity ρ and mean molecular mass M_w is

$$\sigma_{poly}^2 = Z^2 \left(\frac{\mathrm{d}(\ln V_r)}{\mathrm{d}(\ln M_w)} \right)^2 (\rho - 1) \tag{4-25}$$

Provided other contributions to band broadening are small, the total variance of the migrating sample is given by

$$\sigma^2 = \sigma_{inj}^2 + \sigma_{neq}^2 + \sigma_{poly}^2 \tag{4-26}$$

Improved resolution is therefore achieved by minimising these contributions to the variance. The injection contribution requires the smallest injection volume while remaining sufficiently dilute to avoid overloading (Section 4.1.1.7). Contributions from mass transfer and polydispersity increase over the fractionation as measured by the parameter Z which at elution $Z = L$. These contributions may be improved by reducing the physical channel to as short as necessary for separation, but there are very few options to improve the sample resolution further than this limit.

4.1.1.7 Overloading

In a FFF cell, the sample is compressed onto the accumulation wall. For a dilute sample the solutes behave independently, which is a necessary condition for the relations between retention and diffusion coefficient as described above. For more concentrated samples, and especially for polymers, the concentration independence is threatened and nonlinear retention occurs. This phenomenon, known as "overloading", places an upper limit on the sample size. The local region will have a viscosity different to the bulk carrier and will favour moving through the channel as a gel, moving faster and eluting earlier than the mean profile (Caldwell *et al.* 1988).

This peak asymmetry is characteristic of overloading. Theoretical predictions to the onset of overloading show the parameter λ is indicative of a propensity to overload (Caldwell *et al.* 1988), but the effects of molecular mass and polymer coil interactions were not accounted for. Accordingly, the onset of overloading remains an empirical effect.

4.1.1.8 Sample loading and stopflow

A complication present in FFF is that a sample cannot be simply injected into the flow, as the parabolic flow will enforce a bimodal concentration profile. Figure 4-3a (adapted from Hovingh *et al.* 1970 and Yang *et al.* 1977) illustrates this problem for a sample, introduced evenly across the width of the channel. Under the combined influence of the crossflow and parabolic channel flow trajectories deposit the sample in a concentration profile as shaded. The bimodality may be avoided if $\dot{V} << \dot{V}_c$, but this is impractical for most FFF operation. The strategy used to overcome this is the *stopflow*, a period when the channel flow is diverted once the sample is loaded into the channel such that the sample relaxes into the equilibrium position under influence of the field only. The stopflow time is sufficiently long for the crossflow to sweep one channel (void) volume. Stopflow is simple to implement but does lengthen experimental time and the pressure fluctuations are responsible for baseline instability.

As an alternative to stopflow the use of stream splitters for stopless sample relaxation has been proposed (Giddings 1985, Lee *et al.* 1989). The stream splitter allows the sample introduction to be separate from the main channel flow (Figure 4-3b). In doing so, the mixing across the velocity profile is limited and the sample is introduced close to an equilibrium position. The parabolic flow profile is established within 2 mm of the end of the split inlet (Liu *et al.* 1991).

Figure 4-3 Sample relaxation in flow FFF. (a) Relaxation trajectories and solute concentration profile from initial narrow slug to bimodality, due to the interaction of field and channel flow. (b) Inlet splitting where sample compression broadens the elution profile.

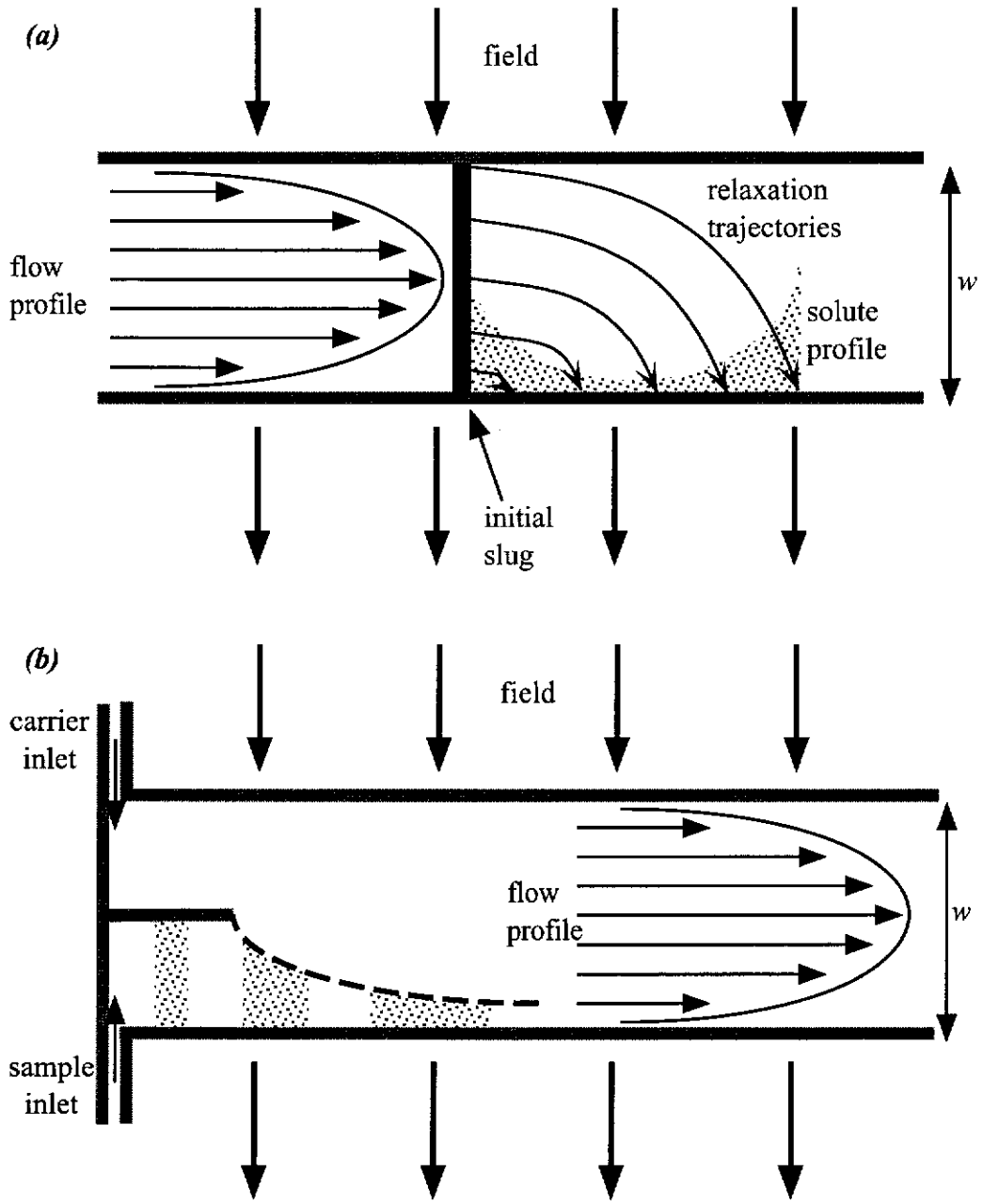

Problems with the splitter are shown by Figure 4-3b, with the injected sample pulse experiencing band broadening as it encounters the main channel flow. Giddings (1990) noted the difficulty in accurately suspending the splitter such that the flows may pass and not clog with the sample. A thin steel sheet between two layers of spacer material may act as a splitter, but the channel thickness becomes three times greater than that of the single spacer and is inconsistent with an effective fractionation in the thinnest possible channels. Even with these considerations, the flow splitter is attractive due to the ease of automation and baseline stability.

Another form of sample relaxation has been reported through the use of frit elements (Giddings 1990) in which the channel flow is introduced independently of the sample through a frit similar to the depletion (upper) wall and the field flow. This channel-flow frit is implanted within the upper wall but separated from the field frit by an impermeable dam. This method of relaxation is gentler than the stopflow procedures, limiting sample adsorption onto the membrane and shear effects on fragile polymers, but requires careful introduction of the sample into the fractionator channel.

Liu *et al.* (1991) compared the effectiveness of flow splitters, frit elements and stopflow relaxation for latex particles. Stopflow gives better resolution with less zone broadening but a less stable baseline. The performance of the flow splitters and frit elements is similar, but as the two FFF cells used had different widths comparison is limited. There exists limited empirical data for further comparison with model solutes, and none for the fractionation of synthetic polymers and polyelectrolytes. For shear-sensitive macromolecules, Giddings (1990) provided calculations demonstrating the reduction in shear stress by the use of split or frit relaxation.

4.1.1.9 Signal enhancement

The overloading effect (Section 4.1.1.7) places an upper limit on sample volume and concentration. A sample in a FFF channel is compressed onto the accumulation wall and by directing only the carrier liquid eluting near this wall to the detector the signal is improved and allows smaller sample sizes. This skimming procedure may be implemented using a flow splitting at the outlet exactly analogous to the inlet stream splitting. Wahlund *et al.* (1986) demonstrated the feasibility of this method with two sample outlets, one placed low in the channel and another higher near the upper (depletion) wall. Although the increase in signal did not match the ratio of the flows, suggesting some sample does elute out the carrier outlet stream, the increase in signal is useful nonetheless. The difficulties associated with tubes protruding into the narrow channel are considerable, but the method has been adopted for commercial flow FFF channels by installing a dam in the upper wall. The dam allows excess carrier to be skimmed rather than diluting sample in the detector line, as shown in Figure 4-4, essentially the reverse of the frit inlet method (Section 4.1.1.8).

Figure 4-4 Signal enhancement using a frit outlet to skim the majority of the carrier to avoid detection difficulties due to dilution during fractionation.

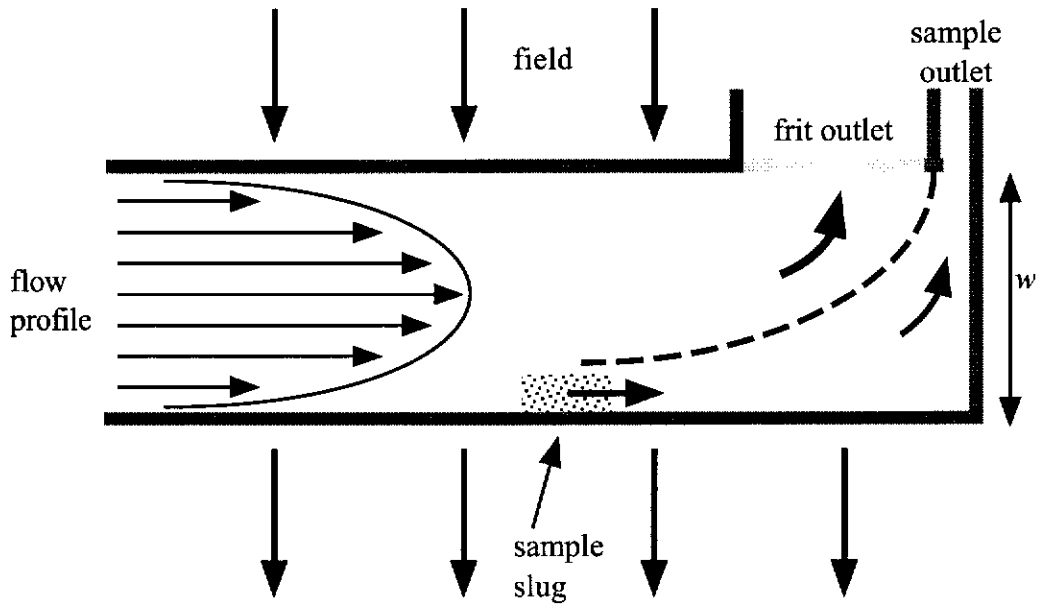

4.1.1.10 The asymmetric variant

A variant to the flow FFF methodology is to replace the porous upper (depletion) wall with an impermeable glass window, developed by Wahlund and Giddings (1987). Carrier liquid may be fed in both ends of the channel and passes through the accumulation wall, such that the carrier acts as both the axial and field flow. The theoretical basis for the technique is complicated, as the two flows do not act independently with the solute. Nevertheless, the technique has been shown to work well, with many applications provided for biological samples (Section 4.1.3).

4.1.2 FFF optimisation

The theoretical basis of FFF suggests a number of methods to optimise the resolution of eluting samples. The theory allows optimisation of the channel flows and physical dimensions of the channel, but does not account for optimisation of the sample interacting with the carrier fluid and membrane. This section outlines the issues and strategies involved.

Sample optimisation involves minimising the injected volume while using the lowest detectable concentration. Large volumes provide an overly broad sample pulse, which will only increase in breadth during passage through the FFF channel. At the same time, a low volume of highly concentrated sample will prevent the analytes from behaving independently. High concentration of polymers are a concern, as the local viscosity must increase, giving rise to effects such as overloading, peak asymmetry, or the polymer eluting as a gelatinous slug. Increasing the molecular mass of a polymer will, for a given mass, reduce the number of molecules present and thus higher concentrations of increasingly viscous sample are required to ensure a signal from a concentration sensitive detector. The development of sample

enhancement methods (Section 4.1.1.9) reduces the lower sample volume and concentration limits such that overloading of the sample should be always avoided.

Higher channel flow rates (increased $\dot{V}$) shorten retention times, but increase the non-equilibrium contribution linearly. This may be overcome by increasing $\dot{V}_c$, as the non-equilibrium contribution is dependant to the first power in $\dot{V}$ and third power in $\dot{V}_c$, to give a net second power decrease to non-equilibrium effects for a proportional increase of both flow rates (Wahlund *et al.* 1986). However, this is a "brute-force" method, as too high a field may permanently adsorb the solute onto the membrane and lead to temporary immobilisation or permanent sample loss.

Many of the zone broadening considerations may be offset with intelligent channel design. The channel thickness w is a parameter fundamental to the equations. The critical parameter λ, and therefore retention of sample, is dependent upon w^{-2} and by using channels as thin as possible both resolution and selectivity is improved. However, as channels get thinner the effects of membrane roughness on the laminar flow is enhanced and non-equilibrium effects increase. This is not a concern in the mirror-smooth thermal FFF channels, where spacers of less than 0.1 mm thickness are routinely used, but for flow FFF 0.25 mm is a practical minimum thickness.

To make the channel as short as possible limits the contributions of pulse injection to band broadening, as this increases with the length of the channel. Compared to other techniques the efficiency of FFF, as measured by the height equivalent of a theoretical plate, is quite poor and the good resolution available to FFF is a function of the excellent mass transfer characteristics of the open channel. By shortening the channel length to limit the band broadening the cost is therefore to the available resolution.

An alternative channel design is to make the channel narrower over its length to reduce sample dilution for improved detection. Litzén and Wahlund (1991) utilised a

trapezoidal channel, as shown in Figure 4-5. As the sample progresses through the channel, the mean carrier velocity increases towards the narrow end of the channel in accordance with Pouiselle's Law, thereby counteracting the entropic effects of sample dilution during elution due to longitudinal diffusion.

Figure 4-5 Channel designs for flow FFF: (a) standard rectangular and (b) trapezoidal.

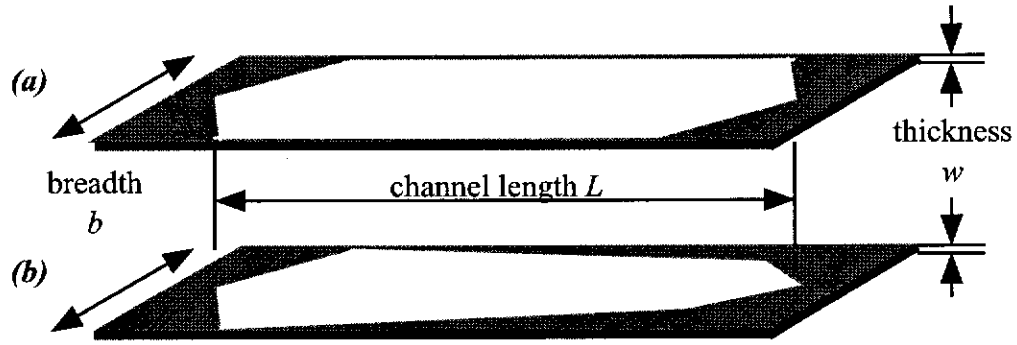

The theory of FFF is derived from the hydrodynamic behaviour of particles in an ideal channel and does not account for the carrier or membrane properties. Both of these factors may exert an influence upon the fractionation. Carrier characteristics are chosen to prevent coagulation of particles or phase separation of polymeric solutes. Membrane are chosen to be sufficiently porous to allow a good carrier flux, while retaining the smallest solutes and at the same time being as smooth, incompressible and swell-resistant as possible. The membrane surface chemistry must also be compatible with the carrier liquid and sample, such that irreversible adsorption cannot occur. Most membranes in the fractionation of polymers will require a conditioning run to place a monolayer of adsorbed material on the *ca.* 0.005 m^2 of exposed membrane surface. This is in contrast to SEC, where the surface area is typically many thousand times greater and sample loss due to adsorption is a continual problem (Benincasa and Giddings 1997).

The final approach to optimising a FFF system is reducing the dead volume of the system, an important consideration in any liquid chromatography apparatus. Tubing is chosen to be as short and as narrow as possible. Limits to this approach

are the pressure drop along the tube and sample shear considerations, as discussed for PAAm in Section 3.5.

It is clear that the theoretical basis to FFF lends itself to strategies to optimise the system, although some aspects are choices based upon experimental conditions and demand lengthy studies to select.

4.1.3 Previous studies of macromolecules by Flow FFF

The first significant paper on the fractionation of synthetic water soluble polymers by flow FFF was by Giddings *et al.* (1978), who converted commercial polystyrenes to the corresponding sulphonic acid salts and polyacrylic acids to the sodium salt with molecular mass ranges $0.02\text{-}0.5\times10^6$ and $0.15\text{-}2\times10^6$, respectively. Transformation of the elution data into Stokes' diameters for the polyelectrolytes demonstrated the diameter calculated was dependent upon the sample size and the salt concentration. The self-consistency was demonstrated by running the experiment under different field strengths. While the position of the elution changed, the shape of the distribution remained constant.

Recent publications on the normal-mode symmetric flow FFF technique as applied to synthetic water soluble polymers include Giddings *et al.* (1991), Giddings *et al.* (1992), Benincasa and Giddings (1992) and Kirkland *et al.* (1992). The polymers so studied included cationic (polyvinylpyridine M_W $28\text{-}240\times10^3$), anionic (polystyrene sulphonate M_W $4\text{-}690\times10^3$) and nonionic (polyethylene oxide M_W $18\text{-}996\times10^3$; polyvinylpyrrolidone M_W 387×10^3). Giddings (1989) considered flow FFF suitable for macromolecules in either aqueous or organic solvents. Although this has been demonstrated to be true by Kirkland and Dilks (1992), the fractionation in organic solvents is more rapid and selective in thermal FFF, while flow FFF elution profiles are characterised by broad, tailing peaks in any solvent (Benincasa and Giddings

1992). Benincasa and Giddings (1992) also reported oddities in the aqueous fractionation of anionic polystyrene sulphonates with varying ionic strength. The behaviour was suggested to be an effect of reduced sample loading but the anomaly remained unsolved. The fractionation of anionic polystyrene sulphonate with molecular mass over 1×10^6 has been recently reported by Thielking and Kulicke (1996) in 0.1 M sodium nitrate. The elution profile showed standards at this size have a very broad molecular mass distribution. This paper also presented a linear decay field program, which did improve the elution profile.

Biological macromolecules have attracted more attention than synthetics. Early investigation utilised proteins (Giddings *et al.* 1976) although separation of DNA fragments under thirty minutes has been reported (Liu and Giddings 1993). The asymmetric flow FFF variant (Section 4.1.1.10) has also been employed successfully with biological macromolecules (Wahlund and Litzén 1989, Litzén 1993). Of particular interest is the analysis of two viruses of molecular masses 1.8×10^6 and 50×10^6, both eluting in less than five minutes (Litzén and Wahlund 1989). Unfortunately, the paper presents no experiment demonstrating whether a mixture of these viruses could be separated by the technique. Asymmetric flow FFF also requires a membrane, so success with these samples suggests strongly that the same method may be transferred to symmetric fractionation.

The single published fractionation of PAAm over 1×10^6 was reported by Benincasa and Giddings (1997) in dilute sodium sulphate carrier, and presents an elution profile with a half-height width over 90 min. No molecular mass calculations were provided for PAAm. Eluting polymer was detected by UV absorbance at 200 nm, which given the poor chromophores of PAAm in a background of 25 mM Na_2SO_4, requires an astonishingly sensitive detector. The propensity for PAAm to undergo intermolecular interactions and physical entanglement was cited in this paper as complicating effects. An overloading study for molecular mass 0.5×10^6 noted with some surprise the lack of overloading effects for PAAm up to 13.6 μg of sample.

This result shows analytical fractionation of PAAm by FFF is feasible, although the results presented by these authors clearly represents only preliminary work.

4.1.4 Flow FFF summary

The flow FFF technique provides a separation based on sample diffusion coefficients. More powerful are the possibilities of programming the fractionation to tune the separation as it is occurring. Flow FFF has only a few constraints, such as eliminating sample-membrane interaction and locating the critical size of the steric inversion. When accounted for, the elution time of a sample may be converted directly to diffusivity and a molecular mass distribution.

4.2 EXPERIMENTAL

4.2.1 Reagents

Purified water was delivered from a Milli-Q Plus 185 unit with resistivity over 18 MΩ cm^{-1} (Millipore, Bedford, Massachusetts). AR grade formamide, sodium chloride, nitric acid and acetic acid (BDH, Poole, England) were used as received. All dilute solutions were freshly vacuum filtered through a 0.22 μm filter (Millipore, type GV).

PAAm standards were obtained from Polymer Laboratories (Birmingham, England) with cited weight-averaged molecular masses 0.35, 1.14, 5.55 and 9.00×10^6 and polydispersity indices *ca.* 2.3. Aqueous solutions of standards were prepared in Milli-Q water freshly filtered through a 0.02 μm syringe filter (Anotop 25 Plus, Whatman, Maidstone, England). PAAm stock solutions were produced by adding portions of polymer piecewise to solvent, agitated manually until the polymer had commenced swelling, then shaken overnight on an orbital shaker at 150±5 rpm (Braun TM-1, Basel, Switzerland). All solutions were prepared in a laminar flow cabinet (Gelman HWS, Ann Arbor, Michigan).

The commercial PAAms used were Magnafloc 333 and Magnafloc 351 ("M333" and "M351", respectively) from Allied Colloids (Bradford, England), and FA920VHM, FA920BMP and AN910VHM from SNF-Floerger (Saint-Etienne, France), all used as flocculants in the mineral processing industries except FA920BPM, which is used for slurry rheology modification. Polymer solutions were made up in Milli-Q water freshly filtered through a 0.1 μm filter (Millipak 40 "gamma gold", Millipore). PAAm stock solutions were produced by adding portions of polymer piecewise to solvent pretared in a screwtop glass jar in a manner described above. Stock concentrations used were, in units of mg mL^{-1}, 3.98 (M333), 4.08 (M351) 3.85

(FA920VHM), 4.12 (FA920BPM) and 4.90 (AN910VHM). For the low-concentration M333 experiments, solutions at 2.07 and 0.50 mg mL^{-1} were prepared.

All commercial flocculants were checked for hydrolysis and imidisation by ^{13}C NMR (Chapter 7), and by CHN elemental analysis (performed by Graeme Rowbottom, Central Science Laboratory facility, University of Tasmania). The cited 10% anionicity of AN910VHM was 10.3% by NMR and 10.2% by elemental analysis. No other PAAm samples showed detectable hydrolysis. No polymer solution exhibited detectable imidisation.

Polystyrene-divinylbenzene latex standards were obtained from Duke Scientific (Palo Alto, California) and Coulter Electronics (Luton, England) for the sub- and supramicron diameters, respectively.

4.2.2 Scanning electron microscopy

Images were taken of carbon sputtered membrane surfaces in a Jeol JSM-5800LV (Tokyo, Japan) at 20 keV accelerating potential.

4.2.3 Flow FFF apparatus

The arrangement of the fractionator and associated equipment is presented in Figure 4-6. The flow FFF channel was type FO-1000 from FFFractionation (Salt Lake City, Utah) with ceramic upper and lower frits in an acrylic block. The upper frit was split into two sections, with the last 20 mm used as a frit outlet (Section 4.1.1.9). The channel shape was defined by a 0.25 mm thick Teflon spacer sheet sandwiched between the upper and lower blocks. The channel was symmetric 20 mm wide and 260 mm long tapering a further 20 mm (illustrated by Figure 4-5a) to total length 300 mm.

Figure 4-6 Flow field-flow fractionation apparatus. Tubing is shown colour-coded by flow type: red = recycling field flow; blue = channel flow; green = flow from the frit outlet; purple = flow to detectors. Tubing for stopflow relaxation omitted for clarity.

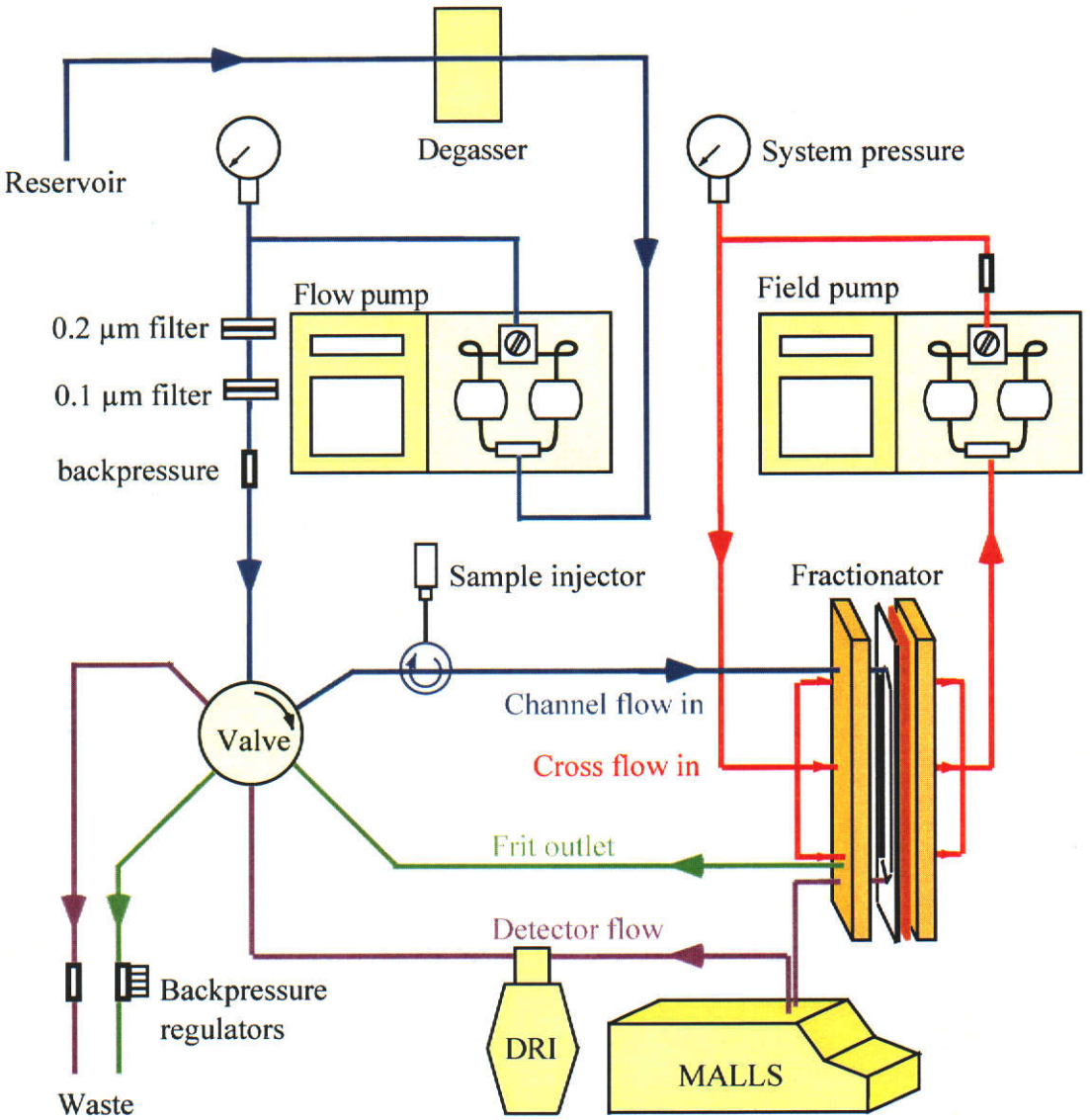

Between the spacer and the lower frit was placed an asymmetric regenerated cellulose membrane (Amicon YM-10, Houston, Texas) rated at 10^4 molecular mass cut-off. The upper and lower blocks sandwiched the spacer and membrane between them with eighteen evenly spaced bolts torqued to 3.5 N m.

All polymer-carrying tubing ("channel flow in", "detector flow") to and from the FFF channel used 0.51 mm internal, 1.59 mm external diameter (0.020" i.d., 1/16'' o.d.) polyether-ether-ketone (PEEK) tubing. Tubing unions, tees and crosses

were also made of PEEK with matching bores, sealed to the tubing with PEEK nuts and polypropylene ferrules. Other liquid-carrying lines consisted of 3.2 mm (1/8") polypropylene tubing. The device was plumbed as described below.

From the magnetically stirred carrier liquid reservoir of 1 L capacity, the carrier passed a 10 μm pore inlet filter and a Shimadzu GT-102 inline degasser (Shimadzu GT-102, Kyoto, Japan) through polypropylene tubing. The line connected into a dual-piston reciprocating pump (Shimadzu LC-10AD) with a 10 μL piston volume. The pump is equipped with a 200 μL pulse dampener and 2 μm line filter. The flow line passed through another inline filter rated at 0.22 μm (Millipore GV, in a stainless steel Millipore filter holder) then a 340 kPa (100 psi) PEEK-Teflon backpressure regulator. The 340 kPa regulator provides sufficient backpressure for the pump's checkvalve operation. The flow line passed a ten-way valve (Valco, Houston, Texas) and entered a sample injector (Rheodyne 7125, Cotati, California) equipped with a 20 μL stainless steel loop, before a final 300 mm (60 μL volume) length of PEEK tubing to enter the FFF cell. The positions of the ten-way valve during normal operation and stopflow are shown by Figure 4-7.

The crossflow was generated by a second Shimadzu LC-10AD pump, passing an identical backpressure regulator and system pressure meter (Ashcroft, Germany) and was introduced behind the upper frit at three separate entry ports into the upper field chamber. Beneath the lower frit, in an identical chamber, carrier liquid was withdrawn at the same rate and recycled back to the same crossflow pump, such that during the stopflow procedure this is a closed loop.

Behind the outlet frit, effectively the last 20 mm of the channel, bulk carrier liquid was skimmed off the compressed sample zone to emerge through another PEEK tube, into the Valco valve and out to waste at a rate regulated by a stainless steel needle valve (Nupro, Willoughby, Ohio).

Past the frit outlet the final detector line entered a UV detector (Shimadzu SPD-10AV) at 230 nm, then a Wyatt Technology (Santa Barbara, California) DAWN-DSP multi-angle laser light scattering ("MALLS") photometer. The MALLS detector uses a 5 mW vertically polarised laser at 632.8 nm wavelength, as described in Section 3.2.8. After the MALLS detector, the effluent entered a further 600 mm (120 μL) tubing to a Wyatt Technology Optilab 903 differential refractive index (DRI) detector. The flow line then re-entered the Valco valve, through a crosspiece and 140 kPa (40 psi) PEEK-Teflon backpressure regulator, to emerge into waste.

The ten-way Valco valve is arranged such that the flows as described operate during elution, while during the stopflow procedure the channel flow does not enter the injector-channel-detector stream but bypasses instead into a length of 0.26 mm (0.010") i.d. PEEK tubing (Figure 4-7). The bypass tubing is cut to provide backpressure identical to that generated by the injector-channel-detector stream, thereby limiting the system pressure changes during stopflow operation. The arrangement differs from that suggested by FFFractionation in their commercial systems, in that the detector stream is included within the stopflow circuit, and the sample does not pass the Valco valve itself, eliminating a high shear region.

The MALLS detector was calibrated and normalised (as described in Section 3.2.8) and set to ×100 sensitivity by removing all jumper leads. The DRI detector was installed with a P100 cell (10 mm sampling length) and set to ×20 attenuation. The refractometer was kept at 35.0±0.1°C by a Grant LTD 6 water bath (Cambridge, Great Britain) connected together with Tygon tubing.

Figure 4-7 Function of the ten-way valve showing operation during (a) normal elution and (b) stopflow modes. Under normal operation the fractionator and detectors are connected to the channel pump and signal enhancement (frit outlet) is governed by the needle valve. During stopflow the FFF cell is not subject to the channel flow, while the bypass loop simulates the pressure drop across the FFF cell and detectors.

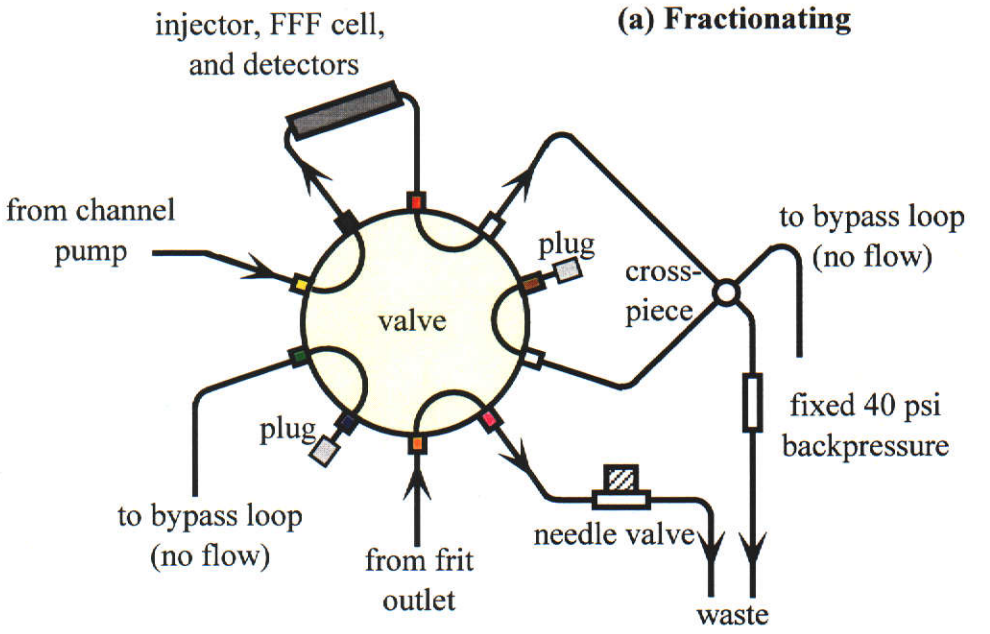

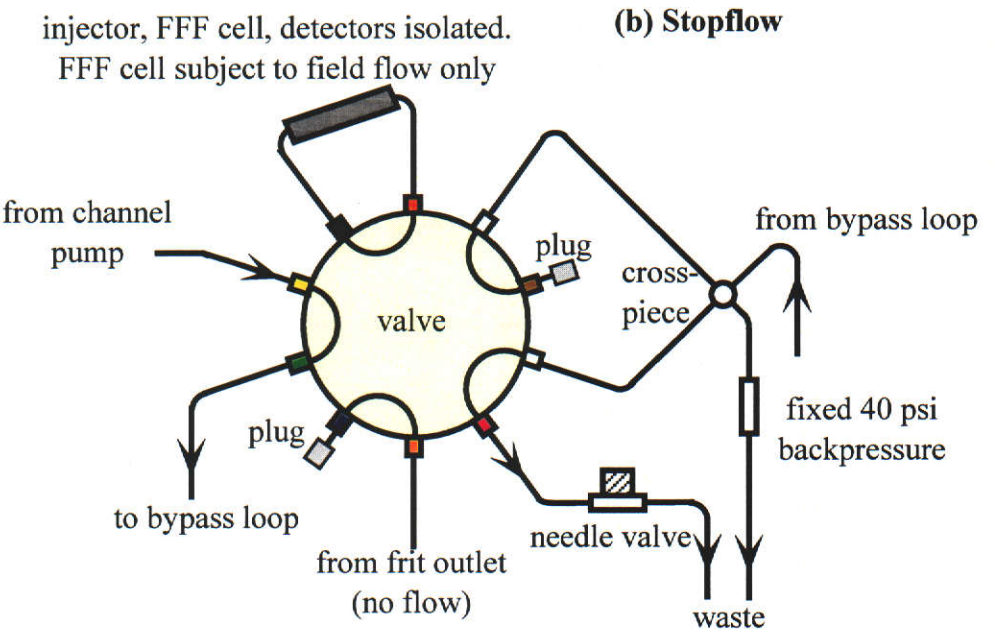

4.2.4 Static ultraviolet spectra

The UV spectra of selected solutions were measured on a Hewlett-Packard 8452A diode array spectrophotometer (Palo Alto, California) using a quartz cell of path length 10 mm.

4.2.5 Light scattering data processing

Molecular mass determinations required the MALLS detector be used as a chromatographic detector. The DRI was the primary concentration detector, with refractive index increment $(\frac{dn}{dc})$ of 0.190 mL g^{-1} and calibration constant 1.0327×10^{-5} rad^{-1} (±1.4%). The UV output was monitored routinely but not used for data processing. A set of MALLS detectors was chosen which produce the lowest residual error of molecular mass. This detector set was used consistently. For the chromatographic output, fitting by the Debye formalism with a fourth-order angular dependence gave the most reasonable results with the lowest error for all experiments. Light scattering data was processed by ASTRA 4.20 software from Wyatt Technology. The use of the MALLS and DRI detectors to characterise fractionated PAAm is described in detail in Section 4.3.6.

4.2.6 Molecular mass calculation

With a MALLS detector characterising FFF eluent, molecular mass can be calculated in two ways. Direct measurements arise when the FFF acts passively, separating the sample into near monodisperse slices for treatment by the MALLS according to equation (2-5). Molecular masses may also be calculated indirectly from FFF retention. Equations (4-15) and (4-21) show retention is dependent solely upon

diffusion coefficient for flow FFF under normal mode operations. The diffusion coefficient is in turn strongly dependent upon molecular mass according to the standard expression

$$D = A\ M_w^{\ b} \qquad (4\text{-}27)$$

where A and b are empirically determined constants for a given polymer-solvent-temperature system. Substitution of equation (4-27) into (4-15) or (4-21) gives the final indirect determination of molecular mass.

4.2.7 Mean molecular mass determination of commercial flocculants

4.2.7.1 Viscometry

Capillary viscometry, as described in Section 3.2.7, was performed with an Ubbhelode viscometer. Complementary viscometry measurements were made on an inner-rotating cylinder viscometer (Brookfield, Stoughton, Massachusetts) equipped with an UL adaptor. In both cases viscosity measurements were made over a range of concentrations and extrapolated to infinite dilution.

4.2.7.2 Static light scattering

The MALLS detector was used for batch determinations of molecular mass, using described calibration and normalisation methods. Stock polymer solution was diluted 1:1 with 0.22 μm filtered 0.20 M NaCl. Solutions were extruded slowly from 10 mL syringes (Terumo, Elkton, Maryland) by a syringe pump (Razel A-99, Stamford, Massachusetts) at 8 mL hr^{-1} through a length of 0.51 mm i.d. PEEK tubing and into the K5 flow cell (Section 3.2.8). Solvent offsets were taken from 0.10 M NaCl. Processing of the light scattering data used detectors 6 through to 17

with a fifth order angular fit and first order concentration fit by applying DAWN 3.01 software with the AURORA module from Wyatt Technology.

4.2.8 Degradation studies

Commercial PAAm was degraded by an XL2020 ultrasonic horn (Heat Systems, Farmingdale, New York) rated to 475 W at 20kHz. A 100 mL beaker was filled with 75 mL of stock polymer and a magnetic stirrer introduced. The beaker was placed in a larger volume of water to act as a crude temperature regulator. The horn was immersed into the centre of the solution and operated at 15% power (60 W) over a 20 s pulse period, using a 5 s pulse following a 15 s pause to limit sample heating. Reported degradation times refer to total degradation time rather than sonication time. Degraded polymer was allowed to cool before fractionation. No solution deoxygenation steps were taken, so avoiding radical depolymerisation.

4.3 METHOD DEVELOPMENT

There are a number of issues that must be addressed to apply the flow FFF-MALLS technique to characterising PAAm. Flow FFF fractionates samples based on their diffusion coefficients, which according to the Stokes-Einstein equation are related to the sample's hydrodynamic diameter. However, the rms radii, determined from light scattering, are not directly comparable with hydrodynamic diameters. FFF theory also assumes there are no sample-membrane interaction during elution (Section 4.1.2). Ideally the dead volume of the tubing is minimised but narrow tubing may agglomerate or shear the sample (Section 3.5). For very large samples, the possibility of elution under the "steric" mode (Section 4.1.1.5) and coelution of sample is of concern. The sample must be concentrated enough for detection, but for polymers the viscosity creates an upper concentration limit due to sample-sample interaction and poor mass transfer, while a large volume of low concentration sample interferes with resolution (Section 4.1.1.6). Only if all these criteria are satisfactorily addressed can a meaningful molecular mass distribution be provided.

This Section describes the means by which the FFF system was made operational. The optimisation process was subdivided into considerations of cell materials, cell flow rates and hydrodynamics, membrane surface and carrier chemistry problems. Complicating the optimisation process was the now apparent need to optimise these interacting variables in a specific order. While this process involved extensive experimentation, including several unsuccessful lines of approach, only the results relevant to the eventual outcome will be discussed. A final subsection describes the processing of the detector output.

4.3.1 FFF cell materials

During the method development process, numerous FFF cells made from a range of materials were investigated. The cell design on which all initial studies were focussed featured metallic frits (sintered stainless steel, mean pore 5 μm) and a body of nylon. These materials were chosen to resist highly caustic conditions found in the Bayer process for refining bauxite to alumina. Cell dimensions matched the commercial type FO-1000 from FFFractionation (Salt Lake City, Utah) as described in Section 4.2.3. The cell body developed a distinct distortion along its length during a year of use. It is unclear whether this warping may be attributed to thermal expansion of the stainless steel frit, or a tension generated when the upper and lower bodies of the cell were bolted together. This effect lead to continuous leakage from the cell and deviation from ideal FFF parallel plate behaviour.

A secondary effect noted with this cell was that model polystyrene latex samples took at least twice as long to elute as expected (Section 4.3.2), even before the cell distortion dominated. Although the hydrodynamic and membrane effects were not fully optimised at this time, the influence of metallic frit cannot be discounted, perhaps as an electrostatic interaction between the frit and polystyrene latex retarding elution. All reported flow FFF studies have used ceramic frit materials and the issue of frit material modifying membrane effects remains unknown.

The fractionator used in all subsequent work reported in this study was a commercial FO-1000 cell with aluminosilicate frits of mean pore size 10 μm installed into a clear Perspex (polymethyl methacrylate) cell body.

4.3.2 Hydrodynamics

For a 2.5×10^{-4} m wide channel at 298 K and aqueous carrier viscosity of 8.90×10^{-4} kg m^{-1} s^{-1} (Weast and Astle 1982), the elution time (t_r, seconds) for a particle of Stokes' diameter d_s under isocratic conditions can be calculated from substitution into equation (4-20)

$$t_r = \frac{\pi\eta w^2}{2kT}\frac{\dot{V}_c}{\dot{V}}d_s = \frac{1.75\times10^{-10}}{8.23\times10^{-21}}\frac{\dot{V}_c}{\dot{V}}d_s \qquad (4\text{-}28)$$

This expression is not corrected for the frit outlet, in which the flow through the detectors will be slower, or for local viscosity inhomogenities due to sample, but is a good approximation for well retained solutes. It must also be noted that the manufacturer-cited latex sample diameters are characterised by electron microscopy, which is not identical to the sample's d_s. A polymer latex (cited diameter of 0.265 μm) eluted with a peak at 22.4 minutes under cross- and channel flow rates of 0.25 and 1.00 mL min^{-1}, which upon substitution into the above equation gave a measured Stokes' diameter of 0.25 μm. Changing the channel flow to 0.50 mL min^{-1} and injecting 0.121 μm diameter latex, a peak eluted after 19.5 minutes for a calculated diameter 0.11 μm. The good agreement between the calculated diameter and cited sample value demonstrates satisfactory fractionator operation for this ideal sample.

4.3.3 Membrane effects

From the MALLS sizing, PAAm coils are approximately 0.35 μm diameter for a molecular mass of 2×10^7, so an expected size for 1×10^6 molecular mass is 0.09 to 0.15 μm, dependant upon polymer configuration. Injection of PAAm standards, at cross- and channel-flow rates 0.25 and 0.50 mL min^{-1} respectively, repeatedly showed no elution apart from a void peak. Repeating flow rates used by Benincasa

and Giddings (1997) did not show any polymer elution at all, even using the extremely sensitive light scattering detector. However, a molecular mass sensitive separation did occur when the stopflow relaxation was not used, albeit with poor resolution. This observation suggested that compressing the polymer, even in the gentle crossflow, is either able to agglomerate the coils or allows a membrane adsorption effect.

An extensive series of experiments were used to select membranes for use in the FFF system. Most promising were polypropylene (Accurel 1E-PP, Akzo-Nobel, Wuppertal, Germany), supported regenerated cellulose (PLTK, Millipore, Bedford, Massachusetts; YM-10, Amicon, Houston, Texas) and 0.1 μm pore polycarbonate (Poretics, Livermore, California). Figure 4-8a shows a mix of three polystyrene latices (0.12, 0.26 and 0.50 μm) adsorbed onto the polypropylene membrane. The pore size is large enough to account for the observed sample retardation, as small samples permeate the membrane. Fractionation experiments repeated with the smoother surfaced polycarbonate membrane (Figure 4-8b) allowed elution of latex standards at predicted peak elution times. Clearly, surface texture of the membrane is a consideration for flow FFF. The elution experiments repeated with PAAm showed a very broad peak when using polypropylene and cellulose-based membranes, but no elution whatsoever in the presence of the polycarbonate. From these observations it is concluded that while surface texture is a consideration to optimise the system, sample-membrane interactions determine if elution may be achieved at all. A corollary is that polypropylene and polycarbonate membranes exhibit near pH independence, while the surface chemistry of the regenerated cellulose membrane may be influenced by carrier solutions. Therefore, for all experimentation the YM-10 regenerated cellulose membrane was used.

Figure 4-8 SEM of flow FFF membranes after fractionation of mixed 0.121, 0.265 and 0.497 μm polystyrene latex standards. Membranes are (a) polypropylene and (b) polycarbonate.

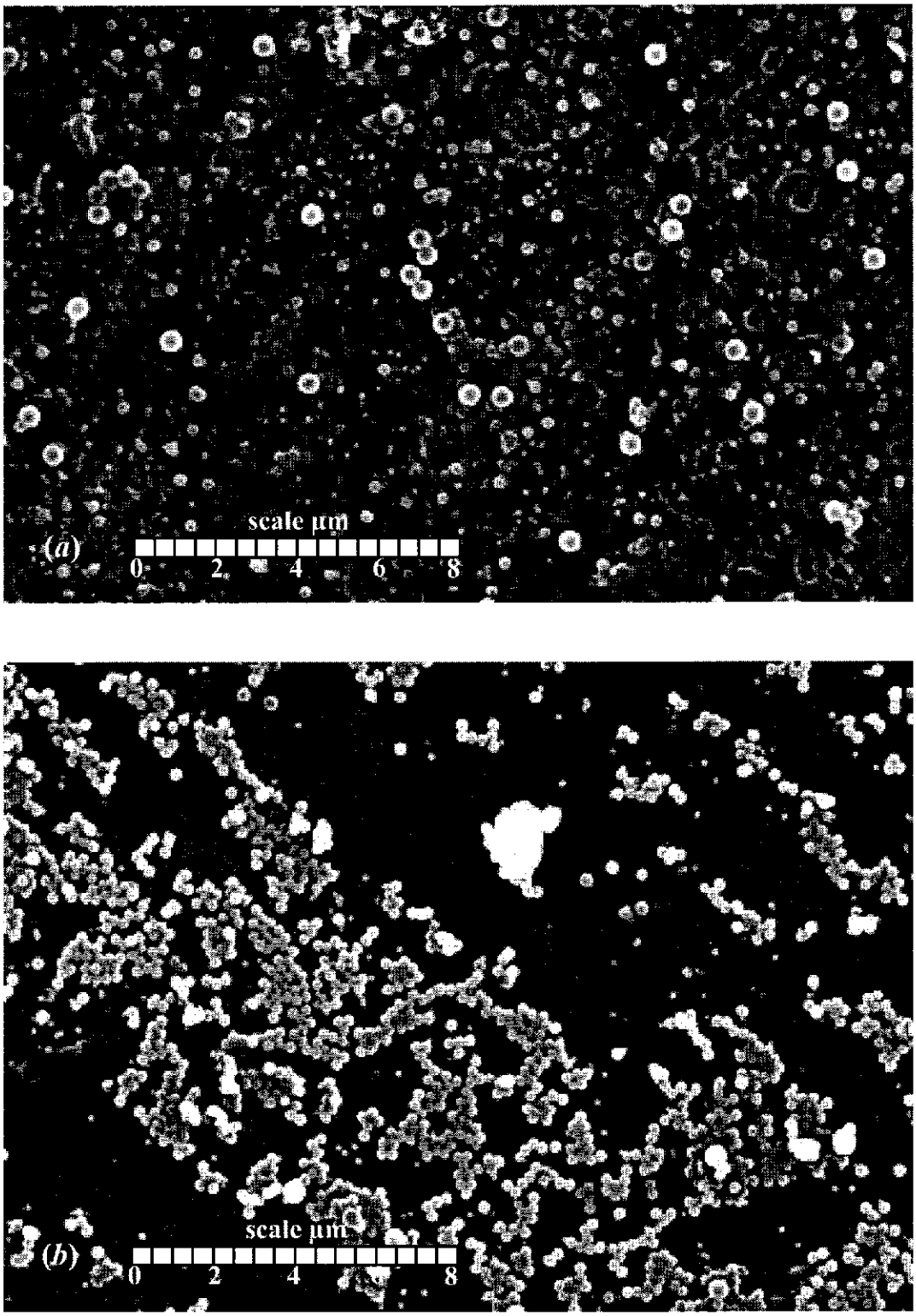

4.3.4 Carrier chemistry

It was shown in Chapter 3 that the existence of agglomerates in PAAm may be suppressed by the presence of formamide, which favours polymer-solvent over polymer-polymer interaction. The presence of acetate has a similar effect, and introducing acetate into the system as acetic acid may also protonate PAAm slightly (as shown in Figure 4-9), thereby enhancing intermolecular repulsion. Amides are weakly basic compared to other carboxylic acid derivatives, due to the reduced electronegativity of the nitrogen as compared to the oxygen; for example, acetamide has a pK_a in the range -0.5 to -1.0 (Sykes 1986, p. 68). It is feasible by this mechanism that the presence of acid leaves an amide moiety charged. For PAAm, if only 10% of the amide groups accept the charge, self agglomeration becomes less likely due to electrostatic repulsion. The electrostatic repulsion will "stiffen" the polymer from a spherical to rodlike conformation in a low ionic strength medium.

Figure 4-9 Effect of pH on the amide moiety.

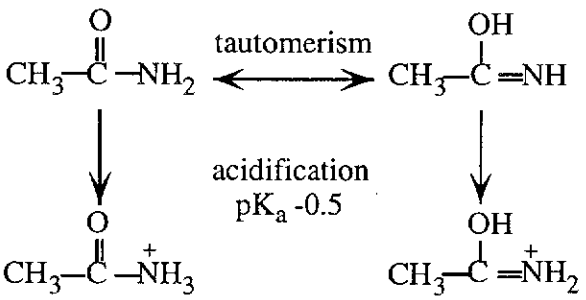

Injections of 20 µL of PAAm standards, prepared to *ca.* 5 mg mL^{-1} and aged for two days, were made into the FFF cell. The carrier solution was 2%-v/v formamide in water, adjusted to pH 2.5 with acetic acid, with channel and field flowrates 0.30 and 0.25 mL min^{-1}, respectively. The times to peak maxima from injection are given in Table 4-1.

Table 4-1 Elution times and calculated sizes of polyacrylamide standards.

M_w of standard	Elution time (peak)	Stokes' diameter (calc'd)
1.14×10^6	18.3 min	0.173 μm
5.55×10^6	30.3 min	0.287 μm
9.00×10^6	40.0 min	0.379 μm

Although conversion to the equivalent Stokes' diameter uses an estimated viscosity (local inhomogenities preclude an accurate calculation), there is a reasonable size progression. As the nature of the polymer-solvent system is invariant, the calculated diameter increases at some power reflecting the polymer coil packing density.

$$d_s = K(M_w)^a \qquad \ln(d_s) = a\ln(M_w) + \ln(K) \tag{4-29}$$

A least-squares fit of the data in Table 4-1 using the logarithmic form of equation (4-29), gave a correlation coefficient over 0.98, with the "packing coefficient" $a = 0.37$ indicating a near spherical conformation. Whether this indicates that (a) the dissolution of the microgels from the presence of the formamide aids the fractionation, or (b) the acidity of the carrier influences the cellulose membrane rather than protonating the polymer, is unclear from this result.

PAAm adsorbs weakly in the UV, peaking at 192.5 nm (Soponkanaporn and Gehr 1987) with detection commonly applied in the range 200-215 nm (Holzwarth *et al.* 1988, He *et al.* 1990, de Laat and van den Heuvel 1993). However, the admixture of formamide and acetic acid adsorbs too strongly in the UV range for the PAAm chromophores to be detected, and furthermore produce an erratic refractometer baseline. Although both formamide and acetic acid absorb in the ultraviolet region (acetic acid λ_{max} 208 nm, ε_{max} 32 in ethanol; formamide λ_{max} 205 nm, ε_{max} 58;

Grasselli and Ritchey 1975), the adsorption of an aqueous mixture is greater than the sum components' contributions, possibly arising from a charge-transferring species (Figure 4-10). Unusual properties of formamide-acetic acid mixtures have been observed by Verstakov *et al.* (1981). Further evidence for the presence of such a hydrogen-bonded species is shown by the acidification of the carrier with a mineral acid (nitric acid) instead of acetic acid, which at the same pH eliminates the refractometer oddity.

Figure 4-10 Formamide-acetic acid complex: example dimer.

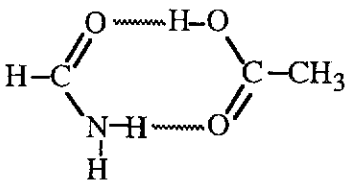

The presence of formamide continues to prevent UV detection of PAAm. Removing the formamide still allowed successful fractionation of PAAm, leaving only nitric acid at pH 2.5 as the carrier solution. This result also clarifies the earlier problem raised on page 160, demonstrating that the presence of the acid, rather than the formamide, is important: membrane effects, more than polymer agglomeration, need be accounted for. The NO_3^- group, like most common anions, also adsorbs below 250 nm (Wieteska 1986) obscuring the PAAm. However, by using more dilute nitric acid, at pH 3.8, a window exists where the polymer is detectable above the nitrate, and the carrier is sufficiently acid to avoid adsorptive loss of the PAAm.

In summary, the optimal carrier for the fractionation of polyacrylamide in a flow FFF cell fitted with a cellulose membrane was found to be dilute nitric acid in Milli-Q water at pH 3.8±0.1, bulk filtered to 0.2 μm.

4.3.5 Shear minimisation

While flow rates through the fractionator should be kept as low as possible to avoid shear-induced agglomeration, this requirement must be balanced by the need to achieve elution within a reasonable time. As discussed in Section 3.5, all polymer-carrying tubing was 0.51 mm diameter and channel flow rate was 0.30 mL min^{-1}, to avoid shear-derived artefacts. There are still points where shear can be influential, such as the syringe loading, but these were also minimised using slow injection.

4.3.6 Characterisation of fractionated PAAm

The light scattering signal of a polymer, as measured by the excess Rayleigh ratio (Section 2.1.3), is dependent upon both molecular mass and concentration. That is, for an equivalent number-based concentration, the light scattering detector signal and angular dependence are greater for larger bodies than smaller. For a polymer eluting from the flow FFF cell, Figure 4-11 shows the output from two of the MALLS detector angles and that from the concentration-sensitive refractometer. Immediately following the void peak, at elution time *a*, the concentration signal is strong while the light scattering is barely above baseline, commensurate with many (high concentration) small bodies (minimal light scattering). At time *b* the light scattering signal is stronger, indicating that polymer coils eluting here have a greater radius than at *a*. Elution at point *c* is similar to *b* but the angular dependence of the measured scattering, combined with the detector response for the low concentration, shows the radii are larger still.

Figure 4-11 MALLS and DRI detector output for fractionated polymer. The blue line follows the concentration-sensitive detector (DRI) while the red line is the MALLS signal. Two angles from the MALLS are shown: at 90° scattering (solid) and at 60° (dashed).

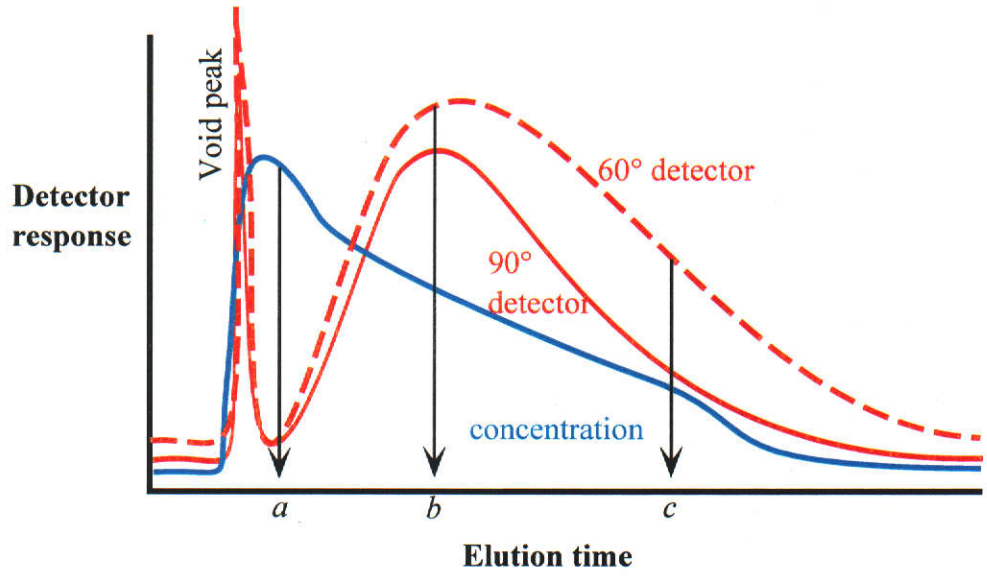

Figure 4-12 Light scattering data using elution times taken from Figure 4-11, as a Debye plot. Dashed line shows the extrapolation to zero angle, from where the mean molecular mass is directly calculated.

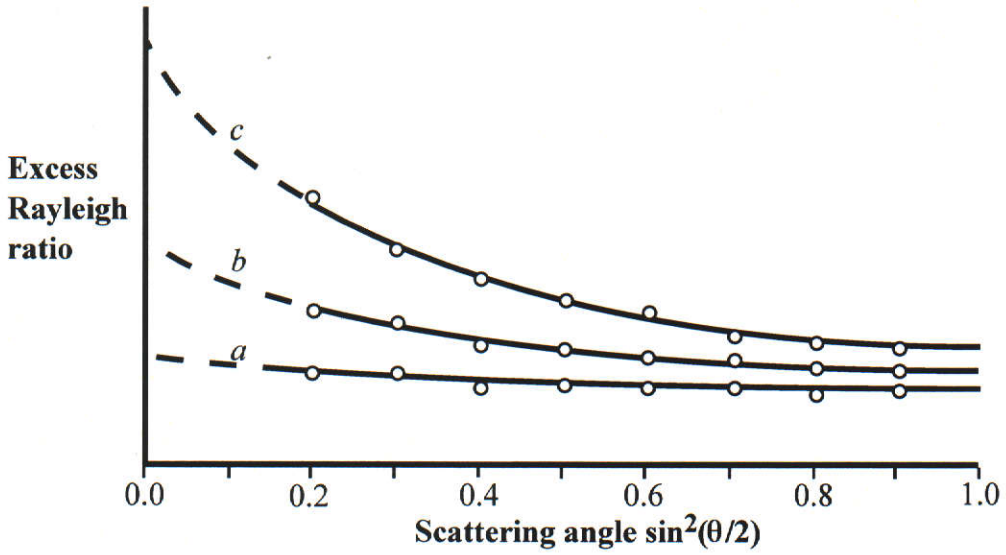

For calculating the molecular mass for each output slice, the excess Rayleigh ratio of the scattering is plotted against scattering angle in a Debye plot, which from equation (2-4) the molecular mass is given from the intercept extrapolated to zero angle. For elution at times *a*, *b* and *c* from Figure 4-11, the light scattering data for all available detectors is presented by Figure 4-12. The effect of the angular dependence upon the extrapolation to zero angle is clear.

For most of the fractionated polymer elution profiles reported herein, only the concentration curve is shown. To present the profile as the scattering intensity at a particular angle requires separation of polymer coil size and concentration effects in the discussion. This complication is avoided through showing elution profiles ("fractograms") in terms of the concentrations generated from the refractometer. Where necessary the light scattering will be explicitly shown.

4.4 *Fractionation of Standards*

4.4.1 *Comparing flow FFF and MALLS*

From the isocratic experiments (Table 4-2), the excessive band broadening of the slower moving components may be limited by field programming (Wahlund *et al.* 1986). Conditions chosen were exponential decay of time constant τ of 60 minutes with the decay commencing immediately after the end of the stopflow relaxation period (τ_0 = 0). Measured outlet flow rates remained constant during the fractionation and therefore the inter-detector time was fixed.

A series of PAAm standards (0.45 mg mL^{-1}) prepared in 0.02 μm filtered water produced the fractionation profiles shown by Figure 4-13, using concentration-sensitive refractive index detection. The stated molecular masses of the standards were the mean values cited by the manufacturer.

The position of the pre-experiment time and stopflow is marked to the left of the plot. Considering only the peak maxima retention times, corresponding to the greatest concentration of polymer, substitution into equation (4-21) gave diffusion coefficients as listed in Table 4-2. For comparative purposes, a diffusion coefficient calculated from the cited mean molecular mass is included (Schwartz *et al.* 1980) for PAAm in water at 20°C. The calculated and predicted diffusion coefficients compare surprisingly well, suggesting the DRI peak maximum is a reasonable indicator of the sample's mean elution time.

Figure 4-13 also exhibits a degree of overlap in the sample elution profiles. Caldwell *et al.* (1988) describe the sources of band broadening in terms of injection volume, mass transfer (non-equilibrium) effects and sample polydispersity. In a subsequent publication, Caldwell (1991) concluded that for polymeric materials the

polydispersity contributions are most significant, and the fractogram is an accurate representation of the molecular mass distribution.

Figure 4-13 Elution profile of PAAm standards with cited mean molecular masses 0.35, 1.14 and 5.55×10^6. DRI detection, 0.45 mg mL^{-1} polymer concentration, exponential field decay with τ 60 min.

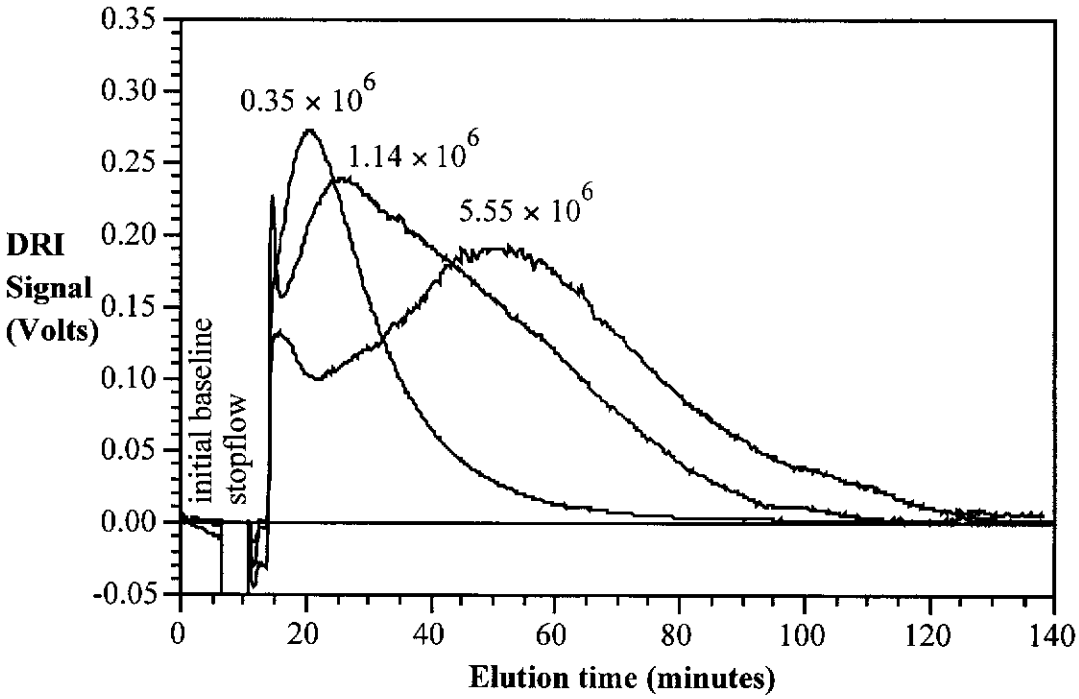

Table 4-2 Elution of PAAm standards under fractionating conditions and prediction based on relationship presented by Schwartz *et al.* (1980).

M_w of standard	Peak elution time	Calculated diffusion coefficient (m^2 sec^{-1})	Predicted diffusion coefficient
0.35×10^6	10.5 min	2.02×10^{-11}	1.43×10^{-11}
1.14×10^6	16.0 min	1.26×10^{-11}	7.64×10^{-12}
5.55×10^6	40.0 min	4.07×10^{-12}	3.30×10^{-12}

The presence of artefacts arising from overloading effects manifest as a fronting asymmetry with a shift of peak concentration to shorter retention times (Caldwell *et al.* 1988). These effects depend strongly upon concentration and viscosity. Figure 4-14 shows for 100 μL injections of a 1.14×10^6 PAAm standard at concentrations of 0.43 and 3.75 mg mL^{-1} the elution profile is unchanged. Loads of up to 375 μg for this standard clearly did not affect the fractionation. The upper limit to the onset of overloading remains unknown, as beyond the high concentration injected PAAm becomes unmanageably viscous.

Figure 4-14 Concentration (overloading) effects for a 1.14×10^6 PAAm standard.

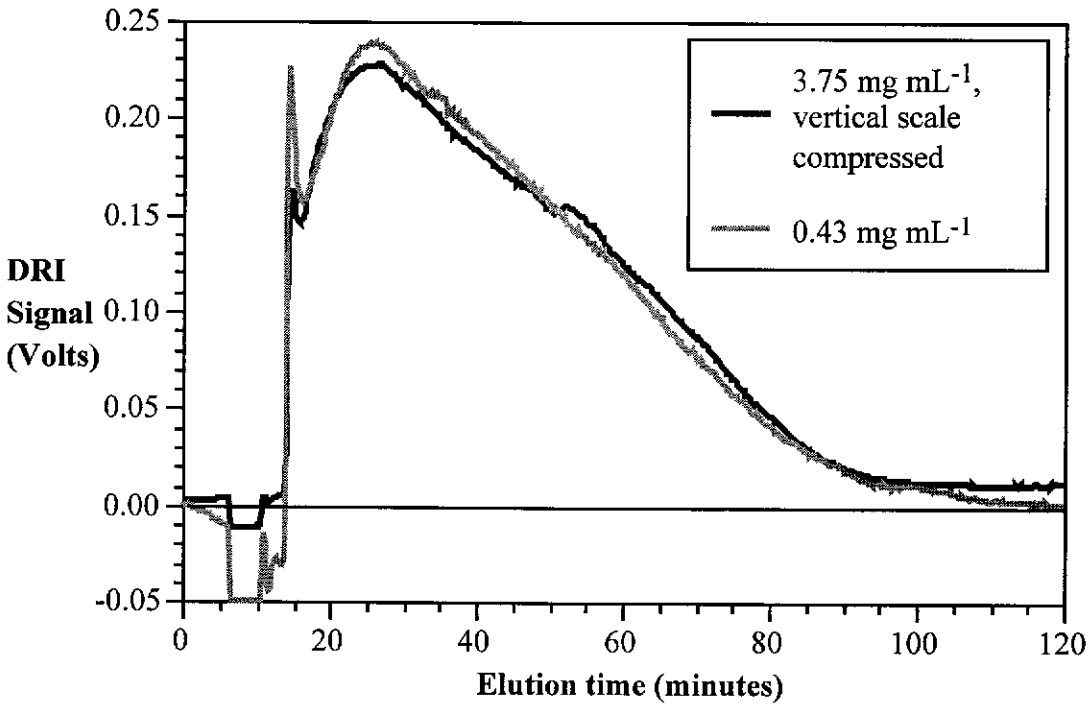

Processing the data using the light scattering and including a 9.00×10^6 standard a molecular mass-elution time relationship is given in Figure 4-15. Figure 4-15 clearly demonstrates that a given polymer molecular mass elutes at a reproducible time, independent of the source, concluding that the broad fractograms are intrinsic to the standards. Interestingly the distribution of the 1.14×10^6 molecular mass PAAm appears unusually wide with species of molecular masses of 50×10^6 present, although it is plausible that they represent many individual polymers intimately

coiled. Confirmation of this result was achieved by changing the fractionation field decay parameter τ to 90 minutes. The molecular mass range and the shape of the elution profile did not change, while the distributions presented in Figure 4-13 shifted to longer retention times in accordance with equation (4-21).

Figure 4-15 Molecular mass determinations by MALLS of PAAm standards eluted from the FFF.

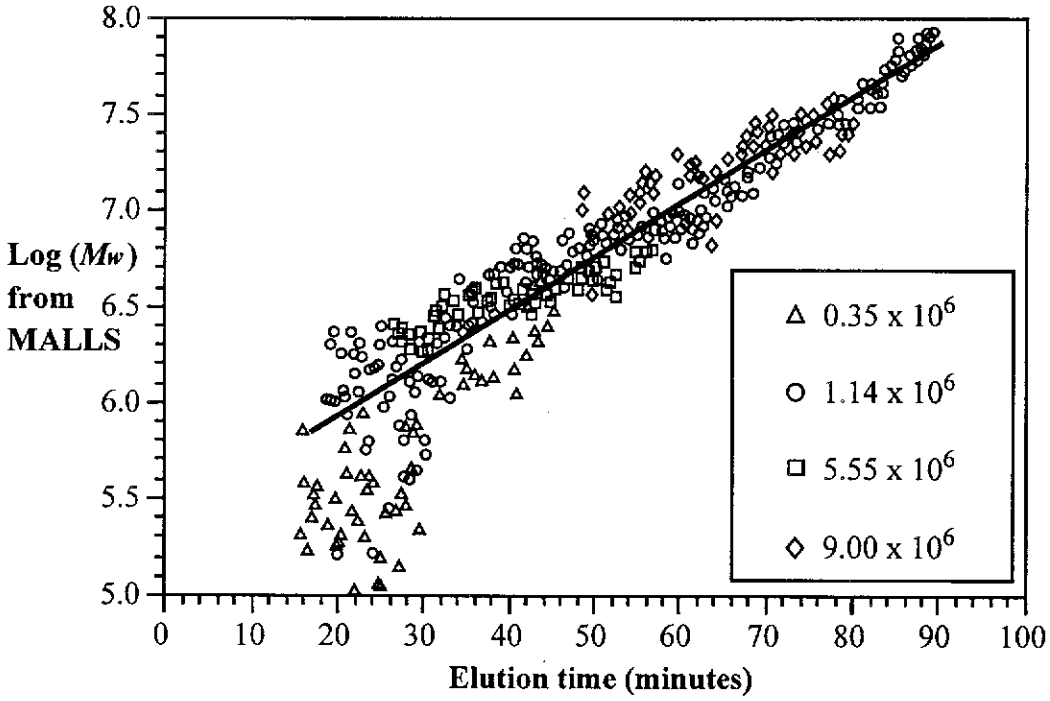

Recalling the theory discussed earlier (Section 4.1), molecular masses may be evaluated directly via light scattering or indirectly from FFF retention. The light scattering results (direct method) are shown in Figure 4-15. The linear regression featured fits well with correlation R^2 0.90 and provides a calibration for molecular mass *versus* elution time. The time axis of Figure 4-15 was transformed into a diffusion coefficient for Figure 4-16 according to the relationship of equation (4-21). This provides a test of the indirect molecular mass determination. For comparative purposes, two older molecular mass-diffusion coefficient relationships for PAAm are presented, together with measurement conditions.

Figure 4-16 Empirical diffusion coefficients for PAAm.

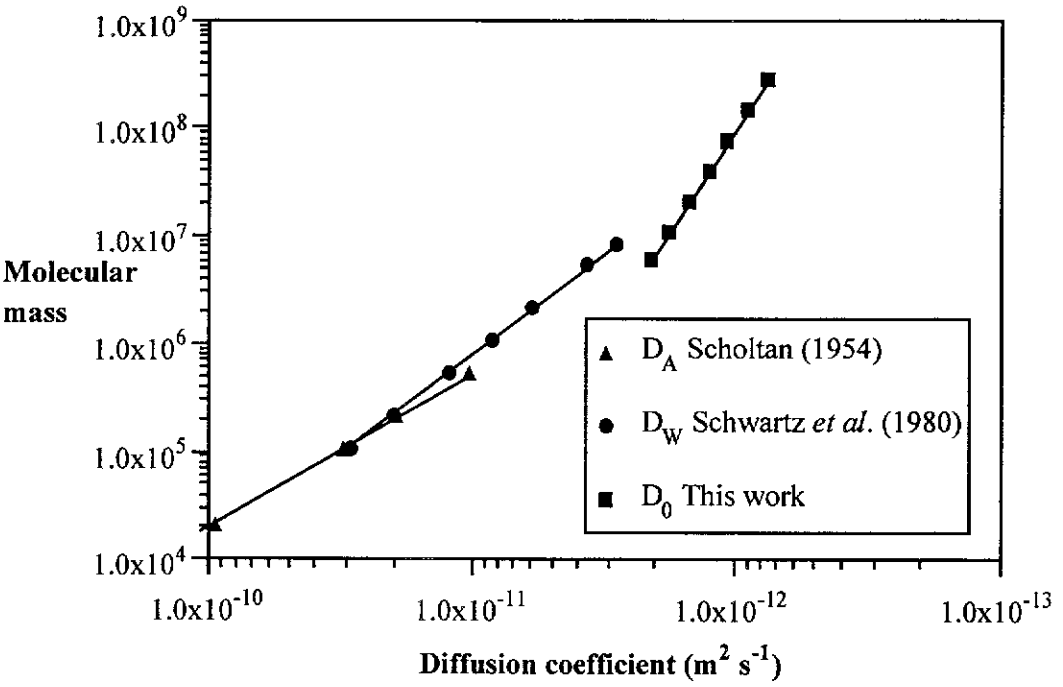

$$D_A = 8.46.10^{-4}\ M_{SD}^{-0.69} \qquad \text{water}, 20°C, 0.02 - 0.53 \times 10^6 \qquad (4\text{-}30)$$

$$D_w = 1.24.10^{-4}\ M_w^{-0.53\pm0.01} \qquad 0.1\,\text{M NaCl}, 0.13 - 8.2 \times 10^6 \qquad (4\text{-}31)$$

Equation (4-30), reported by Scholtan (1954), is an area-averaged diffusion coefficient derived from sedimentation measurements of low mass species, while equation (4-31), from Schwartz *et al.* (1980), lacked temperature control, and as such the two may not be directly comparable.

Extrapolation of the older M_w-D relationships to the higher molecular masses studied here shows the range and domain are consistent, although the gradient is greater than expected. Reasons for this include the extreme sensitivity of Figure 4-16 to the least-squares fit of Figure 4-15, and the presumption that the diffusion coefficients calculated from the FFF are accurate. The last point is significant, as it demands immediate sample response to the decaying field, and no analyte-membrane interaction, which has been demonstrated during the method development to be an issue. Giddings (1997) and Wyatt (1998) have also raised these concerns about FFF theory. Indirect molecular mass measurements, contingent upon ideal fractionator

operation and good diffusion-molecular mass conversion, may be less reliable than direct light scattering detection for PAAm.

4.4.2 Comparison with size-exclusion chromatography

The upper limit imposed on sample concentration due to viscosity has been a problem in some SEC studies of PAAm, for which the injection of larger sample volumes give the required sensitivity, but at the cost of resolution. For the SEC characterisation of PAAm with a mean M_w of 3×10^6, injected volumes of 0.5 mL were typically required (He *et al.* 1990), with elution times of over three hours (Kulicke and Böse 1984). The FFF-MALLS technique therefore offers a significant improvement in sensitivity over SEC.

4.5 *Fractionation of Commercial Flocculants*

4.5.1 *Bulk solution characterisation*

Viscosity is the most widely used technique for characterising commercial flocculants during manufacture. Table 4-3 collates the viscosities of commercial flocculants used in this study by both measurements.

Table 4-3 Dilute aqueous solutions of commercial PAAms. Mean molecular masses (cited by manufacturer and light scattering), and viscosities (reported as extrapolation to infinite dilution and extrapolation correlation coefficient) are presented.

Flocculant commercial designation	Mean molecular mass		Solution viscosity	
	Manufacturer cited $\times 10^6$	MALLS[A] M_w $\times 10^6$	Capillary[B] mL mg^{-1}	Rotational[C] $\times 10^3$ kg m^{-1} s^{-1}
M333	19-22	20.2	2.21 (R^2 0.98)	1.61 (R^2 0.98)
M351	15-17	10.8	0.73 (R^2 0.95)	0.91 (R^2 0.97)
FA920VHM	22-25	23.2	0.75 (R^2 0.98)	0.96 (R^2 0.99)
FA920	16-19	13.0	1.47 (R^2 0.97)	0.95 (R^2 0.99)
FA920BPM	7-9	11.6	0.41 (R^2 0.95)	0.80 (R^2 0.99)

A: solutions unfiltered, 5th order Debye fit, dn/dc 0.190 mg mL^{-1}, in 0.1 NaCl.

B: Ubbhelode viscometer (no. 75, 0.01017 cSt.s^{-1}) at 35.0°C.

C: Brookfield inner-rotating cylinder, with UL spindle adaptor.

The samples M351 and FA920VHM are identical according to viscometry, differing only by 3.5% and 4.4% from capillary (Ubbhelode) and rotational (Brookfield) measurements respectively, although the M351 shows a greater concentration dependence in the extrapolation to infinite dilution. The viscosity of FA920BPM is

much lower, reflecting its lower mean molecular mass. For most samples the capillary and rotational viscosity determinations are similar, but for M333 and FA920 the capillary measurement is notably greater. For all cases, the viscosity numbers given by both methods provide no more than an indication of mean molecular mass, and no indication whatsoever of molecular mass distribution. For comparison, the mean molecular masses of the polymers (determined in 0.1 M NaCl for signal stability) are included, clearly demonstrating that without a molecular mass distribution, the mean M_w or viscosity alone provides limited characterisation.

4.5.2 Commercial flocculants versus polyacrylamide standards

Ideally, flow FFF fractionates PAAm based on sample diffusion without regard to the source, to produce a near-monodisperse slice for subsequent characterisation. In Figure 4-15 molecular mass *versus* elution time was, based upon comparison of the fractionation of PAAm standards, internally consistent. This consistency is shown again by Figure 4-17, where the time-molecular mass relationship of the standards and the linear regression is compared with the elution of the commercial flocculant M351. The slight dip in the measured molecular mass of M351 at high retention is a feature shared by the lower mean molecular mass samples M351 and FA920BPM, and is discussed further in Section 4.6.

4.5.3 Fractionation of commercial flocculants

The elution profiles of the nonionic commercial flocculants is shown by Figure 4-18. The fractionation of the samples M351 and FA920VHM, exhibiting a similar viscosity, differ in their elution profiles where FA920VHM shows a very low amount of low molecular mass material.

Figure 4-17 Comparison of fractionation of PAAm standards and of the commercial flocculant M351.

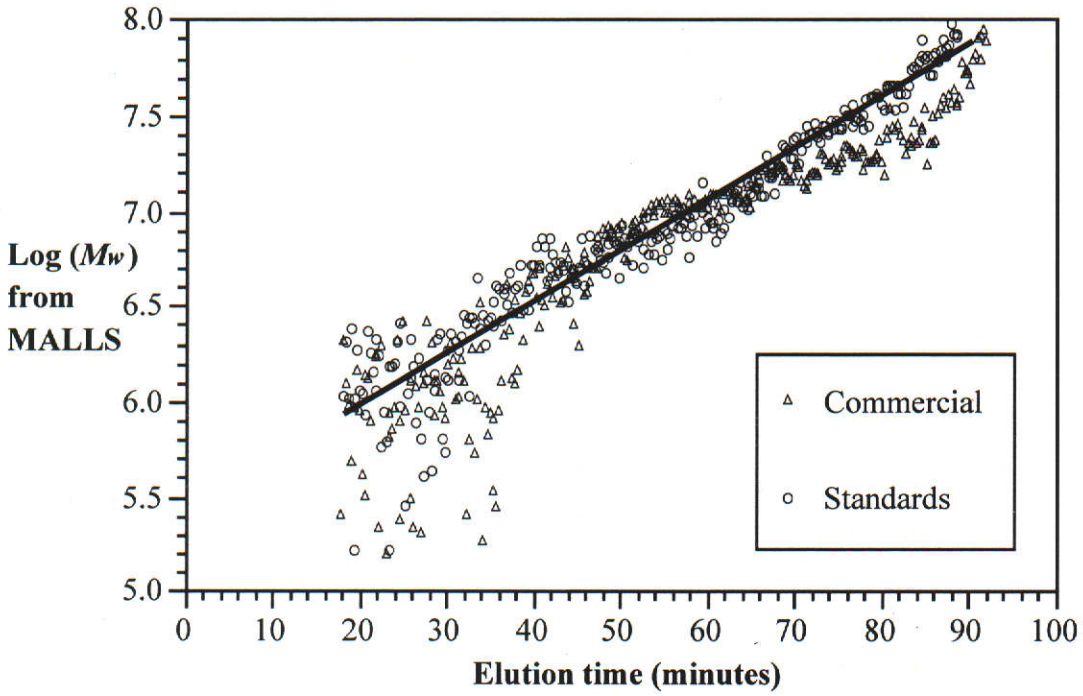

Figure 4-18 Fractionation of commercial polyacrylamide flocculants aged for two days under standard conditions.

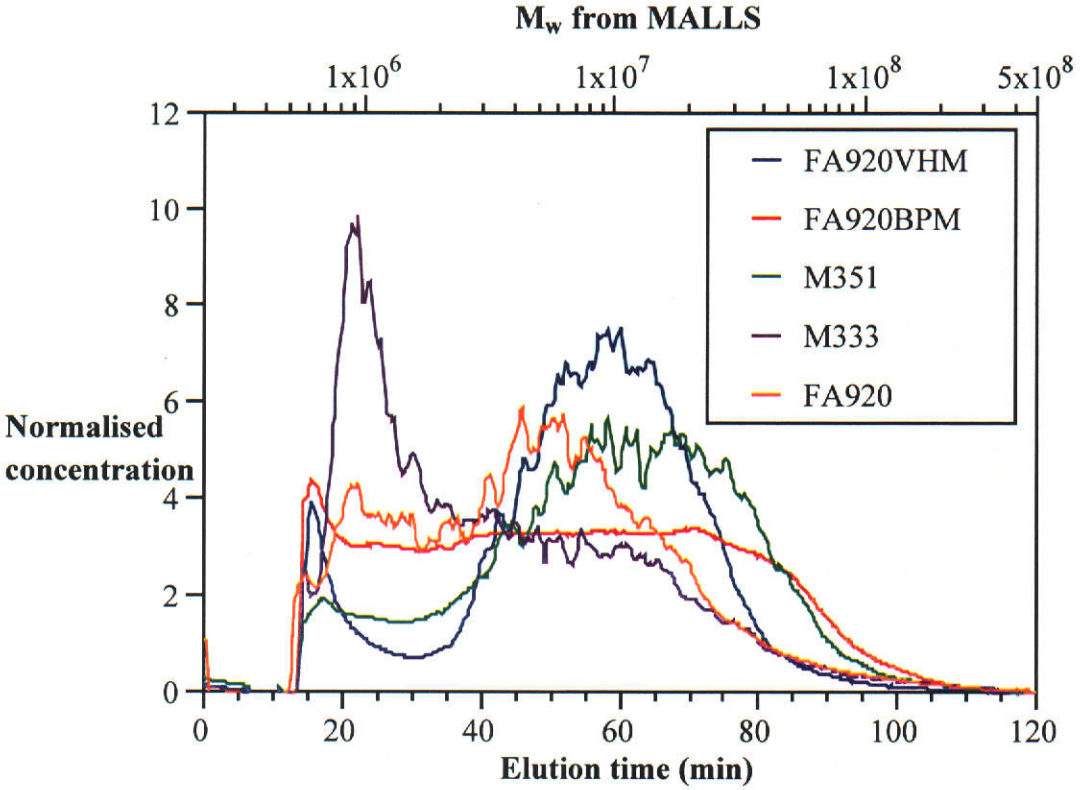

The slightly lower viscosity of M351 matches the broader size distribution, expected where the smaller polymers act as solvent or plasticiser for the larger species (Yau *et al.* 1979). The M351 sample will be discussed further in Section 4.5.4. FA920BPM has both a lower viscosity and mean molecular mass but the fractionation shows it to be very polydisperse, featuring a much greater number of low molecular weight species. All solutions were made to approximately the same concentration on a mass basis, therefore the lower mean molecular mass BPM will have a greater number-based concentration. Differences in the molecular mass distribution between the commercial flocculant samples are clearly observed. The effect of such differences upon flocculation activity is the subject of Chapter 5.

The fractionation of the more viscous M333 differs from M351, showing a higher concentration of rapidly eluting material. From Section 3.3, M333 is known to agglomerate to supramicron size in solution, with a volume-based measurement showing a peak number at around 10 μm diameter. Agglomerates this size would coelute with finer material, according to the parallel normal/steric mechanisms of FFF, and would explain these early peaks in the fractogram. For comparison, injection of a 9.1 μm polystyrene latex elutes with peak 7.2 min after the end of the stopflow (raw elution time 17.2 min) for the fractionation conditions. This result suggests the early peaks in the M333 fractionation are agglomerate-derived.

Proof that the early peak of the M333 fractionation is due to agglomerates is provided by Figure 4-19, which compares contemporaneous slices of the polymer fractionation with M351. The light scattering detector, in accordance with equation (2-5) from Section 2.1.3, has a scattering angular dependence determined by the architecture function $P(\theta)$, which is in turn a function of the rms radius of the polymer coil; specifically, a greater curvature identifies the presence of larger species (Section 4.3.5). Comparing the light scattering after 20 minutes elution the M351 curve is flat, indicating materials eluting at this time behave as isotropic scattering bodies, and therefore must be sufficiently small to be subject to the normal mode elution. A slice taken later, at 60 min elution, has a similar curvature for both M351

and M333 samples, although with different concentrations of sample, indicating that the material eluting at this time is the same size regardless of source as predicted by Figure 4-17. The curvature of the M333 sample after 20 min is greater than the curvature at 60 min and identifies the presence of a larger species. Although light scattering is a function of both scatterer radius and concentration, the curvature states definitely that the early peak in the M333 fractogram is due to agglomerates and to elute so early must be large enough to be subject to the FFF steric mechanism.

Figure 4-19 Excess scattering of fractograms from MALLS detector for a given elution time slice for flocculants M333 (solid line) and M351 (dashed).

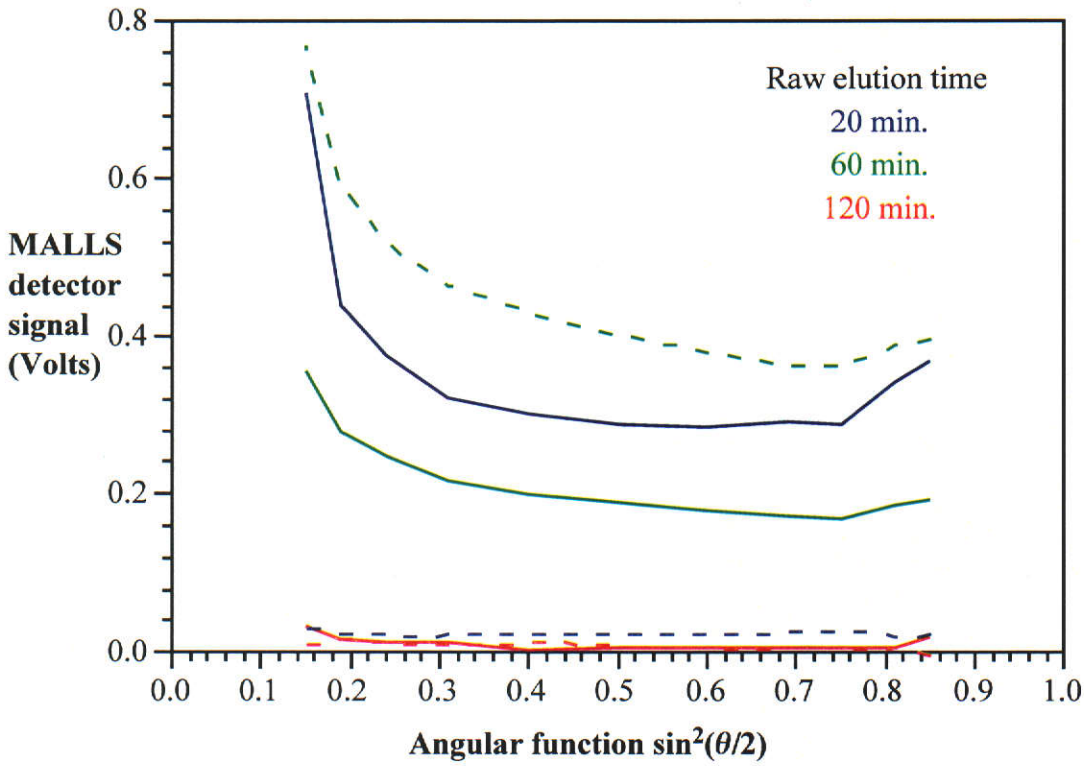

However, quantifying the size of the agglomerates found in the M333 fractionation is not simple. Sizing by the light scattering signal is influenced by the coeluting material and the superposition of the large, low concentration material which influences predominantly the lower angle detectors with the smaller, higher concentration fractions affecting all detectors will provide an angular dependence less than expected for the agglomerates alone. Extraneous dust in the PAAm samples would also elute at this time. Sizing by the MALLS detector is less reliable than the molecular mass determination, as the intercept is far more robust than the curvature

function towards the detector fluctuations. The FFF theory demonstrates retention based solely upon diffusion for submicron species, but for agglomerates affected by the steric mechanism the complication of lift forces has so far meant there is no first-principles function for calculation of size from elution time.

4.5.4 Ageing effects

The fractionation of M351, with detection from the concentration-sensitive refractometer, is shown in Figure 4-20a. From the fractogram the peak concentration of polymer elutes at 60 minutes and corresponds to a molecular mass of $10^{7.1}$, or 12.5×10^6. There remains a substantial amount eluting later in the period 70 to 80 minutes, equivalent to $10^{7.3\text{-}7.6}$, or $20\text{-}40\times10^6$. The distribution, reprocessed as a cumulative concentration profile, is summarised by Table 4-4.

Table 4-4 Cumulative elution concentration profile, as percentage of total DRI signal, for commercial flocculant M351.

Solution age		Cumulative % mass below M_w			
(days)	log (M_w) =	6.50	7.00	7.30	8.00
2		18.5	48.9	70.7	98.6
15		21.4	53.0	74.5	98.8
38		21.8	53.6	74.6	98.3

By concentration, about 22% of the polymer elutes as species with mean molecular mass over 20×10^6 (log M_w 7.30). There is only a slight ageing effect for M351: after 15 days there is no discernible difference to the molecular mass distribution from the 38 day old solution.

Figure 4-20 Elution profiles of stock solutions of flocculants (a) 4.08 mg mL^{-1} M351 and (b) 3.98 mg mL^{-1} M333 as a function of solution ageing.

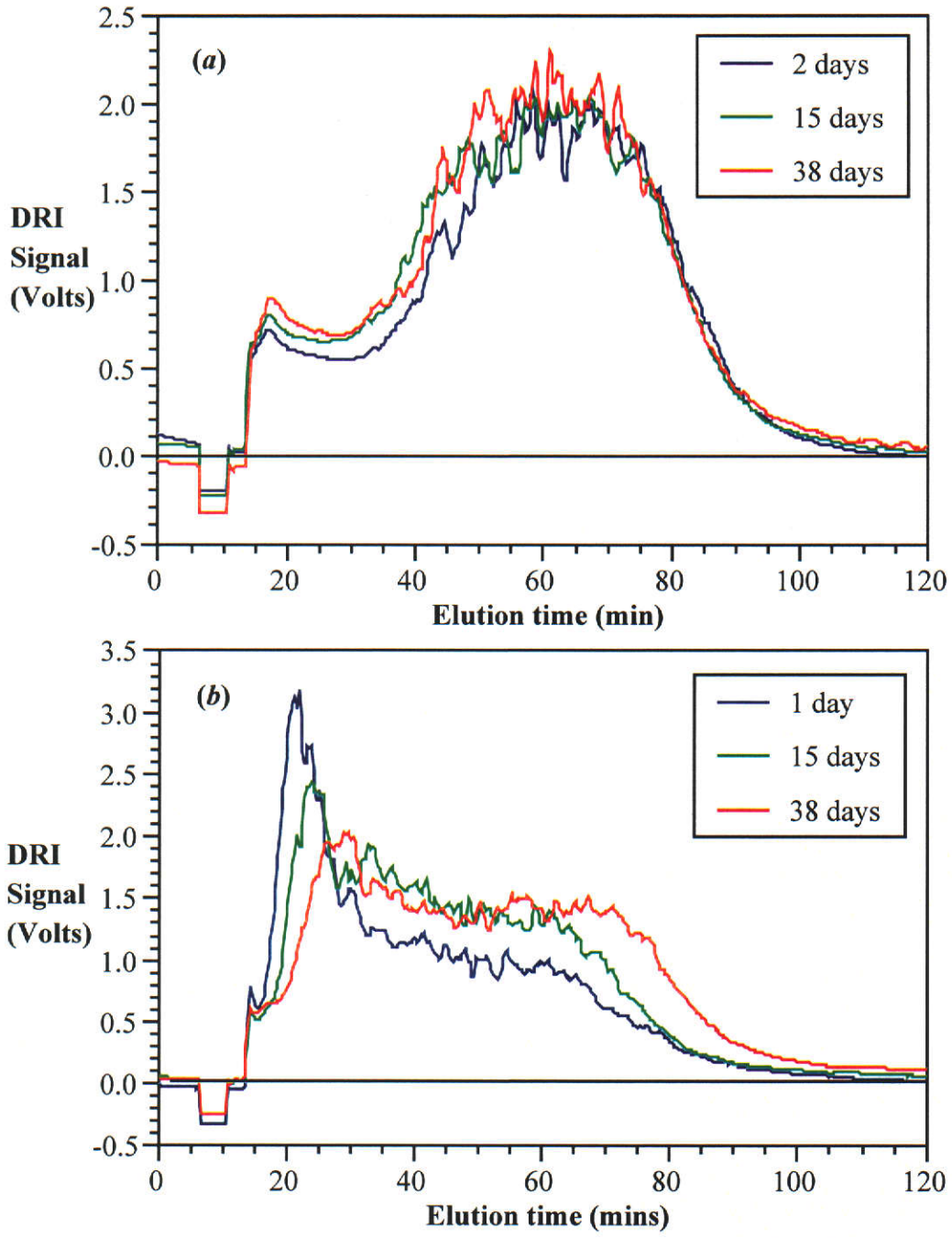

In contrast, M333 exhibits a dynamic fractogram, reflecting a clear ageing effect (Figure 4-20b). The supramicron peak around 20 minutes shifts to a later elution, which under a steric mechanism indicates a general decrease in size and therefore agglomerate dispersion. At the same time, free polymer coil peaks, which elute later than 60 minutes (matching the 15-25×10^6 PAAm), become increasingly dominant. These coils are subject to the FFF normal mode mechanism. The effect may be attributed to (a) the agglomeration/entanglement of the smaller coils, (b) an increasing coil radius due to some swelling mechanism, (c) polymer conformation change, or (d) from the erosion of agglomerates to free coils. Agglomeration of small coils is unlikely as it is not observed in the dynamic ageing behaviour of the otherwise identical M351 sample, and further swelling should not occur as the polymer in solution is already extensively solvated. Conformation change is known to occur in PAAm with ageing (Kulicke *et al.* 1982) but a shift of the magnitude observed is too great. The erosion of supramicron agglomerates and freeing discrete polymer coils (d) is therefore favoured. Only a small number of agglomerates need to degrade to provide a significant increase in the concentration of free polymer coils. This result is in agreement with Section 3.3, where a decrease in the size of supramicron counts of M333 was observed with time. Further, the result concurs with both Gardner *et al.* (1978) and Scott *et al.* (1996), where ageing results in an increasing viscosity with time, matching an increasing number of polymer coils in solution.

4.5.5 Supramicron agglomerates

In Chapter 3, PAAm agglomeration was shown to be dynamic and dependant upon solution ageing. For high molecular mass M333 in water, agglomerates as large as 20 μm diameter were shown to exist, but by number were estimated at less than 0.001% of the total polymer. Due to the method used in that series of experiments, species

smaller than 0.6 μm diameter were undetectable. Clearly, flow FFF is a complementary technique, capable of observing submicron species.

Agglomeration processes were shown to have definite concentration dependence, with more dilute polymer showing fewer, smaller agglomerates (Section 3.3). For the M333 polymer samples at less than 1.0 mg mL^{-1} concentration no agglomerates were observed. The effect of injecting increasingly dilute M333 solutions on the agglomeration (steric elution mode) region is shown by Figure 4-21. For comparative purposes, all signals are scaled to an equivalent 5.0 mg mL^{-1}. Preparing the PAAm solution at 2.0 mg mL^{-1} shows the agglomerate peak shifting to greater retention, commensurate with smaller agglomerate species. The same sample prepared at 0.50 mg mL^{-1} exhibits a complete suppression of this region between 15 and 25 minutes. This result reliably, although only qualitatively, matches the result the earlier reported concentration effect. Flow FFF is therefore not the ideal technique for directly characterising molecular mass distributions for highly agglomerated samples like M333. However, sample preparation steps to remove or suppress agglomerates may assist analysis, as discussed in the following two Sections.

4.5.6 Filtration to remove agglomerates

Samples of M333 were filtered slowly through a 5 μm filter, with the measured rotational ("Brookfield") viscosities increasing from 1.61 to 1.80×10^{3} kg m^{-1} s^{-1}. Filtration to 5 μm does not measurably change the concentration of polymer but was shown to clearly disperse the agglomerates (Figure 3-5), increasing both the number of free molecules in solution and viscosity, as observed. To understand this result more completely, fractionation of the filtered polymer was performed. PAAm samples aged for 15 days were filtered through a 5 μm syringe filter and the collected effluent was injected. The distributions are presented by Figure 4-22.

Figure 4-21 Effect of M333 stock concentration on fractionation, all scaled for comparison to equivalent 5.00 mg mL^{-1} concentration. Region displayed shows elution of supramicron diameter species under the steric mode.

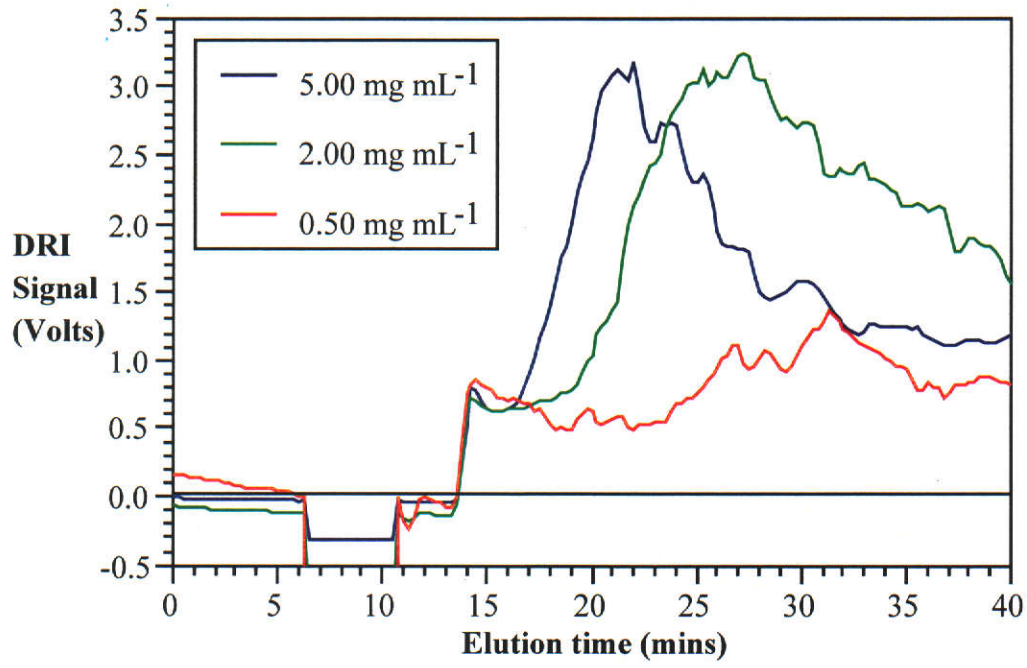

Figure 4-22 Fractograms of 5 µm syringe filtered and unfiltered M333 prepared to 3.98 mg mL^{-1} in water.

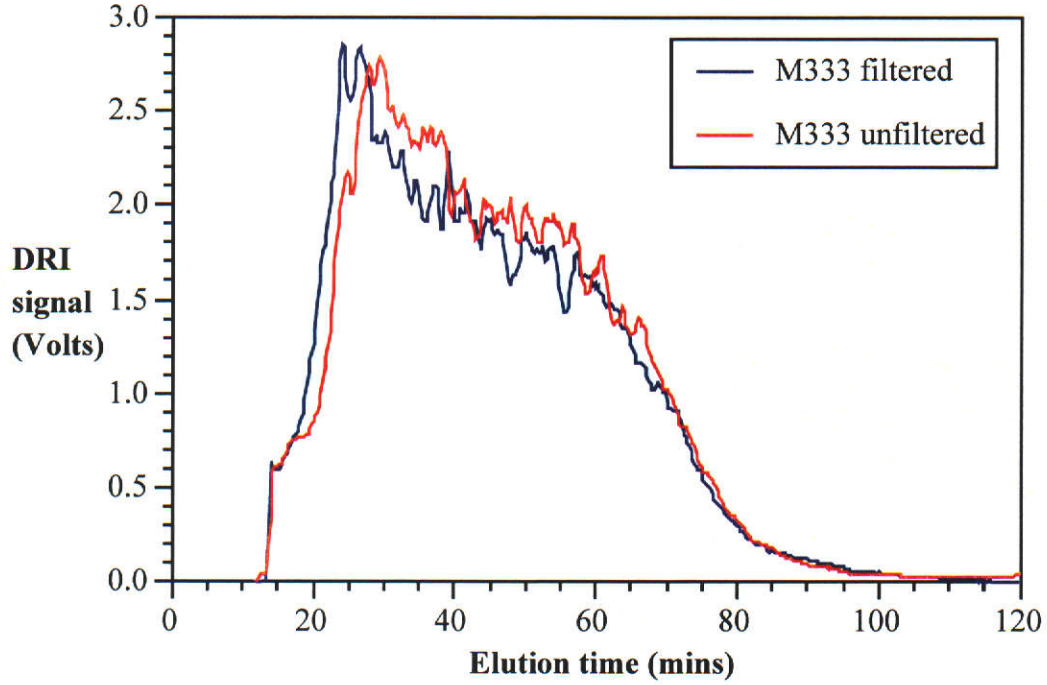

Magnafloc 333 shows, in the main, little change upon 5 μm filtration. However, the supramicron agglomerates (eluting at *ca.* 30-40 min.) were observed to shift to earlier elution and, due to the steric FFF mechanism, a larger size. Passage through the filter has entwined some of the polymer. The agglomerates present in M333 prevent derivation of a molecular mass distribution, and filtration is unable to remove these interferents. Interestingly the similarity between the filtration and ageing fractograms suggests filtration effectively reverses the effect of ageing upon PAAm. Filtration through smaller pore sizes has not been possible, as solutions at this moderate concentration are too viscous to pass the membranes.

4.5.7 Dispersion by adding salt

Dupuis *et al.* (1994) claimed chloride ions, at a concentration of 0.1 mol L^{-1}, are an effective dispersant for PAAm, which was confirmed with the Sizing Counter in Section 3.3. However, the viscosity of commercial flocculants in water are in apparent conflict with the (static) light scattering measurements taken in chloride (Table 4-3). The FFF-MALLS was used to reconcile these observations. The samples were identical to those used for the static light scattering, with stock flocculant solutions diluted to 0.1 mol L^{-1} NaCl. The presence of chloride on the fractionation is shown in Figure 4-23. The large void peak is expected, as the refractometer is sensitive to the unretained chloride. Upon comparison with chloride-free fractionation (Figure 4-18), FA920VHM showed little agglomeration and the presence of chloride resulted in little change in the elution profile. Recalling that M351 showed a viscosity nearly as high as FA920VHM, yet only half the mean molecular mass, fractionation of dispersed M351 shows a severe change in the molecular mass distribution, with a concentration maximum shifting from 65 to 45 minutes (equivalent to molecular masses from 15 to 5×10^6).

Figure 4-23 Effect of dilution of polymer stock to 0.1 M NaCl solution on fractionation.

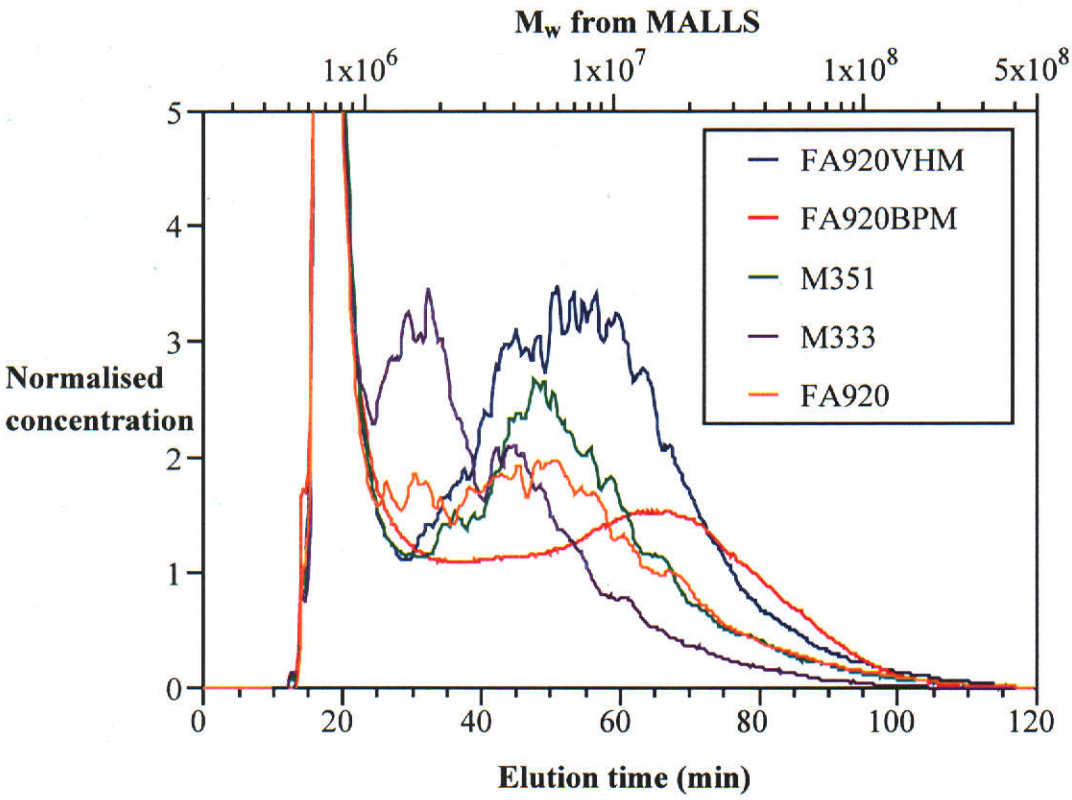

4.5.8 Ultrasonic degradation

The shear degradation of long chain polymers has been extensively studied. In an industrial thickening application, the flocculant solutions may commonly be pumped up to 500 m from preparation to dosage sites. Degradation as a consequence of pipe flow has been postulated as a cause of reduced flocculant activity. Conversely, ultrasonic degradation has been used to deliberately reduce polymer molecular mass in order to improved NMR analysis (Section 7.1). Flow FFF-MALLS represents an ideal approach to characterise such changes.

A commercial flocculant, M351, was degraded ultrasonically as described in Section 4.2.8, sampled and fractionated. The superimposed fractograms presented in Figure 4-24 may be read as changing molecular mass distribution with degradation

time. These show a large shift to lower molecular mass. After extended degradation virtually all the polymer has been reduced to below 10^6.

Figure 4-24 Degradation and fractionation of commercial M351 (4.08 mg mL^{-1}) over a series of sonication periods presented as total degradation time.

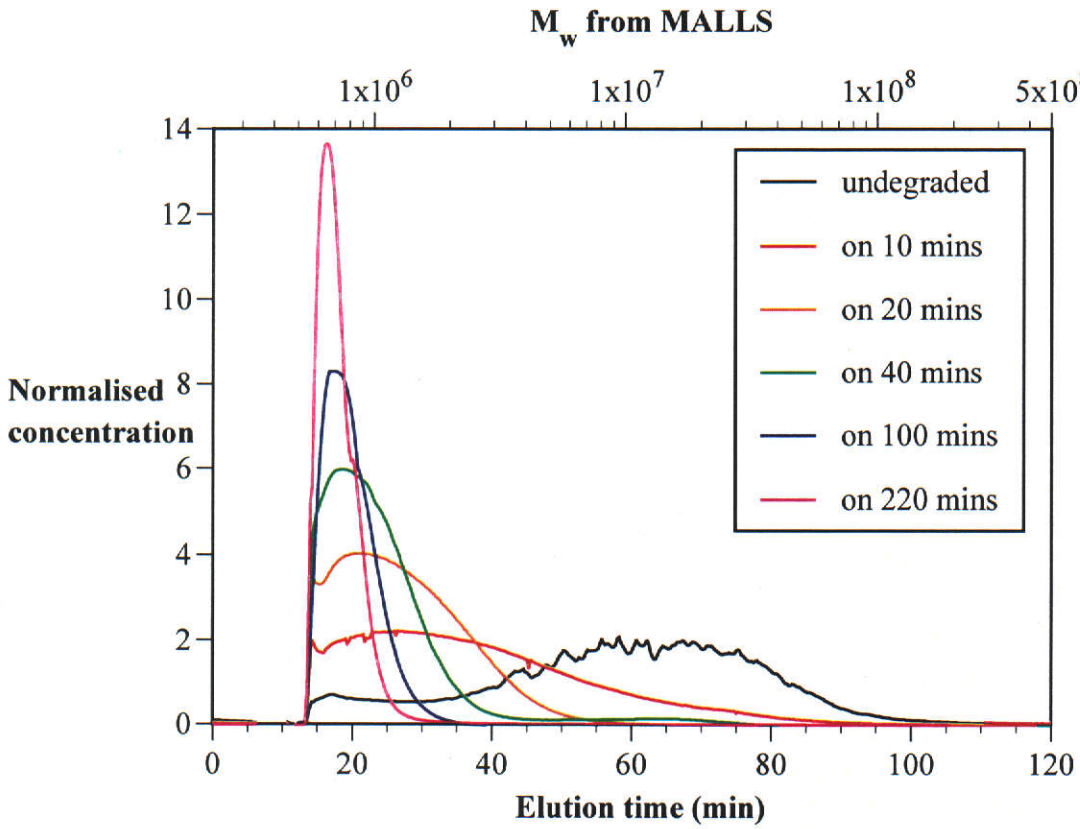

Chiantore and Guaita (1993) showed degradation can be monitored on the basis of measured polydispersity but required an accurate molecular mass distribution, while Kulicke *et al.* (1993) measured the mean molecular mass during ultrasonic degradation to show the typical exponential decrease in mean M_w with degradation time. The results cannot be easily compared as, according to Koda *et al.* (1994), the intensity of energy and dispersion is rarely reported. Reporting the degradation of pullulan, Koda *et al.* (1994) used SEC to measure molecular mass distributions but with unimpressive resolution and therefore an erroneous determination. The PAAm degradation presented in Figure 4-24 shows a very rapid loss of the highest molecular mass species. This quantitatively matches chain scission processes rather

than depolymerisation. The greater resolution available to FFF-MALLS over SEC is well demonstrated by this example.

4.5.9 Hydrolysed flocculants

Many of the PAAm-based flocculants used by the mineral processing industries are at least partially hydrolysed. Figure 4-25 shows the fractionation of AN910VHM, found to be 10.3% acrylate, and clearly the charged groups provides a number of differences.

Figure 4-25 Example 10% hydrolysed flocculant AN910VHM compared with the elution profile of unmodified PAAm from the same manufacturer and similar cited mean molecular mass.

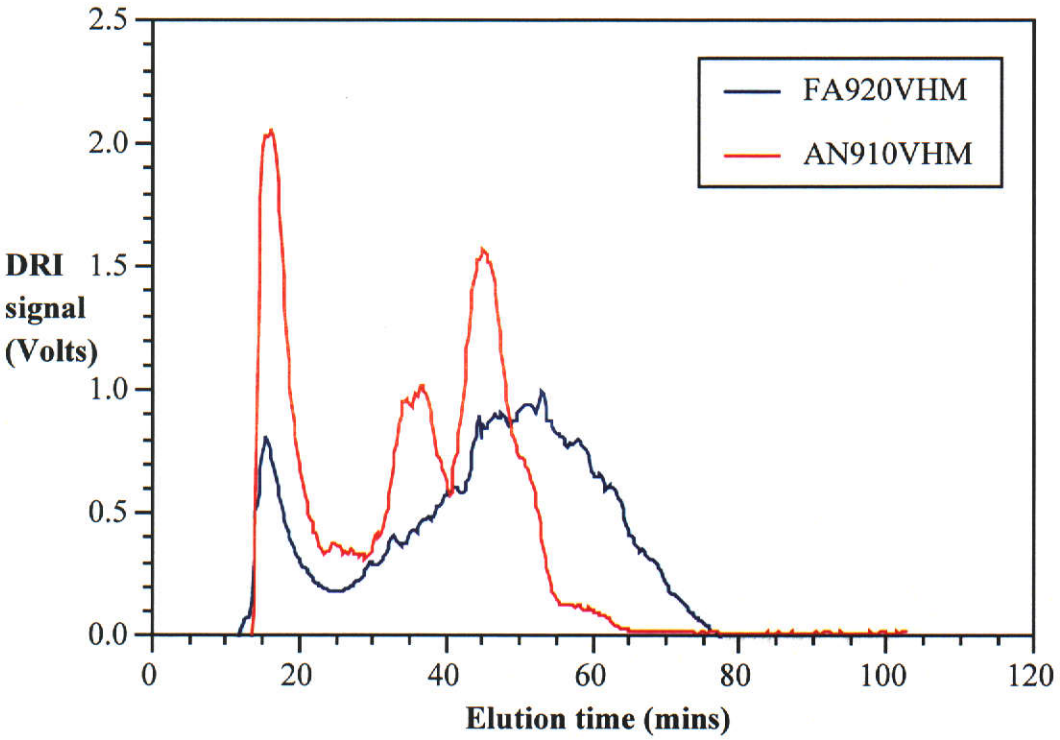

At ambient pH and ionic strength the screening of the anionic groups is not present and mutual repulsion forces the polymer into a stiffer, more rodlike conformation. In turn, the molecular mass-diffusion relationship is dependant upon ionic strength and pH, and therefore the FFF elution will vary from that of nonionic PAAm. The

anionicity affects also the mutual repulsion of the coils, and increased solubility in polar solvents such as water, both effects contributing to the suppression of agglomerates.

Most striking for this fractionation is the very narrow distribution. Since anionic flocculants are hydrolysed from the nonionic polymers, the reduced polydispersity is not due to manufacture but suppression of agglomerates. The distribution is, relative to the equivalent nonionic polymer, eluting earlier. Whether the earlier elution is due to reduced polymer-membrane interaction or a different M_w-D relationship is unclear. Also of interest is an apparent bimodality of the polymer peaks at 35 and 45 min elution. The bimodality may be intrinsic to the sample or may have arisen from chain shearing during preparation or analysis. This result merits further study to expand the range of the flow FFF-MALLS method for polymer analysis.

4.6 AGGLOMERATES AND ENTWINED POLYMER

An important issue to clarify why the samples FA920BPM and M351, with low mean molecular masses, apparently have the widest elution profile of any of the commercial flocculants (Figure 4-18). Linked to this is the tendency of the molecular mass-elution time plot to "flatten" at higher retention, a feature seen in Figure 4-17 where the curve of the commercial flocculant M351 dips slightly after 70-80 minutes. For ultrahigh molecular mass PAAm solutions, the molecules exist in one of three solvated states. The first state, representing the bulk of the material, is of well dispersed individual coils. The fractionation and light scattering of these is well described by theory, and follows the same molecular mass-retention effects of the standards (Section 4.4). The second state is of supramicron agglomerates, eluting according to the FFF steric mode, and has been covered extensively in Chapter 3 and again in Figure 4-19. The third state is of several entwined polymers coils, a term chosen to differentiate from agglomeration. The FFF separation, sensitive only to diameter, allows their elution later than the individual coils, while the MALLS detector observes each molecule in the entwined body as an individual. The mean molecular mass-retention curve then "flattens" as the species radius increases (FFF elution) but the molecular mass remains the same. These different polymer states are shown schematically in Figure 4-26, eluting in overlapping "zones" from the FFF cell.

Further evidence for entwined polymers comes first from the degradation experiments (Figure 4-24), where the material retained to at least 70 minutes dispersed very rapidly. This is attributed to the loss of entwined polymers, eluting in zone 3, which are more weakly bound than the covalent bonds that comprise the polymer backbone and therefore cleave most easily. Secondly, for a charged polymer featuring intermolecular repulsion this entwinement is not favourable and is absent from the fractionation of the anionic flocculant (Figure 4-25). The remarkable breadth of the low mean molecular mass commercial flocculants M351 and

FA920BPM is therefore assigned to the presence of these entwined polymers. Lower mean molecular mass implies, for solutions prepared on a mass basis, more molecules in solution to favour entwinement.

Figure 4-26 Elution of the three "phases" of PAAm in aqueous solution. The polymer state is shown in red (not to scale) and elution region in green. Zone 1 is for solution state 1, the well-dispersed PAAm. Zone 2 features the agglomerates coeluting with the smallest polymers. Zone 3, with the longest retention, are the largest submicron-diameter "entwined" polymers.

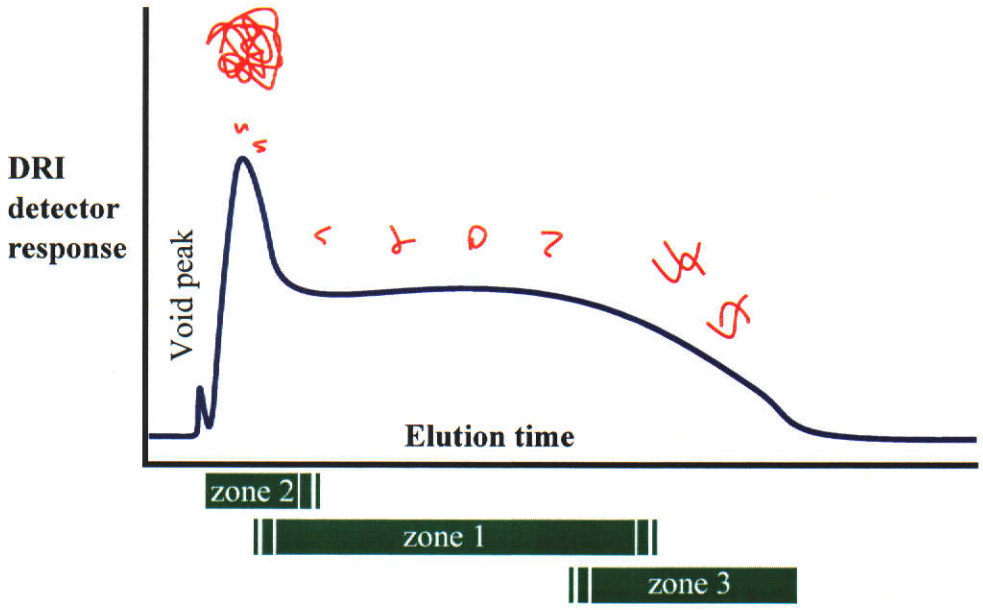

The presence of the three zones means separation of PAAm by the flow FFF remains viable, but interpretation of the fractograms using the MALLS detector is not as straightforward as for the standards. A number of strategies to simplify the fractograms may be pursued.

- *Decrease polymer solution concentration*

  The concentration chosen was appropriate for flocculant stock solutions used in the mineral processing industries. Agglomeration and entwinement are concentration dependant (Figure 3-7, Figure 4-21) and injecting more dilute polymer may suppress the presence of zones 2 and 3 from the fractionation. The dilute polymer will be more difficult to detect, but this may be offset somewhat through the adjusting the frit outlet facility of the fractionator for

signal enhancement (Section 4.1.1.9). This method is potentially useful but does not solve the coelution difficulties.

- *Modify flows used in the FFF*

  Changing the flows may separate the elution of the agglomerates in zone 2 from the submicron species through affecting the steric mechanism. The point of steric inversion is empirically known to be dependent on flow conditions, although the relationship is poorly understood even for model latex systems. Flow adjustment will necessarily affect system pressures and sample relaxation, so system reoptimisation becomes an issue.

- *Modify the field decay*

  More promising is to install a time delay, that is τ_0 from equation (4-21) becomes non-zero. A sufficiently long delay may allow supramicron agglomerates to elute separately from the retained submicron material. The difficulties are twofold: the size distribution is a continuum so a total disengagement of coelution is not possible, while the higher field and longer experiment times may lead to a commensurate loss of resolution (equation 4-24).

- *Modify the carrier solution to disperse polymer agglomerates*

  Salt has been shown to aid dispersion, but the chloride was detected by the refractometer (Figure 4-23). Adding salt to both the polymers upon preparation to match salt added to the carrier solution would allow a fractogram of salt-dispersed PAAm without the salt peak. Salt, however, is aggressive and incompatible with metal components in the fractionator. The effect of salt on polymer-membrane interactions is unknown. As well, the ubiquitous presence of salt is known to decrease the sensitivity of the DRI, effectively masking the polymer.

4.7 *Conclusions*

Flow field-flow fractionation has been successfully applied to the fractionation of ultra-high molecular mass PAAms, with full elution in less than two hours. This improves upon size-exclusion chromatography in terms of both throughput and resolution. Careful control of the carrier chemistry is required to avoid surface adsorption and loss of sample, while at the same time preventing interference to concentration-sensitive detectors.

The relationship between molecular mass and elution time was shown to exhibit a good degree of linearity. Direct (light scattering) methods are preferred for the determination of molecular mass distribution., as the indirect method relies upon ideal circumstances where the polymer coils do not interact with the membrane and retard their passage, or alter configuration and therefore change their hydrodynamic diameter and diffusion coefficient. However, for commercial materials the FFF provided information about the solution state agglomerates and entanglements for which the light scattering detector was incompletely characterising.

PAAm solutions are more complicated than a discrete collection of coils, existing also as entanglements of a few polymer coils and as agglomerates of many molecules. The agglomerates are difficult for the fractionator to characterise, due to the parallel separation mechanisms of the FFF, and cannot be removed by simple filtration. Nevertheless, the elution of agglomerates was shown to match behaviour from a complementary agglomerate-characterising technique.

The application of the technique to the study of flocculant degradation and hydrolysed flocculants was briefly explored. The value of flow FFF-MALLS for degradation studies was clearly demonstrated. Both aspects are now the subjects of ongoing research.

4.8 REFERENCES

Benincasa, M.A. and Giddings, J.C., 1992, 'Separation and molecular weight distribution of anionic and cationic water-soluble polymers by flow field-flow fractionation', *Analytical Chemistry*, vol. 64, pp. 790-798.

Benincasa, M.A. and Giddings, J.C., 1997, 'Separation and characterization of cationic, anionic, and nonionic water-soluble polymers by flow FFF: sample recovery, overloading, and ionic strength effects', *Journal of Microcolumn Separations*, vol. 9, pp. 479-495.

Caldwell, K.D., 1991, 'Polymer analysis by field-flow fractionation', in *Modern Methods of Polymer Characterisation,* eds. Barth, H.G. and Mays, J.W., John Wiley and Sons, New York, pp. 113-150.

Caldwell, K.D., Brimhall, S.L., Gao, Y. and Giddings, J.C., 1988, 'Sample overloading effects in polymer characterisation by field-flow fractionation', *Journal of Applied Polymer Science*, vol. 36, pp. 703-719.

Chiantore, O. and Guaita, M., 1993, 'Experimental and methodological aspects in the characterisation of polymers undergoing degradation', *Journal of Applied Polymer Science: Applied Polymer Symposium*, vol. 52, pp. 1-10.

de Laat, A.W.M. and van den Heuvel, G.L.T., 1993, 'Competitive and displacement adsorption of polyvinyl alcohol and the ammonium salt of a polyacrylic acid on $BaTiO_3$', *Colloids and Surfaces A: Physicochemical and Engineering Aspects*, vol. 70, pp. 179-187.

Dupuis, D., Lewandowski, F.Y., Steiert, P. and Wolff, C., 1994, 'Shear thickening and time-dependent phenomena: the case of polyacrylamide solutions', *Journal of Non-Newtonian Fluid Mechanics*, vol. 54, pp. 11-32.

Gardner, K.L., Murphy, W.R. and Geehan, T.G., 1978, 'Polyacrylamide solution aging', *Journal of Applied Polymer Science*, vol. 22, pp. 881-882.

Giddings, J.C., 1979, 'Field-flow fractionation of polymers: one-phase chromatography', *Pure and Applied Chemistry*, vol. 51, pp. 1459-1471.

Giddings, J.C., 1985, 'Optimised field-flow fractionation system based on dual stream splitters', *Analytical Chemistry*, vol. 57, pp. 945-947.

Giddings, J.C., 1989, 'Field-flow fractionation of macromolecules', *Journal of Chromatography*, vol. 470, pp. 327-335.

Giddings, J.C., 1990, 'Hydrodynamic relaxation and sample concentration in field-flow fractionation using permeable wall elements', *Analytical Chemistry*, vol. 62, pp. 2306-2312.

Giddings, J.C., 1997, 'Factors influencing accuracy of colloidal and macromolecular properties measured by field-flow fractionation', *Analytical Chemistry*, vol. 69, pp. 552-557.

Giddings, J.C., Benincasa, M.A., Liu, M.-K. and Li, P., 1991, 'Separation of water soluble synthetic and biological macromolecules by flow field-flow fractionation', *Polymeric Materials Science and Engineering*, vol. 65, pp. 21-23.

Giddings, J.C., Benincasa, M.A., Liu, M.-K. and Li, P., 1992, 'Separation of water soluble synthetic and biological macromolecules by flow field-flow fractionation', *Journal of Liquid Chromatography*, vol. 15, pp. 1729-1747.

Giddings, J.C. and Caldwell, K.D., 1984, 'Field-flow fractionation: choices in programmed and nonprogrammed options', *Analytical Chemistry*, vol. 56, pp. 2093-2099.

Giddings, J.C., Lin, G.C. and Myers, M.N., 1978, 'Fractionation and size distribution of water soluble polymers by flow field-flow fractionation', *Journal of Liquid Chromatography*, vol. 1, pp. 1-20.

Giddings, J.C. and Schure, M.R. 1987, 'Theoretical analysis of edge effects in field-flow fractionation', *Chemical Engineering Science*, vol. 42, pp. 1471-1479.

Giddings, J.C., Yang, F.J. and Myers, M.N., 1976, 'Theoretical and experimental characterisation of flow field-flow fractionation', *Analytical Chemistry*, vol. 48, pp. 1126-1132.

Grasselli, J.G. and Ritchey, W.M., 1975, *Atlas of Spectral Data and Physical Constants for Organic Compounds*, 2nd ed., CRC Press, Cleveland, Ohio.

Hansen, M.E., Giddings, J.C., Schure, M.R. and Beckett, R., 1988, 'Corrections for secondary relaxation in exponentially programmed field-flow fractionation', *Analytical Chemistry*, vol. 60, pp. 1434-1442.

He, Q., Young, T.-S., Willhite, G.P. and Green, D.W., 1990, 'Measurement of molecular weight distribution of polyacrylamides in core effluents', *Society of Petroleum Engineers Reservoir Engineering*, vol. 5, pp. 333-338.

Holzwarth, G., Soni, L., Schulz, D.N. and Bock, J., 1988, 'Absolute MWD's of polyacrylamides by sedimentation and light scattering', in *Water-Soluble Polymers for Petroleum Recovery*, eds. Stahl, G.A. and Schulz, D.N., Proceedings of the National Meeting of the American Chemical Society, Plenum, New York, pp. 215-229.

Hovingh, M.E., Thompson, G.H. and Giddings, J.C., 1970, 'Column parameters in thermal field-flow fractionation', *Analytical Chemistry*, vol. 42, pp. 195-203.

Janca, J., 1988, *Field-Flow Fractionation: Analysis of Macromolecules and Particles,* ed. Cazes, J., Chromatographic Science Series vol. 39, Marcel Dekker, New York.

Jensen, K.D., Williams, S.K.R. and Giddings, J.C., 1996, 'High-speed particle separation and steric inversion in thin flow field-flow fractionation channels', *Journal of Chromatography A*, vol. 746, pp. 137-145.

Kirkland, J.J. and Dilks, C.H., 1992, 'Flow field-flow fractionation of polymers in organic solvents', *Analytical Chemistry*, vol. 64, pp. 2836-2840.

Kirkland, J.J., Dilks, C.H. and Rementer, S.W., 1992, 'Molecular weight distributions of water-soluble polymers by flow field-flow fractionation', *Analytical Chemistry*, vol. 64, pp. 1295-1303.

Koda, S., Mori, H., Matsumoto, K. and Nomura, H., 1994, 'Ultrasonic degradation of water-soluble polymers', *Polymer*, vol. 35, no. 1, pp. 30-33.

Kulicke, W.-M. and Böse, N., 1984, 'Bestimmung der Molmassenverteilung sowie Stabilitätsgrenze von Polyacrylamiden unter Benutzung einer kombinierten Ausschlußchromatographie/Kleinwinkel-Laser-Streulichtphotometer Anlage', *Colloid and Polymer Science*, vol. 262, pp. 197-207.

Kulicke, W.-M., Kniewske, R. and Klein, J., 1982, 'Preparation, characterization, solution properties and rheological behaviour of polyacrylamide', *Progress in Polymer Science*, vol. 8, pp. 373-468.

Kulicke, W.-M., Otto, M. and Baar, A., 1993, 'Improved NMR characterization of high-molecular-weight polymers and polyelectrolytes through the use of preliminary ultrasonic degradation', *Makromolekulare Chemie*, vol. 194, pp. 751-765.

Lee, S., Myers, M.N. and Giddings, J.C., 1989, 'Hydrodynamic relaxation using stopless flow injection in split inlet sedimentation field-flow fractionation', *Analytical Chemistry*, vol. 61, pp. 2439-2444.

Litzén, A., 1993, 'Separation speed, retention, and dispersion in asymmetrical flow field-flow fractionation as functions of channel dimensions and flow rates', *Analytical Chemistry*, vol. 65, pp. 461-470.

Litzén, A. and Wahlund, K.-G., 1989, 'Improved separation speed and efficiency for proteins, nucleic acids and viruses in asymmetrical flow field-flow fractionation', *Journal of Chromatography*, vol. 476, pp. 413-421.

Litzén, A. and Wahlund, K.-G., 1991, 'Zone broadening and dilution in rectangular and trapezoidal asymmetrical flow field-flow fractionation channels', *Analytical Chemistry*, vol. 63, pp. 1001-1007.

Liu, M.-K. and Giddings, J.C., 1993, 'Separation and measurement of diffusion coefficients of linear and circular DNAs by flow field-flow fractionation', *Macromolecules*, vol. 26, no. 14, pp. 3576-3588.

Liu, M.-K., Williams, P.S., Myers, M.N. and Giddings, J.C., 1991, 'Hydrodynamic relaxation in flow field-flow fractionation using both split and frit inlets', *Analytical Chemistry*, vol. 63, pp. 2115-2122.

Martin, M., van Batten, C. and Hoyos, M., 1997, 'Retention in field-flow fractionation with a moderate nonuniformity in the field force', *Analytical Chemistry*, vol. 69, pp. 1339-1346.

Myers, M.N. and Giddings, J.C., 1982, 'Properties of the transition from normal to steric field-flow fractionation', *Analytical Chemistry*, vol. 54, pp. 2284-2289.

Scholtan, W., 1954, 'The determination of the molecular weight of polyacrylamide by means of the ultracentrifuge', *Makromolekulare Chemie*, vol. 14, pp. 169-178.

Schwartz, T., François, J. and Weill, G., 1980, Dynamic dimensions in the polyacrylamide-water system', *Polymer*, vol. 21, pp. 247-249.

Scott, J.P., Fawell, P.D., Ralph, D.E. and Farrow, J.B., 1996, 'The shear degradation of high-molecular-weight flocculant solutions', *Journal of Applied Polymer Science*, vol. 62, pp. 2097-2106.

Soponkanaporn, T. and Gehr, R., 1987, 'Quantitative determination and peak molecular weight analysis of acrylamide-based polyelectrolytes by size exclusion chromatography', *International Journal of Environmental Analytical Chemistry*, vol. 29, pp. 1-14.

Sykes, P., 1986, *A Guidebook to Mechanism in Organic Chemistry*, Longman Scientific and Technical, Harlow, England.

Thielking, H. and Kulicke, W.-M., 1996, 'On-line coupling of flow field-flow fractionation and multiangle laser light scattering for the characterisation of macromolecules in aqueous solution as illustrated by sulphonated polystyrene samples', *Analytical Chemistry*, vol. 68, pp. 1169-1173.

Verstakov, E.S., Kessler, Y.M., Kireeva, Z.N. and Filimonova, Z.A., 1981, 'The viscosity properties of formamide-acetic acid mixtures', *Zhurnal Strukturnoi Khimii*, vol. 22, no. 4, pp. 180-182.

Wahlund, K.-G. and Giddings, J.C., 1987, 'Properties of an asymmetrical flow field-flow fractionation channel having one permeable wall', *Analytical Chemistry*, vol. 59, pp. 1332-1339.

Wahlund, K.-G. and Litzén, A., 1989, 'Application of an asymmetrical flow field-flow fractionation channel to the separation and characterisation of proteins, plasmids, plasmid fragments, polysaccharides and unicellular algae', *Journal of Chromatography*, vol. 461, pp. 73-87.

Wahlund, K.-G., Winegarner, H.S., Caldwell, K.D. and Giddings, J.C., 1986, 'Improved flow field-flow fractionation system applied to water-soluble polymers: programming, outlet stream splitting, and flow optimisation', *Analytical Chemistry*, vol. 58, pp. 573-578.

Weast, R. C. and Astle, M. J., 1982, *CRC Handbook of Chemistry and Physics,* CRC Press, Boca Raton, Florida.

Wieteska, E., 1986, 'Inorganic applications', in *Comprehensive Analytical Chemistry,* ed. Svehla, G., vol. 19, Elsevier, Amsterdam, p. 391.

Williams, P.S. and Giddings, J.C., 1994, 'Theory of field-programmed field-flow fractionation with corrections for steric effects', *Analytical Chemistry*, vol. 66, pp. 4215-4228.

Wyatt, P.J., 1998, 'Submicrometer particle sizing by multiangle light scattering following fractionation', *Journal of Colloid and Interface Science*, vol. 197, no. 1, pp. 9-20.

Yang, F.J., Myers, M.N. and Giddings, J.C., 1977, 'Peak shifts and distortion due to solute relaxation in flow field-flow fractionation', *Analytical Chemistry*, vol. 49, pp. 659-662.

Yau, W.W. and Kirkland, J.J., 1984, 'Nonequilibrium effects in sedimentation field-flow fractionation', *Analytical Chemistry*, vol. 56, pp. 1461-1466.

Yau, W.W., Kirkland, J.J. and Bly, D.D., 1979, *Modern Size-Exclusion Chromatography*. New York: John Wiley and Sons.

Chapter 5

Flocculation Activity of Characterised Polymers

5 *FLOCCULATION ACTIVITY OF CHARACTERISED POLYMERS*

In Chapter 1 the issue of the effect of the flocculant's molecular mass distribution on flocculation was raised. This question can now be addressed, using the techniques to characterise supra- and submicron domains of PAAm from Chapter 3 and Chapter 4, respectively. Sections 5.1and 5.2 describe the methods used to study the flocculation of kaolin as a model substrate. Section 5.3 compares the observed activity of five commercial flocculants, while Section 5.4 links the activity with characteristics of the flocculant.

The solution behaviour of PAAm is complex. Distinct differences have been demonstrated in the fractionation profiles of flocculants in solution. The polymer coils do not exist in solution as discrete units; rather there can be a mixture of single molecules, entwined polymer consisting of several coils and large agglomerates of many coils (Section 4.6). The flocculation activity of the polymer is, therefore, not a function only of the free coils, but instead a superposition of the activities of the coils, the submicron entwinements and the supramicron agglomerates.

The fold-out page overleaf collates the characterisation results. Included are the elution profiles of the flocculants prepared in water and in 0.1 M NaCl (Figure 5A, Figure 5B), presented earlier as Figure 4-18 and Figure 4-23, respectively. The solution viscosities by capillary and rotational methods are also presented as Table 5A, seen earlier as Table 4-3. Table 5B is a compiled list of the solution state features of the five commercial flocculants, identifying whether the presence of entwinements and/or agglomerates was featured in the elution profiles. Table 5B also categorises each flocculant behaviour type according to the solution-state properties of PAAm, as formally assigned in Section 5.3.3.

Figure 5A Molecular mass distributions of commercial flocculants prepared in water and aged two days.

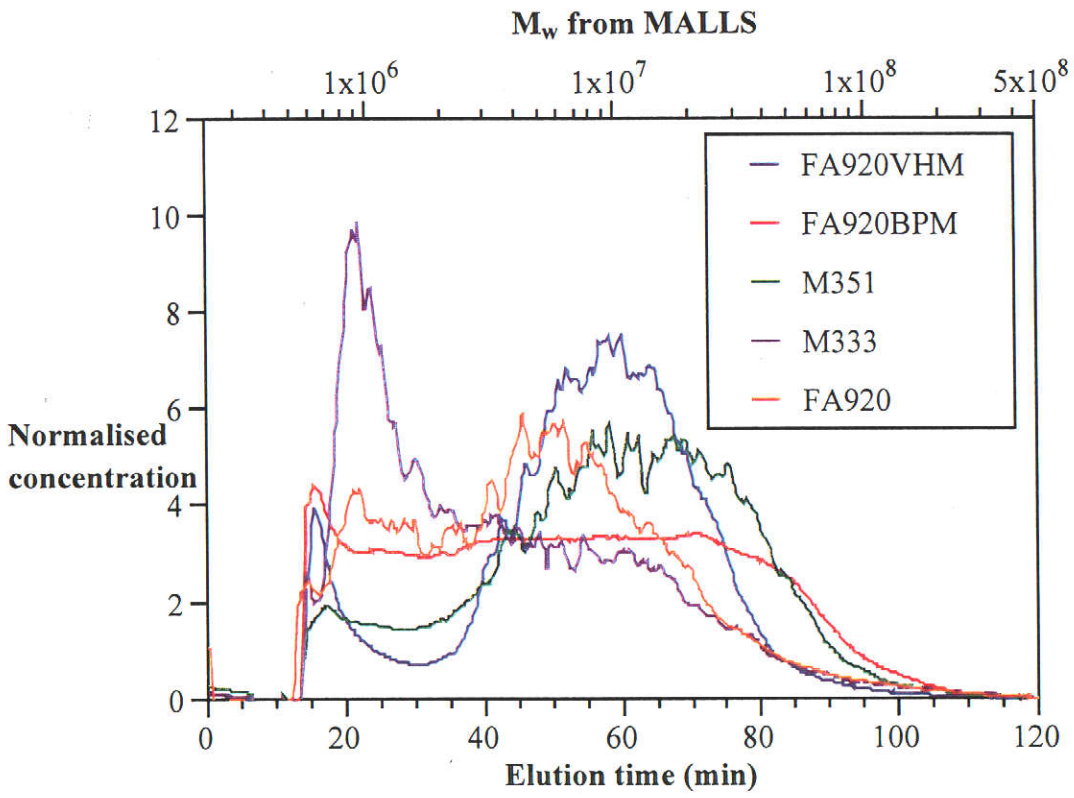

Figure 5B Molecular mass distribution of commercial flocculants prepared in 0.1 M NaCl and aged two days.

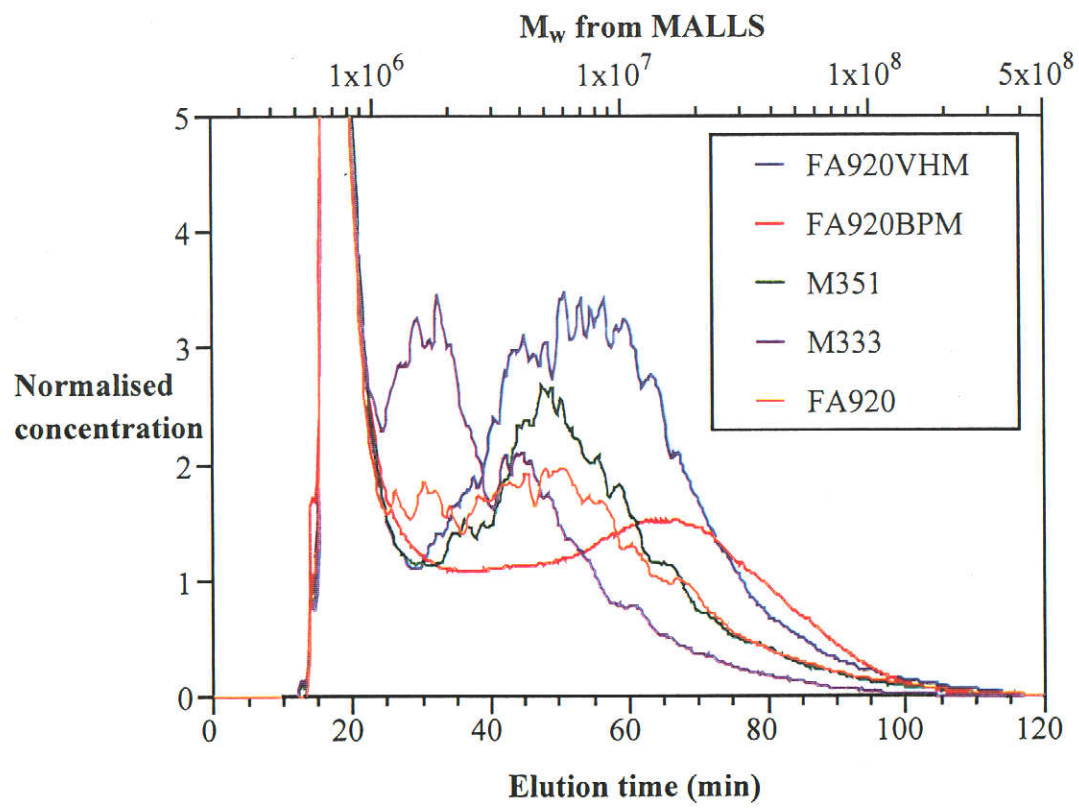

Table 5A Dilute aqueous solutions of commercial polyacrylamides. Mean molecular masses (cited by manufacturer and light scattering), and viscosities (reported as extrapolation to infinite dilution and extrapolation correlation coefficient) are presented.

Flocculant commercial designation	Mean molecular mass Manufacturer cited $\times 10^6$	MALLS[A] M_w $\times 10^6$	Solution viscosity Capillary[B] mL mg^{-1}	Rotational[C] $\times 10^3$ kg m^{-1} s^{-1}
M333	19-22	20.2	2.21 (R^2 0.98)	1.61 (R^2 0.98)
M351	15-17	10.8	0.73 (R^2 0.95)	0.91 (R^2 0.97)
FA920VHM	22-25	23.2	0.75 (R^2 0.98)	0.96 (R^2 0.99)
FA920	16-19	13.0	1.47 (R^2 0.97)	0.95 (R^2 0.99)
FA920BPM	7-9	11.6	0.41 (R^2 0.95)	0.80 (R^2 0.99)

A: solutions unfiltered, 5th order Debye fit, dn/dc 0.190 mg mL^{-1}, in 0.1 NaCl.

B: Ubbhelode viscometer (no. 75, 0.01017 cSt s^{-1}) at 35.0°C.

C: Brookfield inner-rotating cylinder, with UL spindle adaptor.

Table 5B Features of commercial flocculants. Feature present = ✓. Feature indicated or few in number = (). Corresponding flocculation performance is discussed in Section 5.3.3.

Flocculant	Free coils	Submicron entwinements	Supramicron agglomerates	Flocculation type
FA920BPM	✓	✓		type (a)
M351	✓	✓		type (a)
FA920VHM	✓			type (b)
FA920	✓		(✓)	type (b)
M333	✓	(?)	✓	type (c)

Gregory (1989) specified two levels of flocculation, particle and cluster. Particle-particle aggregation is linked to greater fractal dimension, higher density and smaller diameters, as described at length in Section 1.4. These aggregates may in turn be aggregated to a cluster formation featuring a more "open" structure. Polymer agglomerates are suited for flocculating the aggregates to clusters, since they are both sufficiently large and able to multiply bind to the clusters. Based upon the knowledge gained of the composition of PAAm, there are a number of possible flocculation mechanisms. This proposed scale of flocculation is expressed in Figure 5-1. For free particles and dispersed flocculant, the aggregation occurs by a conventional bridging mechanism. For particle clusters the free polymer is unable form a sufficiently strong bridge to resist shearing, leading to a distinct maximum aggregate size. Polymer agglomerates may occupy more surface adsorption sites to make a stronger bridge with better shear resistance. The improved shear resistance would therefore favour the formation of larger aggregates.

Figure 5-1 Particle-particle and cluster-cluster flocculation aggregated by free and agglomerated polymer. Dispersed polymer bridges across free particles to form an aggregate, but the dispersed polymer is poorly able to bind the aggregates to clusters. Polymer agglomerates ably form aggregate clusters.

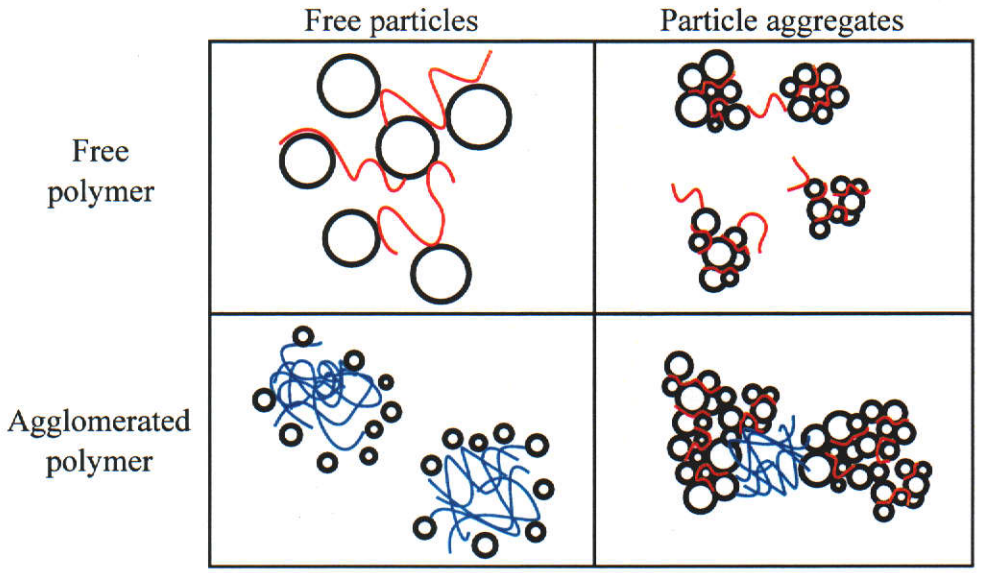

An analogous effect to the mechanism of Figure 5-1 has been reported by Moudgil *et al.* (1993) where the larger particles will be flocculated only with correspondingly high molecular mass polymer, although the flocculant is at least an order of magnitude smaller than the particles. The authors report that the flocculation of coarse particles requires a binding force to be at least as strong as the shearing force.

This Chapter will show that the partition of PAAm in solution between free coils, entwinements and agglomerates indicates, *a priori*, the flocculation activity of the solution. The Chapter concludes by proposing a modified flocculation mechanism.

5.1 TEST METHODS

5.1.1 Shear Vessel: reproducible mixing

An evaluation of flocculant performance is most commonly derived from hindered settling rates and residual turbidities. Hindered settling rates, measured from the rate of descent of a mudline, provide a qualitative indication of aggregate dimensions, while residual turbidities (measured after most of the aggregates have settled) demonstrate the degree of capture of free particles or the properties of small aggregates. These performance parameters are normally obtained from cylinder tests, where dilute polymer is simply dosed into a standard cylinder of slurry and mixed, either by inversion or with plungers. While such tests are simple and convenient, they suffer from ill-defined mixing and are highly operator dependent. The poor mixing can leave polymer-rich and polymer-poor regions, resulting in irreproducible flocculation (Moss and Dymond 1978, Farrow and Swift 1996a).

Farrow and Swift (1996a) developed a new tool to characterise flocculation, which they termed the Shear Vessel. An inner-rotating cylinder generates an annular (Couette) shear zone for reproducible mixing. Flocculant may be added at a number of points, while varying the rotation rate generates a range of agitation intensities. The Shear Vessel has been shown to provide highly reproducible results and allows measurement of both hindered settling rate and turbidity through isolation of the flocculated product in a settling tube. The Shear Vessel flocculates continuously with a controlled residence time, more appropriate for modelling the operation of a thickener feedwell than cylinder testing.

5.1.2 FBRM: aggregate characterisation

Fragile aggregates are a challenge to characterise. For a size distribution, visual measurements of sedimentation are time consuming and prone to operator error (Farrow and Warren 1993), while orifice conductivity fluctuations (Coulter counter) or laser diffraction (Malvern MasterSizer) are not suited to the high solids concentration of flocculated slurries. Microscopic characterisation such as electron or optical microscopies require dewatered samples, leading to irreversible damage (Moudgil and Shah 1986, Moudgil and Behl 1993). For the above techniques sample manipulation and degradation is of paramount concern, and satisfactory measurements therefore demand an in-process technique.

Turbidity fluctuations measure *in situ* the extent of aggregation directly for dilute slurries (Gregory 1991), while sedimentation techniques provide *in situ* size and density (Farrow and Warren 1993). An extensive experimental program to characterise aggregates through sedimentation rates using a "floc density analyser" (Farrow and Warren 1989a, 1989b) was attempted, as described in Appendix 2. Data scatter obscured many subtle aggregation features, and this approach was therefore not continued further.

Focussed beam reflectance measurement (FBRM) is capable of providing real time measurements in a process stream, with measurement over a wide range of solids concentrations. FBRM uses a highly focussed, rotating laser beam projected through a window. When particulate material contacts the focal plane the laser beam is reflected back, and the duration of the reflection is a measure of the particle chord length (Figure 5-2, Figure 5-3). Several thousands of chord lengths are acquired per second. Integration of the chord lengths produces a real-time chord length distribution. While the chord length distribution is not directly comparable to distributions measured by laser diffraction instruments, it provides invaluable data unobtainable by other techniques.

Figure 5-2 Example chord length of a spherical body.

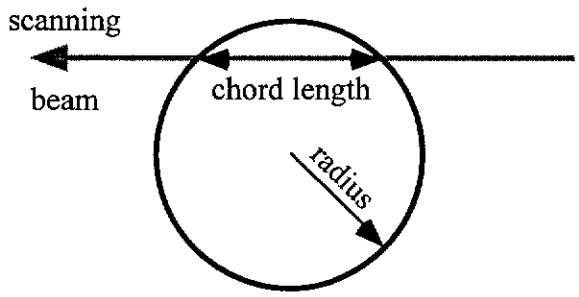

The use of FBRM to study aggregated mineral slurries is still in its infancy. Williams *et al.* (1992) have used the method for silica coagulation and confirmed FBRM data provides a measure of coagula formation rates and mechanical strength. Peng and Williams (1993, 1994) extended the applications of FBRM to investigate silica flocculation by cationic PAAm derivatives, flocculant dosage protocol and aggregate breakage. Recently, Fawell *et al.* (1997) compared the FBRM data with classic cylinder testing for haematite flocculation to find a satisfactory relationship between hindered settling and mean chord length, and between fine counts and turbidity.

5.1.3 Linking the Shear Vessel with the FBRM

Kirwan (1997) has successfully used an FBRM probe in conjunction with the Shear Vessel to monitor the flocculation of kaolin with PAAm. The hindered settling rate of aggregates was correlated to the mean of the weighted chord lengths. The use of FBRM expanded upon the flocculation data available from the Shear Vessel, allowing a more detailed assessment of the extent and efficiency of aggregation achieved.

Figure 5-3 Operation of the FBRM probe: bodies near the sapphire window reflect the rapidly moving focussed laser. Sophisticated electronics convert the reflected signal into chord lengths and a chord length distribution.

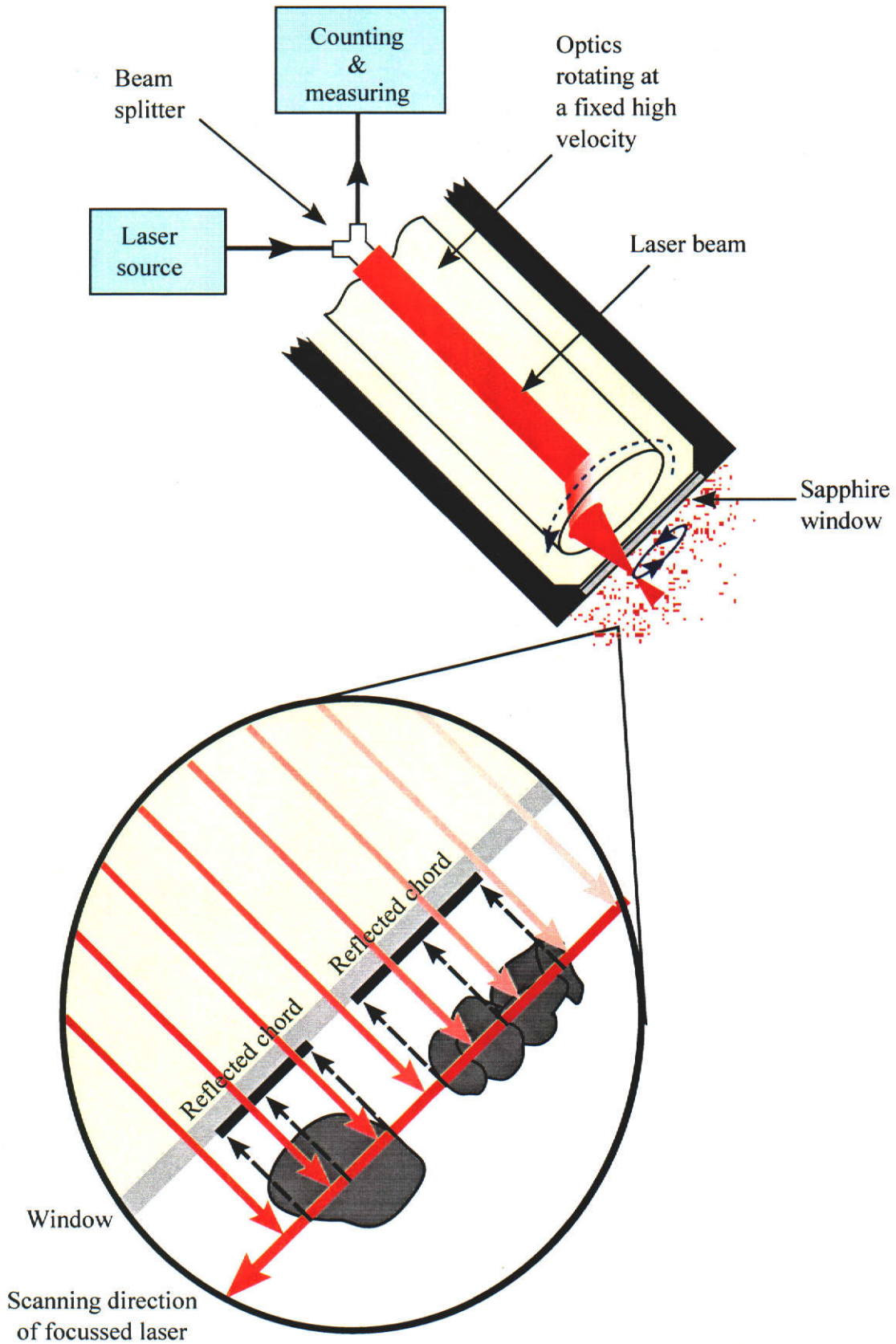

5.2 EXPERIMENTAL

5.2.1 Materials and preparation

5.2.1.1 Substrate

Kaolin RF (12.96 kg, Commercial Minerals, Perth, Australia) was allowed to soak overnight in 80 L of deionised water. This concentrate was recirculated for four hours through an inline mixer (Sulzer SMV4DM25, Wohlen, Switzerland) by means of a self-priming centrifugal pump (Weir Engineering model 25SP-120, Perth, Australia) to reduce the extent of aggregation. The slurry was pumped into a 375 L feed tank, equipped with four equally spaced vertical baffles, and diluted to 4.5 wt.-% solids. The dilute slurry was kept constantly agitated by a stirrer fitted with three 325 mm diameter impellers (Lightnin, Rochester, New York). Sodium chloride (90 g, 5 mM) was added for the benefit of the Shear Vessel's conductivity sensors (Section 5.2.2.1).

Particle size analysis was conducted using a Malvern MasterSizer (Malvern, England) on samples taken immediately prior to entry into the Shear Vessel. The period between sampling and analysis was less than five minutes.

5.2.1.2 *Polyacrylamide*

Polymers used in this study were commercial powder flocculants M333, M351, FA920VHM, FA920 and FA920BPM (Section 4.2.1). Solutions were prepared to *ca.* 5 mg mL^{-1} concentration according to the procedures described in Section 3.2.3. All stock solutions were allowed to age for three days before use. Immediately prior to use the stock was diluted to *ca.* 0.2 mg mL^{-1} by syringe addition into a 2 L beaker, then made up to volume with deionised water or salt solution, added with swirling. Exact flocculant concentrations and dosages are summarised in Table 5-1.

Table 5-1 Flocculant concentrations for stock and diluted. Dosage values are calculated as noted. For samples diluted into NaCl both stock and diluent salt concentrations were identical.

Flocculant	Stock concentration (mg mL^{-1})	Diluted concentration (mg mL^{-1})	Dosage[A] (g t^{-1})
M351	4.83	0.191	108
FA920BPM	4.74	0.190	107
FA920	4.74	0.189	106
FA920VHM	4.64	0.186	105
M333	5.03	0.199	112
M351, 0.104 mol L^{-1} NaCl	4.84	0.192	108
M333, 0.097 mol L^{-1} NaCl	5.03	0.198	110

[A] Flow rate, and therefore dosage, for the addition of diluted flocculant calculated for 4.5 wt.-% kaolin pumped into the Shear Vessel at 400 mL min^{-1} and flocculant at 10 mL min^{-1}. These are the "standard conditions", Section 5.3.4.

5.2.2 Instrumentation

5.2.2.1 Shear Vessel

The Shear Vessel (Figure 5-4) consists of an external fixed cylinder (210 mm diameter) and inner rotating cylinder (200 mm diameter) to generate a 5 mm gap. The inner cylinder was driven by a variable speed motor from 50 to 300 rpm. The cylinders taper at 45° at the base with the 5 mm gap maintained. The shear conditions generated within the Shear Vessel were proportional to the rotation rate of the inner cylinder while the shear in the taper section was much less. Flocculant addition ports were positioned vertically every 50 mm along the outer cylinder. The total volume of the annular gap was 0.760 L with volumes of 0.093 L, 0.254 L and 0.415 L under flocculant Ports 1, 2 and 3 respectively, while the volume of the taper section is 0.223 L. A fourth flocculant port positioned higher, representing an annular volume of 0.576 L, was not used. For a slurry flow rate of 400 mL min^{-1}, (Section 5.3.1) mean slurry residence times are 14, 38 and 62 s for Ports 1, 2 and 3, respectively, although some correction is required for rapidly settling aggregates.

The slurried kaolin was pumped from the holding tank using a peristaltic pump ("pump 1": Masterflex 7550-62, Barrington, Illinois; tubing: Tygon size 17 from Masterflex) at a constant 400 mL min^{-1}. Dilute flocculant was added to the top of the Shear Vessel at a rate between 4 to 14 mL min^{-1}, using another pump ("pump 2": Masterflex 7550-92, size 14 Tygon tubing) corresponding to dosages from *ca.* 40 to 150 g of flocculant per tonne of slurry. The level of material in the Shear Vessel was maintained by third pump ("pump 3": Masterflex 7550-62), withdrawing flocculated slurry at a variable rate as determined by the conductivity sensors.

Figure 5-4 Schematic representation of the Shear Vessel. Slurry is fed into the top of the annular shear region and flocculant may be added in one of three flocculant addition ports. Beneath the body of the Shear Vessel lies the settling tube to measure hindered settling rates, nephelometer for turbidity and the FBRM probe.

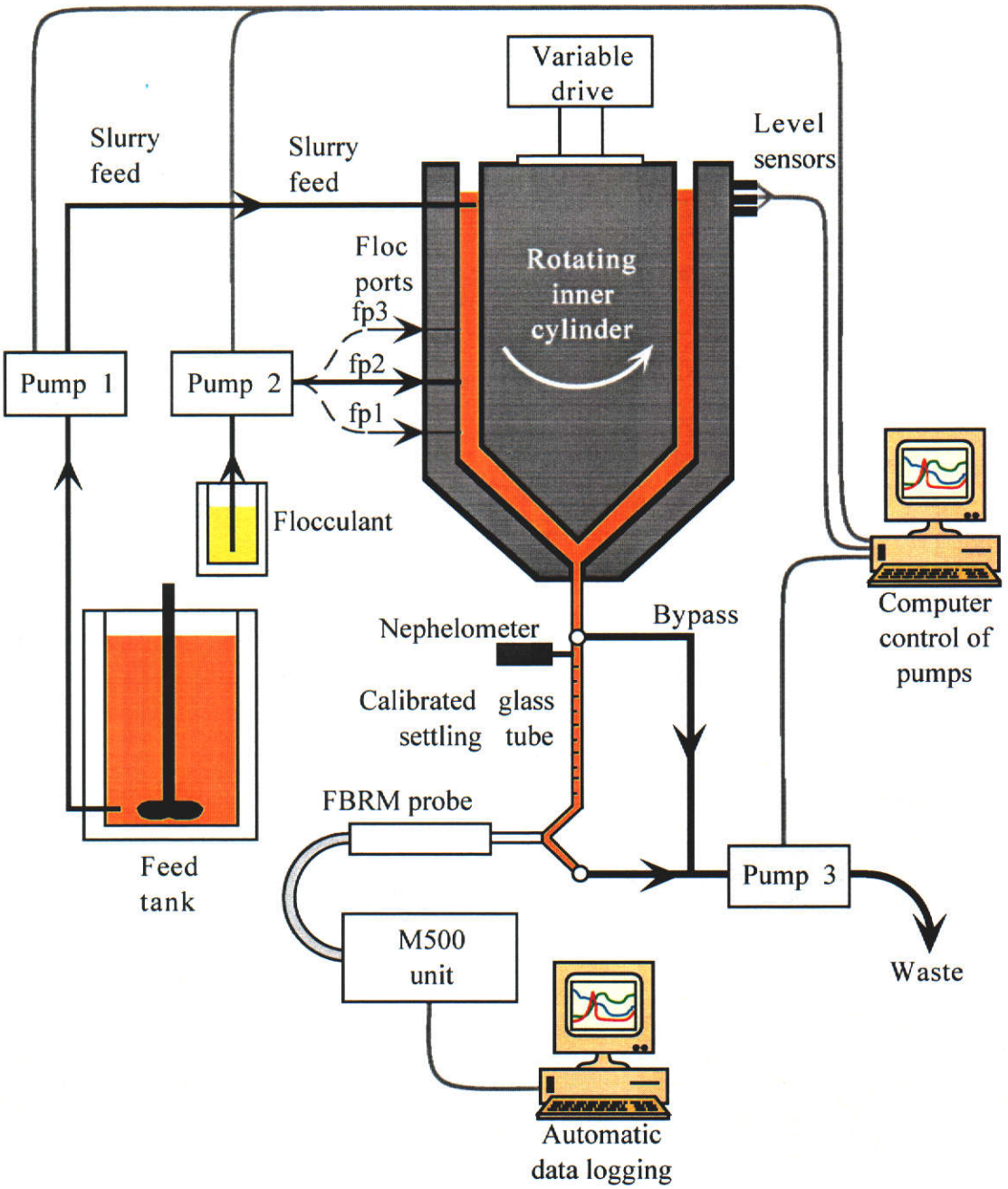

5.2.2.2 *Activity measurements*

A portion of the flocculated underflow from the Shear Vessel was trapped in the settling tube (internal diameter 15 mm) while diverting the flow through a bypass line (Figure 5-4). The flow of slurry and flocculant could therefore be maintained without interruption. The hindered settling rate was calculated from the linear rate of descent of the mudline of the flocculated material. The supernatant turbidity was measured by a nephelometer (Analite, Mulgrave, Australia) installed in the settling tube. The nephelometer was calibrated against a formazin turbidity standard (Hach, Loveland, Colorado).

5.2.2.3 *Focussed Beam Reflectance Measurement (FBRM)*

The FBRM system (Lasentec, Redmond, Washington) consisted of a M500 field unit and a 316 stainless steel laboratory probe with high speed scanning optics. The field unit was fitted with the Lasentec "C" electronics, appropriate for use with aggregated suspensions. The probe is connected to the unit, which contains the scanning drive motor and the controlling electronics, by a 10 m fibre optic cable. The FBRM probe was positioned at 45° to the direction of flow from the Shear Vessel (Figure 5-4) to ensure no dead zones were present in front of the window. The scanning laser was focussed onto the sapphire window. The FBRM probe returns counts from chord lengths of 0.8 to 1000 μm over 38 channels. Data chosen for display on-line were chord length distribution (raw counts per channel and as normalised ratio per channel), weighted distributions and sum of counts in specified ranges. A fuller description of the weighting functions is included in Appendix 3. Data was collected every five seconds and averaged over five consecutive measurements.

The maximum chord length corresponds to the diameter of the largest aggregates. Mean chord length is a function of both aggregate size and shape, as increasing

ellipsoidal eccentricity increases the breadth of chord length distribution compared to a sphere. To quantitatively link aggregate size distribution with chord length distribution is beyond the scope of this research, but the trends in the mean and maximum chord length have been shown to be a good measure of flocculation efficiency (Williams *et al.* 1992, Fawell *et al.* 1997, Kirwan 1997).

Flocculation in the Shear Vessel as monitored by FBRM follows the general form demonstrated in Figure 5-5. As the applied shear is increased from its lowest value the mean chord parameter increases until a maximum is passed. Further increases in shear produce a reduced parameter until a threshold shear is passed, after which the chord parameter remains essentially stable for greater shear. The position of the maximum and threshold vary with flocculant and dosage and therefore reflect fundamental physicochemical attributes.

Figure 5-5 General FBRM-flocculation curve. Shear is imparted onto the slurry and aggregates through the Shear Vessel rotation. Optimum shear gives rises to the greatest mean chord length parameter, while increased shear limits the size of the aggregates.

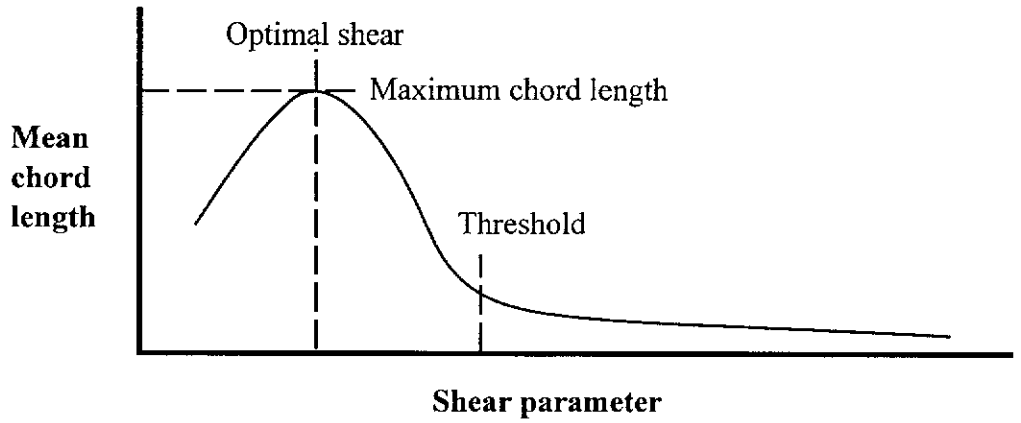

5.2.3 Testing protocols

For a given set of Shear Vessel conditions (rotation rate, flocculant port, flocculant addition rate) data was collected continuously by the FBRM system. When the FBRM signal trend stabilised, measurements for hindered settling rate and

supernatant turbidity was made. Turbidity measurements were low under virtually all conditions, consistent with the observations of Kirwan (1997). It was concluded the majority of unflocculated fines were swept down during the hindered settling process. Turbidities are therefore not reported.

The effect of a range of rotation rates (from 50 to 300 rpm) on hindered settling rate was observed from Port 2 for a given flocculant. The procedure was repeated for shorter and longer residence times (Ports 1 and 3). With Port 2, the effect of flocculant dose was also investigated.

The unflocculated slurry settled at 0.35 m hr^{-1}. For some conditions the flocculated slurry only settled slightly faster than unflocculated material. Hindered settling was observed up to 15 m hr^{-1}. Highly flocculated samples formed macroaggregates and settled independently to give no definite mudline and an unmeasurable settling rate.

5.3 *Results and Discussion of Flocculation Tests*

5.3.1 *Slurry reproducibility*

Kaolin slurry was sampled immediately after the slurry peristaltic pump (Figure 5-4, pump 1) prior to entering the Shear Vessel, and was analysed without further dilution or dispersion. Particle size distributions measured on two separate days are given in Figure 5-6, with the d_{50} of the slurries being 3.97 and 4.40 μm. Samples taken at random and dried overnight during the testing period showed mean solids of 4.35±0.09 g per 100 g of slurry. Slurry density and pH were measured as 1.016 g mL^{-1} and 6.60, respectively, at 20°C.

Figure 5-6 Particle volume-based distribution of slurried kaolin substrate from Malvern MasterSizer.

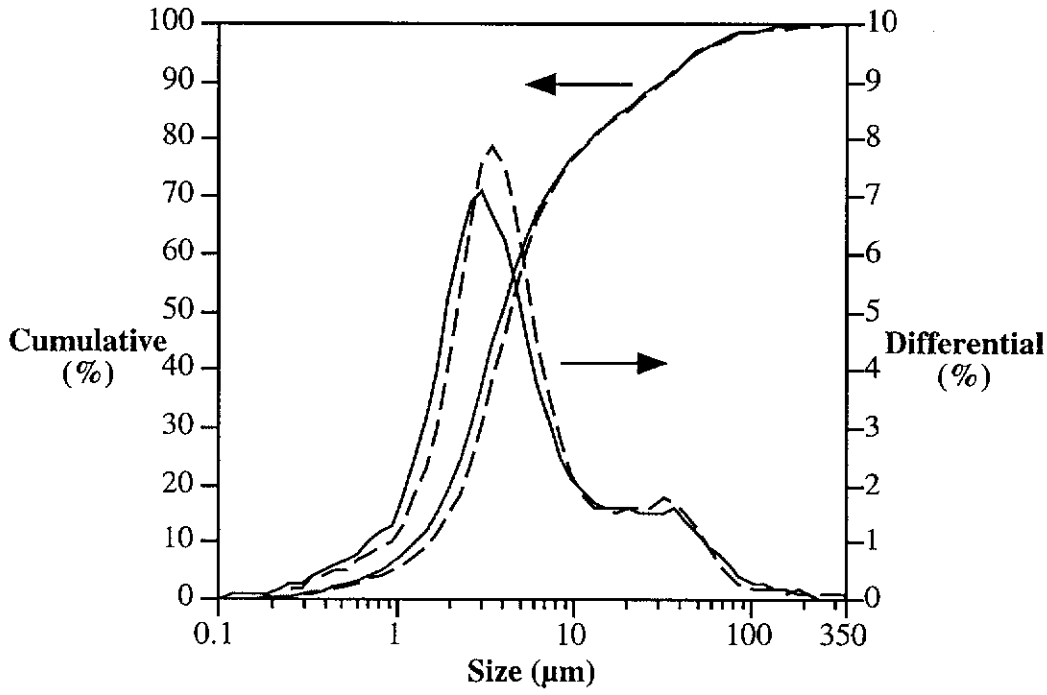

A constant slurry flowrate of 400 mL min^{-1} was selected to ensure a satisfactory presentation of material to the FBRM probe. At low flowrates, fast settling aggregates may not be well presented, while faster flowrates require excessive volumes of slurry (Kirwan 1997). The slurry flowrate was equivalent to 17.7 g min^{-1} of solids.

5.3.2 *Observed hindered settling rate with FBRM*

Kirwan (1997) demonstrated that observed hindered settling rates could be related to mean chord lengths, with improved correlation achieved using the higher order weightings. This correlation demonstrated that the hindered settling rate is dependent upon the coarser aggregates, while being largely unaffected by the presence of fines.

Figure 5-7 Correlation of observed hindered settling rate with FBRM measurements.

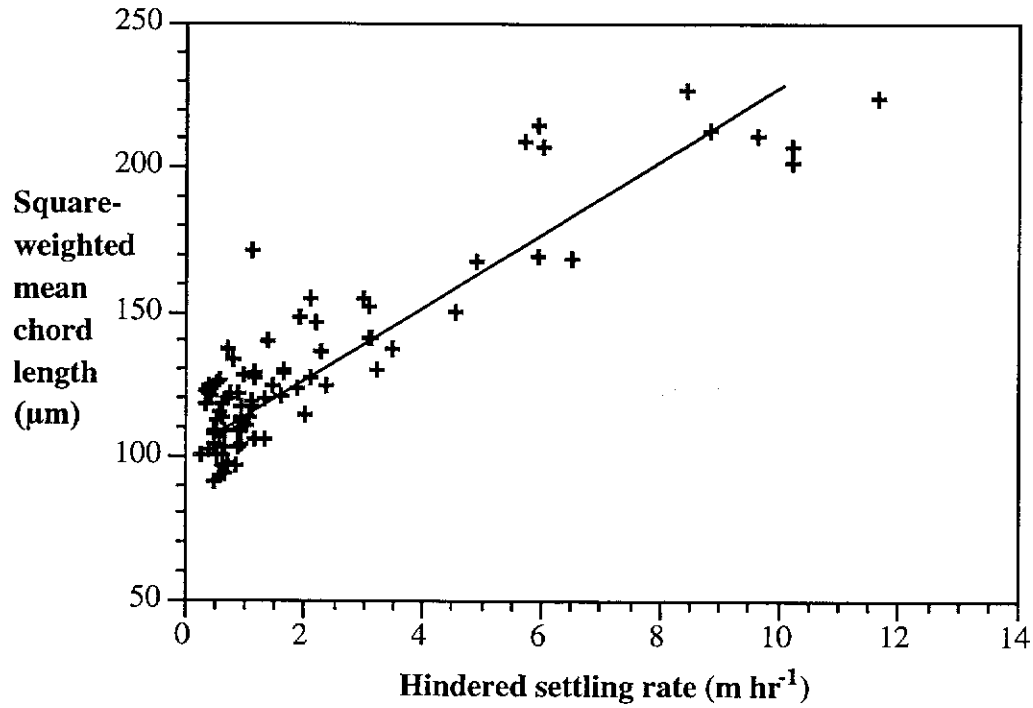

Figure 5-7, which compares the measured hindered settling rate with the FBRM square-weighted chord length over all flocculation conditions (dosage, rotation rate, flocculant type, and residence time), supports Kirwan's result. A least-squares fit between the measurements had a correlation coefficient R^2 of 0.76. This correlation suffers due to the number of points at low hindered settling rates (< 2 m hr^{-1}) where the scatter is greatest. In this region, the hindered settling rate is relatively insensitive to small changes in the state of flocculation, while FBRM readily detects the formation of small aggregates. Aggregate size-dependant density (Farrow and Warren 1993) may contribute to some non-linearity in the correlation.

5.3.3 Flocculation performance of different flocculants

Figure 5-8 shows the FBRM mean chord lengths versus Shear Vessel rotation rates for five commercial flocculants applied at equivalent dosages (Table 5-1). Clearly, there is a distinct response to agitation intensity for each flocculant. Farrow and Swift (1996b), using hindered settling rates and residual turbidities to monitor performance, also observed such differences in the behaviour of flocculants.

Included in Figure 5-8 are the mean number- and square-weighted chord lengths for the unflocculated slurry, at 18 and 59 μm, respectively. The mean chords of the flocculated slurry are always greater than for unflocculated slurry, demonstrating that over the rotation rates investigated, excessive agitation alone does not fully redisperse the particles. The largest aggregates were formed under mild agitation conditions, under 100 rpm. Over rotation rates of 100 rpm, the mean chord lengths exhibit a decreasing size with increasing agitation. This may be attributed to both aggregate densification and rupture processes (Mühle and Domasch 1991).

From Table 5B (fold-out page), flocculants M351 and FA920BPM, termed type (a), feature submicron entwinements of several polymer coils. Type (b) flocculants FA920 and FA920VHM are free of entwinements, while FA920 indicated the presence of supramicron agglomerates. Supramicron agglomerates dominate the type (c) flocculant M333. The three types of flocculants show distinctly different performances (Figure 5-8). M351 and FA920BPM resulted in aggregates with the shortest mean chord lengths with little change over the range of rotation rates. FA920VHM and FA920 gave much larger mean chords but also a marked decrease in chord length with increasing agitation. M333 exhibited similar behaviour to FA920VHM and FA920, but with a distinct maximum performance observed at an "optimum" rotation rate (type c). The following Sections compare and contrast these flocculation behaviours.

Figure 5-8 Effect of agitation intensity on FBRM mean (a) number- and (b) square-weighted chord lengths. Dosages are given in Table 5-1.

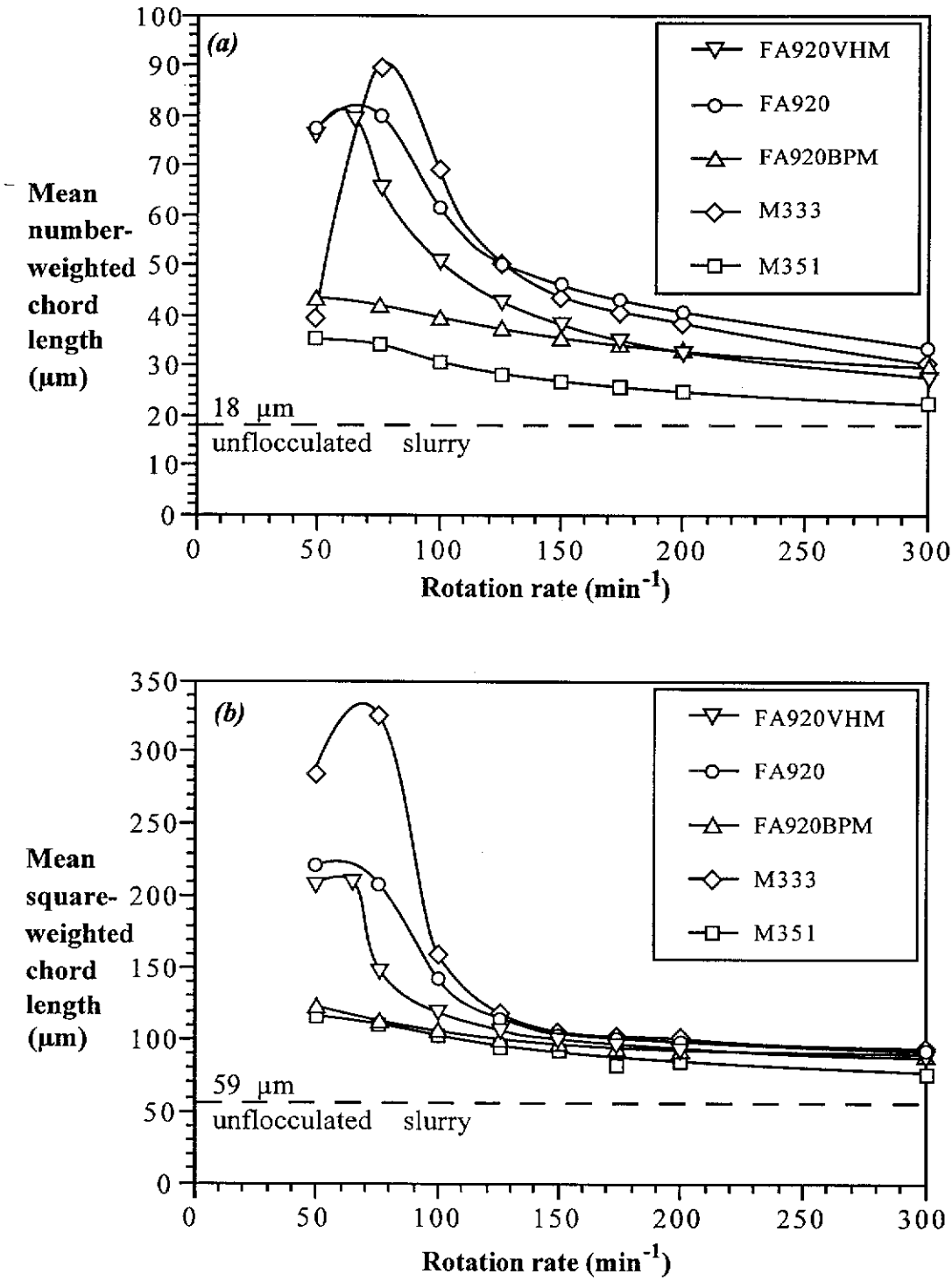

5.3.4 M351 and FA920BPM: type (a) flocculants

Under standard flocculation conditions (*ca.* 105 g t^{-1} dosage through Port 2), the mean square-weighted chord lengths at all rotation rates (Figure 5-8b) for both M351 and FA920BPM were nearly identical. The mean number-weighted chord length (Figure 5-8a) was greater for FA920BPM, indicating this flocculant gave an improved capture of fines compared to M351. Hindered settling rates for both were very poor; at a rotation rate of 50 rpm the measured hindered settling rates were 0.7 m hr^{-1} and 0.4 m hr^{-1} for FA920BPM and M351, respectively.

The effect of Shear Vessel residence time and rotation rate on flocculation performance by FA920BPM is shown in Figure 5-9. The square-weighted chord distributions for flocculated material clearly demonstrated the presence of larger aggregates as compared to the unflocculated kaolin. These distributions were virtually independent of the flocculant addition port used, which represented residence times from 14 s (Port 1) to 62 s (Port 3). The slight shift in the distributions to smaller sizes with increasing agitation reflected the response of the mean chord length shown in Figure 5-8. Interestingly, the maximum chord length, corresponding to the diameter of the largest aggregates, was constant at 250 μm, with neither residence time nor rotation rate a contributing factor. The corresponding data for M351 flocculation showed identical trends. These results indicate flocculation with FA920BPM and M351 formed compact aggregates resistant to shear effects.

The effect of flocculant dosage on the mean square-weighted chord length is presented in Figure 5-10. It is clear that raising the flocculant dosage by 40% led to a slight increase to the mean chord length, and consequently increased the hindered settling rate. For example, the hindered settling rate increased from 0.7 to 2.0 m hr^{-1} once the FA920BPM dosage was raised from 107 to 150 g t^{-1} at 50 rpm agitation intensity. Under the same conditions the mean square-weighted chord length (Figure 5-10) increased from 125 to 147 μm.

Figure 5-9 Effect of residence time and rotation rate for FA920BPM flocculation. Distributions are for the square-weighted chords. Dosage was fixed at 107 g t^{-1}.

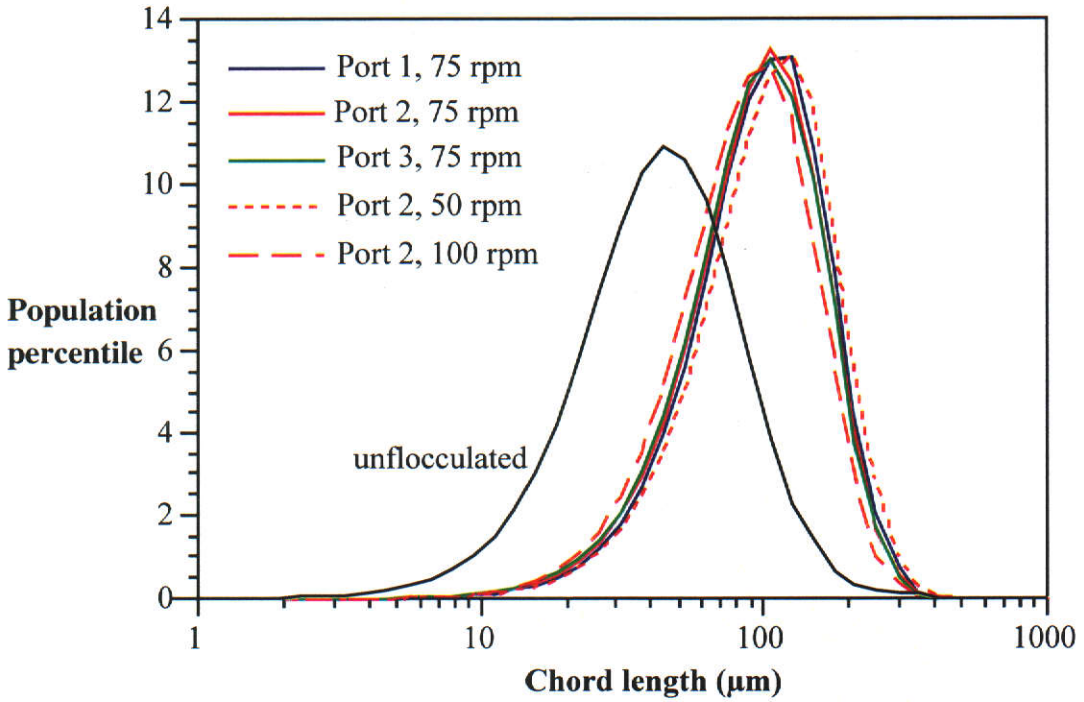

Figure 5-10 Effect of dosage on mean square-weighted chord length for type (a) flocculants. Dosages are: FA920BPM (107, 150 g t^{-1}) and M351 (108, 151 g t^{-1}).

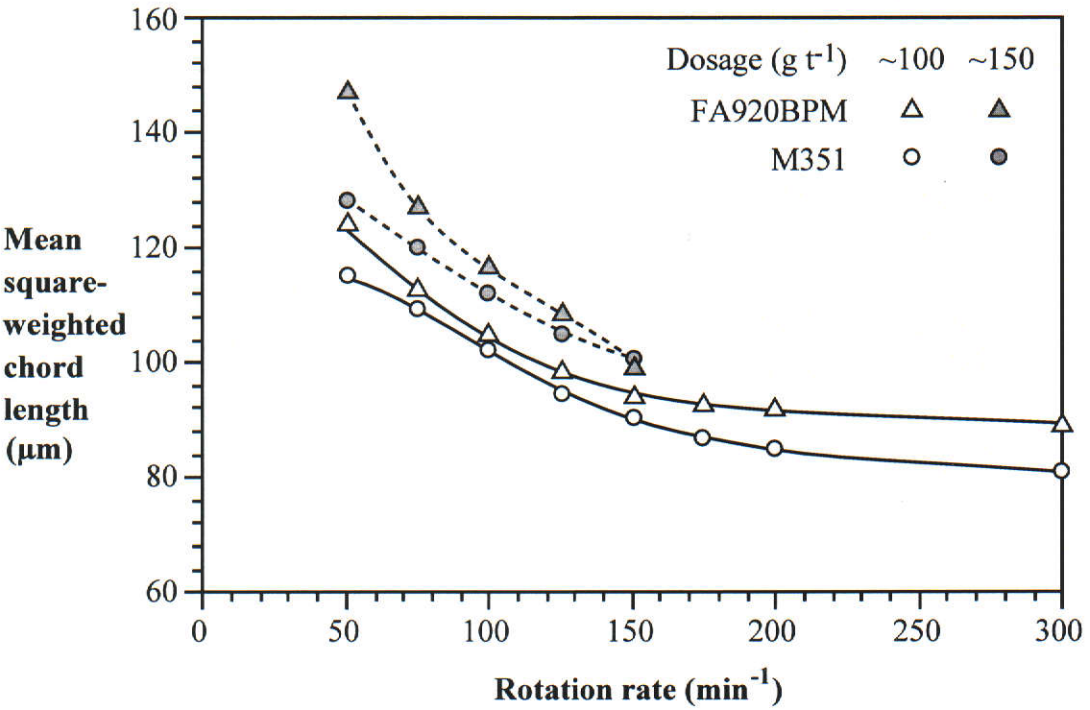

5.3.5 FA920 and FA920VHM: type (b) flocculants

Figure 5-8 showed that FA920 and FA920VHM produced large aggregates at rotation rates below 100 rpm, as monitored by the mean chord lengths. Hindered settling rates measured on the flocculated slurry (Table 5-2) displayed a similar response to agitation intensity, consistent with the chord length-settling rate correlation presented in Figure 5-7. The hindered settling rate for FA920VHM at 50 rpm could not be measured, as extremely large aggregates (up to 5 mm) were formed in the settling tube and no longer settled under hindered conditions, consequently without a clear mudline. Unlike the type (a) flocculants, Figure 5-8 shows these polymers exhibited a threshold shear, beyond which both the mean chord length and the hindered settling rate decreased significantly; *i.e.* performance worsened.

Table 5-2 Hindered settling rates of slurry (m hr^{-1}) with type (b) flocculants FA920VHM and FA920. "Not measurable" indicates no clear mudline was visible.

Rotation rate (rpm)	FA920VHM	FA920
50	Not measurable	11.7
65	10.3	
75	3.1	8.9
100	3.0	3.1
125	1.8	1.6
150	1.7	1.2
200	1.2	0.8
300	< 0.5	< 0.5

The square-weighted chord length distribution (Figure 5-11) shows for both flocculants that the maximum chord length observed was 600 μm. This value was achieved for FA920 and FA920VHM at rotation rates in the range 50 to 75 rpm and 50 to 65 rpm, respectively. In contrast to the type (a) flocculants (Figure 5-9) this maximum chord length is a function of the rotation rate, decreasing to approximately 400 μm at 100 rpm, and further to 350 μm at 150 rpm, for both flocculants.

Figure 5-11 Effect of rotation rate for type (b) flocculants. Distributions are from the square-weighted chords. Dosages are given in Table 5-1.

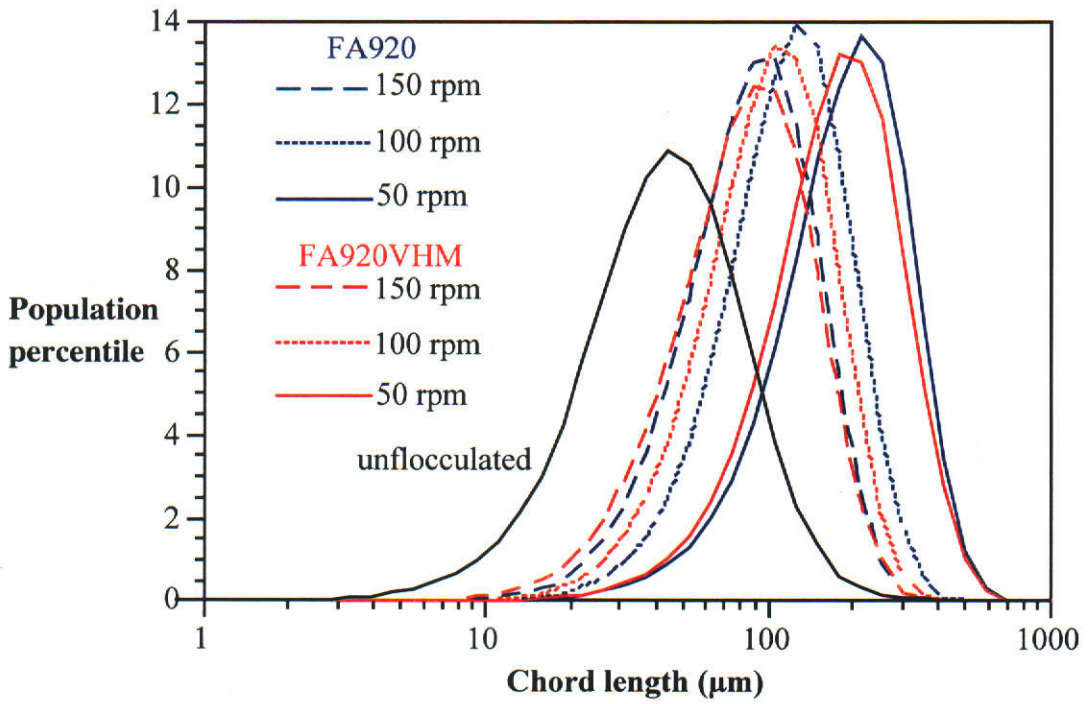

The effect of Shear Vessel residence time for FA920VHM is shown in Figure 5-12. In contrast to the type (a) flocculants, residence time has a significant influence on the aggregate size, as monitored by FBRM measurement. A 14 s residence time (Port 1) produced the greatest mean chord length and hindered settling rate, while increased residence, at 38 s or 62 s (Port 2 and Port 3, respectively), led to a decrease in both parameters. Analogous to Figure 5-11, chord length distributions obtained through Port 1 had a maximum chord length in excess of 1000 μm at 50 rpm. However, the hindered settling rate was not measurable as overflocculation (Section 5.2.3)

precluded a clear mudline. Flocculation with FA920 followed the same trends as described for FA920VHM.

Figure 5-12 Shear Vessel agitation intensity and residence time effects for flocculation by FA920VHM at 105 g t^{-1} dosage.

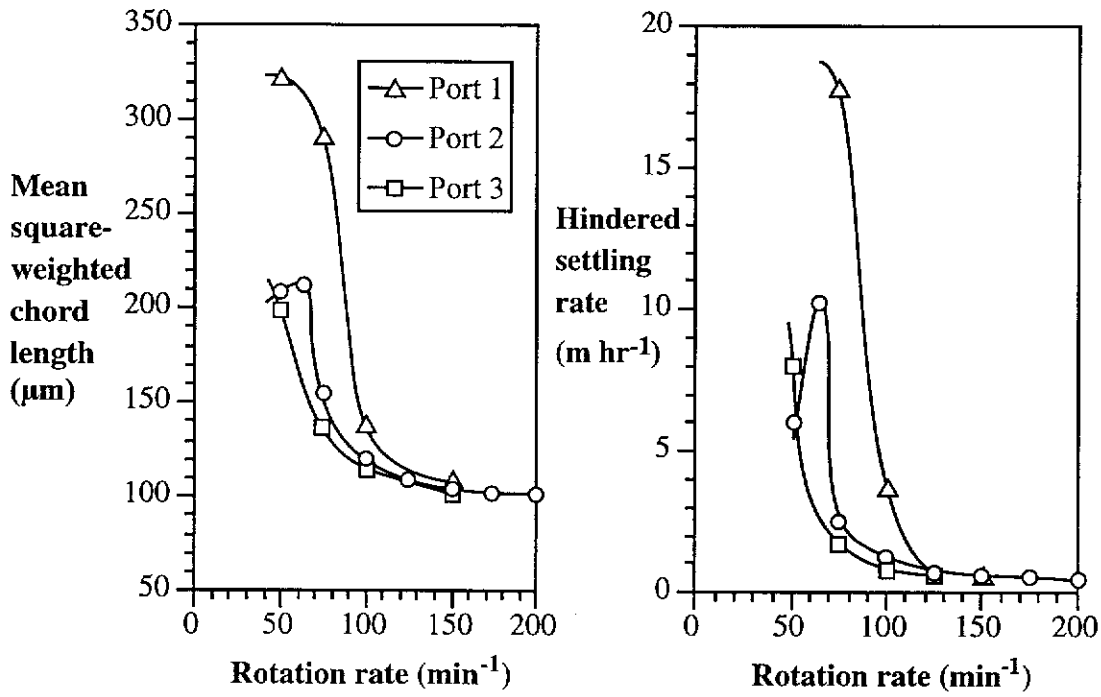

The mean square-weighted chord length, as a function of Shear Vessel rotation rate, for FA920 and FA920VHM over a range of dosages is given in Figure 5-13. Although the concentrations of the two flocculants differed by 1.6% (Table 5-1), this difference was minor compared to the changes in the applied dosage. The two flocculants differed slightly in their response to variations in dosage. At ~75 g t^{-1} FA920VHM behaved similarly to the type (a) flocculants, forming small aggregates. At 150 g t^{-1} the performance of both flocculants was very much enhanced, with "clustering" behaviour observed at rotation rates below 100 rpm. However, the threshold shear for FA920 appears to be greater, suggesting that FA920 formed stronger, more shear-resistant aggregates compared to FA920VHM.

Figure 5-13 Dosage curves for (a) FA920VHM at dosages 146, 105, 73 and 42 g t^{-1}, and for (b) FA920 at dosages 149, 106, 74 and 42 g t^{-1}. Standard flocculation conditions were used with addition through Port 2.

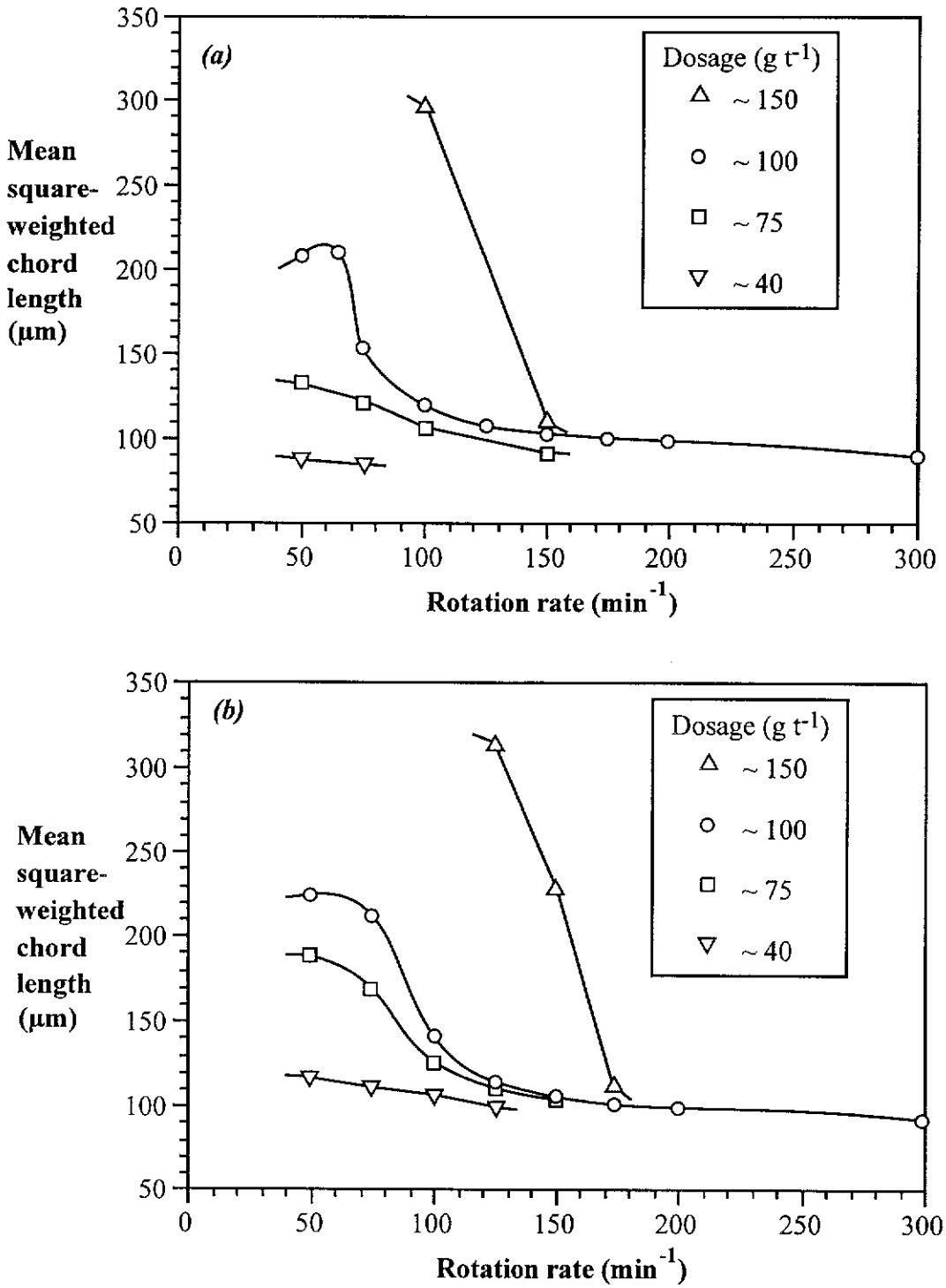

Changes in flocculant dosage influenced the gradient of the mean chord length *versus* agitation intensity plot. Since, from the chord distributions (Figure 5-9, Figure 5-11), an increase in the mean square-weighted length follows a greater maximum chord length and aggregate size, the longer mean chord length achieved with higher dosage is therefore attributed to the formation of larger aggregates. However, as the data in Figure 5-13 shows, higher flocculant dosages were much more effective at low agitation conditions, with convergent results being obtained at ~150 rpm, irrespective of dosage. Large aggregates cannot be formed at higher agitation intensities, even at high flocculant dosages.

5.3.6 M333: type (c) flocculants

M333 is treated separately from the type (b) flocculants based on the distinct optimum agitation needed for good flocculation, as shown in Figure 5-8. The flocculation behaviour of M333 could be attributed to its slightly greater viscosity (as collated in the fold-out page) leading to poor mixing during low agitation. However, for this to be true, the more viscous FA920 would have shown markedly improved flocculation over FA920VHM (type (b) flocculants), and less viscous FA920BPM to be much less active than M351 (type (a) flocculants). Further, the viscosities of the diluted PAAm solutions were so low that they are considered unlikely to influence mixing in the Shear Vessel. For these reasons, good flocculation correlating solely with solution viscosity is rejected, although viscosity-affected activity may be applicable for charged flocculants such as polyacrylate, which exhibit a much higher viscosity in the absence of salt.

At high rotation rates (> 150 rpm) M333 behaved similarly to the type (b) flocculants FA920 and FA920VHM, with only small aggregates formed in the strongly shearing conditions. At moderate rotation rates (75-125 rpm) the FBRM chord length data indicated that M333 is the best flocculant, forming the largest

aggregates. However, M333 behaved differently at the lowest rotation rate (50 rpm), with the mean number-weighted chord (Figure 5-8a) dropping to the level of the type (a) flocculants, suggesting a reduction in aggregate size. At the same time, the mean square-weighted chord still indicated the presence of large aggregates.

Examining the chord length distributions reveals the cause of this behaviour. For the square-weighted distribution (Figure 5-14a), the result matches the mean chord lengths reported, where nearly 15% of the counted chords are greater than 500 μm at 75 rpm. Under more gentle agitation (50 rpm) the square-weighted chord distribution shows a slight shift to shorter lengths, commensurate with more free particles. The number-weighted distribution (Figure 5-14b) shows these effects more clearly. For 50 and 75 rpm the breadth of the distribution is barely changed, and both show distinct bimodality. The increased sub-10 μm chord lengths at 50 rpm is reflected in the tailing of the square-weighted distribution. Collectively these results indicate that M333 forms large aggregates at low rotation rates, but the capture of fine particles is poor.

Comparison of the maximum square-weighted chord lengths shows that M333 formed aggregates over 1000 μm in diameter (Figure 5-14a) at rotation rates 50-75 rpm, while FA920 and FA920VHM were limited to 600 μm at 50 rpm (Figure 5-11), and M351 and FA920BPM to 250 μm (Figure 5-9). Given the matching rotation rates and similar dosages (Table 5-1), the maximum aggregate size suggests M333 had a greater capacity to bridge particles.

Figure 5-14 Square-weighted (a) and number-weighted (b) chord length distribution for aggregation by M333 at 112 g t^{-1} dosage through Port 2.

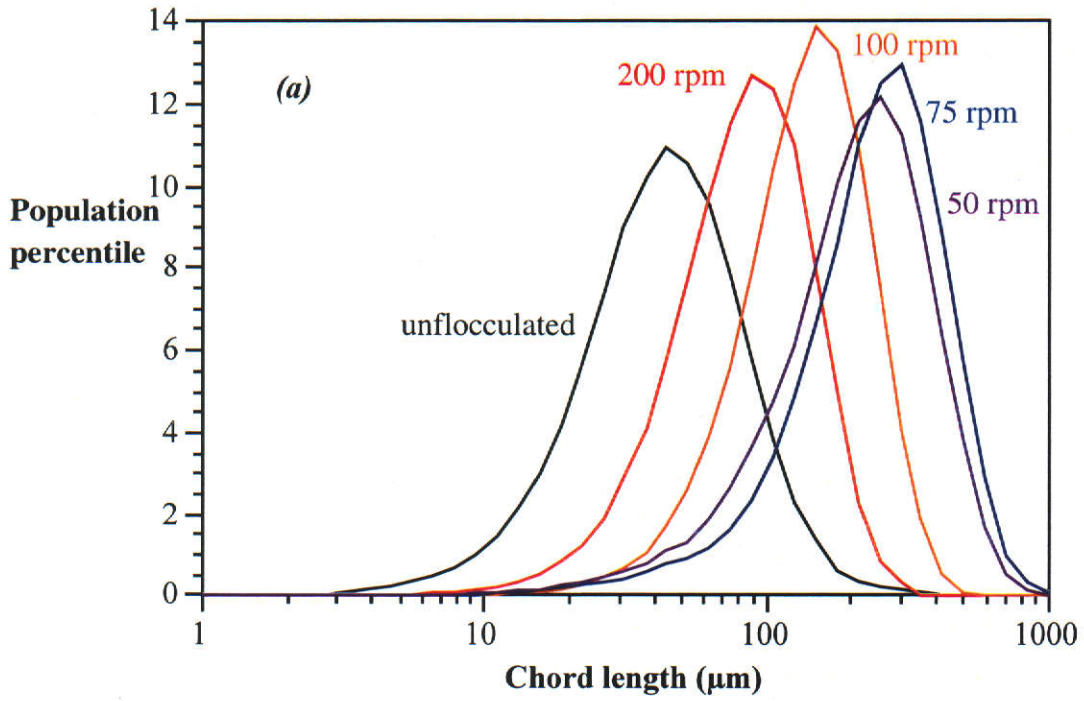

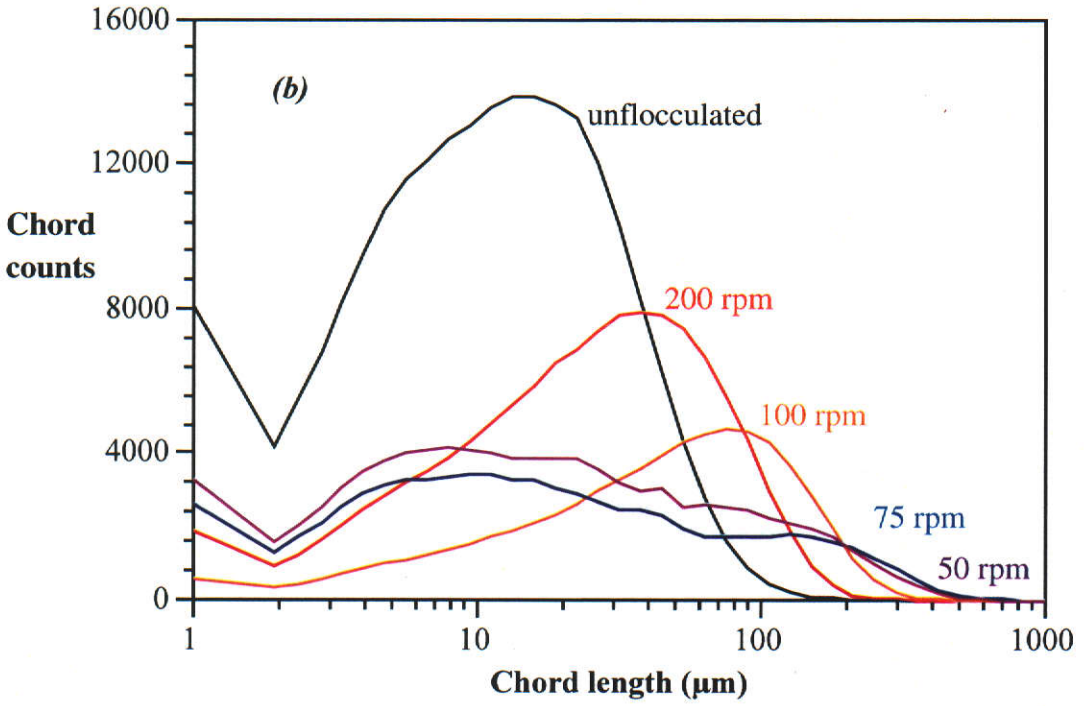

Dosage effects for M333 are presented by Figure 5-15, analogous to the effects presented for FA920 and FA920VHM in Figure 5-13. Dosage did affect the mean square-weighted chord length but, unlike the type (b) flocculants, the gradient of the mean chord *versus* rotation rate plot was invariant, while the position of the threshold increased with dosage. This difference suggests that aggregates formed with M333 increased in strength with increased dosage, but this effect did not depend upon agitation conditions. In contrast for FA920 and FA920VHM, while increased flocculant dosage formed larger aggregates at low agitation, the aggregate strength was not greatly enhanced (as seen from the similar mean chord lengths and distributions at 150 rpm).

For comparison with the type (b) flocculants, Figure 5-16 shows the sub-22 μm chord counts under standard conditions (Port 2, ~110 g t^{-1} dosage). The sizing trend inversion that was observed for M333 at low rotation rates (Figure 5-8, Figure 5-15) is shown, by Figure 5-14, to arise from the presence of fines. At 50 rpm the poor fines capture of M333 compared to FA920 and FA920VHM is clear, while at 75 rpm all flocculants perform approximately equally.

Figure 5-15 Effect of M333 dosage on mean square-weighted chord length on addition through Port 2 at dosages 157, 112, 78 and 45 g t^{-1}.

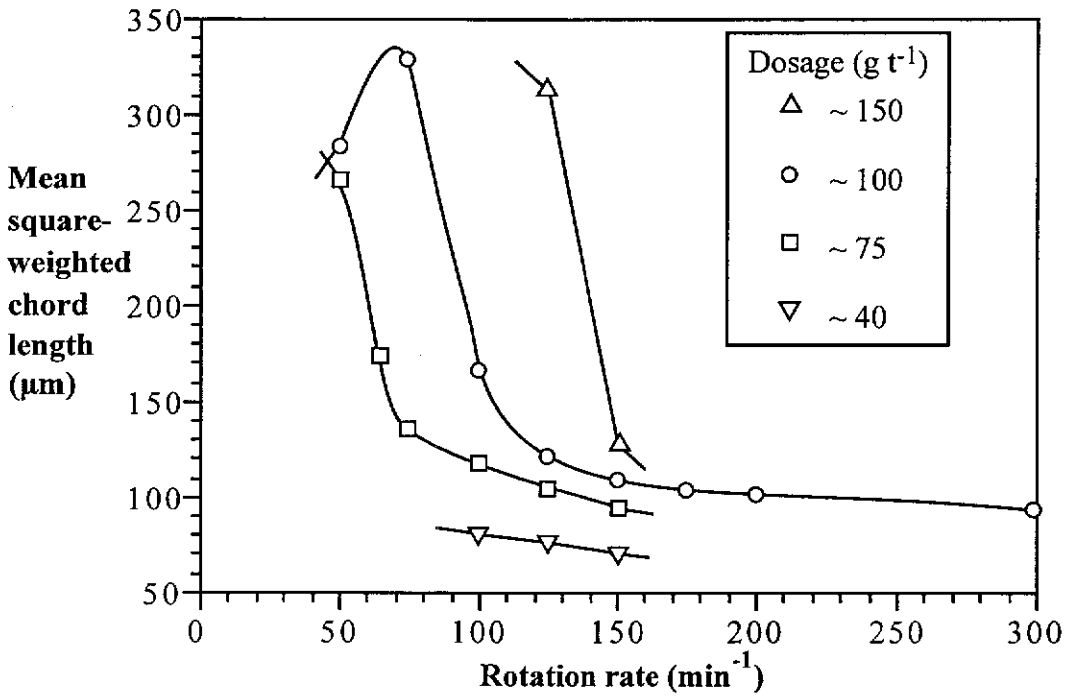

Figure 5-16 FBRM fine (-22 µm) counts for flocculants FA920, FA920VHM and M333. Over 75 rpm FA920VHM, with the highest mean molecular mass, has the highest fine counts. Dosages are given in Table 5-1.

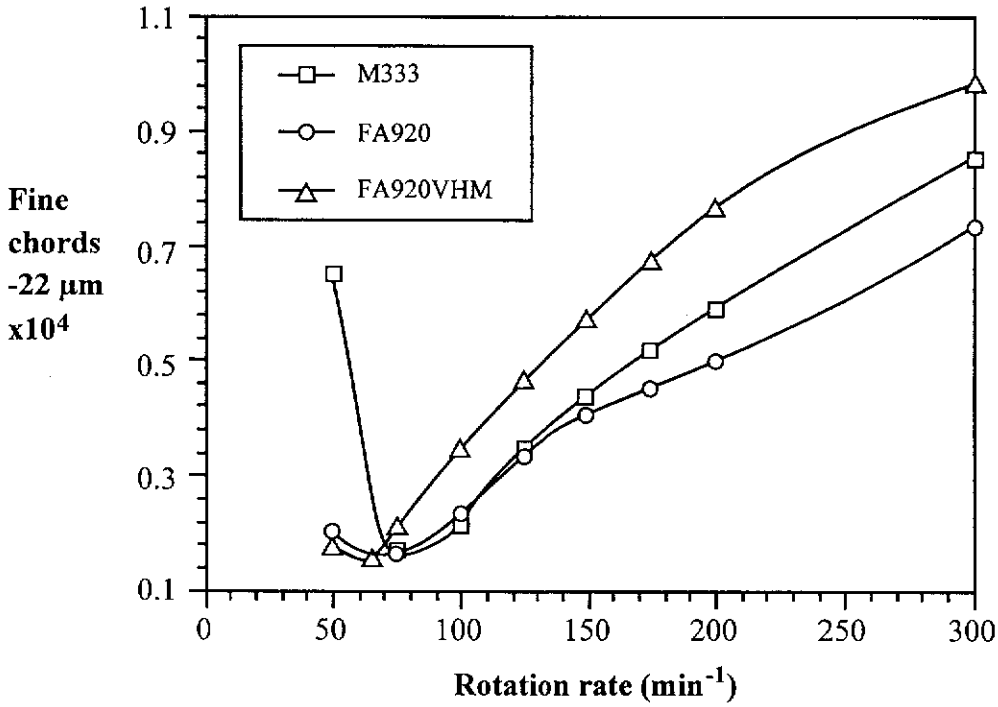

5.3.7 Effects of added salt on flocculation activity

The FFF elution profiles (Section 4.5 and fold-out page) showed a marked change for some flocculants when prepared in salt solution. The profiles of both type (a) flocculants M351 and FA920BPM were found to exhibit polymer entanglement with peak distributions in excess of their mean molecular mass. Upon preparation in 0.1 M NaCl, M351 exhibited a salt-induced dispersal of the entanglements. The type (b) flocculant FA920VHM showed little change when prepared in salt, while M333 (type c) indicated dispersal of the supramicron agglomerates. Although M333 agglomerates were obscured somewhat by the DRI sensitivity to the salt, the shift was distinct. For all flocculants, ^{13}C NMR has shown no anionic character and therefore polyelectrolyte effects upon coil conformation and adsorption are negligible.

The effect of salt on the type (a) flocculants with respect to fines capture is shown by Figure 5-17. This shows an improved flocculation performance with dispersed M351 through an increase in the capture of fines. The dosages of the flocculants (Table 5-1) differ by less than 1 g t^{-1}, and given the dosages required to make a difference in the mean square-weighted chord length (Figure 5-10) this difference is trivial. It is therefore concluded that the improved fines capture arises solely from dispersal of the polymer entanglements to free coils. Dispersion did not improve the hindered settling rates, and the maximum chord length was again 250 μm, as observed earlier for the other type (a) flocculants (Figure 5-9). This means that although there were more molecules available to adsorb onto the fines and bind into aggregates, additional bonding is not significant in terms of increasing aggregate size.

Figure 5-17 Effect of rotation rate on fine (-22 μm) FBRM counts for M351, FA920BPM and salt-dispersed M351 introduced through Port 2. Dosages are given in Table 5-1.

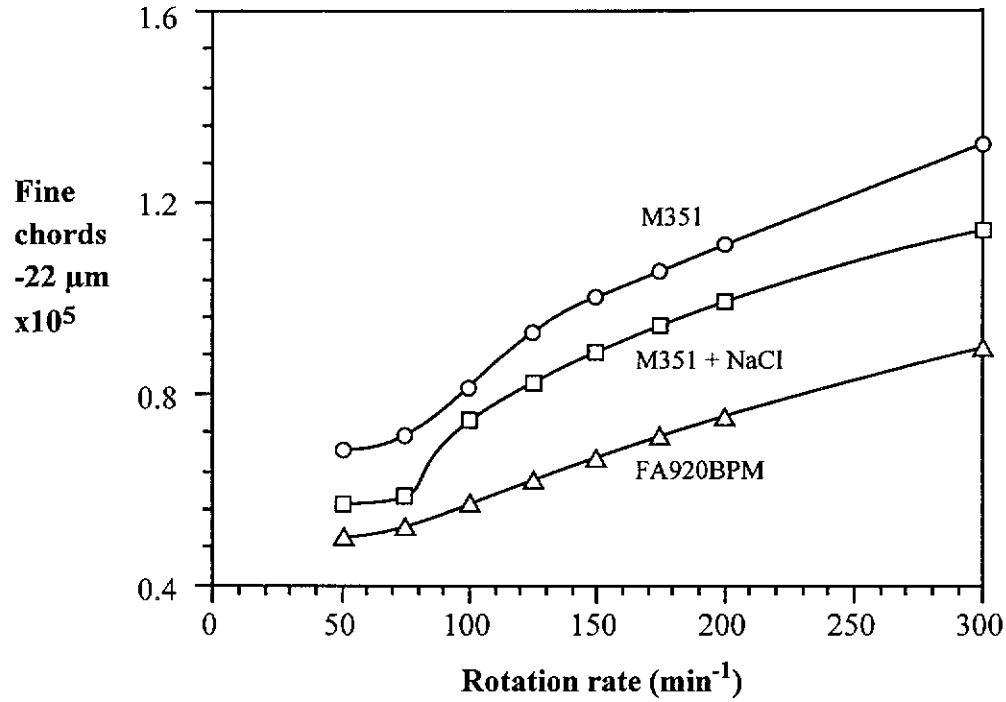

The shift in the FFF elution profile for M351, as a consequence of the flocculant being prepared in 0.1 M NaCl, was shown in Figure 4-23 (presented again in the fold-out page). The profile allows an estimate of the amount of material susceptible to dispersion, but quantification requires removal of the unretained "salt peak" emerging at 20 min. A reasonable approximation was obtained, shown by Figure 5-18, based on the light scattering signal and the salt-free fractionation.

Normalising the M351 elution profiles shows that, for M351 prepared in water as compared to prepared in salt, the loss of material eluting in the 60-80 minute period accounts for approximately 15-20% of the total flocculant concentration. This remains a crude estimate due to the estimates in removing the obscuring salt peak. Dispersion of M351 therefore effectively increases the dosage of free polymer by 15%. Based on interpolation of the dosage curves (Figure 5-10), a 15% increase in M351 dosage would increase performance to slightly less than FA920BPM standard dose, in agreement with the fines capture of Figure 5-17.

Figure 5-18 Elution profiles of flocculants M351 and M333 prepared in water (solid) and in 0.1 M NaCl (dashed). The elution profiles are modified by removing the salt peak arising to the DRI sensitivity to salt eluting in the void volume. The shaded region is where the "salt peak" was removed.

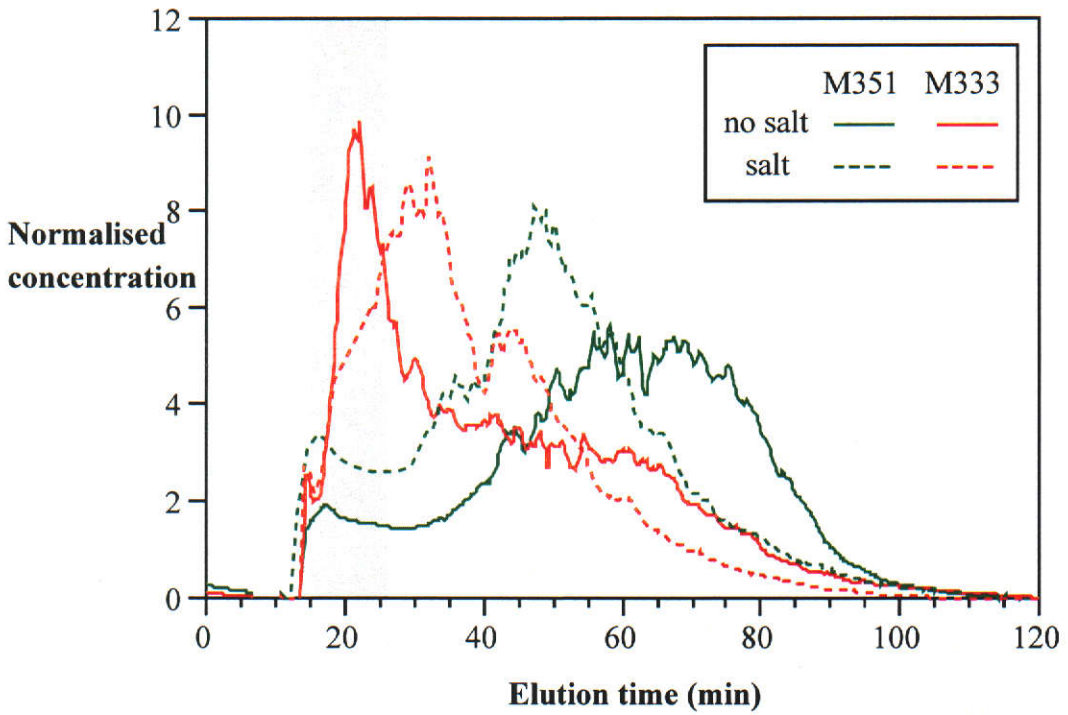

Very different effects were observed for dispersed M333. Comparison of the effect of dosage on mean chord length is shown in Figure 5-19 for M333 with and without salt present. The dosage differences are trivial (110 versus 112 g t^{-1}, respectively, from Table 5-1). For an equivalent dosage, the salt-diluted flocculant performs worse, both in terms of mean chord length and aggregate resistance to shear. The gradient of the mean chord *versus* rotation rate is variable with dosage for salt dispersed M333, an effect seen earlier for the type (b) flocculants (Figure 5-13).

The presence of salt changed M333 flocculation at low shear. For M333 in water, poor fines capture was observed at 50 rpm (shown previously in Figure 5-16), while for salt-dispersed M333 this inversion feature is absent and the fines capture ability improved continually with reduced agitation (Figure 5-20). Included in Figure 5-20 is the fines capture for FA920VHM, and with salt-dispersed M333 showing clearly worse fines capture performance over the entire range of rotation rates. The salt forces the type (c) flocculant to behave as a type (b) flocculant.

Figure 5-19 Effect of dispersed M333 on flocculation. The aggregates formed by salt-dispersed flocculants are less able to resist shear for an equivalent dosage. Dosages are given in Table 5-1.

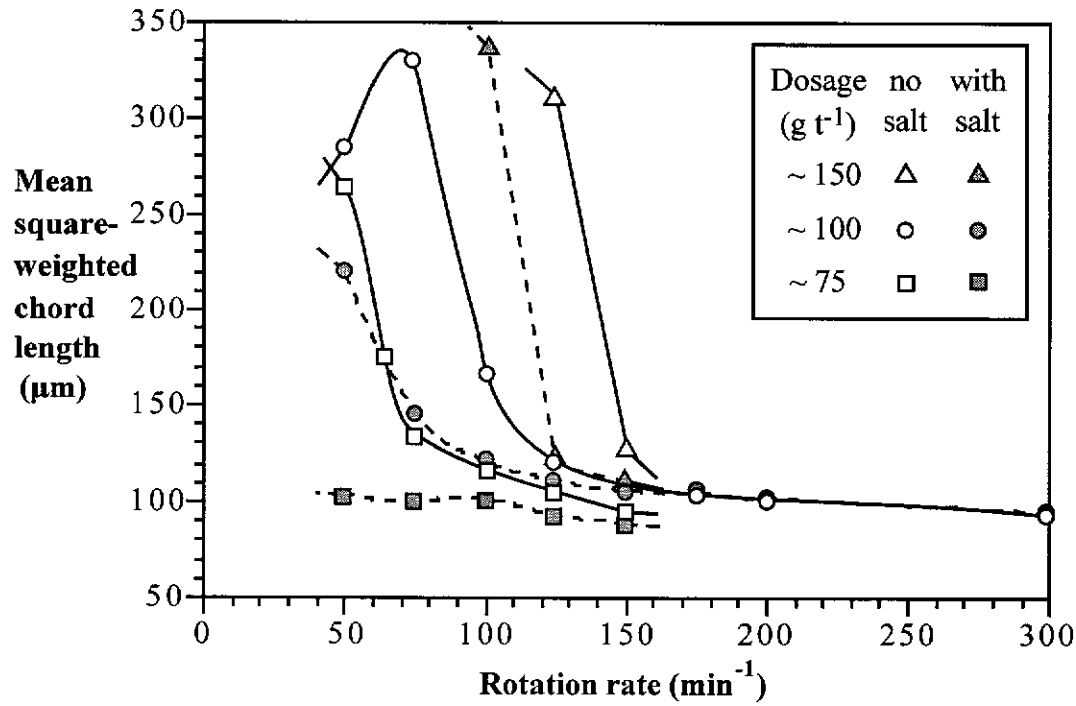

Figure 5-20 Effect of rotation rate on fine (-22 µm) FBRM counts for FA920VHM, M333 and salt-dispersed M333, introduced through Port 2. Dosages are given in Table 5-1.

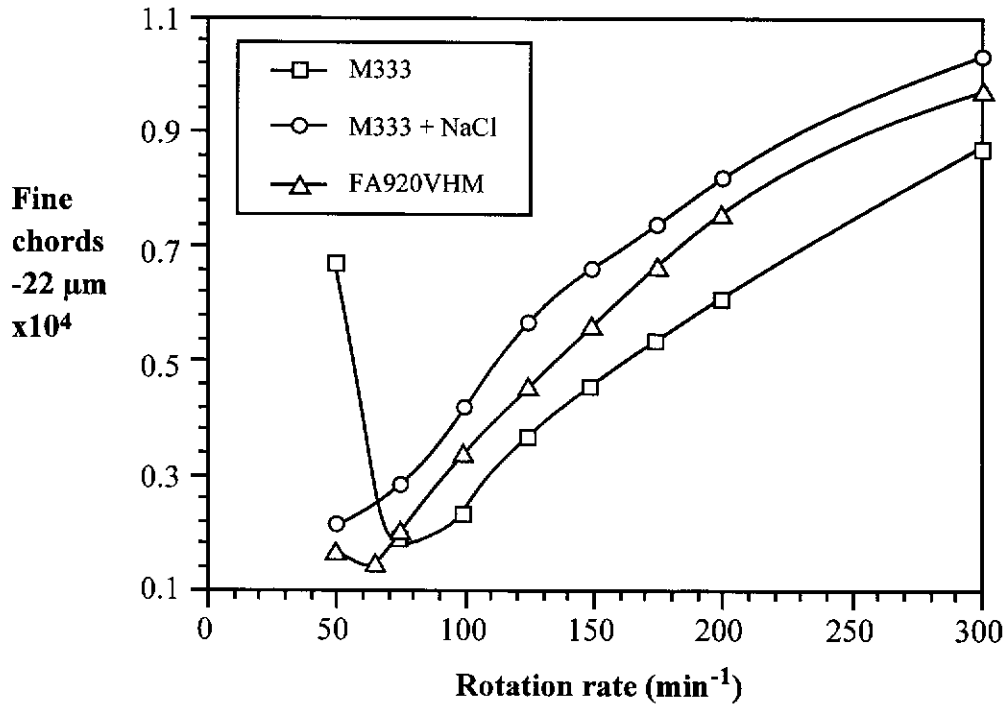

The estimate of the relative change of M333 agglomeration upon addition of salt is, based upon Figure 5-18, extremely difficult due to the FFF coelution problem (Section 4.5.3) and the salt peak masking the elution profile. However, from Chapter 3, supramicron agglomerates in M333 were estimated to be 10^{-3}% of the polymer by number, and an order of magnitude less in the presence of chloride (Section 3.3.5). By volume, an agglomerate 10 μm diameter is over 2×10^5 times greater in volume than a single 0.35 μm coil, assuming size-invariant density. Using the simple bimodal population model noted in Section 3.3.1, a polymer solution consisting of 10^{-3}% 10 μm agglomerates, with the remainder as free coils, would have approximately 18% of the mass of the polymer sample as agglomerates. Although the number concentration of agglomerates is low, their mass and volume contribution may be significant.

5.4 *Effect of Molecular Mass Distribution on Flocculation*

Flocculant performance depends upon slurry composition, as well as the physical and chemical properties of the flocculant in solution. The slurry has been demonstrated to be consistent, and the minor variations in flocculant concentration and dosage are irrelevant, as shown by the extent of dosing needed to provoke a change in aggregation. The ^{13}C NMR of all materials showed signals consistent with PAAm only. Differences in performance therefore are principally a function of flocculant solution features. This section now seeks to provide qualitative correlations with respect to aggregate size, shear and dosage effects.

Bulk flocculant characterisation techniques poorly predict flocculation behaviour. Referring to the fold-out page, M351 and FA920VHM have very similar viscosities but diverse flocculation performance (Figure 5-8), conversely the type (b) flocculants FA920 and FA920VHM have similar flocculant performance but their capillary viscosities are markedly different. Mean molecular mass also correlates poorly with flocculation behaviour, with M333 and FA920VHM having mean molecular masses over 20×10^6, while M351, FA920 and FA920BPM are in the range $10\text{-}13\times10^6$. The presence of polymer agglomerates is apparently indicated by viscosity, when the capillary (Ubbhelode) determination is markedly greater than the constant-shear (Brookfield) measurement.

While the ensuing discussion does consider the mean molecular masses of the flocculants, it focuses primarily on the effect of agglomeration on activity. The techniques used would be expected to be sensitive to minor changes in flocculant properties and performance, but such a study would require, for example, different batches of polymer prepared by the same manufacturer. Despite this, significant observation can be made from the behaviour of the materials studied, based on distinct differences in their elution profiles.

Over the range of rotation rates investigated, aggregates bound with the type (a) flocculants M351 and FA920BPM showed little change with agitation, remaining above their threshold shear (Figure 5-5). Increased dosage showed a slight increase in the mean chord length (Figure 5-10). These flocculants universally had a low maximum chord length and low hindered settling rates. Common to the poorly performing flocculants is a low mean molecular mass and an anomalously wide size distribution attributed to entwined polymer. The entwined polymer may be dispersed by the addition of NaCl, making a slight improvement to fines capture (Figure 5-17) but did not result in significantly enhanced aggregation.

Type (b) and (c) flocculants had a high mean molecular mass but FA920VHM, with the highest mean molecular mass, exhibited the poorest fines capture over 75 rpm (Figure 5-16) and shortest aggregate chord lengths (Figure 5-11). Also unexpected is the performance from the lower mean molecular mass samples FA920. The presence of salt affected both M333 and FA920, indicating loss of agglomerates (Figure 4-23 and fold-out page) but the molecular mass distribution of FA920VHM remained invariant. The shift in the molecular mass distribution may be attributed to dispersal of gross supramicron microgels to smaller agglomerates. The loss of the largest agglomerates appears to be detrimental to M333 flocculation activity as measured by the size of aggregates (Figure 5-19) but aids performance in terms of fines capture under low agitation conditions (Figure 5-20). The results presented here, in conjunction with the mass and volume calculations presented in Section 5.3.7, demonstrate the flocculation activity of these aggregates.

Classic bridging theory of flocculation predicts mean molecular mass to be the dominant parameter, producing larger loops and tails (Ruehrwein and Ward 1952, Kitchener 1972). While this is undoubtedly true of "model" polymers, commercial materials such as FA920, with a molecular mass slightly greater than the type (a) flocculants, perform as well as the higher molecular mass FA920VHM. The best flocculation and aggregate shear resistance is linked with supramicron agglomerated flocculants, M333 and FA920, with the dispersion of agglomerates correlating with a

decrease in flocculation ability. For the low molecular mass type (a) flocculants, featuring submicron-sized entangled polymers, loss of these structures frees polymer coils to improve flocculation by increasing polymer concentration.

At low shear the polymer agglomerates easily coalesce aggregates and free particles to clusters but leave many fines, as demonstrated by the minimum shear necessary for M333 prepared in water. For FA920VHM and salt-dispersed M333, which lack the agglomerates, bridging flocculation between particles remains available but cluster flocculation is poor, leading to more modest flocculation activity. For the low molecular mass polymers, only bridging is available and the relatively short bridges limit the maximum aggregate size. For M333 and F920, the larger aggregates formed indicates the strength of agglomerate binding.

The effect of polymer agglomeration on flocculation is rarely reported in the literature. Shyluk and Stow (1969) associated polymer ageing with agglomerate dispersion, changes in viscosity, and a decrease in flocculant activity. Their reasoning stated agglomerates, which are less likely to take a flattened conformation when adsorbed on a particle, may be expected to favour polymer bridging. Chmelir *et al.* (1980) mentioned that dissolution of polymer aggregates might be one factor linked to deterioration of flocculation activity but gave no experimental details.

Mühle and Domasch (1990) established that different shear regimes allow a maximum aggregate size dependent upon microscale (Kolmogorov) turbulence. Measuring aggregate cohesion, they reported the maximum size and strength of the aggregate is a function of both the molecular mass and concentration of the flocculant. They then claimed that the effect was due to lower hydrophobicity for the larger molecules and therefore stronger particle-substrate adhesion (Mühle and Domasch 1991). A simpler explanation is offered here, since polymer agglomeration is dependent upon molecular mass and concentration. It is reasonable then to state that the agglomerates contribute to production of larger aggregates observed by these authors, rather than an overly subtle hydrophobic effect.

5.5 *Conclusions*

For flocculation in the Shear Vessel, a dispersed, high molecular mass flocculant functioned at low applied shear but performed badly under increasing agitation, as expected for a bridging flocculant. The presence of supramicron agglomerates in the flocculant solution produced stronger, larger aggregates. A mechanism was proposed where the polymer agglomerates contribute significantly to flocculant activity. The agglomerates formed the largest aggregates at lower agitation intensities but with poor fines capture. The dispersal of the agglomerates produced smaller and weaker aggregates but allowed satisfactory fines capture at low agitation intensity.

Classic bridging theory predicts a strong dependence of flocculant molecular mass upon aggregation processes. For a lower molecular mass flocculant, the presence of agglomerates allowed the formation of aggregates as large as those formed by a well-dispersed, higher molecular mass flocculant. However, low mean molecular mass flocculant tends to form entanglements involving several polymer coils. These entanglements inhibited flocculation performance.

5.6 REFERENCES

Chmelir, M., Künschner, A. and Barthell, E., 1980, 'Water soluble acrylamide polymers, 2. Aging and viscous flow of aqueous solutions of polyacrylamide and hydrolysed polyacrylamide', *Angewandte Makromolekulare Chemie*, vol. 89, pp. 145-165.

Farrow, J.B. and Swift, J.D., 1996a, 'A new procedure for assessing the performance of flocculants', *International Journal of Mineral Processing*, vol. 46, pp. 263-275.

Farrow, J.B. and Swift, J.D., 1996b, 'Agitation and residence time effects during the flocculation of mineral suspensions', at *Fourth International Alumina Quality Workshop*, Darwin, Northern Territory, 2-7 June, pp. 355-363.

Farrow, J.B. and Warren, L.J., 1989a, 'The Measurement of Floc Density-Floc Size Distributions', in *Flocculation and Dewatering,* eds. Moudgil, B.M. and Scheiner, B.J., Engineering Foundation, New York, pp. 153-165.

Farrow, J.B. and Warren, L.J., 1989b, 'A new technique for characterising flocculated suspensions', at *Dewatering Technology and Practise*, Australian Institute of Mining and Metallurgy, Brisbane, Australia, pp. 61-64.

Farrow, J.B. and Warren, L.J., 1993, 'Measurement of the Size of Aggregates in Suspension', in *Coagulation and Flocculation: Theory and Applications,* ed. Dobias, B., Marcel Dekker, New York, pp. 391-426.

Fawell, P., Richmond, W., Jones, L. and Collisson, M., 1997, 'Focussed beam reflectance measurement in the study of mineral suspensions', *Chemistry in Australia*, vol. 64, no. 2, pp. 4-6.

Gregory, J., 1989, 'Fundamentals of flocculation', *CRC Critical Reviews in Environmental Control*, vol. 19, no. 3, pp. 185-230.

Gregory, J., 1991, 'Effect of dosing and mixing conditions on flocculation by polymers', in *Advances in the Measurement and Control of Colloidal Processes*, eds. Williams, R.A. and de Jaeger, N.C., Butterworth-Heinemann, Oxford, pp. 3-17.

Kirwan, L., 1997, *Assessment of Flocculation Performance by Focussed Beam Reflectance Measurement,* School of Applied Chemistry, Curtin University of Technology, Perth, Australia.

Kitchener, J.A., 1972, 'Principles of action of polymeric flocculants', *British Polymer Journal*, vol. 4, pp. 217-229.

Moss, N. and Dymond, B., 1978, 'Flocculation: theory and application', *Mine and Quarry Journal*, vol. 5, pp. 1-8.

Moudgil, B.M. and Behl, S., 1993, 'Characterisation Techniques for Agglomerate Structures', in *Handbook on Characterisation Techniques for the Solid-Solution Interface,* eds. Adair, J.H., Casey, J.A. and Vengallia, S., American Ceramic Society, Westerville, Ohio, pp. 223-238.

Moudgil, B.M., Behl, S. and Prakash, T.S., 1993, 'Effect of particle size in flocculation', *Journal of Colloid and Interface Science*, vol. 158, pp. 511-512.

Moudgil, B.M. and Shah, B.D., 1986, 'Selection of Flocculants for Solid-Liquid Separation Processes', in *Advances in Solid-Liquid Separation,* ed. Muralidhara, H.S., Battelle Press, Columbus, Ohio, pp. 191-204.

Mühle, K. and Domasch, K., 1990, 'Floc strength in bridging flocculation', in *Chemical Water and Wastewater Treatment, Proceedings of the 4th Gothenburg Symposium*, eds. Hahn, H.H. and Klute, R., Springer, Berlin, pp. 105-115.

Mühle, K. and Domasch, K., 1991, 'Stabilität von Teilchenaggregaten bei Flockung mit Polymeren', *Chemical Engineering Progress*, vol. 29, pp. 1-8.

Peng, S.J. and Williams, R.A., 1993, 'Control and optimisation of mineral flocculation and transport processes using on-line particle size analysis', *Minerals Engineering*, vol. 6, no. 2, pp. 133-153.

Peng, S.J. and Williams, R.A., 1994, 'Direct measurement of floc breakage in flowing suspensions', *Journal of Colloid and Interface Science*, vol. 166, pp. 321-332.

Ruehrwein, R.A. and Ward, D.W., 1952, 'Mechanism of clay aggregation by polyelectrolytes', *Soil Science*, vol. 73, pp. 485-492.

Shyluk, W.P. and Stow, F.S., 1969, 'Aging and loss of flocculation activity of aqueous polyacrylamide solutions', *Journal of Applied Polymer Science*, vol. 13, pp. 1023-1036.

Williams, R.A., Peng, S.J. and Naylor, A., 1992, '*In situ* measurement of particle aggregation and breakage kinetics in a concentrated suspension', *Powder Technology*, vol. 73, pp. 75-83.

Chapter 6

Conclusions and Further Work

6. CONCLUSIONS AND FURTHER WORK

6.1 CONCLUSIONS

Polyacrylamide finds wide use in the mineral processing industries as a flocculant. The principle attractions are high degrees of polymerisation, water solubility and wide range of surface affinities. Studies of flocculation have been reported often in terms of aggregate characterisation and mixing, while the flocculant itself has been largely overlooked due to the difficulty of characterising ultrahigh molecular mass polyacrylamides. This thesis examined commercial polyacrylamide flocculants solutions in both the sub- and supramicron domains. Flocculant tests using the characterised flocculants confirmed that solution features of the flocculant are important, and a modified mechanism of flocculation was proposed.

Aqueous solutions of PAAm exhibit time-dependant behaviour affecting viscosity, which was ascribed to both individual coil conformation and supramicron polymer agglomeration. Improving solvation of PAAm suppressed the agglomerates, as did manipulation of hydrogen bonding. Unfortunately, to limit agglomeration through improved solvation simultaneously lowered a barrier to polymer interaction, such that under mild shear the extent of agglomeration actually increased.

Agglomerates were never fully eliminated by these manipulations. Commercial powdered polyacrylamides are heated to dryness during their production, and heating was linked to enhanced agglomeration and retarded dissolution. While the presence of imides was confirmed upon excessive heating, many samples exhibited the retarded dissolution without detectable imides, indicating that either imides are highly influential at very low concentrations or that heating has multiple effects.

To characterise the molecular mass distribution of PAAm, flow field-flow fractionation was chosen, primarily for the low shear during separation. Although the technique has existed for thirty years, its application to polymer analysis has

been overshadowed by the simplicity of size-exclusion chromatography. The difficulties associated with the application of FFF to PAAm fractionation were overcome and for the first time the analysis of high molecular mass PAAm in water using the flow FFF-MALLS technique has been reported.

High molecular mass PAAm is relatively fragile and shear degradation may occur under relatively gentle conditions. Simulating conditions of the fractionator environment showed that shear favours polymer coil deformation and enhances agglomeration. This result placed some absolute limits on the fractionation to avoid any shear-induced artefacts in the fractionation.

The conditions chosen to avoid shear matched the predicted elution of model latex standards, but fractionation of polyacrylamide standards required further work to establish a compatibility between carrier and membrane chemistry to avoid surface adsorption and detector interference. Once achieved, flow field-flow fractionation was successfully applied to the fractionation of ultra-high molecular mass polyacrylamides with full elution in less than two hours, which betters size-exclusion chromatography in terms of both sample throughput and sensitivity.

Molecular mass distributions based on the FFF elution time rely upon an ideal circumstance where the polymer coils do not alter configuration and therefore change their hydrodynamic diameter and diffusion coefficient, and that the passage of the polymer through the channel is not affected by membrane. The direct (light scattering) method was preferred for the determination of molecular mass distribution of polymer standards. The relationship between molecular mass and elution time was shown to be highly reproducible.

For commercial polyacrylamides, the presence of supramicron agglomerates was noted earlier. The agglomerates interfere with the fractionation due to the parallel separation mechanisms of the FFF, and cannot be fully removed by simple filtration. A further complication for some commercial samples is coil entanglement. The coils

are of submicron dimensions, and are assigned to entwinement of up to approximately six coils. These entanglements elute from the FFF later than the free polymer coils due to their greater size, and are dispersed in the presence of salt.

A comparison between the characterised polyacrylamides and observed flocculation activity showed polymer with increasing supramicron agglomerates produce the largest and most shear-resistant aggregates. Dispersed, high molecular mass flocculants function at low shear but perform badly under increasing shear stress. Low molecular mass is not necessarily correlated with poor flocculation: a low molecular mass flocculant with featuring supramicron agglomerates forms aggregates as large as a well dispersed high molecular mass polymer. However, low molecular mass molecules often exhibit entanglement of individual polymer coils to submicron sizes, and this feature does inhibit performance.

Polyacrylamide solutions may now be routinely characterised in both supra- and submicron domains. This has direct applicability to both flocculant manufacture and industrial flocculation processes for both quality control and optimising solid-liquid separation efficiency.

6.2 Further Work

A clear picture of the molecular mass distribution of polyacrylamide and its effect on a model flocculation system has been gained. The fractionator elution profile reflects the solution state features well but is difficult to interpret. Improvement to the flow FFF method to simplify the distributions is required. Proposed areas of research are to suppress polymer agglomerates and entanglements by exploring lower concentrations and the addition of dispersants. Alternatively the hydrodynamics of the fractionation could be modified to disengage the sub- and supramicron species in polyacrylamide solutions during fractionation. These issue were described at length in the conclusion of Chapter 4.

From this point there are three applications that demand examination.

(i) Polyacrylamide is only one of a number of flocculants in use. Application of the flow FFF technique to a 10% anionic polyacrylamide derivative has been demonstrated. Increasing charge density is an obvious next step, although the coil conformation sensitivity to ionic strength and acidity will need to be considered. The light scattering of these copolymers is anticipated to be different than polyacrylamide itself, and the copolymer tacticity may have an effect. The self-agglomeration behaviour of other flocculants, arising from different solvent affinities, is anticipated to vary.

(ii) The modelling of the adsorption of polymer onto surfaces predicts the higher molecular mass species will displace lower molecular mass. With the FFF-MALLS system, a method to study this prediction empirically is available. Such data would complement the results presented here to show, for well dispersed polyacrylamide, the effects of polydispersity on flocculation.

(iii) The flocculation activities reported in Chapter 5 are at equilibrium positions, and the effect of molecular mass distribution upon flocculation kinetics, as per

the second issue, is unknown. For example, lower molecular mass PAAm may approach the surface more rapidly and act as a form of surface conditioning prior to adsorption of the higher molecular species. A corollary to this is the effect of polymer molecular mass distribution on aggregate density *versus* dimension relationships.

A further point of interest, although not specifically germane to polyacrylamide characterisation and flocculation, is interpretation of the FBRM chord length distributions of aggregates. The technique is convenient but a comprehensive interpretation of chord length data is complex. The conversion of chord length distribution to a conventional number or volume based measurement would assist elucidation of aggregate formation and breakage mechanisms.

Chapter 7

Appendices

7. APPENDICES

7.1 APPENDIX 1: CARBON NUCLEAR MAGNETIC RESONANCE

The ^{13}C NMR spectra of polyacrylamide and derivatives tests for charge density arising from hydrolysis (to acrylate) and imidisation in the molecule. Unfortunately at the concentrations necessary for a good signal, the solution viscosity interferes with both loading the sample tube and NMR relaxation mechanisms. Degradation of the polymer lowers the viscosity without changing the chemical environments (Kulicke *et al.* 1993). The lower viscosity leads to greater molecular motion, shorter T_1 times and therefore greater spectral resolution through reduced band broadening. Figure 3.1 shows the assignment of peaks in the ^{13}C NMR spectrum of a typical partially hydrolysed polyacrylamide. The fraction of acrylate groups were calculated from the relative areas of the carbonyl peaks (a and a') or of the methine carbon peaks (b and b'). The same principle is easily applied to cationic polyacrylamide derivatives. However ^{13}C NMR requires suppression of interfering magnetic effects, the nuclear Overhauser effect, using the inverse gate pulse sequence (Breitmaier and Volter 1990, pp 46-51).

Figure 7-1 Typical ^{13}C NMR spectrum of a partially hydrolysed polyacrylamide, showing the peak assignments (a) carbonyl, (b) methine, (c) methylene. Peaks marked with apostrophe are from acrylate.

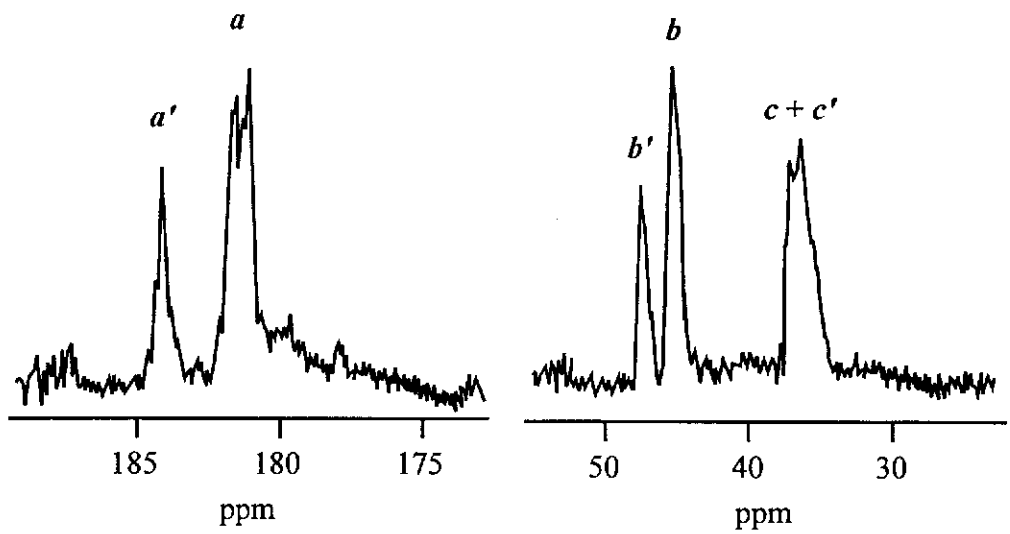

7.1.1 NMR experimental

A concentrated sample of the flocculant (3% w/v) was degraded ultrasonically by an XL2020 at 20kHz from Heat Systems (Farmingdale, New York). Metal fines from the horn were removed by centrifugation (Hettich Mikro 12-24, Tuttlingen, Germany) and clarified polymer was loaded into the sample tube with a quantity of D_2O and *p*-dioxane (standard, 67.4 ppm). Carbon spectra were recorded on a 200 MHz machine (Varian Gemini, Palo Alto, California) using an inverse gate decoupling pulse sequence, where the ^1H decoupler is on only during the pulse and FID acquisition. Prior experimentation determined the 90° pulse width was 18 μs using calibrant of minimum methanol in 2:1 H_2O:D_2O. An inversion-recovery (T_1) experiment, using a polyacrylamide solution, measured the half-life of the carbon atom deexcitation. Regions of interest were the C=O carbonyl (180 to 185 ppm), and aliphatic CH methine (42 to 47 ppm) and CH_2 methylene (35 to 37 ppm) (Leung *et al.* 1985). The relaxation data is shown in Table 7-1. The delay time is ideally at least five times longer than the longest deexcitation time, being the amide carbonyl at 1.39 s.

Table 7-1 Relaxation time for polyacrylamide atoms determined from standard inversion-recovery experiment.

Carbon type	Peak position (ppm)	T_1 time (sec)	Error (sec)
Amide carbonyl	180.4	1.39	0.08
Methine	42.7	0.14	0.02
Methylene	35.5	0.11	0.03

Standard pulse parameters used during the ^{13}C NMR experiments were therefore acquisition 0.267 s, pulse 12 μs, delay 7 s. Typically 10-20×10^4 transients were required for a signal-to-noise greater than 10:1. Although fewer transients would be

required with a longer pulse time, the shorter pulse and commensurate smaller signal vector aids in sample relaxation. With the decoupled spectra the integration of the carbonyl and aliphatic peaks varied by only 5% which is within the limit of accuracy (Tchir and Rudin 1986). Quantisation of the hydrolysis was made on the basis of the integrated 184 ppm acrylate versus 180 ppm amide carbonyl signals. Imides could be detected at 175 ppm (Moradi-Araghi *et al.* 1988). Due to the limits of integration, moieties less than 2% by number were poorly resolved and noted as such.

Tacticity determination of the commercial flocculant samples on the 200 MHz was not possible as the band broadening was too great. The same samples were analysed at 500 MHz (Bruker 500ARX, Rheinstetten, Germany) at supra-ambient temperatures, courtesy of Lindsay Byrne at the University of Western Australia's NMR Centre.

7.1.2 Nonionic and anionic flocculants

At concentrations required for NMR (2-5 wt.-%), solutions of high molecular weight polyacrylamides are extremely viscous, resulting in broad linewidths and poor resolution. Collection of high numbers of scans (>10 000) improves the signal-to-noise ratios, but requires several days of instrument time. After degradation, the ^{13}C NMR spectra showed greater resolution and more rapid acquisition time. No change in the acrylate content was observed as a result of the degradation.

The degrees of anionic character determined by NMR for a range of commercial flocculants are shown in Table 7-2, along with those obtained from microanalysis and the manufacturer's specifications. Values obtained are within the 5% error range, with two exceptions. The nominally 70% anionic flocculant was found to be only 54-57% by number from the NMR determination, a result supported by

microanalysis, suggesting the manufacturer's value was in error. One of the nonionic flocculants had no acrylate detectable by NMR, but gave an apparent anionic character of 22% by microanalysis. It was concluded that this flocculant contained a non-polyacrylamide nitrogen-containing contaminant, which examination by IR spectra clearly supported with a plethora of unexpected peaks.

7.1.3 Cationic flocculants

A range of cationic flocculants, consistent with acrylamide-*co*-trimethylammonium chloride methyl methacrylate copolymers (Lafuma and Durand 1989), have been subjected to ^{13}C NMR analysis using the same procedure. All NMR signals were consistent with the expected structure except for the lower intensity of the carbonyl signal of the cationic functionality. The manufacturer's values for cationic character were from the mass of monomer in the polymerisation while the NMR returns a number measurement. When the number-based estimates were corrected both the NMR and microanalysis results were satisfactorily in agreement with the manufacturer's estimate.

Table 7-3 summarises the analyses for cationic flocculants. This molecular mass correction has a trivial effect when applied to anionic flocculants as there is little difference in molecular mass between acrylamide and acrylate.

Table 7-2 NMR and microanalysis for determination of number-based anionicity.

Expected degree of anionic character	^{13}C NMR analysis: Carbonyl C	Methine C	Microanalysis
100	>98	>98	100.0
80	80.6	77.9	79.0
70	57.4	54.4	60.7
50	50.5	47.7	51.5
30	35.6	35.6	33.3
16	14.1	17.1	12.7
10	11.2	11.5	12.3
10	12.0	10.3	10.2
3	<2	<2	0.9
0	<2	<2	0.3
0	<2	<2	22.3
0	<2	<2	1.9

Table 7-3 Number and mass based determinations of cationicity.

Expected degree of cationic character	Number based estimates ^{13}C NMR	Microanalysis	Mass corrected estimates ^{13}C NMR	Microanalysis
25	10.2	12.0	23.0	23.1
25	9.1	10.0	21.1	26.9
10	1.4	3.4	4.0	8.7
5	1.1	2.8	3.2	7.3

7.1.4 Sequence distribution of anionic flocculants

The sequence distribution of acrylamide and acrylate groups in a copolymer flocculant can have a significant effect on the material's properties (Panzer and Halverson 1989). ^{13}C NMR may be used to determine such distributions, but the slight shifts in resonance frequency produced by changes in the electronic environment require a very high resolution. This could not be achieved on the 200 MHz NMR instrument and all subsequent experiments were carried out at 500 MHz. At ambient temperature there was no discernible improvement in the quality of the results. Increasing the temperature to 45°C substantially reduced the number of scans required from over 20 000 scans to only 700 scans, a remarkable saving in time, but not with sufficient resolution. By far the best results were achieved at 52°C, using a flocculant solution that had been partially degraded. For the acrylamide unit (A) and the acrylate (B), then there are six unique sequences of three monomer triads: AAA, AAB, BAB, BBB, ABB and ABA (Panzer and Halverson 1989).

Figure 7-2 Sequence distribution of 60% anionic poly(acrylamide-*co*-acrylate): carbonyl signals of acrylamide (A) and acrylate (B) exhibit fine structure.

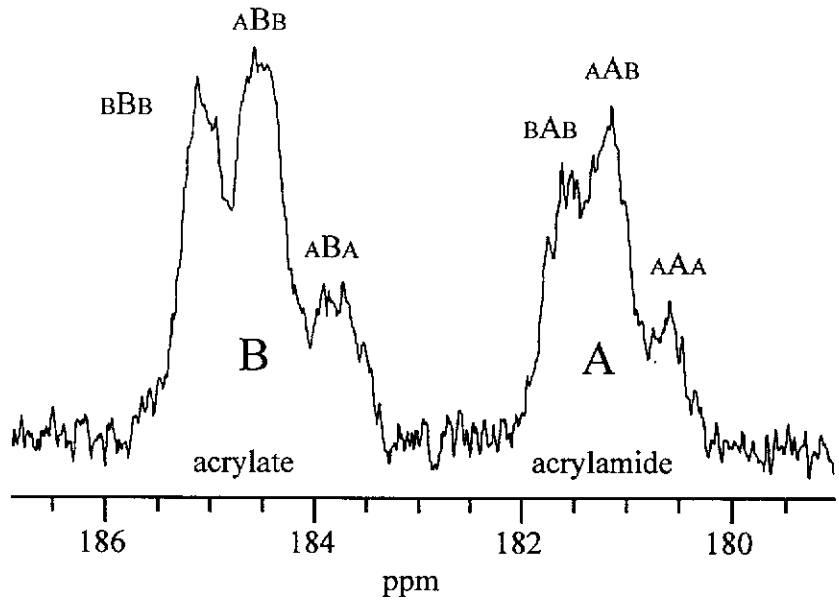

Figure 7-2 shows sufficient resolution to distinguish the peaks for each triad. Integration of these peaks suggest a random distribution of monomers, *i.e.* there are no long sequences of repeated monomers ("blocks"). Blocks may be formed under certain preparation conditions, such as through acid hydrolysis (Halverson *et al.* 1985). This resolution remains insufficient for deconvolution into accurate sequence distributions.

7.1.5 Conclusions

Quantitative carbon NMR is a convenient method for determining the charge density of polyacrylamide derivatives and returns results comparable with elemental analysis.

7.2 *Appendix 2: Aggregate Size and Density*

7.2.1 Use of the FDA

The Floc Density Analyser (FDA) is a device developed for measuring "microscopic properties" of individual aggregates such as size, shape, density and settling velocity within their process liquor (Farrow and Warren 1989a, 1989b, 1993). A video camera, coupled to selected optical lenses, is used to record the sedimentation characteristics of individual aggregates as they settle under the influence of gravity within the analysis cell (Figure 7-3). Strict thermal control is maintained to eliminate convection currents in the cell. A statistically representative number of aggregates (usually two to three hundred) are measured, covering a broad size range. The density may be calculated from aggregate sedimentation and size data, using a modified version of the Stokes' equation for ellipsoidal bodies (Happel and Brenner 1973, p. 233). Equivalently, the aggregate density decreases with increasing size, a function of the fractal nature of aggregates. The density relationship identifies the aggregate structure as compact or loose, as shown in Figure 1-8. A good overview of this phenomenon is provided by Gregory (1998).

Figure 7-3 Observed (projected) area of a freely settling aggregate, represented in a section of the FDA cell. The diameters of the ellipsoidal aggregate are measured from the images, while the settling rate is calculated from the distance travelled versus image capture rate.

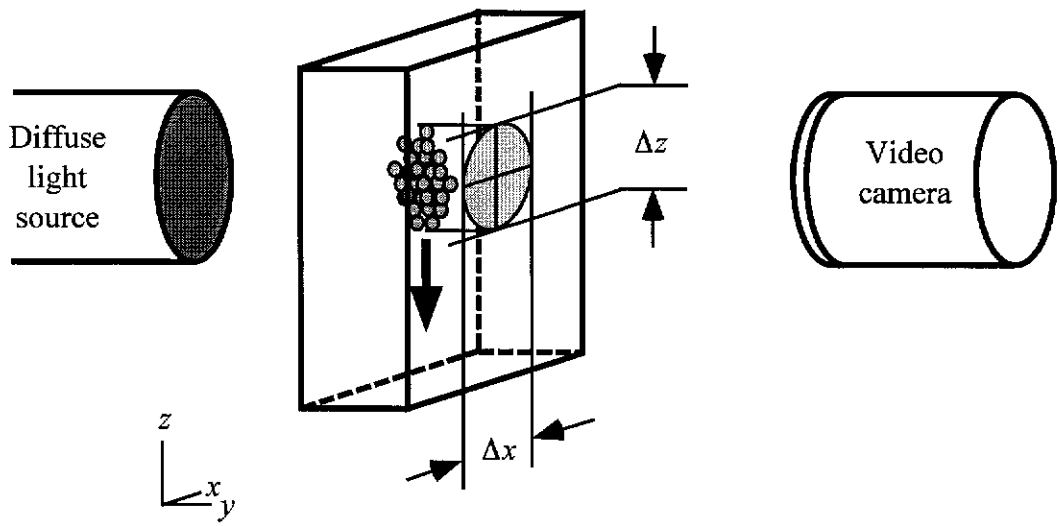

The FDA calculations presume the aggregates are rigid, ellipsoidal with aspect ratio less than 10:1, impermeable to fluid, and that aggregate-aggregate interactions do not occur. The use of Stokes' law requires that the aggregates are settling under steady creeping flow conditions, with a characteristic Reynold's number less than 0.2.

Farrow and Swift (1991) used the FDA to quantify the structure and density relationships of aggregates typical of those formed in mineral processing operations. Upon dilution to 0.5 wt.-% the size-density relationship of aggregates in the underflow differed from those reporting to the overflow, commensurate with dewatering and densification occurring in the thickener bed. The greatest aggregate diameter measured was 300 μm, although bodies as large as 1750 μm were observed. The authors noted an interesting dosage effect from an unspecified flocculant and mixing protocol. Higher dosages led to larger maximum and mean aggregate sizes, and higher hindered settling rates, yet individual bodies had lower sedimentation rates and densities.

To study the effect of the flocculant on mineral aggregate properties a model substrate is required to maximise the opportunities to provide quantitative data. Glass ("Ballotini") spheres were chosen as they are available in bulk, are claimed to be over 97% spherical, and easily refined to a narrow size distribution

7.2.2 Experimental conditions

A model substrate of soda-lime glass spheres was used ("Ballotini spheres", Potters Industries, New Jersey; composition SiO_2 72.5%, Na_2O 13.7%, CaO 9.8%, other (MgO, Al_2O_3, FeO/Fe_2O_3, K_2O) 4.0%). Bulk density was 2.5 g cm^{-3}. A slurry of this material exhibits a time dependency. Monitoring the pH_{25} of a well stirred 1 wt.-% slurry showed a rapid decrease from initial pH 8.2 to 7.3 after 90 minutes and stable thereafter. The measured zeta potential (Rank Brothers

Microelectrophoresis Mark II, Cambridge, England) was measured over a pH range from 4.7 to 10.2 at 25°C. Interpolation shows at pH 7.3 a zeta potential of -47 mV, and extrapolation to a point of zero charge at pH 1.5, comparable to silica at 2.0. This potential is sufficiently repulsive under ambient conditions to avoid coagulation.

The size distribution was refined using a Cyclosizer (Warman, Sydney, Australia) which rapidly separates materials upon passage through a series of five hydraulic cyclones (Kelsall *et al.* 1974). Collected fractions were washed with deionised water, decanted, and washed again before drying overnight at 60°C. Size distributions of the refined material are presented in Table 7-4. For FDA testing the material collected from cyclone 5 (d_{50} 13.2 μm) was used.

Table 7-4 Malvern MasterSizer volume-based distribution of glass spheres. Cyclone 1 (coarse) had no significant amount of material reporting to it.

Sample	d_{10} (μm)	d_{50} (μm)	d_{90} (μm)
As received	1.67	16.83	54.17
Cyclone 2	30.46	42.74	61.55
Cyclone 3	21.45	28.22	36.85
Cyclone 4	13.34	18.72	25.46
Cyclone 5	9.81	13.22	16.89

The free settling of the spheres was observed with the FDA. The experiments were run at 30.0°C with the 20-fold magnification lens. A standard slurry of refined glass spheres in water was made (0.2 g solids, 10 g deionised water) and left to age at temperature for 90 minutes in a small vial. The slurry was subject to gentle dispersion in an ultrasonic bath (47 kHz, Cole-Parmer Ultrasonic Cleaner model 08849, Chicago, Illinois). Sampling from the cylinder was accomplished with a wide

bore syringe (i.d. 2 mm, 0.2 mL sample volume). The entire sample was transferred directly into the FDA settling chamber and allowed to settle freely in the quiescent conditions.

For flocculation studies, flocculants used were FA920VHM and FA920MPM (SNF-Floerger, Saint-Etienne, France) with nominal molecular masses 20 and 10×10^6, respectively. A range of flocculant solutions of concentrations *ca.* 200, 100, 50 and 25 $\mu g\ mL^{-1}$ was prepared. Flocculant (0.5 mL, equivalent to a dosage *ca.* 250 $g\ t^{-1}$ for 100 $\mu g\ mL^{-1}$) was added to the vial containing the slurry. Mixing was accomplished over one minute by a cylinder inverter operating at 15 rpm. Sampling and injection into the FDA was performed as above.

7.2.2.1 Data fitting

For each body, the settling rate and the maximum aggregate dimensions are measured. From the settling rate and aggregate size the density is calculated, and the relationships are fitted to the power functions (equations 7-1, 7-2)

$$U = K(d)^x \tag{7-1}$$

$$\rho_a = A(d)^{-n} + \rho_l \tag{7-2}$$

where the settling rate, U, and aggregate density, ρ_a, is related to a body of diameter d in a medium of density ρ_l by the constants K and x, and A and n, respectively.

An aggregates was not considered if it was

- excessively out of focus, where the sizing function becomes meaningless;
- excessively eccentric, with an aspect ratio greater than 4:1;
- within three diameters of another body, subject to "slipstreaming" effects.

7.2.3 Results of FDA studies

An accurate measurement by the FDA is possible only if the settling bodies are in sharp focus. Either side of the focal plane the bodies appear slightly larger. Single particles, modelled by Stokes' law, settle at a rate proportional to their radii squared and their density is invariant with size. The settling rate data, fitted to a power law, returned exponents $x = 2.2$ and $n = 0.2$. When accounting for optical oversizing, a -1.8 μm correction for both axes brought the settling rate exponent to 1.99, in satisfactory agreement with Stokes' equation. The same correction also restored the exponent of the size-density relationship to the expected value of zero.

For a flocculated sample, Figure 7-4 shows the effect of measured size on free settling rate and density, and clearly with increasing diameter the settling rate increases. The points at 365 and 372 μm diameter are retarded somewhat, most likely from wall effects of the settling cell and, in agreement with Farrow and Swift (1991), are ignored. The remaining data, when fitted to equation (7-1), returns a settling rate exponent of 1.59. The density curve of Figure 7-4b shows larger particles contain more entrained water and the overall density approaches that of the liquid.

Closer observation of the settling rate data suggested a discontinuity at around 70 μm. Fitting the power curves to bodies under 70 μm, an exponent of 1.72 was returned, while for the interval 80-250 μm the exponent was 1.38. This result indicated smaller bodies, of no more than ten primary particles, are more densely packed and settle with less entrained liquid, while the opposite is true for larger species. However, the bodies may be not homogeneously packed, and especially for larger bodies, exist with clusters of densely-packed spheres separated by regions containing mostly liquid.

Figure 7-4 FDA measurements for (a) free settling rate and (b) density versus size with flocculation by 250 g t^{-1} FA920MPM.

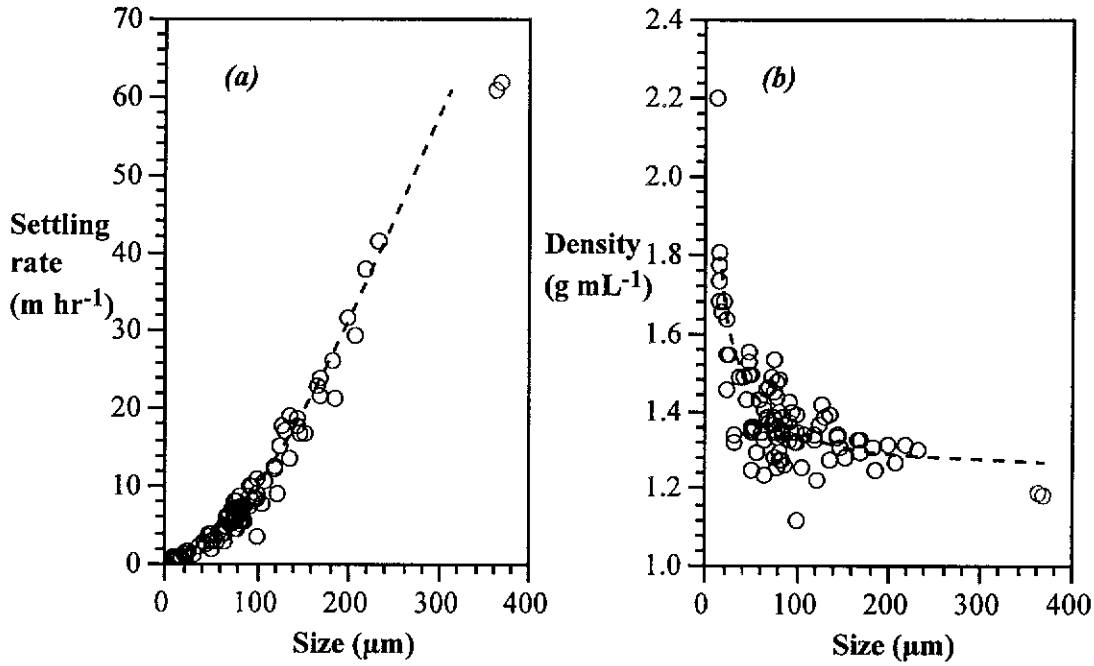

Settling rate exponents are summarised in Table 7-5. A fair comparison between the flocculants may be made on a dosage basis (same mass of polymer) or on an equivalent molecular basis (100 g t^{-1} of FA920MPM has approximately the same number of molecules as 200 g t^{-1} FA920VHM). Unfortunately any comparisons are obscured, as the scatter in the exponents is greater than for any differences between the flocculants. It is unclear whether the differences are real or a function of sampling methods, although the difference in the exponents for the higher dosages suggests the problem lies in the sampling of the aggregates. The other issue is of the size distribution. If the packing is a function of size, a large number of smaller aggregates will weight the curve fitting differently to a more representative measurement range. As the equipment stands, the FDA is an ideal tool for characterising thickener overflow solids and gross differences between compressed bed and underflow aggregates (Farrow and Swift 1991) but may lack the sensitivity to observe differences in aggregates arising from varying flocculation.

Table 7-5 Settling rate exponents for glass spheres flocculated with FA920MPM and FA920VHM over all size ranges.

Flocculant dosage (g t^{-1})	FA920MPM (10×10^6)	FA920VHM (20×10^6)
62	1.56, 1.70	1.73, 1.74
125	1.57	1.35
250	1.51, 1.59	1.51, 1.66
500	1.32, 1.53	1.55, 1.85

There are, however, a few options that may assist sensitivity. Automated image processing allows many more data points to be gathered for a more statistically robust experiment. Also, the glass spheres used were quite coarse (d_{50} 13.2 μm), and a finer substrate may be more influenced by the flocculant. Finally, the flocculation mixing and sampling will greatly affect the aggregates and require an extensive study.

7.3 *Appendix 3: FBRM Data Weightings*

The FBRM probe records the time of reflection of light, which multiplied by the scanning speed, gives a chord length. The discrimination circuit sorts the chord lengths into a number based (frequency) distribution over z chord length channels of mean length M for channel 1, 2 ,..., z. For the M500 probe there are 38 channels ($z = 38$). The raw chord counts are amenable to chord length weightings to an upper number of channels k, where $2 \leq k \leq z$, as given below in a cumulative format.

Number-weighted mean chord ("unweighted chord")

$$C_n = \frac{\sum_{i=1}^{k} n_i M_i}{\sum_{i=1}^{k} n_i} \qquad (7\text{-}3)$$

Length-weighted mean chord

$$C_l = \frac{\sum_{i=1}^{k} n_i M_i^2}{\sum_{i=1}^{k} n_i M_i} \qquad (7\text{-}4)$$

Square-weighted mean chord

$$C_s = \frac{\sum_{i=1}^{k} n_i M_i^3}{\sum_{i=1}^{k} n_i M_i^2} \qquad (7\text{-}5)$$

Cube-weighted mean chord

$$C_c = \frac{\sum_{i=1}^{k} n_i M_i^4}{\sum_{i=1}^{k} n_i M_i^3} \qquad (7\text{-}6)$$

Intuitively C_l is a measure of aggregate diameters, C_s of projected areas and C_c of volumes, but these are derived from chord lengths and are not comparable directly to classical particle size distributions. Becker (1997) has shown that for spherical particles, the cube-weighted chord length distribution is very similar to the particle size distribution obtained with a Coulter counter.

7.4 REFERENCES

Becker, R., 1997, *Personal Communication.*

Breitmaier, E., and Volter, W., 1990, *Carbon-13 NMR Spectroscopy,* VCH Publishers, Weinheim.

Farrow, J.B. and Swift, J.D., 1991, 'Improving thickener technology', at *Fifth Extractive Metallurgy Conference*, Australasian Institute of Mining and Metallurgy, Perth, Australia, 2-4 October, pp. 227-232.

Farrow, J.B. and Warren, L.J., 1989a, 'The Measurement of Floc Density-Floc Size Distributions', in *Flocculation and Dewatering,* eds. Moudgil, B.M. and Scheiner, B.J., Engineering Foundation, New York, pp. 153-165.

Farrow, J.B. and Warren, L.J., 1989b, 'A new technique for characterising flocculated suspensions', at *Dewatering Technology and Practise*, Australian Institute of Mining and Metallurgy, Brisbane, Australia, pp. 61-64.

Farrow, J.B. and Warren, L.J., 1993, 'Measurement of the Size of Aggregates in Suspension', in *Coagulation and Flocculation: Theory and Applications,* ed. Dobias, B., Marcel Dekker, New York, pp. 391-426.

Gregory, J., 1998, 'The role of floc density in solid-liquid separation', *Filtration & Separation*, vol. 35, no. 4, pp. 367-371.

Halverson, F., Lancaster, J.E. and O'Connor, M.N., 1985, 'Sequence distribution of carbonyl groups in hydrolyzed polyacrylamide', *Macromolecules*, vol. 18, pp. 1139-1144.

Happel, J. and Brenner, H., 1973, *Low Reynolds Number Hydrodynamics*, Noordhoff International Publishing, Leyden.

Kelsall, D.F., Restarick, C.J. and Stewart, P.S.B., 1974, 'Technical note on an improved cyclosizing technique', *Proceedings of the Australasian Institute of Mining and Metallurgy*, vol. 251, pp. 9-10.

Kulicke, W.-M., Otto, M. and Baar, A., 1993, 'Improved NMR Characterization of high-molecular-weight polymers and polyelectrolytes through the use of preliminary ultrasonic degradation', *Makromolekulare Chemie*, vol. 194, pp. 751-765.

Lafuma, F. and Durand, G., 1989, '^{13}C NMR spectroscopy of cationic copolymers of acrylamide', *Polymer Bulletin*, vol. 21, pp. 315-318.

Leung, W.M., Axelson, D.E. and Syme, D., 1985, 'Determination of charge density of anionic polyacrylamide flocculants by NMR and DSC', *Colloid and Polymer Science*, vol. 263, pp. 812-817.

Moradi-Araghi, A., Hsieh, E.T. and Westerman, I.J., 1988, 'Role of imidization in thermal hydrolysis of polyacrylamides', in *Water-Soluble Polymers for Petroleum Recovery,* eds. Stahl, G.A. and Schulz, D.N., Proceedings of the National Meeting of the American Chemical Society, Plenum, New York, pp. 271-278.

Panzer, H.P. and Halverson, F., 1989, 'Blockiness in hydrolyzed polyacrylamide', in *Flocculation and Dewatering*, eds. Moudgil, B.M. and Scheiner, B.J., Engineering Foundation, New York, pp. 239-249.

Tchir, M.F. and Rudin, A., 1986, '13C NMR Characterisation of Structures of Water-Soluble Polymers', in *Water-Soluble Polymers,* ed. Glass, J.E., ACS Symposium Series 213, American Chemical Society, Washington DC, pp. 71-83.